NOTE TO USERS

Description and Evolutionary Significance of the Sauropodomorph Dinosaurs from the Early Jurassic (Hettangian) McCoy Brook Formation

by

Timothy J. Fedak

Submitted in partial fulfilment of the requirements
for the degree of Doctor of Philosophy

at

Dalhousie University
Halifax, Nova Scotia
December 2006

Your file Votre référence
ISBN: 978-0-494-27192-6
Our file Notre référence
ISBN: 978-0-494-27192-6

DALHOUSIE UNIVERSITY

To comply with the Canadian Privacy Act the National Library of Canada has requested that the following pages be removed from this copy of the thesis:

Preliminary Pages

Examiners Signature Page (pii)

Dalhousie Library Copyright Agreement (piii)

Appendices

Copyright Releases (if applicable)

Dedication

For Max, who makes everything of value so easy to share;
and my family for your patience and encouragement.

In memory of Marilyn Smith.

Table of Contents

List of Tables

List of Figures

Abstract

A rich bone bed of prosauropod dinosaurs was discovered in the Lower Jurassic (Hettangian) McCoy Brook Formation of Nova Scotia. At least five individuals are present within the bone bed, based on unique femora and coracoids, therefore the new bone bed is now the richest site in North America for prosauropod dinosaurs. Based on the morphology of the ilium and sacral vertebrae from these new specimens, the McCoy Brook prosauropods are not referable to cf. *Ammosaurus*, but rather represent a new taxon, *Fendusaurus eldoni*. A phylogenetic analysis of the holotype, which includes the first cranial material from the McCoy Brook Formation, and three other articulated specimens referred to *Fendusaurus*, place this new taxon within the terminal branches of Massospondylidae. *Fendusaurus* is unique among Massospondylidae, for the extreme elongation of the cervical vertebrae, a four vertebrae sacrum that includes a dorsosacral and caudosacral, the elongate postacetabular process of the ilium, and an expanded anterior distal process of the tibia. Morphological variation within the bone bed is attributed to intra-specific variation; although additional specimens remaining to be collected from the bone bed may provide further information to identify at least one other taxon. The two skulls of *Anchisaurus* (=*Ammosaurus*) have been misinterpreted for over one hundred years, and the new preparation and description of these skulls further clarifies the morphology of the cranial and braincase elements. The absence of *Anchisaurus* and the presence of a the new massospondylid *Fendusaurus*, further strengthens the similarities between the McCoy Brook Formation and the Lower Jurassic deposits of the western USA, China, and South Africa.

Acknowledgements

A project of this size is impossible to complete without the help of many generous people. Thanks to Ian Morrison and Hans Sues for the initial idea to travel east, and Paul Olsen for encouragement to stay and thoughtful advice. A special debt is owed to the literally dozens of people who have helped with field work over the past nine years; as this shows, the struggles through rain, snow, and sun were not in vain. Preparation staff and volunteers in the museum lab have of course spent more time with these specimens than I have, for which I remain grateful; particularly to Kathy Goodwin (FGM) and Molly Kernohan. The generous support and interest by all other staff at the FGM has been important over the course of this project, especially that of Ken Adams, Rose MacAloney and Leisa Babineau. Other staff at the Nova Scotia Museum, including D. Skilliter, B.Ogilvie and R.Grantham, have provided important administrative support. I am grateful to have had stimulating interactions with members of the Hall lab, especially M. Vickaryous, A. Gillis, J. Stone, and T. Franz-Odendaal, and to Michael and Krista who provided a second home. Also, special thanks to P. Galton and P. Barrett for encouragement and editorial advice.

Funding for field work, museum travel and specimen preparation has been provided by: Nova Scotia Museum (NSM) Research Grants (1997 and 2000), the Royal Canadian Geographic Society, the Jurassic Foundation, NSERC (PromoScience), the Canadian Geological Association, the ERI Education Grant, the Samuel P. Welles Grant (Berkeley), the Patrick Lett Fund (Dalhousie), the Fundy Geological Museum and the Faculty of Graduate Studies. The funding was instrumental in the completion of this project and is greatly appreciated.

My research has been directly funded by NSERC Post Graduate Scholarships, Systematics Supplement (NSERC and NSM) and the NSERC grant of my advisor, Brian Hall. My sincere appreciation is extended to Brian for his constant availability to answer questions and offer advice. I am grateful to the other members of my committee, who have provided their time and advice on the development of this project.

Chapter 1 – Introduction

Sauropod dinosaurs include the largest animals to ever walk on the earth, which is most certainly the basis of their popularity with movie audiences (*Brachiosaurus* in Jurassic Park) and museum visitors around the world. The Sauropodomorpha (von Huene 1932) includes these popular long necked herbivorous giants, the Sauropoda (Marsh 1898), as well as the smaller and more basal taxa from the Late Triassic and Lower Jurassic, some of which form a monophyletic group, the Prosauropoda (von Huene 1932). Several research projects have focussed upon some of the more important basal sauropodomorph taxa during the past decade. These studies include the small *Thecodontosaurus* (Benton et al. 2000) from the Late Triassic of Britain, description of a new genus, *Saturnalia* (Langer 2001), from the Late Triassic of South America, and the restudy of the medium-sized taxa from the Lower Jurassic, such as *Massospondylus* (Sues et al. 2004) from South Africa, and *Lufengosaurus* (Barrett et al. 2005) from China. *Anchisaurus*, from the Lower Jurassic of eastern North America, has historically been identified as a prosauropod dinosaur (Marsh 1896, von Huene 1932, Lull 1953, Galton 1976), but was recently recognized as being more closely allied with the sauropod clade (Yates 2004), and therefore identified as one of the smallest sauropod dinosaurs. While the first phylogenetic analysis of the Sauropodomorpha (Gauthier 1986) concluded Prosauropoda represented a paraphyletic grade of taxa at the base of the sauropod tree, the recent studies (Yates 2003c, Sues et al. 2004, Yates 2004, Barrett et al. 2005) have reaffirmed the monophyletic status of Prosauropoda, although the clade now excludes many of the smaller taxa that represent more basal sauropodomorphs.

With the recent attention directed toward the morphology and relationships among basal sauropodomorph taxa, the identity of the dinosaur specimens from the Wasson Bluff section of the Lower Jurassic McCoy Brook Formation, located near Parrsboro, Nova Scotia, are of greater significance. Isolated and disarticulated 'prosauropod' dinosaur skeletal remains discovered from the McCoy Brook Formation in the mid-1970's were referred to cf. *Ammosaurus* (Olsen et al. 1982), a genus that is now considered a junior synonym of *Anchisaurus* (Chapter 3). As already mentioned, while *Anchisaurus* has historically been considered a prosauropod dinosaur, it has recently been

recognized as being more closely allied with the Sauropoda clade (Yates 2004). Therefore, the Nova Scotia dinosaur specimens would potentially provide some important additional information about this genus. However, the initial material collected from the McCoy Brook Formation did not include diagnostically significant a fact which has limited the phylogenetic and biostratigraphic significance that could be drawn from these specimens.

Following the discovery of the first dinosaur material, the McCoy Brook Formation became increasingly important as the Fundy basin was recognized as the largest and most exposed rift basins in the Newark Supergroup (Olsen 1978, Olsen et al. 1982, Olsen and Gore 1989). The discovery of rich deposits of small vertebrate fossils (Olsen et al. 1987, Shubin et al. 1994) at Wasson Bluff, provided important evidence for interpretations of the ecological turnover at the Triassic-Jurassic boundary. Although much attention has been directed toward these small vertebrate fossils, the study of the dinosaur fossils was hampered by the lack of sufficiently diagnostic material.

A new dinosaur specimen was located at Wasson Bluff in 1997 and from my study of this specimen and additional field work at the site (Chapter 4), a rich bone bed was discovered that includes at least five individuals. These new specimens provide the first diagnostically informative skeletal material from the McCoy Brook Formation. These specimens are described (Chapters 5-8) in order to clarify if the specimens are referable to *Anchisaurus* (=*Ammosaurus*), or rather if the specimens represent some other, or perhaps new taxon. The phylogenetic relationship of the McCoy Brook dinosaur specimens are then examined in relation to other recently published studies of basal sauropodomorph dinosaurs (Chapter 9).

As a consequence of the previous referral of the Nova Scotia dinosaur specimens to cf. *Ammosaurus*, the specimens of this taxon *Anchisaurus* (=*Ammosaurus*) were examined directly for comparative reference. In the course of this work, it became apparent that the most complete skull of *Anchisaurus* has been misinterpreted for over 100 years, and new information about the braincase and skull of *Anchisaurus* was subsequently gathered after conducting additional preparation of a second smaller skull. After presenting a redescription of these two skulls (Chapter 3) a hypothesis is proposed that the small size of *Anchisaurus* specimens is due to young age and skeletal immaturity,

which is then considered within a phylogenetic context (Chapter 3). As an introduction to these topics of ontogenetic variation and skeletal immaturity, a series of unresolved issues related to ontogeny among sauropodomorph dinosaurs is reviewed (Chapter 2); this is then followed by a re-examination of a small 'juvenile prosauropod' specimen that was previously recovered from the McCoy Brook Formation (Olsen and Gore 1989).

Chapter 2 – Growing Issues of Sauropodomorph Dinosaur Ontogeny and a 'Juvenile Prosauropod' Reconsidered (as *Protosuchus*)

Introduction

Sauropodomorph dinosaurs include the largest animals to ever have walked on the earth, some sauropods exceeded an estimated body size of 75,000kg (Peczkis 1994) and include popular taxa such as *Apatosaurus* and *Diplodocus*. Considering a sauropod hatchling mass estimate of 7.5 kg (Britt and Naylor 1994), which correlates well with an egg volume of 800 cm^3 (Chiappe *et al.* 2004), these gigantic sauropods increased in mass by a factor of 10,000 during post-hatchling growth. With one of the largest ontogenetic size increases found among terrestrial vertebrates, the identification of skeletal maturity is especially important for phylogenetic studies of sauropodomorph dinosaurs, especially given the importance of comparing specimens of equal growth stages (Wiley *et al.* 1991). Taxonomic bias, the misidentification of immature specimens as separate taxa from adult forms (Coombs 1990), remains a significant problem in systematic studies of Dinosauria since the allometric differences during ontogeny can be greater than the differences between mature specimens of closely related taxa (Currie 2003). Unfortunately, the level of ontogenetic variation remains undocumented for most sauropodomorph taxa (Galton and Upchurch 2004).

Several outstanding issues related to sauropodomorph ontogeny are considered here while reviewing the recent literature related to sauropodomorph ontogeny and ontogenetic variation. Due to the importance of documenting sauropodomorph ontogeny, a small 'juvenile prosauropod' (Olsen and Gore 1989) from the Lower Jurassic McCoy Brook Formation is then examined, and based on the available material is reinterpreted as postcranial material of a protosuchid crocodylomorph.

Sauropodomorph Ontogeny

Maturity and Size

As with ontogeny, maturity is a continuum that is artificially divided into stages in order to facilitate appropriate comparisons between taxa. *Skeletal maturity*, the stage after which a specimen demonstrates the morphologically derived skeletal characteristics of its taxon (Brochu 1992), is of central concern to systematic studies that are based solely upon morphological characters. Skeletal maturity is attained when the morphology and size relationships of the skeletal elements have stabilized to a level to permit appropriate comparisons between taxa. With extant taxa, time (age) is often used as a proxy for maturity and has the benefit of permitting comparison of specimens *within* a species that are either equally immature or fully mature. However, taxa mature at different rates, therefore age is not a reliable staging factor *between* taxa, except when specimens can be assessed as old and confidence in skeletal maturity is therefore high. Comparisons that are based on mature skeletons are preferred, as they are not biased by ontogenetic differences between the specimens. How then do we determine if a specimen is skeletally mature?

If dinosaur skeletons are associated with eggshells or nesting structures, such as the sauropods from Argentina (Chiappe et al. 2001, Chiappe et al. 2004), or prosauropods from South Africa (Reisz *et al.* 2005), maturity state can often be explicitly described with terms such as embryo (within an egg) or hatchling (within or around a nest). Beyond these early stages, determination of skeletal maturity becomes more complicated, especially when evaluating a sample of perhaps fragmentary specimens.

Various methods are used to judge sauropodomorph skeletal maturity, including size, suture fusion patterns, bone surface texture, tooth morphology and bone histology, but fundamental to the validity of these approaches is confirmation of maturity patterns within a well preserved growth series. The factors used to determine maturity state are not always consistent, often being variable between closely related taxa. For example, neurocentral and cranial sutures act as joints between skeletal elements and are locations of active bone growth (Fedak *et al.* 2003). While sutures are typically open during immaturity, close, and then fuse later in maturity, sutures can also remain open in otherwise mature skeletons (Maisano 2002). Furthermore, it can be difficult to determine

the difference between closed and fused sutures without sectioning, and closed sutures can still permit significant bone growth (Brochu 1996). While suture fusion is one-way (closed/fused sutures are not known to reopen), the point at which a suture closes (if ever) can be variable even between closely related taxa (Maisano 2002). These variations and characteristics of suture fusion patterns complicate their unequivocal use in the assessment of skeletal maturity.

Of course, vertebrate skeletons either maintain or increase (grow) in size, with no known examples of animals that become smaller with increasing age, therefore enormously large specimens are likely old and skeletally mature. However, small specimens are not necessarily young (immature) – take for example dwarf taxa. Jianu et al. (1999) attempted to test a hypothesis put forward by Nopsca (1914) that *Magyarosaurus,* from the Upper Cretaceous of Transylvania, represents a dwarf sauropod. A central requirement for this test was the identification of mature *Magyarosaurus* specimens. Unfortunately, specimen maturity was based on rather speculative evidence, including joint surface characteristics and an assumption that the largest specimens are adults. Mussel and Weishampel (2000) attempted to improve upon this study by including more measured variables, however their conclusions that *Magyarosaurus* is a dwarf taxon would be greatly strengthened by additional assessment of maturity that is not related to size, such as osteohistological age estimates. As this taxon demonstrates, the fundamental problem of skeletal maturity is with small specimens, for which evidence of skeletal maturity must be gathered and evaluated.

Terms such as baby, juvenile, and sub-adult are often used as synonyms for immaturity, yet these terms hold little value for facilitating the appropriate comparison of equally immature specimens; two sub-adult specimens may still have significantly different maturity states. Carpenter and McIntosh (1994) offer an explicit size-based definition for baby specimens as "arbitrarily set as less than one-sixteenth adult size" (p. 265). Although not stated, they clearly intend this to refer to a mass-based measure, as no appendicular specimen in their study of "baby sauropods" is smaller than one-sixth adult linear size (e.g. the smallest humerus at 227 mm is 19% of the length of the largest at 1195 mm). Accepting for now their assumption of limb isometry, the change in linear length of a skeletal element is generally proportional to the cube root of the volume/mass

change of the animal, therefore the baby definition represents any linear dimension that is less than $(^1/_{16})^{1/3}$ or 40 % adult linear size. While this definition has been adopted by others (Wilhite 1999), the biological significance is not stated, and being dependant upon a comparison with the largest sized specimen which may or may not be mature, the definition is not helpful in explicitly assessing skeletal maturity.

The small ("baby") sauropod material also demonstrates that data is currently lacking for the first 15% of sauropod post-hatching linear growth (i.e. femur size between 100 and 300 mm). The recent discovery of sauropod eggs from Upper Cretaceous of Argentina (Chiappe et al. 2001), suggest sauropod hatchlings had a femur length of approximately 100 mm (Chiappe pers. comm. 2004), while the smallest post-hatchling sauropod femur known is 330 mm long (Carpenter and McIntosh 1994).

Knowledge of ontogenetic variation is important for the proper assessment of significant differences between specimens and taxa. Proportional characters are common among phylogenetic analyses; for example 34% of character descriptions involved proportions within or between skeletal elements in a recent phylogenetic study of basal sauropodomorphs (Yates 2004). Some ontogenetically variable skeletal proportions are well known and occasionally used to identify skeletons as immature, but in general more work is required to document ontogenetic variation among sauropodomorph dinosaurs.

Allometry

Ontogenetic allometry involves the analysis of shape change due to growth and development (Hall 1999). The proportions within or between elements can either increase or decrease (positive or negative allometry) or remain constant (isometric growth). Recently, studies of sauropodomorph locomotion (Bonnan 2003), systematics (Yates and Kitching 2003), and life history growth strategies (Erickson *et al.* 2001) have relied on the assumption of limb isometry during sauropod ontogeny, citing two studies (Carpenter and McIntosh 1994, Wilhite 1999) that attempted to quantify limb proportions through ontogeny. However, accepting the assumption of limb isometry among sauropod dinosaurs based on these studies is not recommended due to inappropriate mathematical analysis, uncertain taxonomic identifications and species pooling.

The methodology adopted by Wilhite (1999) was inappropriate for identifying allometry among sauropod limbs as he sought to find the most effective regression of the form $y=mx^k$ only where k was a positive integer (1, 2, and 3), and therefore was unable to consider more realistic allometric coefficients such as $0.8 < k > 1.2$ (Dodson 1975a). Furthermore, allometric variation of proportions *within* an element, and allometric variation *between* elements or body size are separate relationships. Both Wilhite (1999) and Carpenter and Macintosh (1994) examined only proportional changes within elements and did not consider the relative proportions between a standard metric of body size.

While Carpenter and McIntosh (1994) concluded the proportions within *Apatosaurus* humeri did not change during ontogeny, the significance values of their analyses were not provided and the study was limited to only four small and two large humeri. Also, they point out that the circumference to femur length ratios of adult and juvenile *Camarasaurus* specimens differ (0.40 compared to 0.44) and suggest this difference "is not unreasonable to expect in an immature animal" (p 275), implying allometric variation of this ratio during ontogeny. Allometry in sauropod growth is further supported by a recent report of an immature specimen of *Alamosaurus sanjuanensis* (TMM 43621-1), which demonstrates a ulna to humerus length ratio (0.77) that is larger than in adult specimens (0.65) (Lehman and Coulson 2002). Negative allometry of the forelimb (humerus and ulna) has also been demonstrated for the prosauropod *Massospondylus* (Reisz et al. 2005), the sauropodomorph with the most complete and well-documented growth series.

It is uncertain if pooling the *Camarasaurus* species into a single ontogenetic series (Wilhite 1999) affected the possibility of identifying ontogenetic variation, although taxonomic identification may have been a contributing source of error. Two "baby" specimens from Oklahoma (OMNH 01277 and 02115) were used in both the *Apatosaurus* (Carpenter and McIntosh 1994) and the *Camarasaurus* (Wilhite 1999) data sets, with each study justifying identity based on similarity of the "baby" humeri to the respective adult proportions. The use of proportional similarity of small and large specimens for determining taxonomic identification must be avoided in studies that

attempt to determine if proportional changes occur during ontogeny, otherwise circular reasoning prohibits an unbiased result.

The allometric growth of limbs can have significant implications for systematic studies as well as for reconstructing their ecology and biomechanics. The holotype of the oldest known sauropod, *Antetonitrus ingenipes* from the Late Triassic of South Africa, was identified as immature based on open cervical and dorsal neurocentral sutures (Yates and Kitching 2003), yet the immaturity of the specimen was not considered an issue of systematic importance as "the appendicular skeleton of sauropodomorphs experiences little, if any, allometric change with growth" (p 1755). Unfortunately the evidence for this statement is traced back to the studies mentioned, which do not adequately support this assumption. Also, in dinosaurs with well documented growth series, allometric growth of the appendicular skeleton can result in a shift from bipedal posture in juveniles to a quadrupedal posture in adults, such as has been hypothesized for *Maiasaura peeblesorum* (Dilkes 2001).

Additional study of sauropodomorph appendicular allometry is needed to determine the amount and direction of proportional changes that occur during ontogeny. The position of the fourth trochanter along the length of the femur has been used as both a phylogenetic character (Galton and Upchurch 2004, Yates 2004), as well as for reconstructing total femur length when distal areas are missing (Galton 1976) in studies of sauropodomorph dinosaurs. However, Dodson (1975) demonstrated that the fourth trochanter length of *Alligator mississippiensis* is positively allometric during ontogeny ($a=1.09$; $y= (0.5)\ x^{1.09}$), while the total femur length is negatively allometric ($a=0.97$). These allometric relationships result in the distal migration of the fourth trochanter down the shaft of the femur with increasing size/age. With a 13 times linear size increase during *A. mississippiensis* ontogeny (femur lengths: 19 to 247 mm) the trochanter is distally repositioned 10% of total femur length, from 26% femur length to 36% femur length.

Over the course of ontogeny some sauropodomorph dinosaurs undergo a larger linear size increase than *A. mississippiensis,* therefore a 10% distal migration of the fourth trochanter could be taken as a minimum amount of potential variability. Until specimens are available to demonstrate the nature of ontogenetic variation among

sauropodomorph dinosaurs, the use of the position of the fourth trochanter should only be used with caution for systematic studies or reconstructing femur lengths.

Allometry of the manus/pes has also been noted among some basal sauropodomorphs. Specimens of *Massospondylus* show ontogenetic variation in the broadness of the pes, being narrow in young individuals and broad in mature skeletons (Galton and Upchurch 2004). Conversely, pes proportions have been used to distinguish between *Ammosaurus* and *Anchisaurus* taxa from the Connecticut Valley and Arizona (Galton 1976, 1990); however, other authors have argued for synonymy of *Ammosaurus* and *Anchisaurus*, suggesting the pes proportions are likely ontogenetic (Sereno 1999, Yates 2004). The proportions within the manus or pes are problematic for phylogenetic characters, unless character codings are explicit in their application to fully mature skeletal specimens.

Three embryonic titanosaurid skulls recently described from the massive egg layer of the Upper Cretaceous Acua Maheuvo Formation (Salgado *et al.* 2005) provide additional evidence for the nature of cranial ontogenetic variability possible during sauropodomorph ontogeny. Five adult Eusauropoda synapomorphies were identified in the embryonic skulls; 1) ventral process of postorbital much longer than the anteroposterior length of the postorbital dorsal margin, 2) snout with stepped anterior margin, 3) no contact between the squamosal and quadratojugal, 4) elongate and distally expanded rostral process of quadratojugal, and 5) antorbital fossa absent. Some caution may be warranted with the first and fourth characters. With an elongate ventral process found in the smallest skull of *Massospondylus* but not the adult, it is possible ontogenetic variation could confound comparisons of this character between embryonic and adult stages. Conversely, an elongate rostral quadratojugal process is found in the adult but not the small *Massospondylus* skull (pers. obser.), therefore although the ontogenetic variation is in the inverse direction there remains evidence of variability during growth.

Furthermore, the frontal contributes significantly to the large orbits of the embryonic skulls, whereas in adult Eusauropoda the frontal is reduced or excluded from the orbital margin (Salgado et al. 2005). Therefore the authors suggest the frontal contribution may decrease during ontogeny (as it does in Sauropoda phylogeny). Thus, phylogenetic studies that include the amount of frontal contribution to orbital margin (for

example Galton and Upchurch 2004) must be especially diligent to ensure all skeletal specimens are mature or that ontogenetic variability is accounted for within character descriptions.

Due to the tremendous potential for differential growth of the morphological complex cranial elements, ontogenetic variation exhibited within taxa is of great importance. Characters meant to discern phylogenetic patterns should not be confounded by ontogenetic variability through misidentifications of skeletal maturity.

Aside from their gigantic size, the elongate necks of sauropodomorph dinosaurs perhaps their most commonly recognized feature. Neck elongation by addition of extra cervical vertebra has occurred twice, while extreme elongation of individual cervical vertebra appears to have evolved three times among sauropod dinosaurs (Wilson and Sereno 1998). Considering the latter method of neck elongation, allometric growth of the cervical vertebrae among sauropodomorph dinosaurs during ontogeny seems not only possible but probable.

The embryonic sauropod skeletons from the Auca Mahuevo Formation did not include ossified vertebral centra although ossification of the skulls and periosteum of many of the limb elements had occurred, a pattern consistent with avian development (Salgado et al. 2005). However, based on well preserved and apparently late stage *Massospondylus* embryos (Reisz et al. 2005), prosauropod cervical vertebrae grew with positive allometry (compared to femur length), whereas dorsal vertebrae grew isometrically. The proportional length of cervical vertebrae is a common character used in analyses of sauropodomorph dinosaurs, and the allometry demonstrated by *Massospondylus* suggests careful consideration of ontogenetic variation is required in phylogenetic analyses.

The new data provided by the *Massospondylus* embryos suggests that the holotype of *Mussaurus patagonicus* (Bonaparte and Vince 1979), currently the smallest articulated sauropodomorph post-embryonic skeleton (estimated body length=200 mm), likely has a short neck (Durand 2001) due to ontogeny rather than phylogeny. Being only slightly longer than the *Massospondylus* specimens embryos, *Mussosaurus* represents a young specimen of larger specimens recovered from the same locality (Casamiquela

1980), although detailed description of these larger specimens is still required before proper assessment can be made (Galton and Upchurch 2004).

Bonaparte (1999) noted possible ontogenetic variation in the proportion of neural arch to centrum height of anterior dorsal vertebrae in *Riojasaurus*. The smaller *Riojasaurus* specimen (UPLR 56) has a neural arch taller than the centrum height, whereas the larger holotype specimen (PVL 3808) has a neural arch that is shorter than the centrum height; therefore centrum height is suggested to increase in proportion to neural arch height during maturity. However, comparing the figured vertebrae (Bonaparte 1999, Figs 5B-D, 7D, and 8A), the larger specimen has well developed parapophyses on the centra of c10, d1, and d4, which are not found on vertebra d1, d2, or d3 of the smaller specimen. The development of parapophyses late in maturity would be unique, and suggests the location of the vertebrae along the axial skeleton has been misinterpreted or the specimens are not conspecific. The smaller specimen was fully articulated so vertebral identity seems quite reliable. In contrast, the holotype specimen is missing at least several dorsal vertebral (Bonaparte 1971), suggesting it was disarticulated when collected. Although ontogenetic variation in the height/length proportions of individual vertebrae is possible, the example of *Riojasaurus* anterior dorsal vertebrae requires clarification, to rule out the possibility of misidentified vertebral identity. Neural arch height is often used as a character in phylogenetic studies of sauropodomorphs; therefore it is of some importance to confirm if (and how much) the height may change during maturation.

The diversity and distribution of pneumatic cavities among sauropod vertebrae provide yet another way vertebrae morphology can vary during ontogeny. Wedel (2003a) reviewed the diversity and distribution of pneumatic cavities among Sauropoda, noting an evolutionary trend toward increasing cavity complexity from simple fossa, to camerate then to camellate morphologies. The occurrence of *coels*, areas where there has been active resorption of bone by osteoclasts around fossa, was suggested as evidence of pleurocoel development during growth (Wedel 2003a). Wedel was also explicit in pointing out the ontogenetic variability of pneumatic structures; mature *Apatosaurus* vertebrae have complex camerate pneumatic cavities, whereas the most immature vertebrae of *Apatosaurus* examined had simple lateral fossae and even younger

specimens were predicted to have no pleurocoel development. Considering these observations, phylogenetic analyses of sauropod dinosaurs that include the presence and morphology of vertebral pneumaticity (Upchurch et al. 2004, Yates 2004)) must be certain of skeletal maturity when coding taxa for this character. Considering the proposal that *Anchisaurus* represents a basal sauropod (Yates 2004), the lack of pleurocoels in this taxon may be an ontogenetic rather than phylogenetic state if the small skeletons are immature.

The complex vertebral laminae of derived sauropods provide increased structural support while reducing vertebral mass, but may have initially developed as a response to increased pneumatic diverticulae surrounding the vertebrae (Wilson 1999, Wedel 2003a). Unfortunately, the ontogenetic variation of laminae morphology has been mentioned only superficially (Mook 1917, Wilhite 1999). Additional study of the possible ontogenetic variability of vertebral laminae seems justifiable, especially since both laminae and pleurocoels are associated with diverticulae, and pleurocoel morphology has been noted as ontogenetically variable.

Suture Fusion

The use of neurocentral suture fusion patterns as a means for evaluating maturity of fossil skeletons results from the detailed study of suture fusion among *A. mississippiensis* (Brochu 1996). Brochu found that the sutural fusion pattern did correlate well with age and skeletal maturity, the sutures of the caudal vertebrae fusing prior to hatching, while the remaining (dorsal and cervical) neurocentral sutures closed in a posterior to anterior sequence. Therefore, open neurocentral sutures in fossil skeletons can provide evidence of young age and skeletal immaturity. For example, a specimen of the sauropod *Alamasaurus sanjuanensis* has been identified as skeletally immature based on its small size (less than half the size of the type specimen) and unfused neurocentral sutures (Lehman and Coulson 2002).

As noted, studies of Sauropodomorpha vertebral structure and variation have generally focused upon either the morphology of vertebral laminae (Bonaparte and Mateus 1999, Wilson 1999) or pneumaticity (Wedel 2003b, Wedel 2003a). A detailed study of neural arch morphology and neurocentral suture fusion patterns would also be

helpful to evaluate the appropriateness of neurocentral suture fusion patterns for evaluating sauropodomorph skeletal maturity. For example, the "neurocentral" suture of anterior dorsal vertebrae of *Camarasaurus grandis* is located well above the neural canal (see Ostrom and McIntosh 1966, Plate 23). The dorsal location of the suture does not permit the suture to increase neural canal size during growth. While neural canal growth may still have occurred by extensive bone remodelling, the location of the suture suggests neural canal growth may not be the only function of the suture. Comparative study of sauropodomorph suture locations and fusion patterns may clarify the functions and characteristics of the suture during vertebral growth.

Galton (1999) considered in detail the sacrum of a diverse selection of dinosaurs and concluded that the plesiomorphic condition for Dinosauria (excluding *Herrarasaurus*) is a three vertebrae sacrum that includes the "primitive" two vertebra sacrum of more basal archosaurs, SI and SII, and a "sacralized" caudosacral (SI, SII, cS1). Novas (1996) offers an alternative view, proposing that the plesiomorphic sacrum of Dinosauria is composed of the two primordial sacral and a dorsosacral (dS1, SI, SII), a view which has been accepted by other workers (Hutchinson 2001b, Yates 2004). Galton also reiterated a point raised by Mook (1917) - the number of vertebrae fused to the sauropodomorph sacrum increases with ontogenetic age. Therefore, it is clearly important to consider only skeletal mature specimens when coding the number of sacral vertebrae.

Number of sacral vertebrae has been used as a phylogenetic character in studies of sauropodomorph relationships (Upchurch 1998, Upchurch et al. 2004, Yates 2004). These studies concluded that Prosauropoda is composed of taxa with a three vertebrae sacrum, while members of Sauropoda have four or more sacral vertebrae. While Cooper (1981) suggested the prosauropod *Massospondylus* has a four vertebrae sacrum, subsequent authors (Galton and Heerden 1998, Galton 1999, Yates 2004) have dismissed this claim; Galton suggested the incipient dorsosacral (dS2) was too far forward to contact the ilium, leaving *Massospondylus* with three vertebrae sacrum (dS1, SI, SII). Indeed, Cooper's hypothesis of a second dorsal vertebra being incorporated into the sacrum seems to have been the premise for a "postulated cartilaginous extension of the

anterior iliac spine" (Cooper 1981, Figure 35), a suggestion for which there seems to be no evidence (Langer 2003).

Saturnalia tupinquim from the Late Triassic of Argentina, is alternatively considered to be a basal sauropodomorph (Langer et al. 1999, Langer 2003) or a basal prosauropod (Galton and Upchurch 2004). Langer has not offered an assessment of skeletal maturity in any of the publications that describe *Saturnalia*. The sacrum of *Saturnalia* is composed of SI, SII, cS1; however an additional centrum is located between the postacetabular processes of the ilium although it does not contact the medial surface of the ilium or the lateral processes of cs1 (Langer 2003). The uncertain skeletal maturity of the specimens may affect the certainty of sacrum morphology demonstrated by *Saturnalia*; if the specimens are immature it is possible a fourth sacral may have been added during growth, a morphological state that would likely position *Saturnalia* higher within Sauropodomorpha.

Age Estimates, Growth and Maturity

Osteohistology provides important information about fossil specimens, including age estimates, growth rates, and tissues that signify growth completion (Horner et al. 1999a, Padian et al. 2004). These topics are considered specifically in relation to recent studies of sauropodomorph dinosaurs.

Age-at-death estimates generated from analysis of fossil bone tissue provide important data for the evaluation of skeletal maturity. Bone tissue accretes during growth, and different bone tissue types have different growth rates (Chinsamy-Turan 2005), therefore a cyclical change in bone tissue type will often represent a regular fluctuation in overall body growth rate and provide a means to estimate age. However, tissue patterns can vary for reasons that are not temporally cyclical (mechanical properties, egg production, food quality, injury or disease). Consequently, reliable age estimation of fossil bones is founded upon the identification and correlation of tissue patterns with temporal cycles in extant taxa.

Extant and fossil bone tissue is commonly described by its vascularity, arrangement of collagen fibres, and growth marks (de Ricqlès *et al.* 1991). Viewed under cross-polarized light, growth marks include a *zone,* which is generally broad,

opaque, and represents rapid bone growth, whereas an *annulus* is thinner, bright, and represents a period of slowed growth. A *line of arrested growth* (LAG) represents a temporary cessation of bone growth. A zone/annulus group (and LAG if present) can represent a biological signal that is often correlated with an annual cycle, and has been widely noted in the bones of fish, snakes, turtles, and amphibians as well as mammal teeth (Peabody 1961, Kumbar and Pancharatna 2002). The visual distinction between a zone and annulus is not due to a difference in mineral density, but rather represent differences in tissue type (de Ricqlès et al. 1991); for example the fast growing zone might be woven fibered bone and the annulus composed of the slower growing lamellar fibered bone.

LAGs are commonly used to estimate ontogenetic age, and experimental evidence from the grey mouse lemur (*Microcebus* murinus*)* suggests photoperiod plays an important role in LAG development (Castanet *et al.* 2004). However, additional experimental evidence to consider if LAGs and other manifestations of tissue growth may also reflect mechanical, environmental or other stress factors that affect bone growth may still be warranted (Horner et al. 1999a). Importantly, the distribution and number of LAGs can vary across and within skeletal elements (Horner et al. 1999a), which has prompted many researchers to adopt a standard sampling site such as the femur directly below the fourth trochanter (Chinsamy 1993, Sander 2000). Importantly, others have noted that in some sauropodomorphs the femur may not be the best element for age estimation (de Ricqlès 1983) and advocate sampling across many elements (Rogers 1999). The variability in tissue patterns between elements of the same skeleton reflects the variability in growth rates and mechanical properties of the elements (Horner et al. 1999a); which again suggests appendicular allometry is present among sauropod taxa.

LAGs were used for age estimation of a growth series of nineteen femora of the Lower Jurassic prosauropod *Massospondylus carinatus* (Chinsamy 1993). Femur length correlated well with age estimates, and a power curve was the best fit of femur length with age regressions. The peripheral cortex of the largest specimens of *Massospondylus* did not show closely spaced resting lines, and Chinsamy (1993) suggested that this was evidence of indeterminate growth. Another possible explanation is that larger and more

mature specimens of *Massospondylus* remain to be discovered (Chinsamy-Turan 2005), and that current samples of *Massospondylus* may represent immature specimens.

While LAGs are a common bone tissue feature of prosauropod dinosaurs such as *Massospondylus* and *Plateosaurus* (Chinsamy 1993, Klein 2001) they are not typical for sauropod dinosaurs, being present only in the largest (oldest) specimens, if at all (Rogers 1999). Consequently, alternative methods for estimating ontogenetic age from sauropod bones have been proposed.

Tissue periodicity was first noted in a pelvis from an unidentified sauropod from the Middle Jurassic (Reid 1981), the bone tissue showing fluctuations in collagen fibre composition (woven and parallel fibered versus lamellar bone). The alternation between a zone of fibro-lamellar bone and thin annulus of lamellar bone was *assumed* to reflect an annual fluctuation in bone growth rate.

At around the same time, de Ricqlès (1983) drew attention to lines of periodicity in the osteohistology of a sauropod humerus, observed using light reflected from polished transverse sections of whole bones or thick sections. Based on these lines observed on polished surfaces, de Ricqlès estimated the age of 18-26 years for a humerus that had attained fifty percent adult linear size. Adopting a similar technique, Sander (2000) used "polish lines", to estimate the age of four sauropods (*Brachiosaurus, Barosaurus, Dicraeosaurus*, and *Janenschia*) from the Tendaguru fauna from the Upper Jurassic of Tanzania. Sander also identified three types of fibrolamellar bone; "hatchling" bone with large irregularly shaped, reticular or plexiform vascular canals, "juvenile" bone with large, elongate and laminar vascular canals parallel to the bone surface and "adult" fibrolamellar bone with smaller yet laminar vascular canals. All four taxa were suggested to have continuous growth, reaching sexual maturity at 40-80% maximum linear size, corresponding to an estimated age of 11 years for *Janenschia*, the specimens of which died at an estimated 38 years of age (Sander 2000). While the polish lines offer tremendous promise for aging apparently fast growing sauropod bone tissue, experimental validation in extant taxa is still needed to confirm a temporal, let alone annual cycle for these features.

Rogers (1999) examined the histology of an assembled growth series of eleven *Apatosaurus* forelimb samples divided into four growth stages based primarily on size.

The bone of all age classes was highly vascular fibrolamellar bone, with LAGs only found in the peripheral cortex of the largest elements (Class III and IV), suggesting rapid growth through much of ontogeny. Rogers was only able to estimate the age of the scapulae from Class I and II (at five and ten years respectively), based on *fluctuations in vascularity* (interpreted as representing relatively slowed periods of otherwise rapid growth). However, there is no data from extant taxa that supports the correlation of vascular fluctuations with a temporal cycle, therefore the age estimates for *Apatosaurus* remain rather speculative.

Vascular "growth rings" similar to the *Apatosaurus* vascular fluctuations noted in the sea turtle *Dermochelys coriacea* could not be correlated with a temporal cycle, but rather may correlate with migration into boreal waters, changes in energy allocation associated with egg laying, or fluctuations in food quality (Rhodin 1985). In contrast, a study of osteohistological age validation in two sea turtle taxa (*Caretta caretta,* and *Lepidochelys kempii*) was able to accurately estimate specimen age based on LAGs but fluctuations in vascularity were not mentioned (Snover and Hohn 2004). While fluctuating vascularity was also reported the ichthyosaur *Omphalosaurus*, again no experimental evidence was forwarded to support a temporal correlation with this tissue structure (Buffrénil and Mazin 1990).

Aside from the inadequate demonstration of temporal correlation in extant taxa, the demarcation of the fluctuation boundaries in the *Apatosaurus* limbs is also subjective. The boundaries between zones of differing vascularity are difficult to identify, therefore if these zones are used to estimate age, considerable variability due to observer interpretation is expected.

Bone vascularity and growth rate of fibrolamellar bone has been experimentally examined during the first month of growth of the Japanese quail, *Coturnix coturnix japonica*. The study (Starck and Chinsamy 2002) was able to demonstrate that fibrolamellar bone is developmentally plastic, with a variable growth rate (from 10-50 μm) depending upon environmental conditions (e.g. nutrition). Therefore the presence of fibrolamellar bone in fossil taxa may not always correlate with fast growth, although in general fibrolamellar bone does grow faster than lamellar bone (Chinsamy-Turan 2005). Also, whereas no significant difference in bone vascularity was found with reduced

growth, vascularity differed between elements and with bone maturity; individual vascular channels get smaller with time as bone is deposited within primary osteons.

In summary, while prosauropod osteohistology provides signals (LAGs) that have been correlated with an annual signal in studies of extant taxa, the bone tissue of sauropod dinosaurs (typically fibrolamellar tissue that is usually associated with fast growth rates) and the tissue patterns (periodicity, polish lines, vascular fluctuations) used for estimating ages of sauropod dinosaurs have not been correlated with annual cyclicity in extant taxa. Therefore, although promising, the sauropod histology techniques remain speculative until verified with extant studies.

With members that include the largest animals to ever walk on the earth, the growth rate of sauropodomorph dinosaurs is a question of great biological interest. A recent study of dinosaur growth (Erickson et al. 2001) concluded that regardless of absolute size, dinosaur growth appears to follow a sigmoidal curve. However, due to the use of uncertain age assessments and the assumption of limb isometry, their conclusions of sigmoidal growth among sauropodomorph dinosaurs are not well supported.

Two sauropodomorph dinosaurs, *Apatosaurus excelsus* and *Massospondylus carinatus*, were included in a study of growth among non-avian dinosaurs (Erickson et al. 2001). The age data for *Apatosaurus* was derived from the age estimates offered by Rogers (1999). In addition, Erickson et al. also include a hypothetical "five year old radius" of 34% adult size, as well as three age estimates not based on histological evidence. Unfortunately, these estimates are highly speculative, and even small changes to these age estimates produce dramatically different regression results. Therefore it is unreliable to infer from the data used by this study that *Apatosaurus* growth fit a sigmoidal growth curve.

Of the six dinosaur taxa examined by Erickson et al. (2001) the *Massospondylus* sigmoidal growth curve had the lowest correlation coefficient (r^2=0.855). The age estimate data for *Massospondylus* was taken directly from the histological analysis based on LAGs (Chinsamy 1993), therefore the age estimates can be considered well supported. However, as suggested by Chinsamy (1993), an exponential curve is much a better fit for the *Massospondylus* growth data (r^2= 0.99), therefore the sigmoidal growth for *Massospondylus* also cannot be accepted based on the current data. While it is possible

that older specimens of *Massospondylus* might yet be discovered and provide data to support a sigmoidal growth curve, this would suggest the current specimens of *Massospondylus* are possibly skeletally immature.

Another analysis of body size evolution among sauropodomorph dinosaurs (Yates 2004), proposes Massospondylidae (*Coloradisaurus*, *Massospondylus*, *Lufengosaurus*) demonstrates a phylogenetic reduction in body size (based on greatest femur length). However, as there is some suggestion *Massospondylus* specimens are immature, the pattern of this group may be due to an ontogenetic artefact rather that an evolutionary reduction in body size.

Aside from age estimates, histological features can provide evidence of skeletal maturity, such as the epiphyseal structure of long bones (Padian et al. 2004) or the presence of an external fundamental system, a narrow band on the external cortex that demonstrates slowed growth at adult stages found in some dinosaur taxa (Horner *et al.* 1999b). The absence of these structures in large specimens does not provide the interpretation large specimens are immature. However, their presence, particularly among small specimens, would provide evidence that growth has slowed and specimens are mature.

In summary, studies of prosauropod bone histology have consistently found abundant and well demarcated growth marks (LAGs), while sauropod bone tissue is generally composed of fast growing fibrolamellar bone with LAGs found in only the outer cortex of the largest specimens. Techniques for estimating the age of sauropod bones based on polish lines or vascular fluctuations would be strengthened by correlation with tissue patterns formed in temporal cycles in extant taxa. These improved methods for estimating ages of sauropodomorph specimens would provide additional evidence with which to assess the relative maturity of skeletons, particularly small specimens. Also, identification of an external fundamental system would provide strong evidence for skeletal maturity in small specimens.

A "Juvenile Prosauropod" Reconsidered

In the various topics discussed the central difficultly remains in discriminating between juvenile specimens that are often small and do not exhibit derived morphologies present in mature specimens, and small specimens that are somewhat mature and represent phylogenetically distinct taxa. A 'juvenile specimen' from the McCoy Brook Formation offers an opportunity to further consider the difficulties of discrimitating between small size attributable to young ontogentic age/maturity.

In 1986, Niel Shubin, Hans-Dieter Sues and Bill Amaral collected a small 'juvenile prosauropod' (FGM000GF18) from the fluvial sediments near the 'fish bed' (see Chapter 3, Stratigraphic Column). The specimen includes several centra and significant portions of the left pelvis and hind limb. In comparison to other prosauropod specimens from the McCoy Brook Formation (Chapter 4-7), the specimen is less than 40% linear size of the next smallest specimen (94GF69) and would therefore be young, occupying the 'baby' size class as proposed by Carpenter and McIntosh (1994)

The specimen was briefly mentioned in a review of vertebrates from the McCoy Brook Formation as: "an articulated pelvic girdle and hind limb found at site K.... referable to a small, presumably juvenile prosauropod. This identification is based on the ischium; more precise designation must await further preparation of the specimen" (Shubin *et al.* 1994, pg. 247). The partial skeleton was found loose in the erosion debris in the strata directly overlying the green "fish bed" (Site K, Olsen and Gore 1989) and additional material could not be located in the cliff (Sues pers. com., 2001).

Confirmation that the specimen is a sauropodomorph dinosaur would be significant due to its small size as well as the location of the specimen low in section; this specimen would be the earliest sauropodomorph remains within the McCoy Brook Formation. Alternatively, the small size may not be due to young age if the specimen is referable to small dinosaur taxa such as *Scutellosaurus* or a non-dinosaurian taxa such as *Protosuchus micmac*; the remains of the latter are abundant in these beds and the nearby talus slope deposits (Sues *et al.* 1996).

Methods

At some time the specimen was apparently dropped, and was broken into many pieces. The sandstone pieces that contain the specimen were therefore reassembled based on textures within the matrix and by aligning bone surfaces. The specimen was then prepared with mechanical tools in order to expose additional skeletal elements. To supplement the morphological information, a mid-diaphysis femur fragment was prepared and sectioned for histological analysis according to standard procedures (Chinsamy and Raath 1992).

Description

A small fragment of a sphenodontian right mandibular ramus (Figure 2.1) was located in a sandstone fragment stored with the specimen; however, no direct connections could be found between the sphenodontian sandstone fragment and the rest of the specimen. The specimen is therefore assumed to not directly associate with the specimen and is not considered further.

The remaining components of the specimen (Figure 2.2) include two vertebrae, a partial left ilium, the proximal portion of the left ischium, a total of ten phalanges from at least three digits, the astragalus, calcaneum, and a distal tarsal, as well as a fifth metatarsal and impressions of the (left?) femur, tibia and fibula. Non-indelible black ink (likely applied during collection) has stained several of the phalanges and the surrounding matrix.

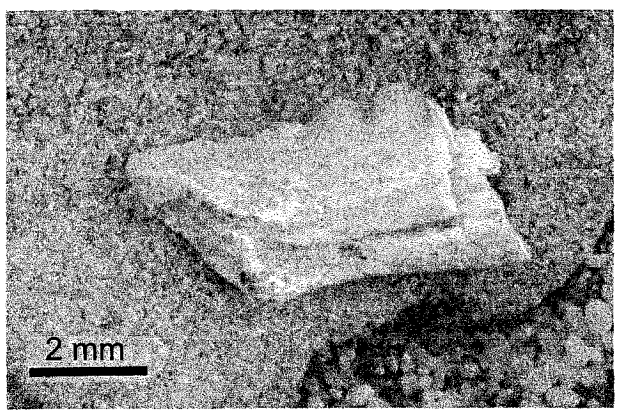

Figure 2.1: An isolated fragment of the symphyseal end of a sphenodontian right dentary included within the specimen.

The two disarticulated amphicoelous centra were dispersed among the hind limb elements. One of these vertebrae (Figure 2.3A) is a caudal, having a bi-faceted chevron articular surface on the posteroventral edge of the centrum. The facets are now asymmetrical due to slight oblique deformation of the vertebrae during preservation. A small foramen is visible on the lateral surface of this caudal vertebra, located centrally within a depression directly below the neurocentral suture. The neural arches of both vertebrae are incompletely preserved; only a small indiscriminate fragment of bone remains above the caudal centra. The articular surfaces of the centra are shield shaped, sub-circular with a flattened dorsal edge, and the anterior and posterior articular surfaces are of similar dimensions. The ventral surfaces of the centra are concave in lateral view and smooth, with no ventral furrows or keels.

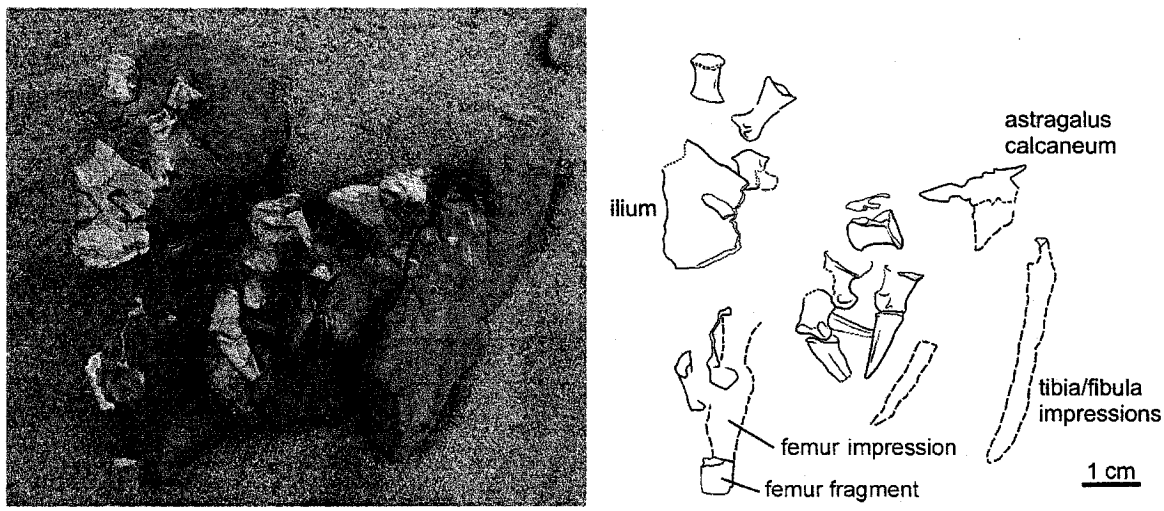

Figure 2.2: The assembled sandstone fragments containing the partial post-cranial skeleton of FGM001GF018.

Most of the posterior portion of the left ilium is preserved, up to a point immediately anterior to the ischial peduncle; the peduncle was broken and lost prior to collection. Radial striations (5-7 mm long) are visible along the posterodorsal and ventral margins of the ilium. Similar striations have been noted in *Orthosuchus* (Nash 1975) and also *Lesothosaurus* (Thulborn 1972), and represent origin surfaces for M. iliotibialis lateralis. A posterodorsally inclined ridge begins in the middle of the blade, directly above the ischial peduncle, likely representing the surface of attachment for the posterior sacral vertebra. The medial ridge terminates at the anteroventral edge of the blade. The

lateral surface of the ilium in this region also bares a small portion of ridge that is concave along the ventral edge. *Kayentsuchus* has a similar structure (Clark 1986), although only a small portion of the ridge is represented in FGM001GF18. A distal fragment of rib lies on the medial surface of the ilium. It cannot be determined if the acetabulum was open or closed medially due to the incomplete preservation of this area after the specimen was broken.

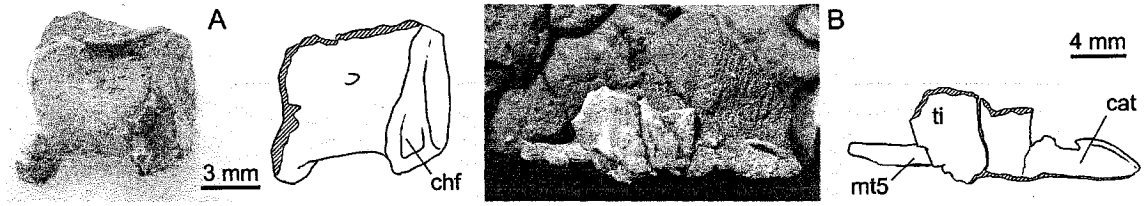

Figure 2.3: The disarticulated caudal vertebra (A) in lateral view, and the distal end of the tibia with articulated metatarsal and calcaneum fragments (B).
Abbreviations: cat, calcaneum tuber; chf, chevron facet; mt5, strap like fifth metatarsal; ti, distal end of tibia. The area below the preserved portions of the tibia and calcaneum was truncated by a fault, and broken bone surface is demarcated with crosshatching.

Only the proximal portion of the right ischium is preserved (Figure 2.4). The ilium articular surface is a long and broad concave surface, a portion of which may have composed the posteroventral part of the acetabulum. A thin and narrow pubic process has a gently rounded articular surface for the pubis and is inflected medially, resulting in the dorsal edge being offset medially.

The pubis is represented by two small fragments that likely come from the same element but cannot be joined. Both pieces show teardrop cross-section demonstrating the pubic shaft was thin along the lateral margin, similar to *Orthosuchus* (Nash 1975). The lateral edge of the pubic fragment is also oriented to suggest it had remained in near articulation with the ilium.

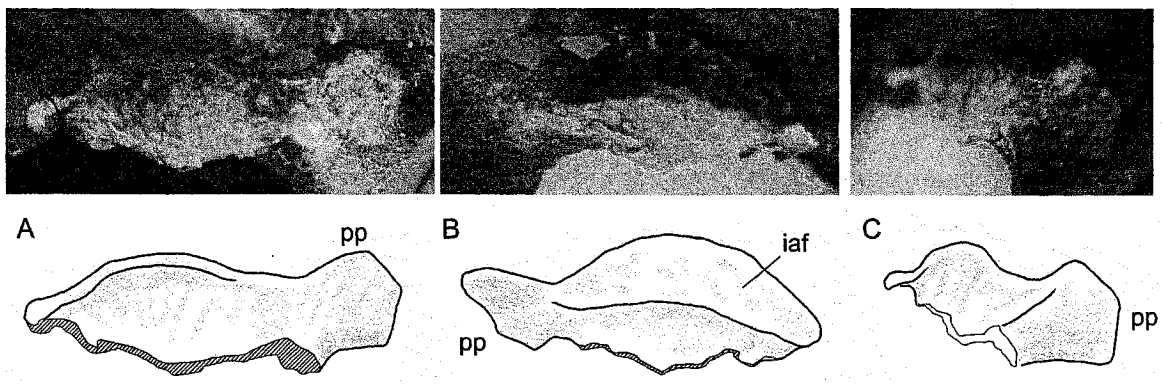

Figure 2.4: Proximal end of the right ischium in lateral (A), dorsomedial (B), and anterolateral (C) views.
Abbreviations: iaf, ilium articular facet; pp, pubic process of ischium.

Except for a small fragment of femur diaphysis (see Histology) and distal fragment of tibia, the femur, tibia and fibula are preserved only as impressions in the fine grained sandstone matrix. The impressions may not represent the complete lengths of the elements, but minimum lengths of 35 mm can measured for both the tibia and fibula.

Attached to the distal tibia? fragment is a portion of the (left?) calcaneum, specifically a portion of the enlarged convex tuber (Figure 2.3B) that is characteristic of Crocodyliformes such as *Protosuchus* (Colbert and Mook 1951). However, the posteriorly directed tuber of GF018 does not have a longitudinal cavity for the reception of gastrocnemus tendons as in *Orthosuchus* (Nash 1975). The calcaneal tuber of *Sichuanosuchus* is grooved only along the posteroventral surface (Wu *et al.* 1997), therefore it remains possible a portion of the GF018 calcaneum was grooved but is now missing. Below and still contacting these elements is the hook-like fifth metatarsal (Figure 2.3B). No other metatarsals are known from this specimen, although the distal portions of at least three digits are preserved.

The largest ungual phalanx (length = 13.0 mm) remains articulated with a proximal phalanx, which is slightly longer on one side (6.8 mm and 7.5 mm). The proximal articular surface of this sub-terminal phalanx is oval, wider than tall, and asymmetrically concave; deeper on the right 2/3 of the surface in proximal view. The long axes of the distal and proximal articular surfaces are parallel. Adjacent and sub-parallel to these elements is another series of articulated phalanges. This includes an ungual phalanx that lacks the distal-most tip (estimated length of 12 mm), articulated to a

phalanx 7.5 mm long, and the proximal-next phalanx that is missing a portion of a distal condyle but was asymmetrical in length (7.0 mm and 8.0 mm).

A third ungual phalanx (8.5 mm long) is located under and oriented perpendicular to the series of three phalanges. Two small phalanges, each 6 mm long, are located at the proximal end of this ungual and appear to be in natural articulation. An isolated phalanx (10.5 mm long) underneath the dorsal margin of the left ilium, appears to be associated with a phalanx 6.5 mm long located near its distal end. If these are associated with the third ungual, this third digit would then contain (at least) five phalanges, alternatively the isolated two phalanges may represent a portion of a fourth digit.

All three ungual phalanges are recurved with developed trenchant sides, lack a ventral tuberosities, and are 140% to 170% longer than the associated penultimate phalanges. The non-ungual phalanges have relatively wider distal ends compared to those illustrated for the pes and manus of *Protosuchus richardsoni* (Colbert and Mook 1951).

Histology

The small fragment of femur diaphysis was examined in order to determine if the bone histology would provide evidence the specimen is a nearly full grown individual of *Protosuchus*. The sample was loose, but most likely represented the central portion of the femur shaft from immediately below the fourth trochanter based on the tight match with the impression remaining in the sandstone.

The bone tissue structure does not provide convincing evidence that the specimen was mature. The sample is a homogeneous texture of highly vascular woven bone tissue, with no signs of slowed growth. Under cross polarized light, the bone tissue is homogeneous and not alternating in light and dark (lamellar) bone. The bone tissue is well preserved, and osteocyte lacunae are clearly visible surrounding the primary osteons (Figure 2.5B). Under high magnification, the caniculae that emanate from the osteocyte lacunae can be clearly recognized.

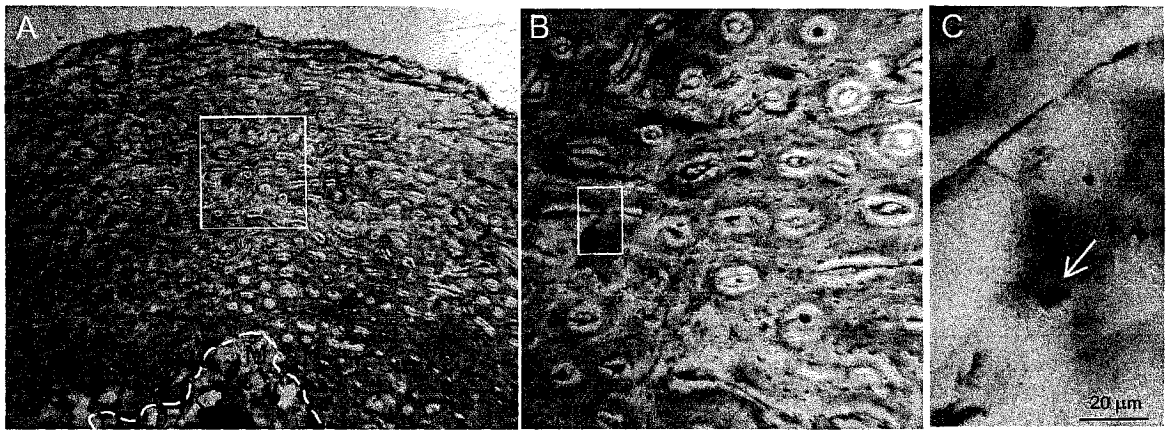

Figure 2.5: Histological sections of femur diaphysis from FGM001GF018, showing (A) the open vascular structure of tissue and infilled medullar cavity (m), (B) the visible osteocyte lacunae surrounding primary osteons, and (C) the individual caniculae that emanate from an osteocyte lacuna.

Although well preserved, the tissue structure of the femur does not provide evidence of maturity; no signs of slowed growth are notable in the periphery of the cortex. Unfortunately, little is known about the tissue histology of protosuchid crocodylomorphs. *Protosuchus* is generally considered to be an active, agile hunter (Colbert and Mook 1951, Carroll 1988), and the open vascular tissue structure may reflect a more active physiology. The tissue structure resembles that of *Terrestrisuchus* (Padian et al. 2004), which has recently been recognized as representing a juvenile *Saltoposuchus* (Allen 2003a, b).

Conclusions

Several issues require additional study in order to further clarify the relationships and life history of sauropodomorph dinosaurs. Allometry of the skeleton of sauropodomorph dinosaurs requires additional examination, using methods appropriate for identifying both allometry between and within elements. Also, experimental and comparative analysis of bone tissue from known age extant taxa is required to consider the appropriateness of using LAGs and other growth marks for estimating ontogenetic age of sauropod dinosaurs. Additional osteohistological sampling of key sauropodomorph taxa (*Anchisaurus*, *Gyposaurus*) would contribute substantial information to further evaluate the skeletal maturity of these specimens. Lastly,

comparative descriptions of the morphology and fusion patterns of sauropodomorph neurocentral sutures would clarify the utility of suture fusion for determining skeletal maturity of sauropodomorph dinosaurs.

Inappropriate inter-taxa comparisons can occur if maturity of representative specimens is assumed and not explicitly evaluated or stated, if maturity is misjudged due to limited or confounding maturity signals, or if specimens are recognized as immature yet still compared with mature specimens from different taxa. Each of these situations results in the inappropriate comparison of specimens representing different and unequal maturity states. The gigantic ontogeny of some sauropodomorph dinosaurs represents a potential for significant ontogenetic skeletal variation, which must be acknowledged in systematic studies based on skeletal morphology.

Based on the morphology of the post-cranial elements described, a specimen previously identified as a juvenile prosauropod (FGM001GF18), is now recognized as the representing a protosuchid crocodylomorph. Many disarticulated and fragmentary remains of *Protosuchus micmac* (Sues et al. 1996) have been recovered from the McCoy Brook Formation (Olsen et al. 1987, Shubin et al. 1994), and the specimen may be referable to this taxon. The bone histology of this specimen is vascular and does not provide evidence for specimen maturity, but is comparable to other crododylomorphs such as *Terrestrisuchus* (= *Saltoposuchus*).

CHAPTER 3 – New Information on the Braincase and Skull of *Anchisaurus polyzelus* (Lower Jurassic, Connecticut, USA; Saurischia, Sauropodomorpha): Implications for Sauropodomorph Systematics

Fedak, T. J. (first author) and Peter M. Galton; Accepted October 2006,
Sauropodomorph volume - Special Papers in Palaeontology.
Printed with Permission – The Palaeontology Society

Abstract

A skull of *Anchisaurus polyzelus* (YPM 1883) has been misinterpreted for over 120 years as a result of deformation during preservation and loss of a small piece of the skull block shortly after collection in 1884. The only other skull of this taxon (YPM 209), from a smaller individual, has been largely ignored in previous studies, on account of distortion and incomplete preparation. Additional preparation of the latter specimen has exposed several new elements, including the nearly complete parabasisphenoid, a region that is damaged and incomplete in YPM 1883. Based on this new information, a phylogenetic analysis supports the recent hypothesis that *Anchisaurus* was a basal sauropod. However, the strength of this hypothesis has been greatly reduced, and is also undermined further by the possibility that the specimens of *Anchisaurus* are skeletally immature. In general, the skull and braincase of *Anchisaurus* resembles those of 'prosauropods' more closely than those of derived sauropods.

Introduction

Historically the basal sauropodomorph specimens from the Portland Formation (Lower Jurassic, Pliensbachian) of the Connecticut Valley, eastern USA, have been attributed to one of two genera, *Anchisaurus* Marsh, 1885 or *Ammosaurus* Marsh, 1891 (see historical review in Galton 1976). However, Yates (2004) has argued convincingly that *Ammosaurus major* (Marsh, 1891) should be regarded as a junior synonym of *Anchisaurus polyzelus* (Hitchcock, 1865), demonstrating that the purported differences between these taxa could be accounted for by ontogenetic variation (as in the case of the width of pes) or specimen deformation during preservation (with respect to the length of

laterodistal groove on the tibia and the absence of a rim to the obturator foramen of pubis, for example).

Only two specimens with cranial material are referable to *Anchisaurus polyzelus* (YPM 1883 and YPM 209). The specimens were collected at the same time (in 1884) and were separated by less than 5 meters horizontally (with YPM 209 about 60 cm higher in the sequence) within Wolcott's sandstone quarry (Lull 1953, Galton 1976), in the Lower Jurassic Portland Formation (Olsen and Galton 1977), in Manchester, Connecticut. Although the skull of YPM 1883 has been described in several studies (see below), the braincase has been misinterpreted for nearly 120 years (Fedak 2003) due to a missing portion (Figure 3.1 A, B). Furthermore, very little has been published on YPM 209 as the specimen has remained largely unprepared until now, with only a few elements visible that were exposed some time prior to 1906.

The skull of YPM 1883 was first described by Marsh (1891), who provided only brief comments and offered no specific details about the condition of the braincase. Marsh (1892, p. 543) published reconstructions of the "somewhat crushed and distorted" skull, along with another short description that includes a brief comparison with the braincase of *Thecodontosaurus* (YPM 2192: Upper Triassic, England). Marsh (1892, p. 546) suggested that *Thecodontosaurus* differs from YPM 1883 (*Anchisaurus)* in its "extended parasphenoid, and the very long basipterygoid processes", and later (1896, p. 148) amended his observations on the braincase, stating that "the basipterygoid processes are unusually short".

The first photographs of the YPM 1883 skull, published by von Huene (1906), clearly demonstrate that a portion of the braincase (Figure 3.1A) has been missing since the time of these early descriptions. Von Huene (1914a) redescribed the skull, providing line drawings of the braincase (Figure 3.1C-E). Contrary to Marsh's opinion, von Huene (1914a, p. 70) contended that the basipterygoid processes were not short: "Near the long basipterygoid processes there is still to be seen on the right the attachment of the pterygoid" (translated from the original German). In these studies, von Huene misidentified a cross-section of the braincase (Figure 3.1D) as the basipterygoid processes.

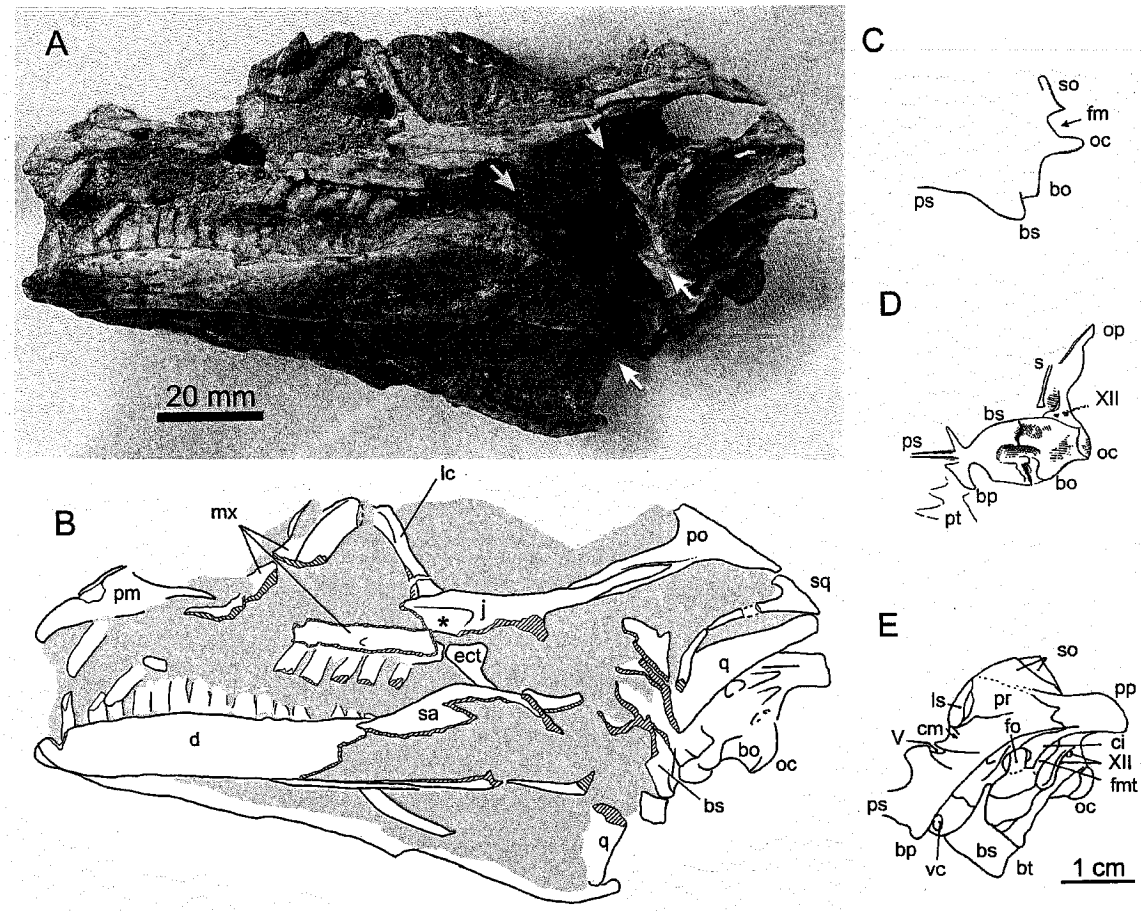

Figure 3.1: Photograph and illustrations of the *Anchisaurus* (YPM 1883) skull demonstrate previous interpretations of the braincase region.
A, a similar view to the first published photograph (von Huene 1906) of the skull in oblique left lateral view; white arrows have been added to demarcate a piece missing since the specimen was collected in 1884. B, the labelled schematic of the same view as the photograph, which shows the posterior end of the maxilla has become disarticulated from its contact (*) with the jugal. Interpretive line drawings of the braincase region from von Huene (1914a) in left lateral (C) and ventral view (D) and, modified from Galton and Bakker (1985), in left lateral view (E). Portions of the broken bone surface of the basisphenoid (between the posterior-most arrows in (A) were previously misinterpreted as the basipterygoid processes (bp) in D-E. Abbreviations as listed on p. 33.

Lull (1915, 1953) made the important observation that, as a consequence of crushing, the basisphenoid appears to have been bent upward and separated from its natural articulation with the basioccipital tubera. Galton (1976) provided a detailed description of the skull of YPM 1883 and, in this and subsequent publications (Galton 1985b, Galton and Bakker 1985, Galton 1990, Galton and Upchurch 2004), followed

Marsh's interpretation, suggesting that, in comparison to *Thecodontosaurus* and *Plateosaurus,* YPM 1883 has relatively small basipterygoid processes (Figure 3.1E). The presence of small/short basipterygoid processes continues to be cited as an apomorphic character for *Anchisaurus* (Yates 2002, 2004).

After re-examination of the braincase and a consideration of the historical documentation of the specimen, it is now apparent that a portion of the skull block (Figure 3.1A), containing parts of the braincase and basipterygoid processes, was lost when the block was broken shortly after the specimen was collected (Fedak 2003). Previous comments on the size and orientation of the basipterygoid processes are based on misidentification of the ventral and bisected surfaces of the basisphenoid. The matrix between the braincase and the stapes, noted in the descriptions and illustrations of von Huene (1914a) and Galton (1976), was removed by W. W. Amaral during preparation of the skull in the early 1980s, revealing many additional details of the braincase anatomy.

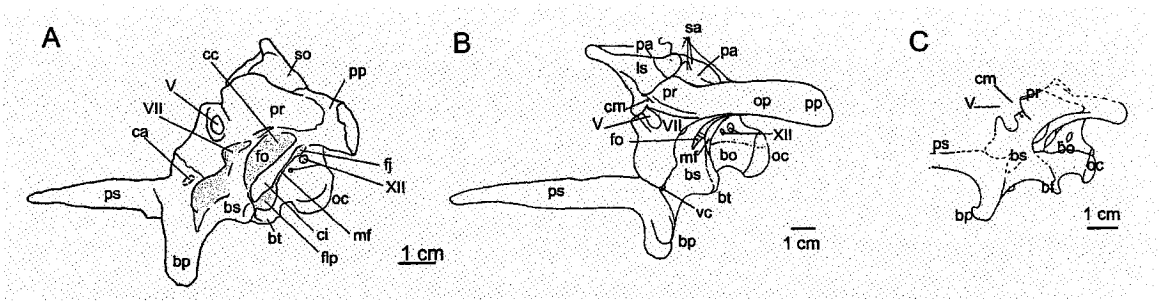

Figure 3.2: Schematic illustrations of basal sauropodomorph braincases in left lateral view. A, '*Thecodontosaurus*' (YPM 2192), the metotic fissure is a continuous structure, composed of the foramen lacerum posterior located anteroventrally and the foramen jugularis posterodorsally. The Vidian canal (internal carotid artery) enters the posterior portion of the sella turcica. B, *Plateosaurus* (AMNH 6810) and C, *Efraasia* (SMNS 12667). All from Galton and Bakker (1985), with (A) modified slightly based on direct observations of the specimen. Abbreviations are listed in the text.

Further preparation of the second, smaller skull (YPM 209) has exposed new elements, including the nearly complete parabasisphenoid (Fedak 2005), details of which are provided herein. The new data provides the first opportunity to consider the proposed synonymy of *Ammosaurus* (YMP 209, holotype of *Anchisaurus solus* Marsh, 1892; referred to *Ammosaurus* by von Huene [1932]; and referred to *A. major* by Galton [1976]), with *Anchisaurus* (YPM 1883) based on cranial characters. A well-preserved braincase of *Thecodontosaurus* (YPM 2192) has been described and figured recently by

Benton *et al.* (2000, p. 85, fig. 3) and we provide brief descriptive comments and an illustration of this specimen here (Figure 3.2A) for comparative purposes and in order to note minor differences in interpretation from previous studies. This new data was added to a phylogenetic analysis to re-evaluate the relationships of *Anchisaurus polyzelus,* which has recently been identified by Yates (2002, 2004) as a basal (and also the smallest) sauropod dinosaur (a result confirmed by Upchurch *et al.* 2005).

Institutional abbreviations. **ACM**, Amherst College Museum, Amherst, Massachusetts; **AMNH**, American Museum of Natural History, New York; **SMNS**, Staatliches Museum für Natrukunde in Stuttgart; **YPM**, Yale Peabody Museum, New Haven, Connecticut.

Figure abbreviations. **ar**, articular; **bo**, basioccipital; **bp**, basipterygoid process; **bs**, basisphenoid; **bt**, basal tubera; **ca**, carotid artery foramen; **cb**, ceratobranchial; **cc** – cavum cochlear; **ci**, crista interfenestra; **cm**, vena cerebalis media; **cp**, crista prootica; **cs**, crista sellaris; **d**, dentary; **ect**, ectopterygoid; **f**, frontal; **fj**, foramen jugularis; **flp**, foramen lacerum posterior; **fm**, foramen magnum; **fmt**, fissure metotica; **fo**, fenestra ovalis; **j**, jugal; **lc**, lachrymal; **ls**, laterosphenoid; **lw**, lateral walls of sella turcica; **mf**, metotic fissure; **mx**, maxilla; **oc**, occipital condyle; **op**, opisthotic; **pa**, parietal; **pra**, prearticular; **pm**, premaxilla; **po**, postorbital; **pp**, paroccipital process; **pr**, prootic; **ps**, parasphenoid rostrum; **pt**, pterygoid; **q**, quadrate; **qj**, quadratojugal; **s**, stapes; **sa**, surangular; **so**, supraoccipital; **sp**, splenial; **sq** –squamosal; **t**, teeth; **vc**, vidian canal for internal carotid artery; **V, VII** and **XII**, foramina for cranial nerves.

METHODS AND MATERIALS

Anatomical terminology follows that used by Bellairs and Kamal (1981) and Baumel and Witmer (1993). The braincases of '*Thecodontosaurus antiquus*' (YPM 2192: taxon restricted to the holotype dentary by Galton 2005) and *Anchisaurus polyzelus* (YPM 1883 and YPM 209) were examined directly. During mechanical preparation of the smaller skull (YPM 209) carried out (by T. F.), a long wave (365 nm) ultraviolet (UV) lamp (UVP Inc. "Mineralight" lamp, Model UVGL-25) was used in an otherwise dark room, which allowed improved discrimination between the thin fossil bone and the

hard calcite matrix. Under long wave UV light, the skeletal elements luminesce bright white, against the dark background of the surrounding matrix, allowing even the smallest of elements to be recognized immediately on exposure. Without UV light it was nearly impossible to discriminate between the small bone elements and large calcite crystals in the matrix. Digital photographs of YPM 209 were taken under similar lighting conditions and using a Tiffen (Haze-1) UV filter mounted on the camera lens.

In order to examine the surface texture of the tooth enamel in YPM 209, epoxy resin casts of a newly exposed left dentary tooth were produced from a high-resolution rubber peel. Several attempts were required in order to capture an accurate surface impression of the tooth, as the initial peels captured emulsion artefacts from the consolidant present on the tooth surface; a similar artefact appears to have occurred during the analysis of the tooth enamel in YPM 1883 (Yates 2004: see below). A suitable mould was produced only after thoroughly rinsing the tooth with acetone to remove all consolidant. The epoxy cast was examined in a scanning electron microscope (SEM).

SYSTEMATIC PALAEONTOLOGY

DINOSAURIA Owen, 1842

SAURISCHIA Seeley, 1887

SAUROPODOMORPHA von Huene, 1932

Genus ANCHISAURUS Marsh, 1885

Type species. Megadactylus polyzelus Hitchcock, 1865.

Diagnosis. As for type species.

Anchisaurus polyzelus (Hitchcock, 1865)

Figures 1, 3-8

	1858	No Name Hitchcock, p. 186.
v *	1865	*Megadactylus polyzelus* Hitchcock, p. 39, pl. 9, fig. 6.
v	1870	*M. polyzelus* (Hitchcock); Cope, 122A-G, pl. 13.
v	1882	*Amphisaurus* Marsh, p. 84 (*Megadactylus* preoccupied).
v	1885	*Anchisaurus* Marsh, p. 169 (*Amphisaurus* preoccupied).

v 1889 *Anchisaurus major* Marsh, p. 331, fig. 1.
v 1891 *Ammosaurus major* (Marsh); Marsh, p. 267.
v 1891 *Anchisaurus colurus* Marsh, p.267.
v * 1891 *Anchisaurus polyzelus* (Hitchcock); Marsh, p. 169.
v 1892 *Anchisaurus colurus* (Marsh); Marsh, p. 543, pl. 15, 16 (figs. 1-2).
v 1892 *Anchisaurus solus* (Marsh); Marsh, p. 545.
v 1896 *M. polyzelus* (Hitchcock); Marsh, p. 147.
v 1906 *Thecodontosaurus polyzelus* (Hitchcock); von Huene, p. 19, fig. 10.
vp 1912 *Anchisaurus colurus* (Marsh); Lull, p. 414, figs 2-3.
v 1914*a* *T. polyzelus* (Hitchcock); von Huene, p. 75, figs. 23-24.
vp 1914*b* *Anchisaurus colurus* (Marsh); von Huene, p. 3.
vp 1915 *Anchisaurus colurus* (Marsh); Lull, p. 130, figs [copied from Marsh 1892] 18-21, pls. 4, 10.
v 1932 *Ammosaurus solus* (Marsh); von Huene, p. 27, pl. 49 fig 1.
v 1932 *Thecodontosaurus polyzelus* (Hitchcock); von Huene, p. 116.
v 1932 *Yaleosaurus colurus* (Marsh); von Huene, p. 119, pl. 14 fig. 1, pl. 54 fig. 3.
vp 1953 *Yaleosaurus colurus* (Marsh); Lull, p. 107, pl. 4, figs. 15-18 [copied from Marsh 1892].
v 1976 *Ammosaurus major* (Marsh) Galton and Cluver 1976, p. 143, figs 8A, J [see also for earlier synonymy].
vp 1976 *Ammosaurus major* (Marsh); Galton, p.3, figs 2A, 23-31.
v 1976 *Anchisaurus colurus* (Marsh); Galton and Cluver, p.132 (= *Anchisaurus polyzelus,* Hitchcock) [see also for earlier synonymy].
v 1976 *Anchisaurus polyzelus* (Hitchcock); Galton and Cluver, p. 132, figs 7A, C, 8E, 9E, H, K, 10A, G, K, 11L, 12B [see also for earlier synonymy].
v 1976 *Anchisaurus polyzelus* (Hitchcock); Galton, p. 2, figs 1B, 3, 5-24.
v 1976 *Anchisaurus solus* (Marsh); Galton and Cluver, p. 143 (=*Ammosaurus major*, Marsh) [see also for earlier synonymy].
vp 1990 *Ammosaurus major* (Marsh); Galton, p. 335.
v 1990 *Anchisaurus polyzelus* (Hitchcock); Galton, p. 335, figs [cop. Galton 1976; Galton and Bakker 1985] 15.3A, 15.4A, 15.6N, 15.8G.
v 2004 *Ammosaurus major* (Marsh); Galton and Upchurch, p. 234.
v 2004 *Anchisaurus polyzelus* (Hitchcock); Galton and Upchurch, p. 234, figs [copied from Galton 1976; Galton and Bakker 1985] 12.3A 12.5A, 12.8N, 12.10G
v 2004 *Anchisaurus polyzelus* (Hitchcock); Yates, p.3, figs 1-8, 9D, 10-11, 12F.

Holotype. ACM 41109, including several vertebrae, part of the left scapula, distal ends of the left radius and ulna, left manus, articulated distal ischial blades, the left femur (estimated length of 180 mm), fibula, proximal tibia and metatarsal IV, and the proximal part of right metatarsal II.

Type locality. Lower Jurassic (Pliensbachian) Portland Formation, Springfield Massachusetts.

Referred Material. YPM 209, a very small (femur approximately 110 mm in length) and nearly complete specimen, which lacks only the distal portion of the tail and right lower fore limb; YPM 1883, a well preserved specimen, femur length 210 mm, which lacks only cervicals 4-10, the tail and left lower fore limb, left ilium and hind limb, and the majority of both ischia; and YPM 208, the largest referred specimen (1.35 times larger than YPM 1883 based on length of metatarsal 3), which includes only the last six dorsal vertebrae, three dorsal ribs and sacrum, proximal part of right scapula and nearly complete pelvis, left hind limb, partial right femur and right pes. These specimens are all from the Wolcott sandstone quarry that was located 1 mile north of Buckland train station, Manchester, Connecticut; Lower Jurassic (Pliensbachian) Portland Formation. See Galton (1976) and Yates (2004) for further details.

Emended diagnosis. Of the autapomorphies of *Anchisaurus polyzelus* listed by Yates (2004), the following remain valid: lateral pit on the distal end of the quadrate above the articular condyle; ventrally opening foramen at the base of the second sacral rib; a large fenestra that pierces the third sacral rib; a long and narrow preacetabular blade of the ilium (twice as long as high at its base); ischium with ventrally emarginated obturator plate and flat coplanar blades; and large obturator foramen that occupies most of the obturator plate of the pubis. In addition, *Anchisaurus polyzelus* possesses a uniquely wide prootic trough.

Additional Information on YPM 1883

Deformation and Damage

During or shortly after the collection of YPM 1883, the skull block was broken. Lull (1915, 1953, p. 61), who summarized Marsh's notes, stated that "Part of the large block was split off at New Haven, and this smaller piece contained the head and part of the neck." Based on the specimen's current condition, the skull block was apparently broken into at least three pieces. A repaired fracture is still visible, traversing the frontals at mid-length, the sutural contact between the jugal and the postorbital on the right side,

and truncating the basisphenoid, left quadrate and left mandibular ramus (Figures 2.1A, 2.3B-D). Although the skull is presently composed of two reattached fragments, at least one other piece of the skull block was not reattached and has apparently been lost. The (missing) third piece was at least 1 cm wide in lateral view; the posterior edge demarcated by the fractured surface of the basisphenoid and the left quadrate, while the anterior surface contacted the broken surface of the left mandibular ramus (Figure 3.1A). The missing portion would thus have included the basipterygoid processes and the ventral end of the left quadrate, including the articular surface for the quadratojugal.

The distal portion of the posteroventral process of the left jugal has also been truncated by the missing area (Figure 3.1A-B). Because of the loss of this area and displacement of the left postorbital (and attached jugal) as a consequence of the transverse crushing of the skull, it is very difficult to estimate the anterior extent of the lower temporal fenestra under the orbit.

The right posterior portion of the skull is deformed, with many of the elements broken, lost or displaced posteromedially (Figure 3.3). The right paroccipital process was bent posteriorly resulting in its fracture. A previously unidentified element, located medial to the right quadrate and anterior to the squamosal (Figure 3.3B), is interpreted as a fragment of the paroccipital process. The morphology of the fragment matches the broken surface of the remainder of the process: when joined these two pieces frame a semicircular canal foramen (Figure 3.3D).

The right lateral wall of the braincase has been rotated clockwise in dorsal view, resulting in the medial surface now being partially visible from the right side, whereas most of the right prootic and the entire exoccipital were apparently destroyed (Figure 3.3A-B, D) during pre-burial deformation. The exposure of the medial surface of the right side of the braincase appears to have been incorporated into the previous reconstruction of the braincase (compare 'cm' in Figure 3.1E with '**' of Figure 3.3B).

The right and left postorbitals are separated from their articulations with the frontal (Figure 3.4), and are displaced posteromedially. The parietals and postorbital did not contact each oher and the frontals do contribute to the supratemporal fenestra (*contra* Yates 2004). The right quadrate is fractured and the supraoccipital is twisted clockwise in dorsal view. The region anterior to the right orbit was also badly distorted: all but the

most ventral part of the right lachrymal is missing; the posterior maxilla is displaced ventrally (Figure 3.1A-B); and the anterior edge of the frontals is displaced toward the left side. The remains of three right maxillary teeth (Figure 3.3B) are oriented perpendicular (83–92 degrees) to the long axis of the maxilla, while the posterior teeth preserved in the left maxilla (Figure 3.1B) are directed more anteriorly (59–77 degrees). However, the left maxilla has been rotated counter-clockwise in lateral view, with its posterior edge disarticulated from the jugal (Figure 3.1B), so the apparent procumbent orientation of the posterior maxillary teeth is likely to be a deformational artefact (contra Yates 2004).

Figure 3.3: Photographs and line drawings of the *Anchisaurus* (YPM 1883) skull (A, B) and braincase (C, D) in occipital (A), right lateral (B), left lateroventral (C), and right ventrolateral (D) views. A, the missing ventral portion of the left quadrate (arrowhead) is truncated by the missing piece of the skull block. The right paroccipital process and posterior portion of the right side of braincase (two black arrows) were fractured prior to preservation. B, the deformation to the right side of the skull exposes the medial surface of the braincase (**), and a fragment of the paroccipital process (not shown: location marked with *) was preserved at the ventral tip of the right squamosal. The white arrows demarcate the repaired oblique crack in the skull block (photographs B and C), and the missing area of the left quadrate and basisphenoid (D), which represents the posterior edge of the missing portion of the skull block. Broken bone surfaces are identified with diagonal lines, matrix and irrelevant elements are shaded grey, and abbreviations as listed on p. 33.

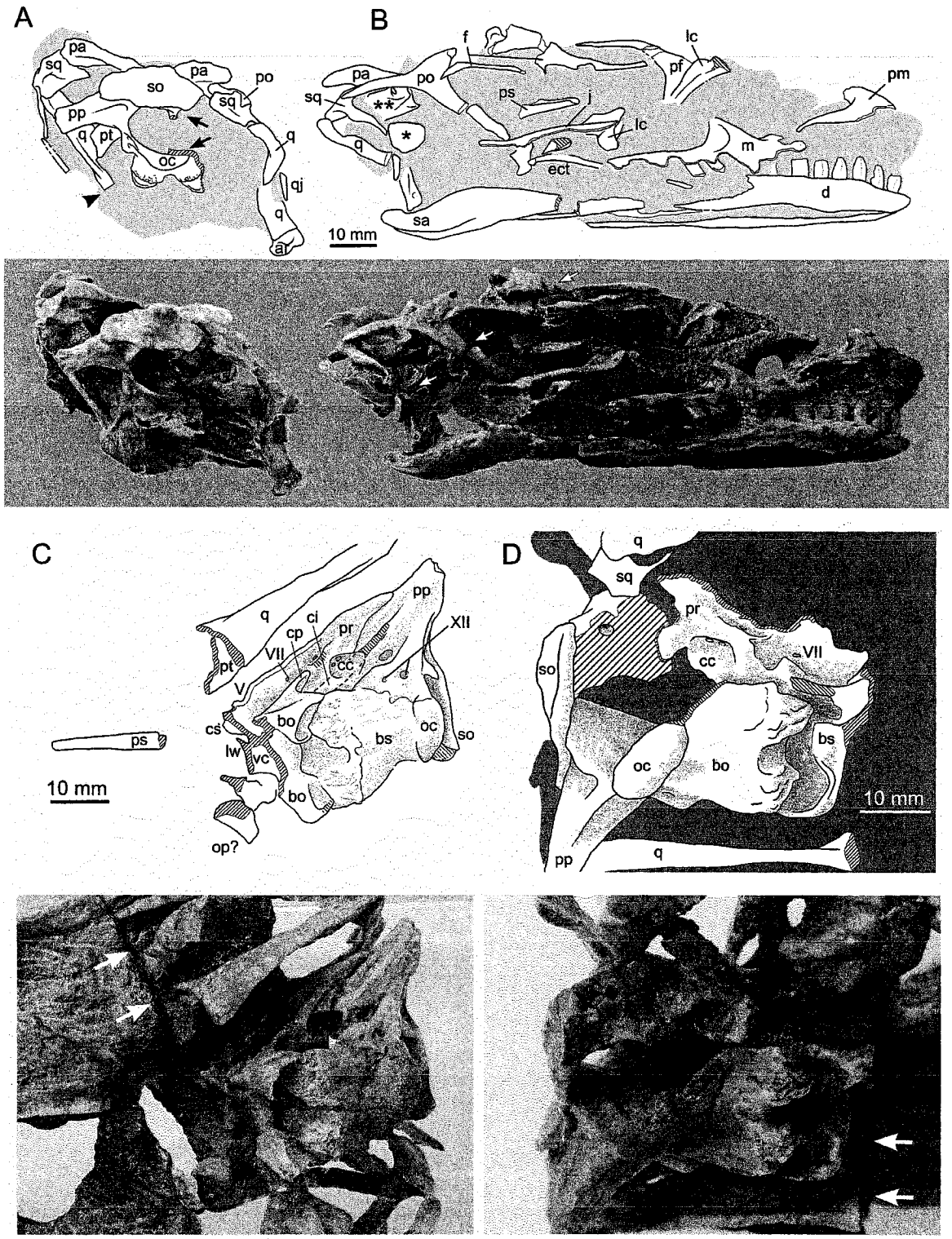
A
pa
sq
so
pa
po
sq
pp
q
pt
oc
q
qj
q
ar
B
f
lc
pa
po
pf
pm
sq
**
ps
j
*
lc
q
m
ect
d
sa
10 mm
C
q
ci
cp
pr
pp
XII
VII
pt
V
cc
bo
cs
bs
oc
so
lw
vc
ps
10 mm
bo
op?
D
q
sq
pr
so
cc
VII
bs
oc
bo
10 mm
pp
q

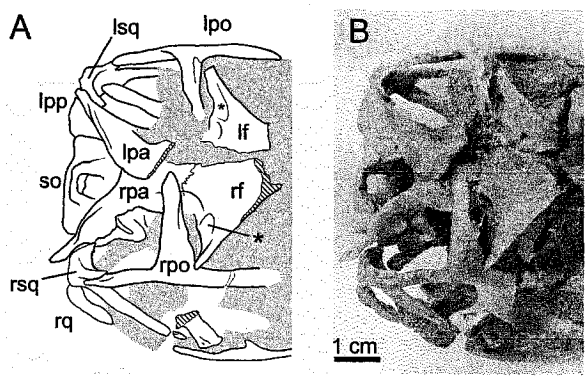

Figure 3.4: Line drawing A, and photograph B, of the posterior dorsal region of the *Anchisaurus* skull (YPM 1883).
The parietal-frontal contact has been lost on the left side, but the open sutural contact remains visible on the right. The postorbitals are displaced posteromedially from their sutural contacts with the frontals (*); the postorbitals did not contact the parietals and the supratemporal fossa on the frontal remains visible, particularly on the right side. The gap between the parietals and supraoccipital is a consequence of deformation and displacement of the braincase. Abbreviations as listed on p. 33, with the addition of prefixes for left (l) and right (r) sides.

The posterior region of the skull is largely intact on the left side although, as Lull (1915, 1953) pointed out, the anterior braincase has been displaced dorsally, separating the basisphenoid from the basioccipital. In left lateral view it appears that the anterior portion of the braincase has been rotated clockwise. This deformation accounts for the separation of the supraoccipital from its sutural contact with the parietal, the fracturing of the right quadrate, and separation of the basisphenoid from the basioccipital at the basal tubera.

The fracture of the right paroccipital process into several pieces, outward rotation of the right side of the braincase, and displacement of the other skull elements, suggests that a force was applied to left lateral area of the skull while it was oriented with its right side on the ground.

Braincase Anatomy

Only the anteriormost 25 mm of the parasphenoid rostrum is preserved, which is visible on the right side. The cultriform process of the parasphenoid is emarginated dorsally, with a 'U'-shaped trough and only a slight extension of the lateral walls, making the cultriform process as a whole as wide as it is tall, at least anteriorly. A small piece (~12 mm) of the parabasisphenoid is missing immediately posterior to the cultriform

process. The anterior end of the parasphenoid extends 33 mm from the base of the basioccipital tubera: the distance is 41 mm in YPM 2192 (*Thecodontosaurus*).

The posterior part of the basisphenoid is bisected by an oblique break that is inclined anterodorsally from a point on the ventral surface of the basisphenoid, slightly anterior to the fenestra ovalis. The break passes anterior to the sella turcica of the left side. The resulting gap is wedge-shaped, being widest on the left side, narrowing toward the middle of the skull and not affecting the dermatocranial elements of the right side.

The right and left Vidian canals are visible on the fractured ventral surface of the basisphenoid. A transverse buttress, that is visible on the dorsalmost part of the broken section, is interpreted as the crista sellaris (sensu Bellairs and Kamal 1981), the posterior wall of the sella turcica, but deformation has repositioned the crista sellaris slightly anteroventrally. Therefore, the internal carotid arteries entered the anteriormost end of the sella turcica, as in *Thecodontosaurus* (Figure 3.2B). The left, and part of the right, lateral wall of the sella turcica can also be seen in section, between the crista sellaris and the Vidian canals (Figure 3.3C).

Only the posteriormost parts of the ventral basisphenoid remain undamaged. The posterior tubera of the basisphenoid are cup like, with a short lateral component (Figure 3.3C), although they have been displaced anteroventrally, so there is now a significant gap between the basisphenoid and the basioccipital. Evidence to suggest that this gap is the result of displacement rather than a true morphological feature (as suggested by Yates 2004) is that the crista prootica (Figure 3.3C), located immediately anterior to the fenestra ovalis, is fractured and displaced anteroventrally from the prootic on the left side. There is an even more pronounced fracture of the right crista prootica. These fractures and displacements demonstrate that the basisphenoid was rotated clockwise in left lateral view, separating the basisphenoid from the basioccipital posteroventrally and the prootic dorsally.

Anterior to the crista prootica, the lateral surface of the basisphenoid forms the widest part and the anterior limit of a deep trough, referred to here as the prootic trough. The trough narrows posterodorsally, terminating at the prootic-opisthotic suture; a similarly located but narrower trough is also found in '*Thecodontosaurus*' (Figure 3.2A). There are two foramina located within this trough in YPM 1883, the facial foramen (for

cranial nerve VII) and a foramen for $VIII_2$, the posterior or acoustic ramus of the auditory nerve, that opens posteriorly into the cochlear cavum (as in *Plateosaurus*: Galton 1985a). Based on the strong deformation of the skull, the open nature of the prootic trough may possibly represent a distortional artefact. However, on the right side the trough is partially visible anteriorly and also appears to be wide, so this may represent a genuine, and autapomorphic, feature.

Dorsal to the prootic trough, the edge of the left prootic is broken and missing, but the trigeminal foramen (for cranial nerve V) appears to be located along this break (Figure 3.3C). The prootic extends posterodorsally and slightly laterally, forming the dorsal margin of the fenestra ovalis, and overlaps the opisthotic posteriorly.

The anteroventral region of the left opisthotic currently exhibits a broken surface where the crista interfenestralis originated (Figure 3.3C). This crest was apparently lost during preservation or preparation because its distal (anteroventral) tip is still preserved dorsal to the suture between the basisphenoid and the basioccipital. The foramen jugularis (exit of cranial nerves X and XI and the vena jugularis), located within the posterior region of the metotic fissure, is immediately ventral to the broken surface of the opisthotic that would have borne the crista interfenestralis. As most of the crista interfenestralis is missing, the cochlear cavum is clearly visible within the left side of the fenestra ovalis. The cochlear cavum exhibits a foramen (for cranial nerve VIII) on its dorsal surface and an anteriorly positioned foramen for $VIII_2$ that communicates with the prootic trough mentioned above.

The basioccipital has a concave ventral surface, is narrow at mid-length, and is widest posteriorly. The exoccipital-basioccipital suture is still visible (Figure 3.3C) and demonstrates that the exoccipital contributes to the lateral corner of the occipital condyle as in all other 'prosauropods' with the exception of *Coloradisaurus* (Galton 1990). The two hypoglossal foramina (for cranial nerve XII) are located dorsal to this suture.

The left paroccipital process is nearly complete, missing only a small fragment distally. The opisthotic merges indistinguishably into the exoccipital posteroventrally to form the paroccipital process, which is overlapped by the prootic anterolaterally and the supraoccipital dorsomedially (Figure 3.3, 2.4).

There are two bones located anterior and ventral to the basisphenoid (Figure 3.3C), which represent broken pieces of the right opisthotic or possibly a posterior fragment of the right pterygoid. Regardless, the fragments further demonstrate that considerable damage to the right side of the braincase occurred prior to, or during, burial.

The Skull of YPM 209 ('Ammosaurus major')

Deformation and Damage

The anterior portion of the skull and mandibular rami remain in articulation, but the posterior portion of the skull is extensively crushed dorsoventrally. Based on the splayed limbs of the fully articulated skeleton (Galton 1976, fig. 30), the skull was buried with the lateral surface of the right mandible resting on the ground and the dorsal edge of the left lateral surface facing upwards; an orientation that also accounts for the oblique nature of the dorsoventral crushing of the posterior skull elements.

Marsh (1892, p. 545) provided the first description of the skull of YPM 209 in which he briefly noted that the specimen exhibited large orbits, a quadrate and numerous teeth that were inclined forward, and that "the skeleton is embedded in a very course matrix, so difficult to remove that preparation is only in part complete". Von Huene (1906) was the first to publish photographs and illustrations (von Huene 1914a) of the skull block, which demonstrate that no significant preparation of the specimen was carried out between 1906 and 2003 (when this project started). Based on the appearance of the rounded and smooth surfaces of the matrix, preparation prior to 1906 was carried out with a hand held grinder, and these early preparation techniques, matched with the hard calcitic matrix and very thin cranial elements, unfortunately resulted in tremendous damage to the specimen. Additional preparation has revealed numerous new anatomical details.

Skull Anatomy

Braincase Elements

The parabasisphenoid is now exposed from the tip of the parasphenoid rostrum to the basisphenoid portion of the basal tubera. The posterior edge of the basisphenoid was

discovered directly under the surface where preparation had stopped in 1906, so it is likely that the posterior-most part of the braincase was destroyed during this earlier preparation.

The long axis of the parabasisphenoid rostrum is aligned with the ventral surface of the basisphenoid. The straight line that joins the ventral surface between the basal tubera and the ridge between the basipterygoid processes is parallel to and 1 mm ventral to the ventral edge of the parasphenoid rostrum. The lateral sides of the cultriform process are well developed, but the process is as wide as it is dorsoventrally tall; a condition that is shared with YPM 1883 (see above), *Massospondylus* (Gow 1990), and *Coloradisaurus* (Bonaparte 1978). The anterior tip of the parabasisphenoid is located 22 mm from the posterior edge of the basisphenoid portion of the basal tubera.

The left, and most of the right basipterygoid processes are preserved. A transverse ridge connects the proximal ends of the processes, extending along the ventral surface of the basisphenoid (Figure 3.6A, C), similar to the situation in *Plateosaurus* (Galton 1984). The left basipterygoid process measures 10 mm from its distal tip to the dorsal margin of the parabasisphenoid rostrum. The process is directed anterolaterally, and in lateral view the distal end is located 8 mm below the dorsal margin. The tip of the left basipterygoid process is located 7 mm from the sagittal midline; therefore the span between the basipterygoid processes is 14 mm, a span that is greater than the width of the basisphenoid portion of the basal tuberae (~10 mm). The right basipterygoid process appears to have been fractured at its proximal base (Figure 3.6B), and the distal edge was lost during previous preparation of the skull.

Premaxilla

The right premaxilla is now partially exposed in medial and lateral view. Most of the dorsal process was lost during earlier preparation, but a small portion of its base remains on the anterior margin of the bone. The roots of the right teeth are exposed due to the loss of the lateral surface of the premaxilla. The long posterior process contacted the medial surface of the maxilla, extending 16 mm posteriorly from the anterior tip of the premaxilla to a point at the base of the ascending process of the maxilla. Four premaxillary teeth are preserved, representing the total tooth count (Figure 3.6E). The

teeth are oriented slightly posteroventrally in relation to the posterior process of the premaxilla, and are mildly recurved. The left premaxilla contains only three partial teeth (Figure 3.6F), which were badly damaged during preparation that took place prior to 1906.

Maxilla

As in other basal sauropodomorphs (Galton 1984, Sues et al. 2004), the maxilla is triradiate, with a subnarial ramus, an ascending process that separates the external naris and antorbital fenestra, and a posterior ramus that contacts the jugal posteriorly. The ascending process and subnarial ramus of the right maxilla are now exposed in lateral view (Figure 3.5B, 2.6E). Although the ascending process of the left maxilla was damaged prior to 1906, preparation has exposed the delicate features at the base of this process, as well as the anterior edge of the antorbital fenestra and the medial surface of the anterior ramus (Figure 3.5A).

The preserved portion of the ascending process is oriented perpendicular to the ventral surface of the maxilla, and extends 5 mm from the dorsal surface of the subnarial ramus (Figure 3.6E), but the anterior edge of this process was damaged prior to 1906, so the full length is uncertain. Three empty alveoli and one partial tooth are visible in the preserved portion of the right maxilla; two of these tooth positions are located anterior to the base of the dorsal process. The dorsolateral margin of the subnarial ramus is partially depressed, which is consistent with the narial fossa being present on the anterior ramus of the maxilla.

Additional preparation of the left maxilla demonstrates that the medial sheet of the ascending process did not extend posteriorly, but rather follows the lateral edge of the process (antorbital fossa), so that the antorbital fenestra is strongly embayed anteriorly. The medial edge of the subnarial ramus is also exposed on the left side, although the lateral surface was apparently destroyed during earlier preparation. A pronounced longitudinal groove is visible on the medial edge that would have accommodated the long posterior process of the premaxilla described above, as in *Plateosaurus* (Galton 1984). Based on the length of the exposed subnarial ramus of the left maxilla, the anteriormost portion probably represents the 'anterior process' (Galton 1984), a small knob-like

process on the maxilla that wrapped medially around the posterior process of the premaxilla. The more lateral, tooth-bearing portion of the anterior ramus would, therefore, not have extended as far anteriorly as the currently exposed medial edge.

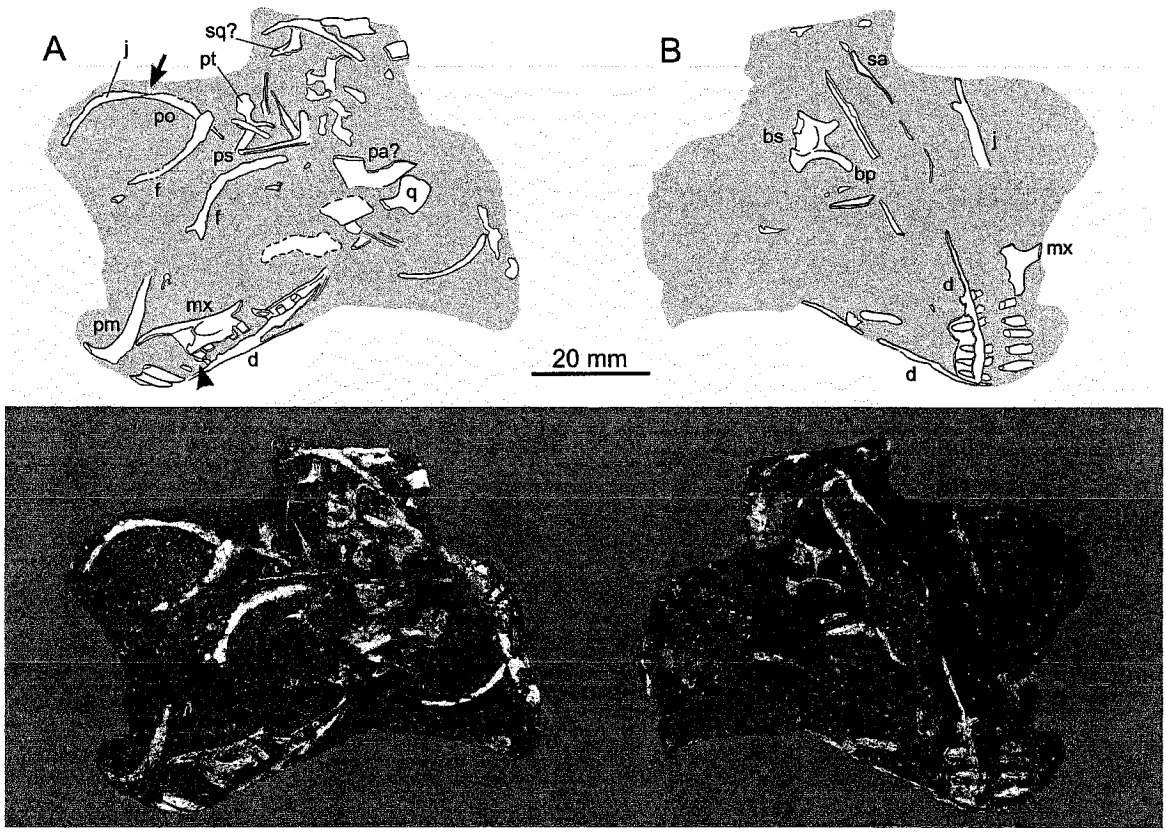

Figure 3.5: Line drawings and long-wave UV light photographs of the small *Anchisaurus polyzelus* skull (YPM 209), in left dorsolateral (A), and right ventrolateral (B) views.
Anterior is toward the bottom left (A) or bottom right (B). The black arrow (A) identifies the boundary between the right postorbital ventral process and right jugal, whereas the arrowhead identifies the location of the dentary tooth examined by SEM. Abbreviations as listed on p. 33.

Four incomplete teeth are preserved within the left maxilla but additional teeth were present prior to 1906; at least one anteriorly and several posteriorly. The preserved maxillary teeth are all oriented perpendicular to the ventral surface of the maxilla and are not inclined anteriorly (contra Marsh 1892). As the anterior maxillary teeth of both YPM 209 and YPM 1883 are not procumbent, the orientation of the posterior maxillary teeth of YPM 1883 is likely to represent a deformational artefact (contra Yates 2004).

Frontal

The orbital margins of the right and left frontals were first identified by von Huene (1914a). While Galton (1976) admitted that these fragments may represent portions of the frontals, he also suggested that the elements may represent parietal fragments. However, von Huene's identification was correct, an interpretation that is consistent with the orientation and dimensions of the other skull elements. The central portions of the frontals were almost certainly ground away by preparation prior to 1906. Alternatively, however, the more medial portion of the frontals may have been minimally ossified due to the immature status of YPM 209. The ossification of the frontals commences along the orbital margins in many extant taxa (e.g. *Alligator mississippiensis*: Rieppel 1993) and the same pattern is apparently present in embryos of *Massospondylus* (Reisz et al. 2005, fig. 2B): only later in ontogeny does the more medial region become fully ossified.

Postorbital

The right postorbital is missing the posterior process and the posterior margin of the ventral process. The ventral process remains in articulation with the jugal (see below); Galton (1976) erroneously identified the latter as a single element (right jugal). As a consequence of the broken surface along the posterior margin of the ventral process, the lateromedial width cannot be determined. The postorbital medial process is disarticulated from, and overlapped, by the frontal.

Jugal

A fragment of the right jugal remains in articulation with the postorbital, and the division between these two elements can still be observed (Figure 3.5A). The posterodorsal process of the jugal contacts the posterior surface of the ventral process of the postorbital, and the orbital margin of the jugal is represented by the external bone surface. However, the remainder of the jugal fragment is truncated by broken bone surfaces. A newly exposed fragment on the right side of the skull appears to represent the ventral portion of the jugal, an interpretation which would require the jugal to have been broken longitudinally during burial.

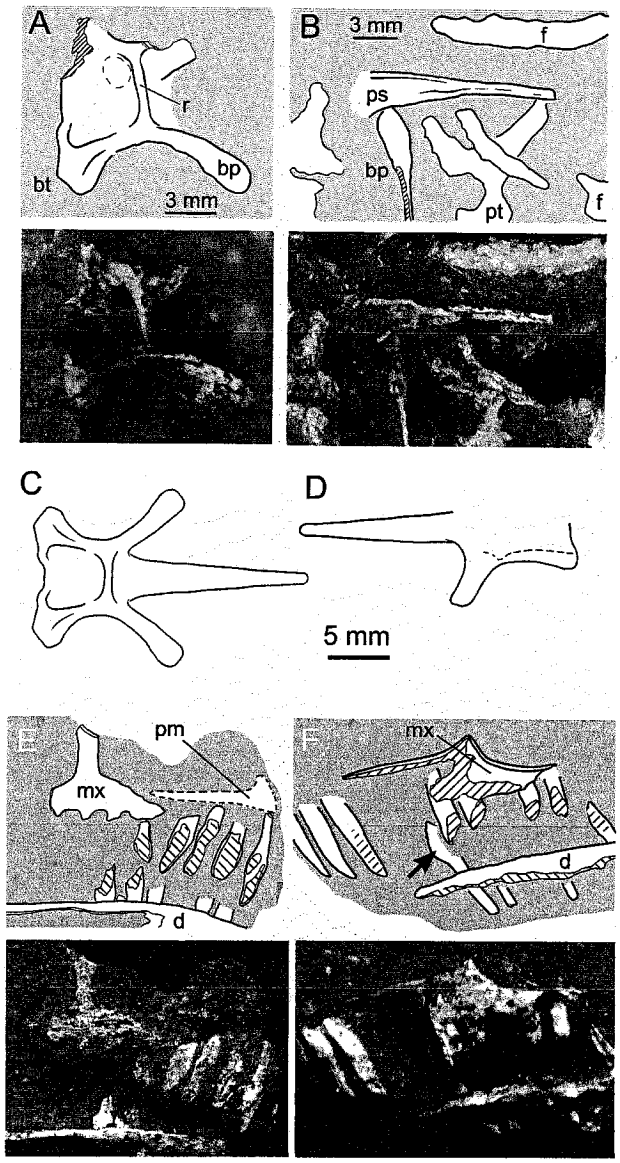

Figure 3.6: ***Anchisaurus polyzelus*** **(YPM 209), line drawings and long wave UV photographs of the posterior basisphenoid in ventral view (A) and parasphenoid rostrum in right lateral view (B). The area demarcated by dashed lines, A, is not a foramen but rather a preparation artefact. The reconstructions of the YPM 209 parabasisphenoid in ventral (C), and left lateral view (D), demonstrate that the ventral edge of the parasphenoid rostrum is parallel to, and 1 mm above the ventral sagittal surface of the basisphenoid (dashed lines in D). The right (E), and left (F), maxilla, premaxillary teeth and dentary in lateral views; the posterior process of the premaxilla is not visible in lateral view (dashed line) but can be seen on the opposite side of the block. Cross-hatched area represents preparation damaged bone surface, and the black arrow in (F) is the dentary tooth that was examined by SEM and is shown in Figure 3.7. Abbreviations as listed on p. 33.**

Quadrate

Prior to further preparation, no element could be identified as a quadrate (contra Marsh 1892). However, the left quadrate is now exposed, having been displaced and rotated prior to burial, so that it is now exposed in medial view. The distal end was lost during previous preparation, but no additional morphological features can be determined from this partially exposed fragment.

Pterygoid

The right pterygoid is now exposed in medial view, located immediately lateral to the parasphenoid rostrum. The rectangular quadrate ramus lacks the thin dorsal process that articulates with the anterior edge of the medial quadrate in *Plateosaurus* (Galton 1984), but this process would probably have been destroyed when this area was removed during earlier preparation. An unidentified thin fragment of bone that overlaid the medial portion of the pterygoid (Figure 3.5A) was removed, exposing the basipterygoid flange. The flange is short, blunt, and directed medially. The palatal ramus is also partially visible in medial view, the anterior tip being located underneath the left frontal fragment.

Mandible

The lateral surfaces of both mandiblar rami were obliterated prior to 1906, so little can be said about the morphology of the individual elements. The mandibular rami diverge from the symphysis at an angle of 45 degrees.

The right dentary is 5 mm deep at its anterior end and reaches a height of 7 mm ventral to the tooth row. The greatest depth of the mandibular ramus (at the surangular) is 11 mm. As in YPM 1883 (Yates 2004), there is no evidence to suggest that the dorsoventral height of the dentary below the tooth row was greater than 20 per cent of dentary length. The dentary length is at least 35 mm based on the tooth-bearing portion visible on the left mandibular ramus, but might have approached 40 mm if the posterior termination occurred at the deepest part of the surangular as in other basal sauropodomorphs (Galton 1984, Sues et al. 2004).

Only five teeth are visible in the right dentary. The small tooth crowns are 3 mm in length apicobasially and oriented perpendicular to the dorsal margin of the dentary. A

space is located adjacent to the symphyseal edge but this represents a missing tooth. The overlying premaxillary teeth obscure the symphyseal edge of the left dentary, but the root and the distal edge of a crown are partially visible, demonstrating that a tooth is located immediately adjacent to the symphysis; consequently, the first tooth is not inset in YPM 209 or YPM 1883 (Sereno 1999, Yates 2004).

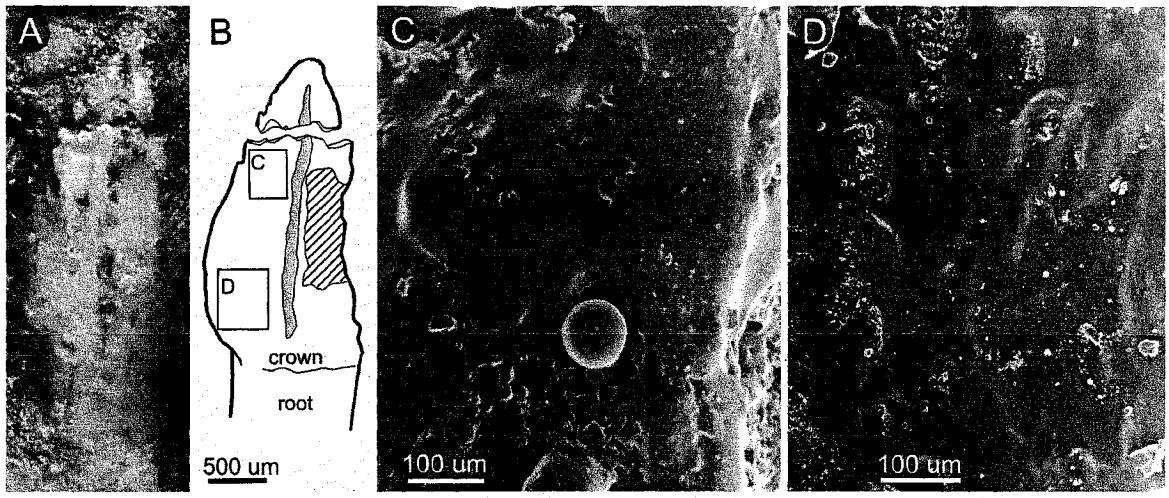

Figure 3.7: A photograph (A), schematic drawing (B), and SEM photomicrographs (C- D), of a recently exposed *Anchisaurus* dentary tooth (YPM 209).
The tooth was damaged by transverse and longitudinal (solid grey) taphonomic cracks and a small portion of enamel is missing (diagonal lines). The preserved tooth enamel exhibits a very fine textured pattern (C-D). The sphere in the middle of (B) is an air bubble present in the mould.

A single empty alveolus is located posterior to the first tooth of the left dentary, followed by four teeth, another empty alveolus, an erupted partial crown, an empty alveolus and one containing a tooth root (the crown was lost during previous preparation). The last preserved tooth is located 25 mm from the symphysis. Two additional tooth positions may have been present more posteriorly, yielding a dentary tooth count of 12. However, the low number of dentary teeth is of uncertain phylogenetic importance due to the immaturity of the specimen (see Discussion).

The recently exposed third left dentary tooth has the best preserved crown. However, like the other teeth of YPM 209 and YPM 1883, it has a centrally located longitudinal crack, suggestive of at least a short period of sub-aerial exposure prior to burial (Behrensmeyer 1978). A transverse crack near the tooth apex is also taphonomic, but several delicate striations appear to be visible in the area near the mesial edge of the tooth (Figure 3.7A, B).

The enamel of this tooth is very lightly textured, and this texture varies over different regions of the tooth crown (Figure 3.7). This texture is much finer than that described for YPM 1883 by Yates (2004), and the size, shape and distribution of the texture present on the teeth of both YPM 209 and YPM 1883 is distinct from the wrinkled enamel of derived sauropods (Wilson and Sereno 1998).

The variability of the enamel textures noted for *Anchisaurus* may represent either variation within the dentition, ontogenetic variation, trauma or disease (Franz-Odendaal 2003, 2004). Also, the textured enamel noted in YPM 1883 (Yates 2004, fig. 6) includes conspicuous fine lines running obliquely to the "the short longitudinal wrinkles", therefore the recorded surface may represent an emulsion (consolidant?) artefact. The significance of the enamel textures on the teeth of *Anchisaurus* is difficult to determine due to an absence of systematic analyses of surface structure among sauropodomorph enamels (Hwang 2005) and the limited quality and number of samples available for *Anchisaurus*.

Other Skull Elements

A fragment located near the posterolateral edge of the skull may represent the right squamosal, and the parietals may also be exposed in dorsal view (Figure 3.5A), but little can be said about the morphology of these fragments.

Specimen Maturity

Galton (1976) was the first to propose that the skeletons of *Anchisaurus* (and '*Ammosaurus*') represent juvenile or sub-adult specimens. Conversely, Yates (2004) proposed that two of the specimens (YPM 1883 and YPM 208) were mature, or nearly mature, as the smaller specimen (YPM 1883) has closed sutures on the posterior dorsal vertebrae. Thus, *Anchisaurus* was identified as a very small, but morphologically mature basal sauropod dinosaur (Yates 2002, 2004).

The prootic-opisthotic, basisphenoid-basioccipital, parietal-parietal, and parietal-frontal sutures remain open, as do the neurocentral sutures of the preserved (anterior) cervical vertebrae, which contradict the hypothesis that YPM 1883 was nearly mature. The small number of teeth also argues for immaturity, as tooth count increases

ontogenetically in other 'prosauropods' (e.g. Sues et al. 2004). A future histological study (by TF) of the *Anchisaurus* material will hopefully provide further evidence with which to evaluate the maturity of the specimens. If all specimens of *Anchisaurus* do prove to be immature, phylogenetic studies incorporating these skeletons should be cautious when scoring characters in order to avoid potential problems with ontogenetic variability.

Phylogenetic Analysis

No significant differences in skull anatomy can be found between YPM 209 and YPM 1883. Thus, all of the specimens from the Portland Formation are considered to represent a single taxon, *Anchisaurus polyzelus* (Hitchcock, 1865). Minor differences between the two skulls can be attributed to ontogenetic variation. However, the smaller skull (YPM 209) is badly deformed and damaged, limiting the comparisons that could be made between the two skulls.

Yates (2004) presented a phylogenetic analysis of basal sauropodomorph relationships, on the basis of 205 characters scored for 17 sauropodomorph ingroup taxa, with two different pairs of outgroup taxa. This analysis included the novel result that *Anchisaurus* was the smallest sauropod dinosaur and was positioned at the base of the sauropod clade (following the stem-based definition of Wilson and Sereno 1998). This was a robust result, with the node uniting *Anchisaurus* and other sauropods supported with a bootstrap value of 97 per cent. In addition, five additional steps were required to remove *Anchisaurus* from this group. Here, we re-examine the strength of this hypothesis by including new information on the skulls and braincases of YPM 209 and YPM 1883 in a phylogenetic analysis.

As a result of the new preparation work described above, several character scorings for *Anchisaurus* used in the Yates' (2004) analysis now require revision (referred to in the following discussion by Yates' original character numbers). As a result of preservational or preparation damage, the anterior portion of the left lachrymal dorsal process is missing (22.1 now 22.?); this has the additional consequence that the anteroventral contribution of the lachrymal to the antorbital fossa is uncertain (23.1 now 23.?). The missing piece of the YPM 1883 skull block truncates the posterior portion of

the right jugal, and transverse crushing of the postorbitals confounds assessment of the position of the anterior limit of the lower temporal fenestra (29.2 now 22.?). Also, the preserved ventral edge of the left quadrate is a broken surface and does not represent the articular surface for the quadratojugal, so the position of the quadrate foramen cannot be determined in either YPM 1883 or YPM 209 (38.1 now 38.?). Further scoring modifications are required as a consequence of misinterpretations of the distorted skull elements of YPM 1883: the frontals did contribute to the supratemporal fenestra (30.1 now 30.0); and there is a lateral component to the cup-like posterior basisphenoid portion of the basal tubera (46. 0 now 46.1).

New information from the skull of YPM 209 also provides additional data to update several character scorings. The region adjacent to the interbasipterygoid space is not preserved in YPM 1883, but there is a well-developed interbasipterygoid septum in YPM 209 (48.0 now 48.1). Moreover, the floor of the braincase has been misinterpreted in YPM 1883 as a result of displacement and the missing portion of the skull block. A new reconstruction, based on the new parabasisphenoid from YPM 209, demonstrates that the ventral edge of the braincase was nearly straight (49.2 now 49.0). Also, the basipterygoid processes of YPM 209 are long and, when scaled to the YPM 1883 braincase, are equal to the dorsal height of the braincase (50.0 now 50.1).

In YPM 1883 and YPM 209, there is no anterior inclination of the maxillary tooth crowns (64.1 now 64.0) or of the dentary tooth crowns (65.? now 65.0) (contra Yates 2004). While the tooth enamel of YPM 209 is textured, this pattern and the 'wrinkled enamel' of YPM 1883 are not necessarily comparable to the wrinkled enamel of derived sauropods (71.1 now 71.?). Finally, the length of the manus of YPM 1883 is 38 percent of that of the humerus length plus radius length (see Galton 1976, Yates 2004, p. 15), so an apparent miscoding was corrected (132.2 now 132.1).

A reanalysis of the Yates (2004) matrix was conducted with the incorporation of the above mentioned modified character scores. Whereas 14 characters were listed as ordered (Yates 2004, p. 23), two additional characters (90 and 94) were also listed as ordered in the character list and were therefore treated as such in the reanalysis of the matrix. The revised data set was analyzed using PAUP 4.0 beta version (Swofford 2002), with branch and bound searches and multistate characters treated as polymorphisms.

A single tree (length 441 steps, CI = 0.58, RI= 0.72) was recovered from this analysis with the same topology as that proposed by Yates (2004), including the position of *Anchisaurus* at the base of the sauropod clade. However, the robustness of this relationship has been weakened. In the new analysis this position has a bootstrap value of 70 percent and a decay index of 2. Only two additional steps are required to place *Anchisaurus* among the 'prosauropod' taxa. A similar result was also found when the modified matrix was further altered to include new information on the skull of *Massospondylus* (Sues et al. 2004).

As mentioned above, it is likely that the specimens of *Anchisaurus* are immature, which would affect the scoring of at least two characters that currently support its inclusion within the sauropod clade. If the scores for two characters are reversed as would be likely with skeletal maturity, character 66.0 to 66.1 (the number of dentary teeth) and 123.0 to 123.1 (relating to the proportions of the appendicular skeleton), then two equally parsimonious trees are recovered. The two trees differ only in the placement of *Anchisaurus*; one tree proposes a topology identical to Yates (2004) while the other places *Anchisaurus* as the sister taxa of 'prosauropods' more derived than *Efraasia minor* [*Anchisaurus* + (R*iojasaurus* + (*Plateosaurus* + (*Coloradisaurus* + (*Massospondylus* + *Lufengosaurus*))))].

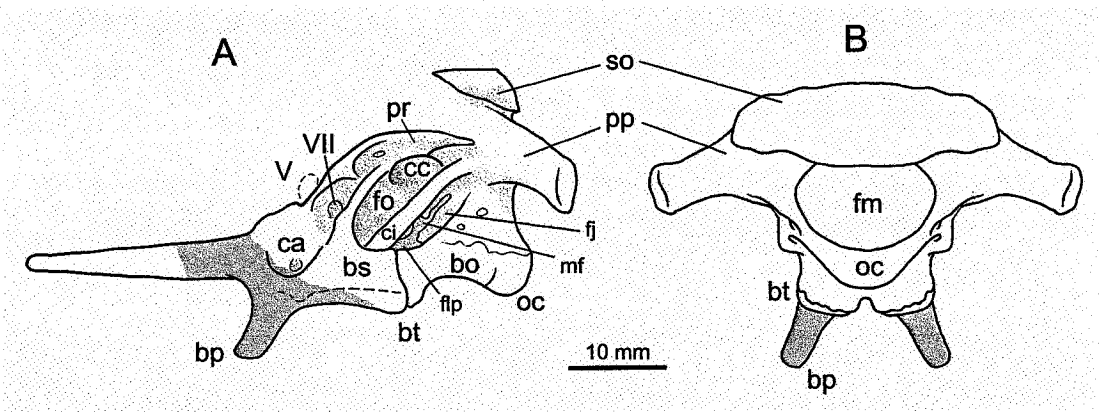

Figure 3.8: Reconstructions of the braincase of *Anchisaurus polyzelus* based on YPM 1883 and a scaled up parabasisphenoid from YPM 209 in left lateral (A), and occipital (B) views. The solid grey area identifies the portion of the YPM 1883 parabasisphenoid that is missing and the dashed line represents the sagittal ventral surface of the basisphenoid. Abbreviations as listed on p. 33.

The classification of *Anchisaurus* also depends on the definition of Sauropoda adopted. Based on a phylogenetic analysis that included an almost complete specimen of

Melanorosaurus (Upper Triassic, South Africa), Yates (2005) noted that many taxa, such as *Riojasaurus, Anchisaurus, Jingshanosaurus, Yunnanosaurus, Massospondylus, Coloradisaurus* and *Lufengosaurus,* are "captured" by the current diagnosis of Sauropoda and, because of this, a new definition of Sauropoda may be required. Yates (2007, in press) proposes a stem-based definition of Sauropoda that excludes *Anchisaurus,* and the other taxa listed above. Although there are differences in the analyses, *Anchisaurus* is also excluded from the stem-based definition of the Sauropoda used by Upchurch *et al.* (2007).

Conclusions

A new reconstruction of the braincase of *Anchisaurus* (Figure 3.8) is based upon the reinterpretation of the braincase elements in YPM 1883 and YPM 209. The estimated basipterygoid lengths for YPM 1883 and the reconstruction are based upon the relative lengths of the basipterygoid processes and parabasisphenoid of YPM 209 (22 mm: 8 mm = 36 percent). The estimated basipterygoid length (12 mm), from distal tip of basipterygoid process to dorsal edge of parasphenoid rostrum, suggests that *Anchisaurus* had long basipterygoid processes, as von Huene (1914a) stated, although his statement was based upon misinterpretation of the YPM 1883 skull.

This new reconstruction differs significantly from that presented in previous studies (Figure 3.1E) and closely resemble those of other 'prosauropods' such as *Thecodontosaurus*, *Efraasia minor* (Galton and Bakker 1985, Yates 2003a) and *Plateosaurus* (Galton 1984, 1985a) (Figure 3.2). The braincase of *Anchisaurus* differs significantly from that of *Camarasaurus* (Chatterjee and Zheng 2005) and other sauropods in that the cultriform process of the parasphenoid is elongate, the ventral surface of the braincase is straight (with the cultriform process being parallel with the ventral surface of the basisphenoid: see reconstruction, Figure 3.8), and the metotic fenestra and foramen ovalis are visible in lateral view (not obscured by a large crista prootica). Interestingly, however, the junction between the basisphenoid and basioccipital does appear to be a deep 'U'-shaped ventral depression in both YPM 209 and YPM 1883, a feature otherwise only found in *Lufengosaurus* (Barrett *et al.* 2005) and derived sauropods.

For over 100 years the skull of YPM 1883 has been misinterpreted because the skull block had fractured and one of the pieces was lost. Both of the skulls of *Anchisaurus* have suffered deformation due to dorsoventral and lateral crushing, which is important to the interpretation of these small and delicate specimens. While commercial developments currently cover the original quarry where the specimens of *Anchisaurus* were recovered, other nearby sites have potential for producing new specimens, which are necessary to further our understanding of this taxon.

Chapter 4 – Discovery of a Prosauropod Bone Bed in the Lower Jurassic McCoy Brook Formation

Introduction

The McCoy Brook Formation at Wasson Bluff, Cumberland County, Nova Scotia, represents a half-graben micro-basin that developed as part of the tectonic reactivation of Palaeozoic faults (Minas Fault Zone) and the formation of the large Fundy rift basin during the break of Pangaea (Olsen and Gore 1989, Olsen and Schlische 1990). Within the western micro-basin at Wasson Bluff, the McCoy Brook Formation on laps the North Mountain Basalt and includes lacustrine, fluvial, aeolian (Tanner and Hubert 1992) and large debris flow units (Tanner and Hubert 1991). The Fundy rift basin is the largest and most northern of a series of rift basins located along eastern North America, termed the Newark Supergroup (Olsen 1978).

The lower-most McCoy Brook Formation has been estimated to be only 200,000 years after the Triassic boundary; the boundary being located in the upper section of the Blomidon Formation, which directly underlies the North Mountain Basalt (Olsen and Gore 1989). The age of the deposits is based upon the similarity of the North Mountain Basalt with the Orange Mountain-Talcott Basalt of the Hartford Basin (Olsen and Gore 1989), in Massachusetts and Connecticut. Furthermore, cyclostratigraphic based timescales developed for the Newark Supergroup (Olsen 1986) have provided the basis for the refined age estimate of the sandstone deposits at Wasson Bluff.

In the mid-1980's, rich deposits of Lower Jurassic small vertebrates discovered among the fossil basalt talus strata at Wasson Bluff (Olsen et al. 1987, Shubin et al. 1991, Shubin et al. 1994, Sues et al. 1996) drew attention to the site as an important record of the vertebrate taxa of the Lower Jurassic period in North America. The rich deposits discovered in the 1980's included small vertebrates such as *Protosuchus*, the sphenodontian *Clevosaurus*, early mammal-like reptiles, and isolated theropod teeth.

The first discovery of dinosaur skeletal fossils in the McCoy Brook Formation occurred in August 1976, by a team from Princeton University (Paul Olsen, Donald Baird, Jack Horner) that collected several disarticulated sauropodomorph dinosaur

vertebrae and appendicular bone fragments. While earlier reports (Carroll *et al.* 1972) of dinosaur skeletal material from the Triassic Wolfville Formation of the Fundy Basin are based on misidentified fragmentary remains (Sues, pers. comm. 2002), the discoveries of dinosaur specimens at Wasson Bluff remain well founded, and these represent the oldest dinosaur skeletal remains in Canada.

The site history for all dinosaur skeletal fossils recovered from the McCoy Brook since 1976 (Fedak 2001) is provided to document the locations of all previous collection sites, and provides an inventory of specimens for considering the morphological and taxonomic diversity that is represented in the McCoy Brook Formation. Field collecting methods used within the bone bed site are then discussed in order to provide the geological context for the specimens within the bone bed, as well as to consider directions for future work. The most dramatic and important modifications of the skeletal material are due to the fault and compression deformation, exhibited by nearly every bone and all sediments within the bone bed. The fault deformation of the bone bed adds complexity to field collecting, and documentation of these features provides the opportunity for improved field collecting techniques for future work. Finally, some elements were affected by post-collection damage, as the internal components reduced in volume while drying, resulting is small pebbles of fractured bone. The process is due to the presence of smectite clays deposited within the bone tissue, and so far, attempts to mediate this damage have been unsuccessful.

To increase the ease of comparing and referring to specimen numbers, abbreviations are occasionally used in this and the subsequent chapters. As an alternative to using the full specimen number (FGM994GF69), only the GF and numeric portion that specifies an individual specimen are used (GF69), after the specimen number has been listed at least once. The abbreviated specimen numbers are adopted in order to limit the amount of redundant information, and therefore improve the ability to compare and discuss multiple specimens.

Site History

The initial discovery of dinosaur remains in the McCoy Brook Formation occurred in 1976 by a team from Princeton University (P. Olsen, D. Baird, J. Horner). As

shown in the sketch made during this field work (Figure 4.1), the disarticulated skeletal material was surface collected across a 10 meter length of cliff, at site 'L' as described by Olsen and Gore (Olsen and Gore 1989). Material collected (YPM PU 22126) includes the proximal end of a right femur, fragments of a pubis, a (third?) metatarsal, a sixth? cervical vertebra, as well as a dorsal and caudal vertebrae. The material was first listed within the appendix of Olsen (1980), and referred to cf. *Ammosaurus* (Olsen and Gore 1989).

In 1986, Neil Shubin, Hans-Dieter Sues, and Bill Amaral collected a small 'juvenile prosauropod' (FGM000GF18) from other fluvial sediments lower in the section (site 'K', Olsen and Gore 1989), near the 'fish bed' (Figure 4.2); however, based on the material that remains available for description, the specimen is now identified as the partial post-cranium of a protosuchid crocodylomorph (Chapter 1). The stratigraphically earliest occurrence of sauropodomorph dinosaur skeletal material at the McCoy Brook Formation therefore occurs at the Princeton site (~ 53 meters up section from the 'fish bed').

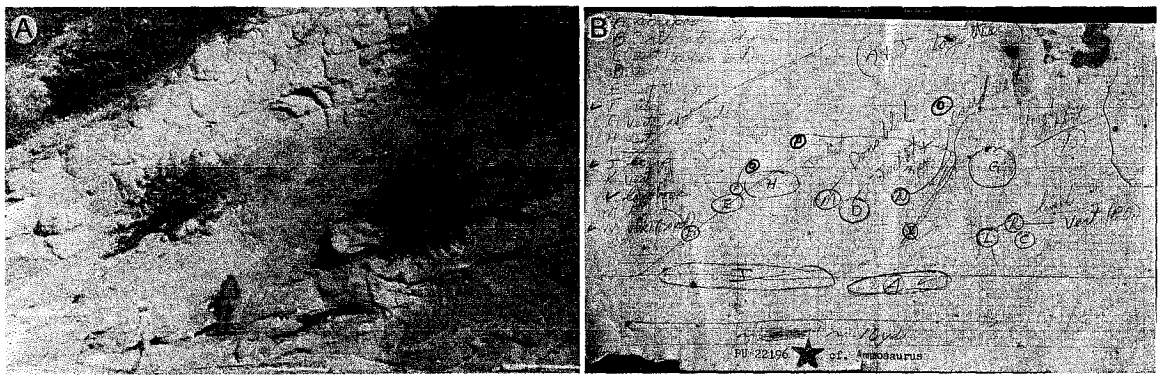

Figure 4.1: Original field photograph provided by P. Olsen (A) and the field map of the collected material (B) stored with the material in the collections of the Yale Peabody Museum.

Another specimen collected by Neil Shubin and the team from Harvard University in 1986, includes a partial pelvis and hind limb, and associated group of gastroliths (NSM005GF009 and FGM998GF46). The specimen was collected from site 'N' (Olsen and Gore 1989), which is located approximately 200 meters west of the Princeton quarry, the exact stratigraphic location relative to the 'fish bed' has not been determined. Gastroliths from this specimen were included in a study of dinosaurian

gastroliths (Whittle and Onorato 2000), and a sphenodontian mandibular ramus located several centimetres from the gastrolith pile has been used to suggest prosauropods may have been omnivorous (Barrett 2000). The study of this specimen (Appendix 2) was unable to confirm the mandibular ramus was associated within the gastral basket, and the recent exposure of a sacral vertebrae from the specimen demonstrates the specimen is distinct from the specimens located in the Princeton site, and possibly represent a theropod dinosaur due to the elongate and low nature of the sacral centrum.

In 1988, a grade nine student (Kevin Murphy, Ellenvalè Jr. High School, Dartmouth, NS) discovered a fragment of a dinosaur bone during a school geology trip to Wasson Bluff section of the McCoy Brook Formation (pers. comm. Bob Grantham 2001). When accessioned, the specimen (NSM 989GF6.1) was identified as a vertebral fragment; however, the specimen is now completely prepared and has been tentatively identified as a posterior fragment of a frontal (Fedak 2001). The fragment is rather difficult to interpret due to the incomplete nature, and alternatively may represent a portion of the acetabular margin of an ilium. The stratigraphic location where the specimen was collected was not recorded, and the original collector could not be consulted. Although the stratigraphic location of the specimen remains unknown, it seems likely that the fragment was discovered at the bone bed site.

While leading a Geological Association of Canada field trip in 1992, Bob Grantham found several fragments of dinosaur bone at the original Princeton site. The fragments then lead to the discovery and collection of a nearly complete and articulated sauropodomorph dinosaur during the following two years. George Hrynewich, a private fossil collector in Nova Scotia, and Ken Adams, the Curator of the Fundy Geological Museum, collected the specimen (FGM994GF69), which includes a nearly complete representation of the skeleton, except for the skull.

I began this research project in 1997, with the preparation and study of the specimen discovered by B. Grantham (94GF69). During my inspection of the site, another specimen (FGM998GF9) was located 3 metres to the west, and over the subsequent nine years, additional disarticulated elements were recovered from this location. Material included to date includes a complete left and distal end of the right femur, left tibia, fibula and fifth metatarsal, a left radius and ulna, coracoid, several

vertebrae and a nearly complete ischium. The radius and ulna are much shorter than expected for the length of the femur and tibia (Chapter 6), therefore this 'specimen' may actually represent the remains of more than one individual.

In 1998, another articulated specimen (FGM998GF13-I) was discovered at the Princeton site; including two dorsal vertebrae, the sacrum and 8-10 caudal vertebrae, the right and left ilium and ischium, the right femur, tibia and fibula, as well as the left tibia, fibula and pes. With additional field work in 2000 and 2004, two other articulated specimens (FGM998GF13-II and FGM998GF13-III) were collected and a rich and localized bone bed was identified. One of these specimens (GF13-II) is nearly complete, including most of the skull; the first associated cranial material from the McCoy Brook Formation (Fedak 2002, 2004).

With these recent field excavations at least five specimens of sauropodomorph dinosaur can now be recognized based on the number of unique femora (and coracoids) within the bone bed. Four of these specimens (GF69, GF13-I, GF13-II, GF13-III) include articulated pelves, and partial axial and appendicular skeletons. A compilation of the field maps from the excavations of 1994-2004 (Figure 4.2) show the distribution of these specimens. The articulated specimens contact and overlap each other, demonstrating rapid emplacement and burial. Field work in 2003 resulted in the discovery of additional bone fragments high in the cliff, within the same stratigraphic layer as the bone bed specimens. The fragments are located approximately 3 meters along the bedding surface north from the site of GF69, and demonstrate that additional material (and specimens?) remain to be collected from the bone bed.

The three specimens of *Anchisaurus* (=*Ammosaurus*) collected from the Wolcott Quarry of the Hartford Basin (YPM 1883, YPM 209, and YPM 208) were separated by 6 meters, and one (YPM 209) was in a layer 60 cm above the others (Galton 1976). The basal sauropodomorphs from the Lower Jurassic of Arizona were collected as isolated, partial skeletons (Galton 1976). Therefore, the McCoy Brook bone bed, containing at least five specimens, and with additional specimens remaining at the site for future collection, now represents the richest site in North America for basal sauropodomorph dinosaurs (Fedak 2006a).

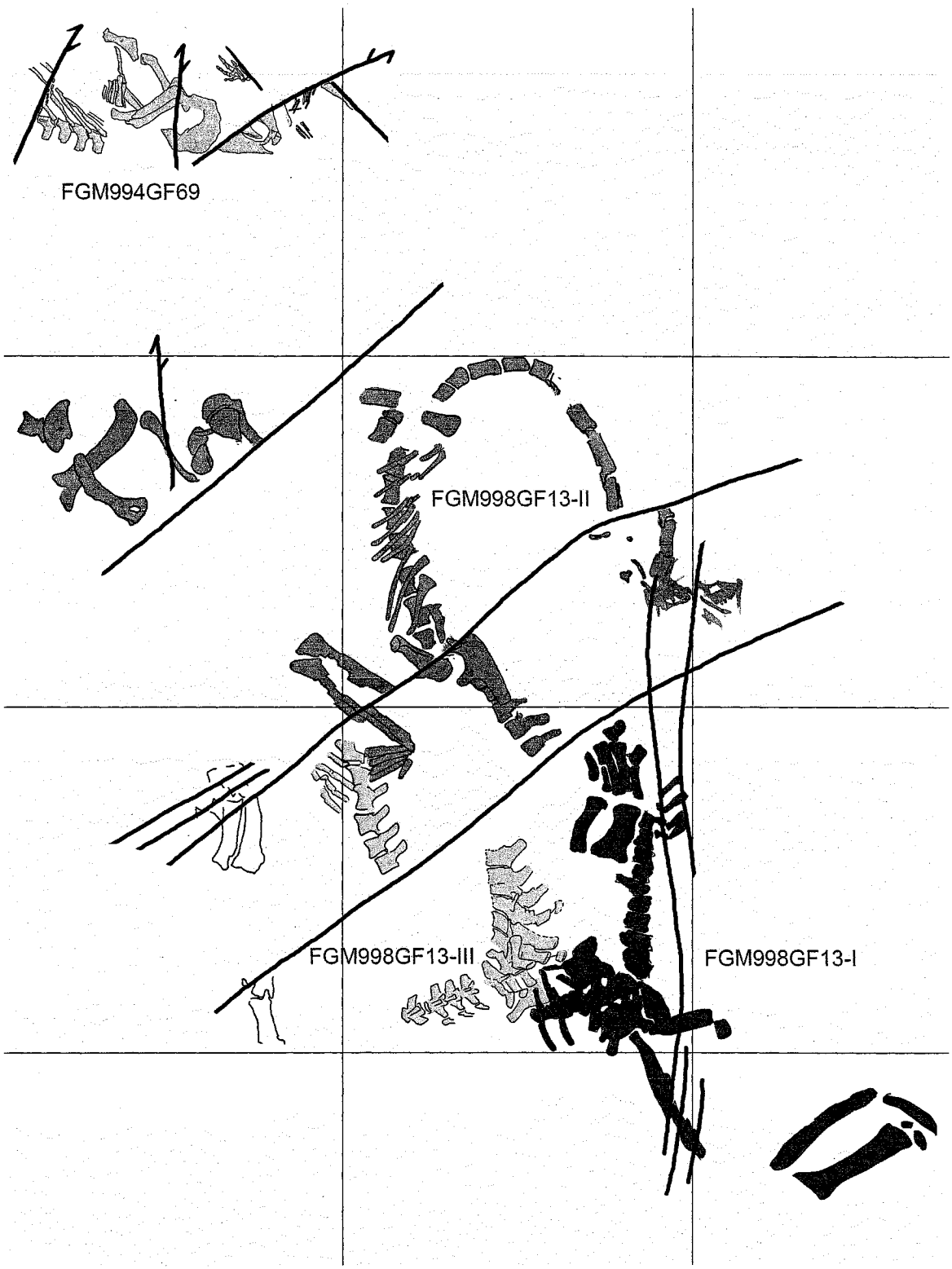

Figure 4.2: Field map of the specimens collected from the bone bed from 1992 – 2004. Grid lines represent 1 meter squares.

Collection and Preparation Innovations

The initial excavations that have been carried out during this research have been carried out as reconnaissance of material in danger of loss or damage due to erosion. During the past several years (2004 – 2006) field work has been more proactive, in exposing and collecting material prior to immediate danger from erosion. The specimens and field research described in this and the following chapters is the result of research carried out under the following Nova Scotia Heritage Research Permits: P1997NS04, A1998NS02, P1999NS02, P2000NS02, P2002NS02, P2003NS03, P2004NS04, P2005NS07, and P2006NS06.

The rate of erosion at the site is extremely high, due to the large tidal range of the Minas Basin, as well as the freeze-thaw affects of the winter seasons and the highly faulted nature of the sandstone exposures. An erosion rate estimate of one-meter a year, is based on observations over extended field seasons at the same locality, and includes occasional periods of extreme cliff erosion due to cliff failure and collapse. An excavator has been used twice (2004 and 2006), to remove large amounts of erosion debris from above the site.

A gas powered (Partner K650) rock saw was used during the initial field excavations to assist with channelling around blocks and removal of overburden. The rock saw was effective at cutting through the soft sandstone. However, due to the excessive dust created and the high speed with which it cut through the sandstone, it was difficult to recognize when unexposed bone was cut by the saw. Also, due to the frequent involvement of volunteers within the field crews, many of whom had little or no field experience, the use of the field saw could only be operated by a portion of the crew who had the appropriate experience and training.

To resolve these issues, a manual circular field saw was developed and proved useful for reducing the damage to fossil specimens. The dust and debris that previously covered exposed bone specimens was reduced, and a tool was now available for all field crew members to easily operate. The manual circular saw was made by mounting an eight inch circular saw blade, which has large carbide tipped teeth, on a metal handle approximately fifty centimetres long. To quickly cut into the soft sandstone matix, the saw was simply pulled toward the operator repeatedly (Figure 4.3). Due to the reduced

speed by which the cut in the sandstone is made, it is easy to recognize if a bone has been cut by the saw, and the cutting can be immediately stopped. Also, because excessive dust is not created, several people can use a pull saw within the quarry at one time, and the loud noise and fumes generated by a gas powered saw are also avoided.

Some skeletal elements within the bone bed become damaged immediately after being collected from the field due to the internal shrinking of the bone as it dries. Initially, salt contamination from the seaside exposure of the site was postulated as a potential cause of the damage (Fedak 2000), but not all skeletal elements were affected by this damage, which is not consistent with salt contamination. The occurrence of smectite clays within the McCoy Brook has been well documented (Tanner 1994). Smectite clays increase and decrease (up to 30%) in volume with exposure to water, as the water becomes incorporated between the mineralogical sheets of the clay. A preliminary x-ray diffraction (XRD) analysis to compare undamaged fossil bone and bone samples that were damaged by internal shrinkage was done to consider the possibility smectite clays were responsible for the damage. The results demonstrated the presence of smectite clays within the bone samples that crumbled upon drying (Fedak 2000).

Attempts to mediate the shrinkage damage by isolating the collected fossil material within the field jacket by including an impermeable barrier (tin foil), and the reduction of drying time within a controlled environment in the museum did not prevent the internal shrinkage. A method for preventing the shrinkage of the smectite clays involved in the permineralization of the bones has not been identified. Fortunately, the presence of the smectite clays within the fossil bone is not widely distributed, and only affects about 20% of the material collected to date.

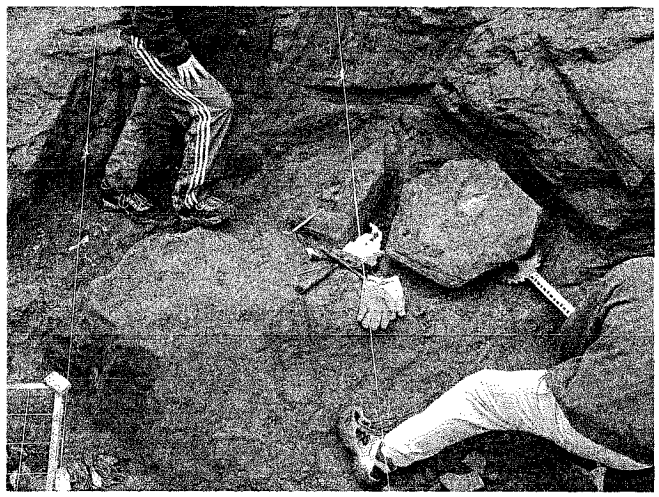

Figure 4.3: Use of manual field saw, to isolate the block containing the pectoral girdle elements of GF13-II (see Chapter 6).
The use of one meter strings and a frame divided into 10 cm squares (bottom left) was used for mapping elements in the quarry. Kathy Goodwin (left) and Jeff Odgen (right), for scale.

The teeth articulated or associated with GF13-II also experience post-collection damage; the dentine of the tooth crowns and roots also shrinks during drying, resulting in small fragments that pull away from the enamel of the tooth crown. The enamel is left unsupported medially and is therefore extremely fragile. A sample of dentine has not been examined with XRD analysis, therefore it is unknown if the shrinkage is due to the presences of smectite clays or simply the result of complete absence of permineralization.

An additional problem of consolidating the bone samples in the field remains unresolved, although several different methods have been attempted. The sandstone is saturated with moisture in the field. When exposing a specimen in the field, the bone is unable to dry out before it requires consolidation. The presence of water in the freshly exposed skeletal material prevents the effective use of typical consolidants (polyvinyl acetate, PVA) that are dissolved in ethanol or acetone solvents. The PVA solution does not penetrate into the damp bone, and when the solvent evaporates, a skin of PVA is deposited on the surface of the bone, but remains soft and only slightly increases the strength and resilience of the skeletal material.

The use of polyethylene glycol (PEG) was also tested in the field; however this water based consolidant results in the deposition of a waxy coating that prevents the stable repair of fragments with glues when the specimen is being prepared in the lab. Attempts to dry the specimens prior to consolidation by flushing the specimen with

ethanol prior to consolidation have also been ineffective. The identification of an archival and reversible consolidant that will set up (harden) while exposed to water would be useful for improving the field collection of specimens within the bone bed; but a consolidant with these properties is not yet available. An increased amount of field preparation would also reduce the preparation time involved in the lab, and therefore reduce the cost of research and specimen preservation.

Consolidation of the specimen with a PVA in a solution of ethanol or acetone within the lab environment has been effective. Due to the involvement of volunteers and students with the preparation of the specimen, a system was developed to monitor the concentration of PVA in the consolidant solutions (Fedak 2006b). The regular monitoring with this technique has improved the consistency of consolidant application, and therefore improved the conservation of the specimens during preparation.

Field Mapping

Mapping of specimens during field excavations provides important taphonomic information (Rogers 1994), including the documentation of specimen orientation, spatial distribution and association of elements. The orientation of the strata in these cliff side exposures, limits the amount of exposed surface of a particular bed, and the extensive faulting of the strata and skeletal material adds complexity to the mapping process. A typical field mapping method of establishing a base line, from which grid lines were created and used to located specimens on a field map proved to be reasonably useful. The faulted nature of the bedding limits the resolution of spatial relationships that could be attained with any mapping system, but the base line method provided the ability to correlate maps from several field seasons into a composite field map (Figure 4.2). The maps from each field season, along with the field notebooks have been deposited in the collections of the Fundy Geological Museum. Although not all specimens are depicted on the composite field map, the high density of the bone bed and stacked nature of the articulated specimens is apparent.

One of the primary difficulties faced during excavation of the bone bed is the faults that deform the skeletal material and sediments. The fault offsets can be large (30 cm), but are typically smaller (2-20 cm). These faults also offset the sedimentary

structural details (mud drapes, ripple layers), further adding to the challenge of systematic collection of single sedimentary beds or bedding sets.

Based on experience from five excavations (1998, 2000, 2002, 2004, and 2006), the faults generally strike in two major directions. Northeast striking left-lateral faults usually include some strike slip (obliquely vertical ~45°), and have generally larger displacements (30 cm). These large sub-parallel faults tend to be 1 meter apart, and therefore divide the strata into a series of discrete faulted sets that when viewed from the beach level, resemble a staircase; single bedding surfaces offset higher and to the left as it is traced into the cliff face.

While destructive to the skeletal elements, the larger faults at least have enough structural presence to be easily mapped and predicted. Excavations in 2000 and 2004 collected material up to boundaries of these larger fault units, effectively dividing the bedding into units that could be excavated within a single field season. The smaller, but more numerous fault offsets are oblique to the larger faults, and more difficult to identify, predict and reconcile during excavation work. Due to the limited (localized) affect of these small faults, only the general direction of displacement can be predicted; the size of the displacement is highly variable, although generally small. When these small oblique faults are in high concentration, the skeletal material can become very damaged by deformation.

In the field map and specimen illustrations in the following chapters, direction of fault offsets are marked by lines with arrowheads showing the direction of relative displacement (Figure 4.6B). If the relative displacement is in downward and upward direction, a triangle is placed on the line so that the apex is located on the side that is displaced downward (Figure 4.6C).

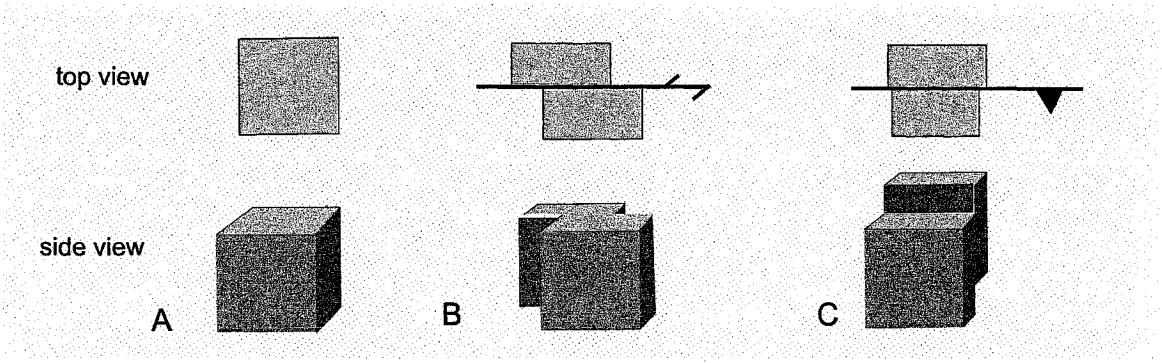

Figure 4.4: Schematic diagram depicted the two symbols used to label fault offsetting of fossil bone and sedimentary structures.
A simple shape such as a cube (A) and the top view (above), can be deformed by a left-lateral fault (B) resulting in lateral displacement as depicted by the relative arrowheads, or a strike slip fault (C) in which the relative movement is downward and depicted with the narrow end of the triangle toward the side that is relatively lower.

Stratigraphic Data and Correlations

In order to clarify the stratigraphic location of the dinosaur bone bed within the western micro-basin at Wasson Bluff, I exposed and measured one meter transects (perpendicular to strike) of the strata located within the inter-tidal beach, from the fish bed up into the column (Figure 4.5). Superficial bed features, such as amount of mud/sand and sedimentological features (ripples, clasts, colour), were noted along with bedform thickness, in order to develop a stratigraphic column (Figure 4.6) within which the bone bed could be placed.

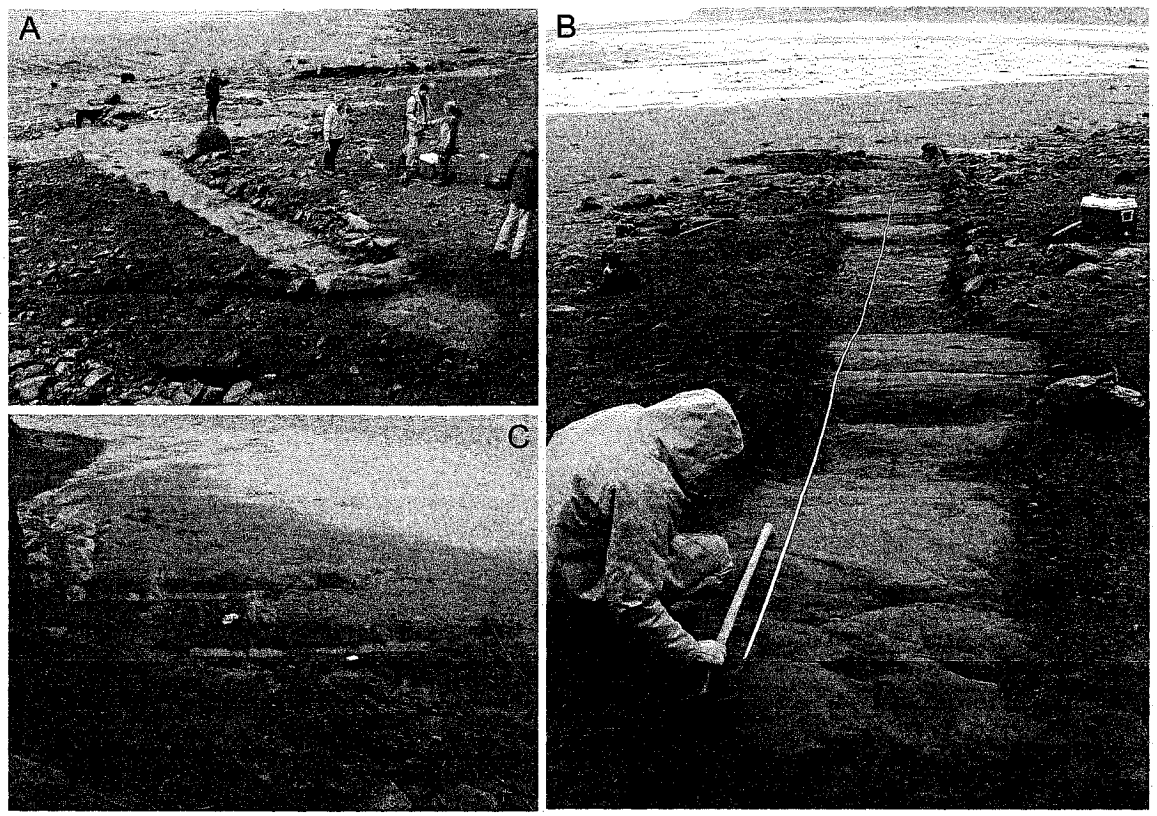

Figure 4.5: The intertidal exposures of the western sub-basin at Wasson Bluff, the lowermost section (A) including the 'fish bed', the upper portion of the measured section (B), and a birds eye view of the upper measured section (C).

The intertidally exposed strata are also faulted, and these faults had to be accounted for in several locations. Exposing the strata perpendicular to strike provided the opportunity to map 28 m of the column up from the fish bed. Much of this lower portion of the micro-basin is dominated by fluvial sandstones, with some interfingered of aeolian beds (Figure 4.6). The observations were generally consistent with those made by previous studies, although the stratigraphic column based on intertidal strata demonstrates the fluvial muddy sandstones are more abundant than proposed for the section by Hubert and Mertz (1984).

Recent field work (2006), confirmed the bone bed can be correlated to the lower 'fish bed' based on a aeolian and muddy sandstone contact at approximately 53 m above the fish bed. Immediately east to the cliff-side exposure of the bone bed, there is a contact of a one meter thick mudstone and thick overlying aeolian sandstone. The boundary between these two units is sharply defined, and has been traced in the inter-

tidally exposed beds immediately to the east of the bone bed. The contact of the mud and eolian unit can also be observed within a ravine to the east of the bone bed, and on the cliff side exposure farther east. The mud stone bed is extensive, as well as thick, and suggests the presence of abundant water during sediment deposition. The bone bed unit is estimated to be within 1-2 meters above this contact boundary, and therefore 53 m above the fish bed. Those interested in making sedimentological observations within or around the bone bed site should appreciate that faulting in this half-graben basin adds tremendous complexity to the interpretation and correlation of the bedding structures within it.

Sedimentological Observations

Initial reports of the prosauropod material from the McCoy Brook formation, reported that the skeletal material was preserved within aeolian dune sands (Olsen and Gore 1989). The quartz grains of the matrix that surrounds the skeletal material is certainly rounded, suggestive of wind-blown abrasion, and large dune cross beds are present in strata immediately above the bone bed. However, there are several sedimentological features directly related to the bone bed strata that do not support an aeolian depositional context.

There are numerous thin mud and muddy sandstone laminations immediately above the rather massively deposited sandstone containing the skeletal remains (Figure 4.6). Also, a larger muddy sandstone unit (10 – 20 cm thick) is present immediately above the bone bearing unit, which has ripple marks and drying cracks on the upper surface, and contains matrix supported basalt cobbles. This muddy sandstone unit also comes into direct contact with some of the skeletal material (skull block). The large and small scale faulting of the strata makes the sedimentological interpretation of these beds difficult. No channel boundaries have been observed within or around the bone bed. However, the sediments containing the skeletal material do have a fluvial nature.

Fault and Compression Deformation

The skeletal material from the dinosaur bone bed at Wasson Bluff is typically deformed by crushing, as well as multiple displacement faults from syndepositional

faulting (Olsen and Gore 1989). The skeletal material has a small amount of permineralization, such as the infilling of osteocyte lacunae and caniculae, but larger open areas within the skeletal elements are general poorly permineralized. The medullar cavities and open structure of internal woven bone, remained unfilled by secondary mineralization during preservation. This lack of secondary mineralization made the skeletal material susceptible to compression forces, which often resulted in the complete closure of the open structures due to structural collapse (Figure 4.7A).

The minimal permineralization of the skeletal material is consistent with high sedimentation rates present within the syndepositionally faulted half-graben micro-basin. The deformation that results from the low level of permineralization can be examined in cross section using CT scanning (Figure 4.7), for at least the large scale deformations. Subduction of the external bone surface under an adjoining external surface occurs due to compression deformation (Figure 4.7B,C).

Faulting of the skeletal material further damages many of the skeletal elements, occurs in a diversity of directions and magnitudes. Unfortunately, the CT scan of a skeletal element will not provide a signal to identify the fault deformation. Therefore recognition and interpretation of faulting can only be done by careful observation of the external surfaces.

The deformation due to compression or faulting can be extreme, and care must be taken when examining specimens to avoid misinterpretation due to deformational artefacts. Unfortunately, the level of deformation is not predictable enough to provide retrodeformation techniques, as proposed by Motani (1997) and others (Sankar 1966, Bambach 1973, Engelder and Engelder 1977).

Fault distortion of the skeletal material is often quite obvious, with the direction and magnitude being consistent across adjacent elements. With careful observation, the faults can be noted both on individual elements and across elements on larger scales, for example across the entire quarry (Figure 4.2). After the fault deformations are documented, photographs of the skeletal deformation can be realigned using common image editing software (such as Photoshop). The offset of faults can therefore be generally accounted for. However, the deformation due to structural collapse cannot be easily corrected for with image editing software. In the descriptive components of the

following chapters, effort has been made to document the direction of fault offsets affecting skeletal material, and occasionally a reconstruction is proposed to provide improved interpretive information.

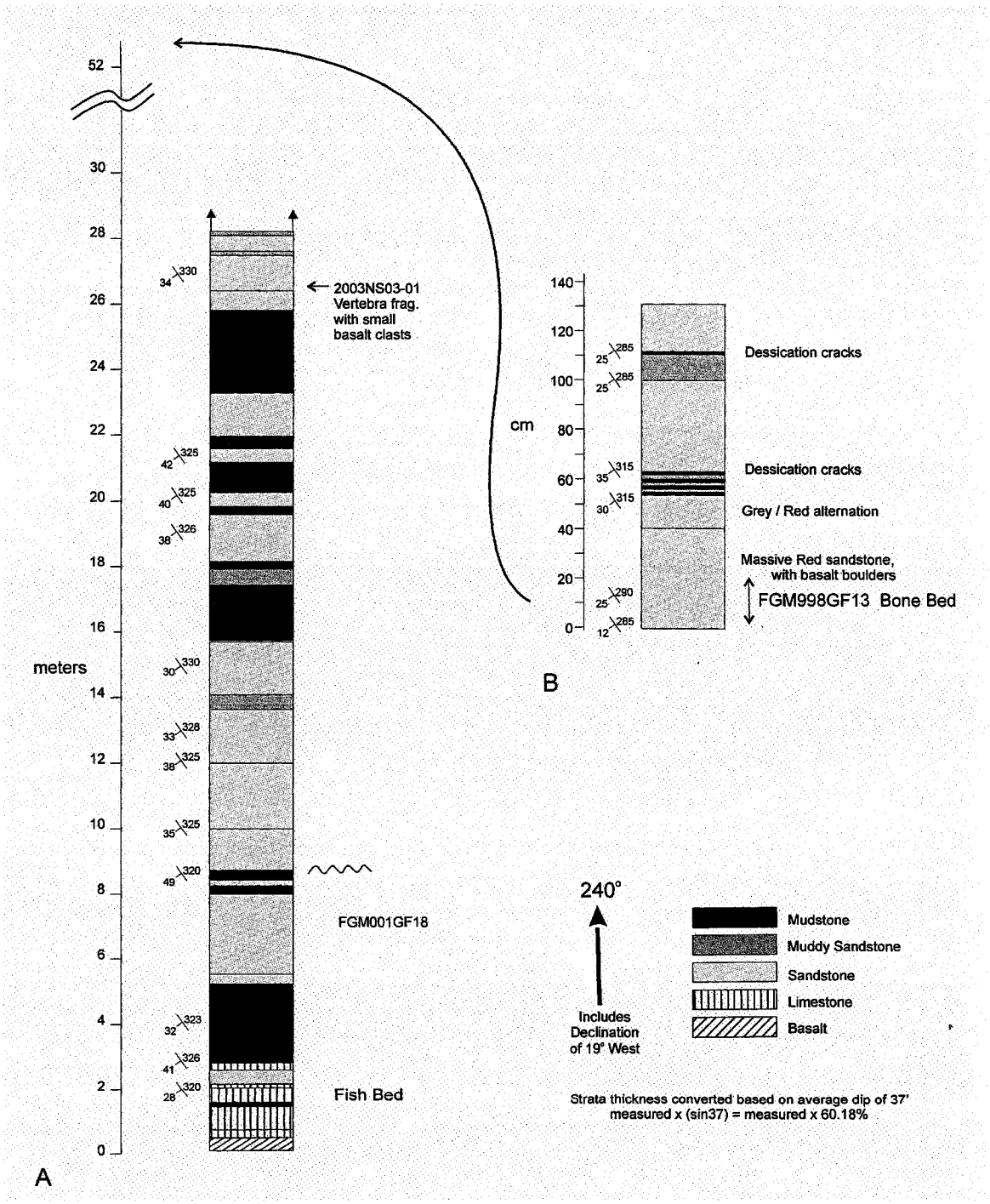

Figure 4.6: Stratigraphic column prepared based on observations of the intertidal and cliff exposures at Wasson Bluff, McCoy Brook Formation, showing the location of the new dinosaur bone bed at approximately 52 meters up section from the 'Fish Bed' Scots Bay member.

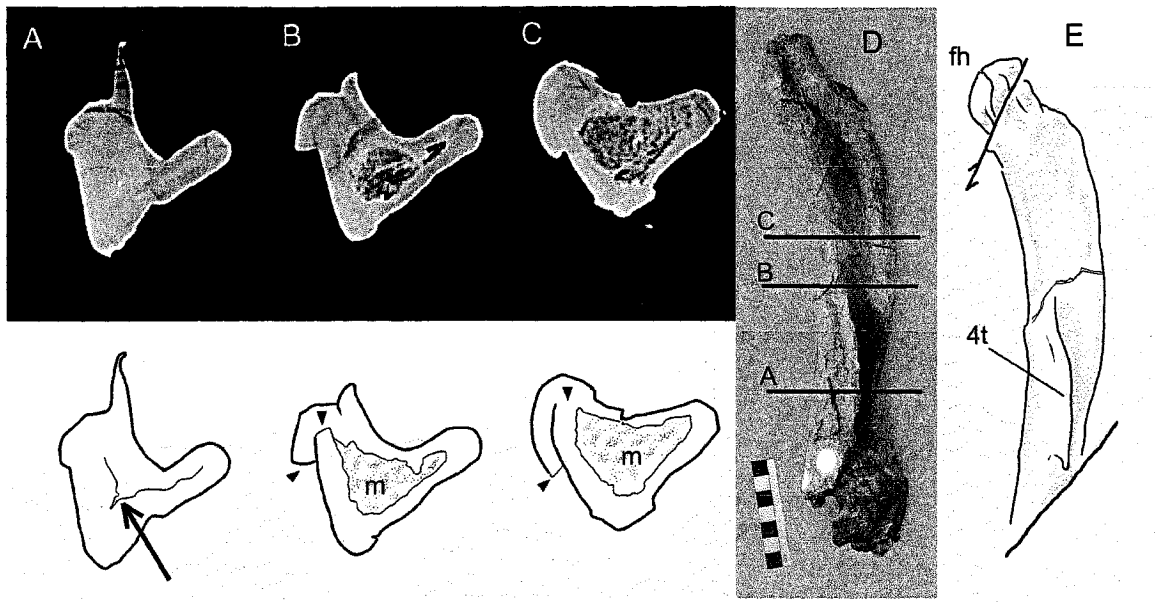

Figure 4.7: Computer tomography (A-C) images of the proximal end of the right femur of GF13-I (D), showing the complete collapse of the medullar cavity (m) in some areas (arrow) and the subduction of the cortical bone in other areas of the shaft (arrowheads).
Faults offsets of the bone (E) cannot be detected in the CT scans.

Conclusions

The recent field work and excavations have identified a rich bone bed of basal sauropodomorph dinosaurs in the Lower Jurassic McCoy Brook Formation. The bone bed can now be recognized as the richest site in North America for prosauropod dinosaurs. Although fault deformation increases the complexity of field work and specimen collection, useful data and specimens can be recovered. Alternative strategies and techniques for collecting in this cliff side exposure have been provided. Additional new techniques are required for the consolidation of wet material in the field, which will help improve specimen quality during preparation.

Chapter 5 – Pelvic Girdle Morphology and Variation of the Bone Bed Specimens

Abstract

As a result of the excavations carried out for this research project, four separate skeletons (GF69, GF13-I, GF13-II, and GF13-III) can be identified based on unique sacra, each of which has at least one ilium. Four ischia have been recovered from the bone bed, but only three are clearly associated with specimens (GF69, GF13-I, GF13-II),. It is considered unlikely that the other ischium (98GF9.19) associates with GF13-III, but rather seems to represents a separate (fifth) specimen. The pubis is the least represented pelvic element, with only two right pubes recovered; one right pubis is clearly associated with the sacrum of GF13-III. A second pubis is morphologically distinct from that of GF13-III, but was not directly articulated with a skeleton. However, based on comparisons with the ilia and ischia, this isolated right pubis likely associates with GF13-I.

Pervious studies referred the Nova Scotia sauropodomorph specimens to *Ammosaurus* c.f. (Olsen and Gore 1989). However, this referral should not be followed based on the new information from the pelvic girdle elements. Rather, the bone bed specimens appear to represent at least one new sauropodomorph taxon. Morphological variation of the pelvic girdle elements does suggest the presence of at two unique morphological forms. The significance of the diversity of pelvic morphology will be considered in a separate chapter after the associated axial and appendicular skeletal elements have been considered in detail.

Description

Ilium

General Comments: The ilia collected from the bone bed have a general morphology that is typical of sauropodomorph dinosaurs such as *Anchisaurus* (Figure 5.1). The acetabulum is bordered posteriorly by a well developed ischial peduncle and

anteriorly by the pubic peduncle. The supracetabular crest is offset anteriorly from the midline of the acetabulum and located on the proximal portion of the pubic peduncle. The dorsal portion of the ilium is composed of a short preacetabular process that is separated from the pubic peduncle by the anterior notch, and a postacetabular process that extends posteriorly from the ischial peduncle.

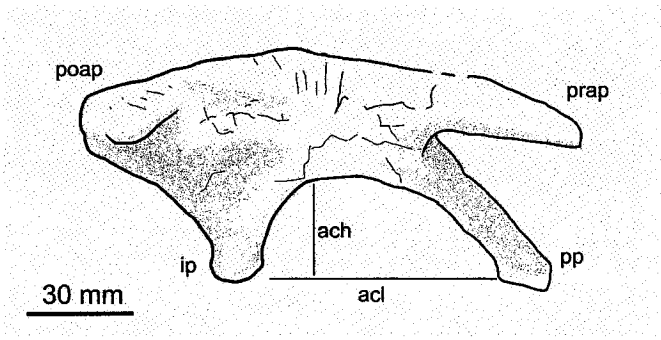

Figure 5.1: The right ilium of *Anchisaurus* (=*Ammosaurus*, YPM 208) in lateral view, demonstrating the elongate nature of the preacetabular process (prap).
Other Abbreviations: ach, acetabulum height; acl, acetabulum length; ip, ischial peduncle; pp, pubic peduncle; poap, postacetabular process.

GF13-I

Both of the right and left ilium remain articulated to the sacrum, although the right ilium (Figure 5.2) has separated slightly from the sacral ribs suggesting incomplete fusion (and possible immaturity). An oblique fault passes through the left ilium, from the anterior notch to the ventral edge of the postacetabular blade, and has offset the dorsal portion of the ilium anteriorly. The right ilium is rather well preserved, although it was severed in two by a rock-saw cut during collection, and the anterior half of the dorsal margin is offset posterodorsally by a small (14 mm) fault. The description of the ilium of GF13-I is based on this well preserved right ilium (Figure 5.2), with supplemental information provided from the left side where appropriate.

The lateral surface of the iliac blade has a strong concave depression above the acetabulum (*fossa iliaca dorsalis*, (Hutchinson 2001b), which is deepest at a level centered above the ischial peduncle and extends anteriorly to the mid point of the preacetabular process. The ventral extent of this dorsal fossa is level with the dorsal margin of the acetabulum above the ischial peduncle and the posterior margin is demarcated by a strongly developed rugose scar that extends obliquely (posteroventrally) from the dorsal margin. Posterodorsal to this rugose scar the ilium blade is inclined

slightly dorsomedially, mildly concave and covered with numerous vertical striations. The dorsal fossa can be inferred to represent the origin for the M. iliofemoralis (Hutchinson 2001b, Langer 2001), while that of the posterodorsal portion of the lateral surface is consistent with the origin of the M. iliofibularis (Langer 2001, and citations therein)

The anterodorsal margin of the right ilium is offset posterodorsally by a 14 mm fault, and after accounting for this displacement the dorsal rim is convex posteriorly and gently concave anteriorly. The ventral edge of the preacetabular process is visible immediately ventral to a rock-saw cut that transects the ilium and the dorsal margin of the preacetabular process is displaced posterodorsally by the fault. The preacetabular process is pointed, with a mildly rugose dorsal surface that is positioned medial relative to the ventral edge. The preacetabular process is short and deep, not extending beyond the pubic peduncle, with a length of 45 mm and a dorsoventral depth of 64 mm at the anterior notch. The ventral edge of the preacetabular process is nearly perpendicular to the long axis of the pubic peduncle.

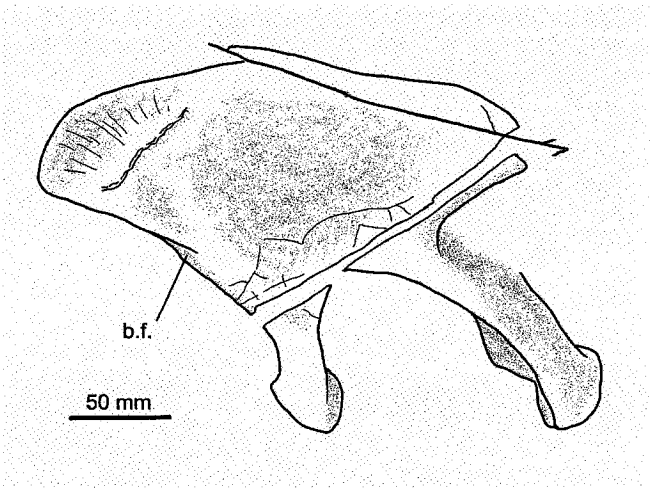

Figure 5.2 The right ilium of GF13-I in lateral view.
The thick grey line denotes the left lateral fault displacement of the anterodorsal rim of the ilium. The location of the anterior point of the brevis fossa (b.f.) demonstrates the short postacetabular blade of this specimen.

Acetabular length is measured as a chord line that joins the ischial and pubic peduncles, whereas the acetabulum height is the highest point perpendicular to this chord (Figure 5.1). The right acetabulum is 95 mm long and 65 mm high, with the

supracetabular crest offset anteriorly and located in front of the anterior notch at approximately pubic peduncle mid-length.

The acetabular margin of the right pubic peduncle appears to be deformed, with a narrow medial margin that backs the acetabulum. Prior to deformation the medial acetabular edge of the pubic peduncle was likely inflected mildly posteromedially as on the left side, and during preservation was bent to the anteroposterior orientation due to mediolateral compression. The left pubic peduncle acetabular surface is both transversely and dorsoventrally concave, with only a short medial edge directed slightly posteromedially. The widest portion of the acetabular margin (54 mm) is located at the midpoint of the supracetabular crest. A faint longitudinal ridge is notable along the midline of the anterior acetabular margin; a similar structure is present in a comparable location in the ilium of *Plateosaurus* (AMNH 2106, pers. observ.) and also noted in *Massospondylus* (Cooper 1981).

The articular facets on the right and left pubic peduncles are differentially deformed; however the facet appears to have been sub-circular, with a nearly straight acetabular margin and a mediolateral width of at least 32 mm. The articular facet of the left ilium pubic peduncle is transversely widest along the acetabular margin (posteriorly), and has a rounded medial edge but a straight lateral edge, the later consistent with deformation. The right articular facet is also widest along the acetabular border with a rounded lateral edge, but the medial edge of the articular facet is straight, due to compression from the medial side.

The right ischial peduncle is still associated but slightly dislocated from the proximal end of the ischium (Figure 5.8), demonstrating the elements were not fused at the time of death. The articular facet faces ventrally and was D-shaped in distal view, with a straight acetabular margin and an anteroposterior length of 33 mm. The preserved mediolateral width of the articular facet (28 mm) is most certainly due to mediolateral compression, as the correlated articular facet on the ischium is 40 mm wide. There is no posteriorly directed surface ('heel' of Yates 2004) on the distal end of either the left or right ischial peduncle. The posterior edge of the acetabulum on the ischial peduncle is only partially prepared, but the exposed portions demonstrate it is concave, both mediolaterally and dorsoventrally.

Immediately posterior to the ischial peduncle the ventral surface of the postacetabular process is mediolaterally convex. Farther posteriorly, the medial edge becomes inflected and positioned dorsally relative to the lateral edge, producing a mediolaterally concave surface that is interpreted as the anterior edge of a shallowly developed brevis fossa (Figure 5.2). The postacetabular process depth can be measured at this transition point, beyond which the process narrows posteriorly. On both the right and left ilia, the length of the brevis fossa is 60 mm from the posterior edge, and the height above the anterior edge of the brevis fossa is 70 mm. The postacetabular component of the ilium is represented by 52 mm of posterodorsal ilium edge. Based on these dimensions, the ilium of GF13-I is recognized as having a short postacetabular blade.

The left ilium is now exposed in ventrolateral and dorsomedial view, with the medial surface of the postacetabular process particularly well prepared. The dorsal portions of the second and third sacral rib complexes are also partially exposed dorsally. The distal end of the third sacral rib-complex is faulted anteriorly 15 mm, which corresponds with similar displacement of the dorsal portion of the left ilium.

GF13-II

Only the right ilium was preserved, and remains fused to the sacrum and only slightly disarticulated from the ischium. Several faults affect the ilium (Figure 5.3A), including a large fault that displaced the preacetabular process and pubic peduncle ventrally 120 mm relative to the rest of the ilium. The other small faults are generally oriented obliquely through the ilium and are able to be traced and measured in the attached sacral vertebrae. The sacrum and ilium were severed twice by rock-saw cuts during collection, but these missing areas have been accurately reconstructed due to the constant thickness of the cuts produced by the saw blade.

Although the preacetabular process and pubic peduncle were displaced ventrally 120 mm relative to the rest of the ilium, the anterior portion of the ilium has been prepared free and can now be positioned adjacent to the fault surface, providing the opportunity to measure and describe these features. The preacetabular process is 62 mm long and 40 mm deep (dorsoventrally) at the base. As preserved the tip of the process

appears to be directed slightly medially. The preacetabular process is more pointed than that of GF13-I, the dorsal edge meets the ventral edge at a 30° angle.

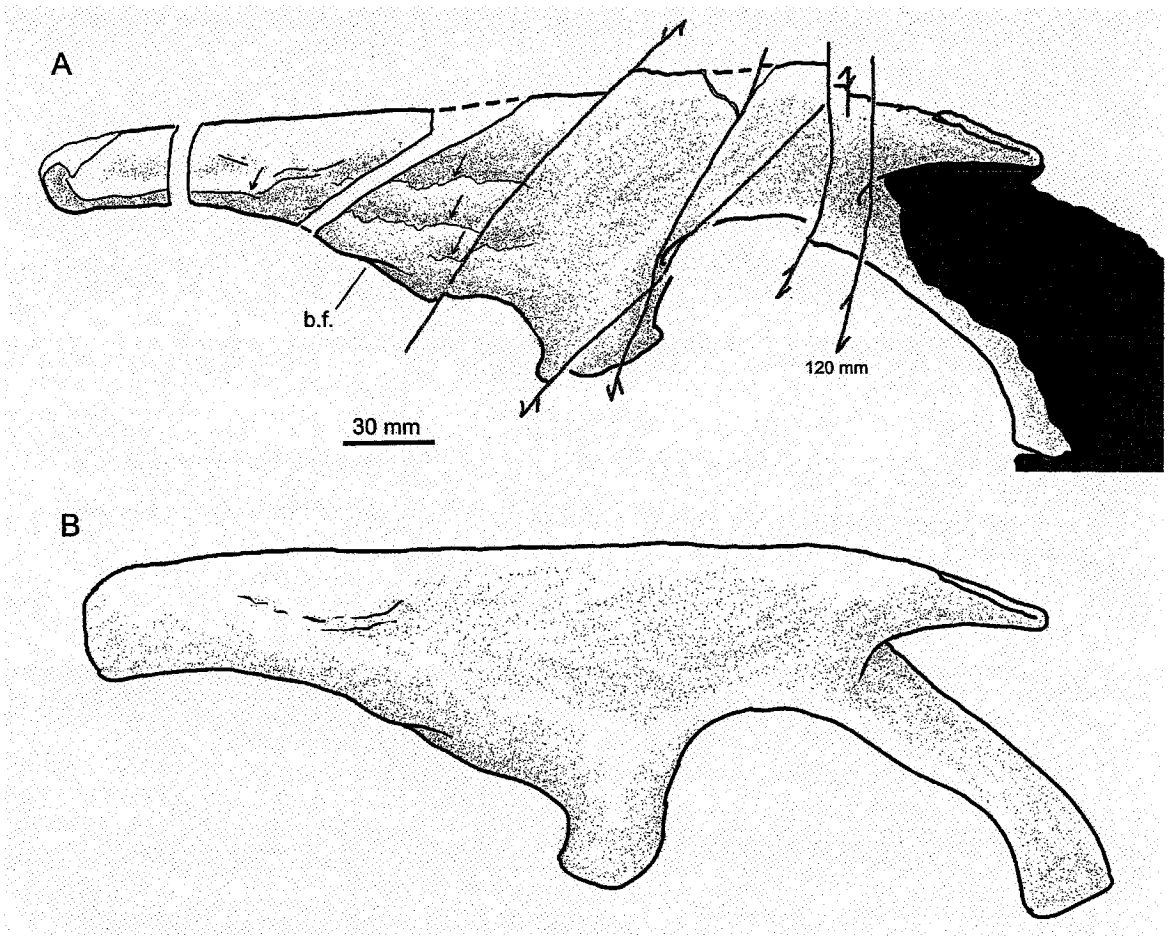

Figure 5.3 Right ilium of specimen GF13-II, in lateral view.
The grey lines denote fault displacements, and the arrows point to collapse structures that resulted from dorsoventral crushing. The location of the anterior end of the brevis fossa (b.f.) and the reconstruction of the ilium (B) demonstrates the very elongate postacetabular process of this specimen. The black area in A represents matrix.

While the postacetabular process length was increased slightly due to fault displacements, these small deformations can be measured and the reconstructed postacetabular process (Figure 5.3B) remains proportionally long. The measured length of the postacetabular process (to the anterior notch) is currently 265 mm, and predefromational length is estimated at 255 mm. The elongate postacetabular blade is at least 180% the depth of the blade at the anterior edge of the brevis fossa (Figure 5.3A); the anterior edge of the fossa is 98 mm from posterior edge of blade, the current depth

above the anterior fossa boundary is 45 mm and the predeformation height is estimated at 50 mm. The lateral surface of the ilium shows at least three telescoping collapse fronts (Figure 5.3A), which demonstrates some dorsoventral compression has occurred prior to the oblique fault offsets. The amount of dorsoventral compression is not expected to have been great (~ 10 mm), because the neural spines of the articulated sacrals show no evidence of dorsoventral compression. The ilium height at the posterior edge of the ischial peduncle is estimated at 117 mm (107 +10 mm). It does not appear that the posterodorsal edge of the ilium was been broken (and lost) prior to preservation, which would artificially increase the length: height ratio. The sacral ribs are fused 11 mm below the dorsal edge of the ilium. This and other general proportions of the postacetabular dimensions are similar to the right ilium of GF13-III.

A dorsoventral and anteroposterior concave depression on the lateral surface of the ilium remains partially visible and extends anteriorly to a point immediately behind the anterior notch. The dorsal fossa becomes shorter posteriorly, occupying only the ventral portion of the blade and terminating posteriorly beyond the mid-length of the postacetabular process. A second depression located immediately posterior to this posterior termination of the dorsal fossa is dorsoventrally short and anteroposteriorly long, and extends the remainder of the postacetabular process. This posterior depression is interpreted as a deformational collapse artefact (Figure 5.3).

Sinuous ridges that border the posterodorsal part of the dorsal fossa are not due to deformation, but represent sites of muscle origin. Similar to GF13-I, the anterodorsal edge of the ridge is located on the dorsal edge of the ilium, immediately above the anterior edge of the brevis fossa, and from here is directed posteroventrally. However, while the ridge of GF13-I continues in this oblique direction until nearly reaching the posteroventral edge of the ilium, the ridge in GF13-II becomes inflected posterodorsally, and thus demarcates a semicircular area on the dorsal edge of the postacetabular blade. The postacetabular blade is extended well beyond this semicircular fossa and many rugose lines on the posterior portion of the blade represent other areas of muscle origin.

The pubic peduncle is 116 mm long, with the supracetabular crest located at about mid-length and anterior to the anterior notch. The acetabular margin on the pubic peduncle is composed of a wide anterior surface and a narrow medial wall (parallel to the

sagittal plane). As in GF13-I, the medial portion of the acetabulum is interpreted as a deformational artefact; the edge of the acetabulum is inferred to have been directed medially and only slightly ventrally, but due to slight mediolateral compression the medial edge has become oriented parasagittally.

The anterolateral portion of the ischial peduncle has been displaced laterally 2 mm, and is otherwise unaffected by deformation. The lateral surface of the articular facet is 30 mm long (anteroposteriorly) and the maximum depth of the ischial articular facet is 29 mm.

As preserved, the acetabulum is proportionally long, and the length (130 mm) is 200% the acetabulum height (65 mm). The acetabular length is only 145% of the acetabular height for GF13-I. The difference does not appear to be attributed to deformation; the pubic peduncle does not appear displaced anteriorly, but rather maintains a convex dorsal edge. As well, a similar acetabulum proportion is exhibited by the right ilium of GF13-III, which like GF13-II is an elongate ilium blade.

GF13-III

The left ilium is in articulation with the sacrum and is now exposed in dorsal, lateral (Figure 5.4) and ventral view. The ilium measures at least 235 mm from the anterior notch to the postacetabular processes distal end. A 30 mm oblique fault through the postacetabular process contributes 15 mm in elongation; therefore the pre-deformation length of the postacetabular process is estimated at 220 mm. Regardless, prior to deformation the postacetabular process was elongate and dorsoventrally short, similar in proportions to the process of GF13-II.

The dorsal edge of the preacetabular process is inflected laterally in relation to the ventral edge, and is rounded and broad, rather than narrow and pointed as in GF13-II. Several rugose ridges can still be identified on the dorsal distal edge of the preacetabular process; therefore the full length and height appear to be preserved. The length of the preacetabular process is equal to the base height (38 mm). It narrows only slightly distally (25 mm). The broad and inflected morphology of the left preacetabular process is interpreted as a deformational artefact (see right ilium).

Above the acetabulum, 40 mm of the dorsal rim of the ilium was damaged during collection and preparation, but the shape of the edge can be accurately reconstructed based on the adjacently preserved portions. The neural spines of the posterior dorsals of GF13-I currently cover a portion of the dorsal iliac edge, posterior to the acetabulum. The lateral surface of the ilium above the acetabulum is concave from the cranial notch to the posterior edge of the ischial peduncle. The ventral edge of this dorsal fossa appears to have been located slightly above the acetabulum.

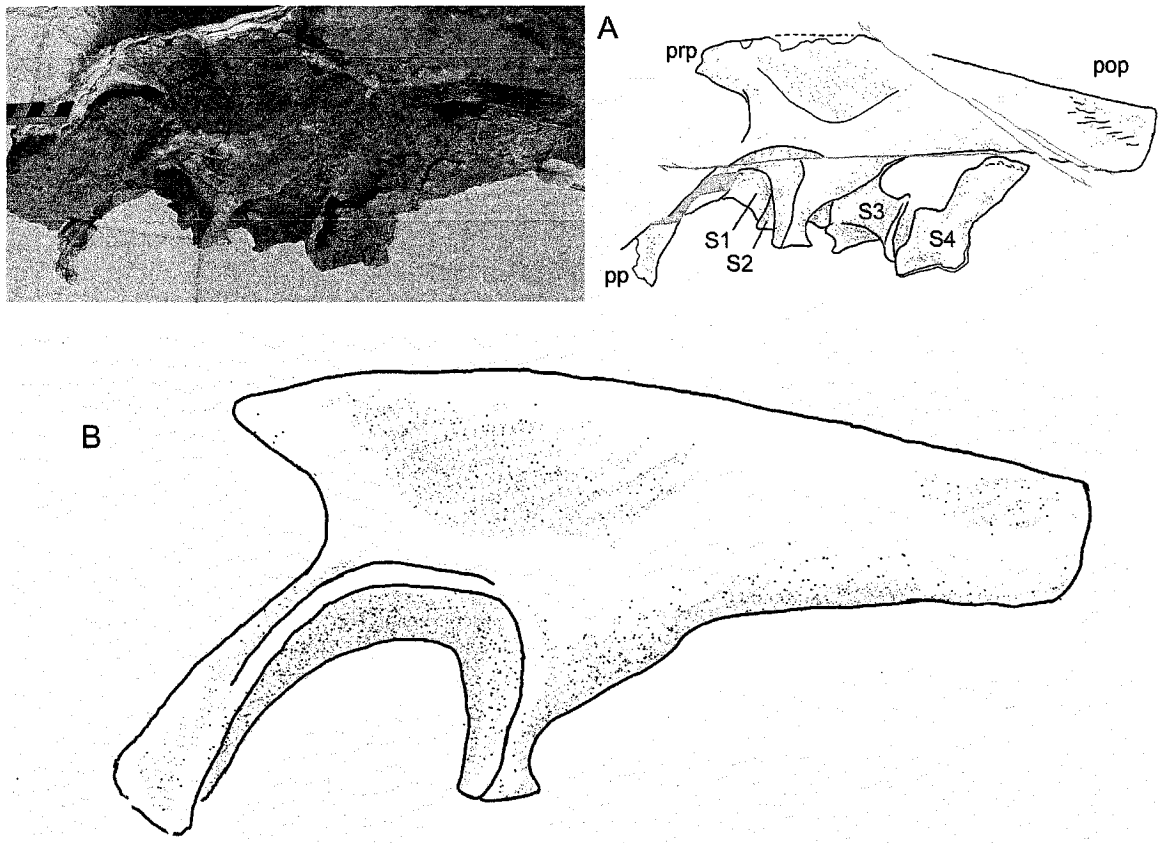

Figure 5.4: The left ilium of GF13-III in lateral view (A) and the reconstruction (B) after accounting for several faults (grey lines) and fault surfaces (grey shading), which demonstrates the elongate postacetabular blade of this specimen.
Abbreviations: pop, postacetabular process; pp, pubic peduncle; prp, preacetabular process; S1-S4, sacrals 1-4.

The 60 mm long ischial peduncle is displaced anteriorly (30 mm) and medially (6 mm), due to a fault that also crosses the distal edges of the third sacral vertebra and postacetabular process of the GF13-I left ilium. The articular surface on the distal end of

the ischial peduncle is widest medially (25 mm), and has rounded anterior and posterior medial-corners, a straight anterior edge (34 mm) and rounded posterior edge. The articular surface is concave, with rugose patterning. The lateral edge of the ischial peduncle is developed into a rather sharp ridge. The anterior edge of the brevis fossa is difficult to identify with certainty in the left ilium due to faulting, although it appears to be located about 140 mm from the distal end, as in the posterior fragment of the right ilium.

The medial edge of the left acetabulum is directed medially, with no ventrally projecting portion. The orientation of the medial edge of the right acetabulum wall cannot be determined, as it remains covered by matrix. The anterior portion of a right ilium (Figure 5.5A) is exposed in medial view. Although currently unable to be connected and attached, a portion of a long postacetabular process of a right ilium (Figure 5.5B and C), was removed several centimetres from the same location in the quarry two years before (1998). It shows the same preservational features, and most certainly represents the posterior portion of this ilium. The right ilium is already accounted for in GF13-I and GF13-II; therefore the ilium can be confidently associated with GF13-III, based on the close proximity of these specimens during collection (Figure 4.2) as well as the similar length of the preacetabular processes (38 mm) and ischial peduncles (60 mm). As the right pubis of GF13-III was preserved in an appropriate position to have been articulated to the pelvis, the right ilium likely disarticulated only a short time before, perhaps as a result of final burial.

The morphological differences of the right and left preacetabular process are interpreted as due to preservational deformation. The right preacetabular process is pointed, the dorsal edge 30° from the ventral edge (similar to GF13-II), with the dorsal rim located medial to the ventral edge. The mediolateral compression and translation of the dorsal edge of the left preacetabular process laterally in relation to the rest of the ilium is consistent with the deformational collapse patterns exhibited by the posterior dorsal centra and ribs of GF13-I. Having not found any other major differences between the preserved portions of the two ilia, it is concluded here the unique morphology of the left ilium preacetabular process is attributable to compression deformation.

The posterior portion of the right ilium includes the posterior end and a dorsoventrally expanded section that is consistent with the posterior edge of the ischial peduncle. In medial view (Figure 5.5A and B), the articular surfaces for the sacral rib complexes remain present as a medially expanded ridge, and this is also interpreted as the medial limit of the brevis fossa. Following this interpretation, the brevis fossa is well developed, and extends to the distal end of the postacetabular process. A similar strong ridge is found on GF13-II, but not on GF13-I.

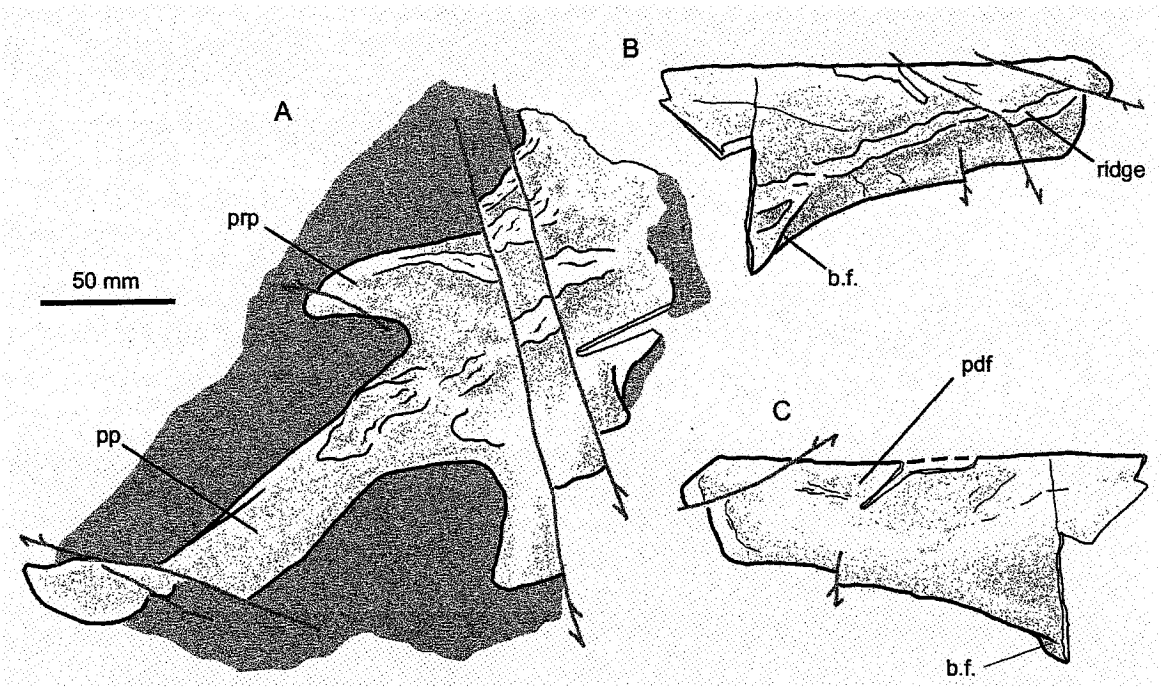

Figure 5.5: Two portions (FGM998GF13.46 – A, FGM998GF13.49 – B, C) of a disarticulated right ilium in medial (A,B) and lateral (C) views.
The preacetabular process (prp) is short and pointed, the pubic peduncle (pp) distal end is faulted anteriorly, and two other faults offset the ischial peduncle dorsally. A very well developed ridge is present in medial view, representing the articular surfaces for the sacral ribs. The anterior point of the brevis fossa (b.f.) is demonstrates the elongate postacetabular process.

The lengths of the left pubic peduncle and acetabulum cannot be reliably determined; the distal portion of the pubic peduncle has been displaced by two faults and the distal end was severed by a rock-saw cut and was apparently lost. The distal end of the right pubic penduncle is translated anteriorly (31 mm), but a reasonable estimate for the peduncle length is 140 mm. The length of the right acetabulum is estimated at 110 mm after accounting for the anterior fault displacement of the distal end of the pubic peduncle. The height of the acetabulum is 50 mm, therefore the proportions of the

acetabulum are similar to GF13-II. The lateral surface of the right postacetabular blade also shows the posteroventral fossa was located similarly as in GF13-II. A series of anteroventrally directed rugose ridges emanate from the posterodorsal corner of the ilium. Again the ridges are similar to those on the ilial lateral surface of GF13-II.

GF69

Although affected by several displacement faults, the right ilium is exposed in lateral (Figure 5.6) and dorsal view, and is nearly complete except for the distal end of the ischial peduncle and a small portion of the postacetabular process. The distal portion of the right pubic peduncle is affected by two small displacement faults, making it appear short; the length can only be estimated at 55 mm. These faults can be traced through the lateral process/rib of the posterior dorsal vertebra and are located anterior to the tip of the preacetabular process; the preacetabular process was therefore not affected by faulting and represents the complete length. The left ilium is now also partially exposed in lateral view, although the region anterior to the middle of the acetabulum is offset dorsally by several faults and is deformed beyond interpretation.

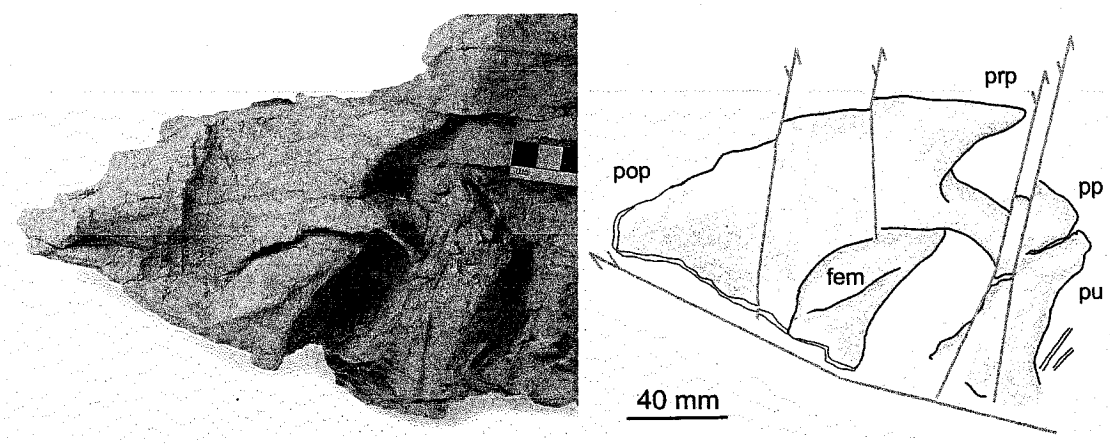

Figure 5.6: Right ilium, pubis (pu) and femur (fem) of GF69 in lateral view.
The pubic peduncle is deformationally shortened by two faults (grey lines), but these faults do not affect the preacetabular process (prp). The postacetabular process (pop) and ischial peduncle are truncated by a large fault.

The right ilium demonstrates that although GF69 is similar in size to the largest *Anchisaurus* specimen (YPM 208), GF69 does not demonstrate the autapomorphic characters of the *Anchisaurus* ilium. The height of the ilium above the acetabulum is the

same for YPM 208 (48 mm) and GF69 (50 mm), and this similarity in size is also reaffirmed by the similar metatarsal lengths of the specimens (see Chapter 5). The length of the GF69 preacetabular process, measured to a line perpendicular to the anterior notch is 34 mm and equal to its depth (height) along this line. This differs from *Anchisaurus*, which has a length more than twice its depth (Yates 2003). Also, as seen in lateral view, the ventral edge is shallowly concave and directed almost 90° to the dorsal surface of the pubic peduncle; therefore the process is not oriented acutely, as in *Anchisaurus* (Yates 2004).

The ilium of *Anchisaurus* (YPM 208) measures 130 mm from the preacetabular to postacetabular process distal ends, while that of GF69 is 160 mm in length. The longer ilium length of GF69 is interpreted here as a feature of the elongate postacetabular blade of GF69. The lateral surface of the preacetabular process is directed dorsolaterally; the ventral edge of the process is lateral to the dorsal edge. The rib of the first sacral vertebra contacts the posterior portion of the medial surface of the preacetabular process. Due to the deformations of the pubic peduncle, the length and height of the acetabulum cannot be determined.

Ischium

General

As a consequence of deformation, a limited number of ischial measurements can be determined. The ischium length is measured from the articular facet for the ilium to the distal edge of the blade. The lateromedial width of a single ischial blade is measured near the mid-length of the symphyseal portion of the blade, and the dorsoventral depth of the blade is the greatest width perpendicular to the mediolateral width. The subacetabular length of the ischium is measured from the pubic articular facet to the anterior edge of the iliac facet. The ischial proportions and sizes are similar for GF13-I and GF13-II, whereas GF9 and GF69 are both about 80% the size of GF13-I.

All ischia from the bone bed have an anterolaterally inclined surface located anterior to the ilial articular facet, which represents the ischial component of the antitrochanter (Fraser et al. 2002, Langer 2004). The ischia differ from that of

Saturnalia, which has an antitrochanter that occupies the entire subacetabular area from the ilia peduncle to pubic peduncle (Langer 2003).

Only one specimen, GF69, has both a pubis and ischium that are confidently associated together. However, the proximal ischium and pubis are deformed by many faults and little comparative information can be gleaned from this specimen. Although GF13-III has a (right) pubis associated by articulation, it remains unlikely the disarticulated ischia (GF9.19) associates with GF13-III due to the apparent small sizes of the ischia. While GF13-I and GF13-II include articulated ischia and lack associated pubi, based on the evidence available the isolated pubis (GF13.130) likely associates with GF13-I. It remains possible the pubis should be associated with GF13-II or represents another specimen altogether. Regardless of the incomplete and faulted nature of most material, the morphologies of the ischia and pubi, and their relative proportions based on the available evidence, provide further evidence for the presence of two morphs.

GF13-I

The right and left ischia (GF13.19) remain tightly articulated along the median symphysis, but the distal 165 mm is offset toward the right side by a 65 mm displacement fault. A second fault displaces the distal 80 mm of the blades 20 mm ventrally (Figure 5.7). The distal ends of the ischial blades are poorly preserved, having undergone internal shrinkage during drying and subsequently were heavily consolidated. The ischia are complete, although the posterior corner of the right proximal end (containing the ilial articular facet) remains attached to the right ilium, and the entire subacetabular region of the left side remains attached to the sacral block.

The symphyseal portions of the ischial blades have also experienced lateral deformation; the left ischial blade displaced into the medial edge of the right blade. Although the ischium is faulted in several places, the length of the ischium can be reasonably estimated at 260 mm, and a single ischial blade is 37 mm wide (measured 110 mm from the distal end) and 15 mm deep. The depth of the distal end cannot be determined due to damage and incomplete preparation.

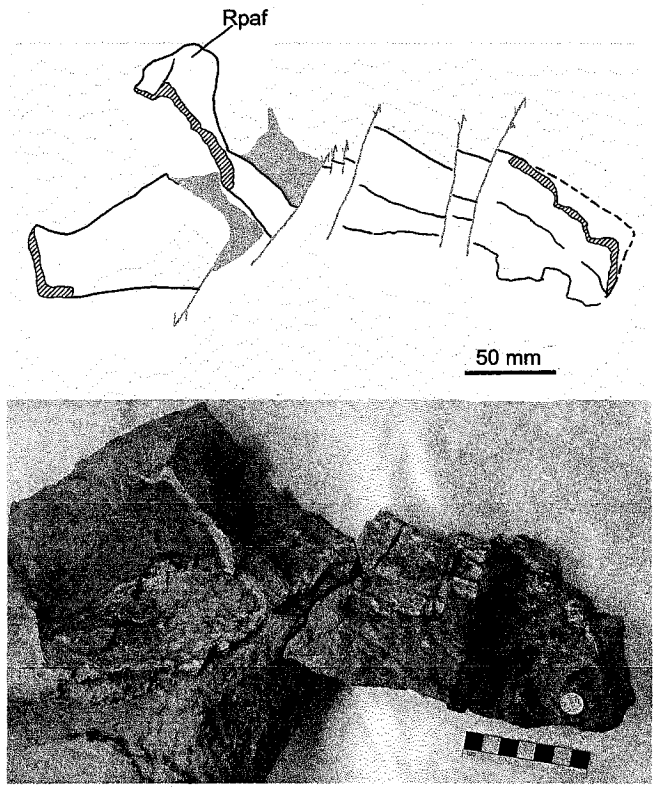

Figure 5.7: The articulated right and left ischia of GF13-I as seen in dorsal view are deformed by several faults (grey lines and shading).
The right articular facet for the pubis (Rpaf) is the only proximal portion that remains in contact with the distal blades, however the rest of the right proximal blade remains with the ischial peduncle of the right ilium and can be reattached (see Figure 5.8). The left proximal portion remains attached to the underside of the sacral vertebrae.

The ilial articular facet is sub-circular, 35 mm long (anteroposteriorly), with a straight anterior margin. Anterior to the ilial facet, a slightly smaller facet-like surface is directed anterolaterally, and represents the ischium component of the antitrochanter (Figure 5.8). The subacetabular portion of the ischium on the right side is 60 mm long, or 63% of the acetabulum length of the ilium (95 mm). The pubis for GF13-I is expected to have occupied the remaining 35 mm of the subacetabular region, and the isolated right pubis (GF13.130) with a subacetabular length of 40 mm is a reasonable match. The relatively shorter pubic subacetabular length differs from that of *Anchisaurus*, *Gyposaurus*, *Jingshanosaurus*, *Riojasaurus* and *Yunnanosaurus,* where the pubic and ischial subacetabular lengths are equal (Galton and Upchurch 2004). The dorsoventral depth of the pubic facet of the ischium is 55 mm.

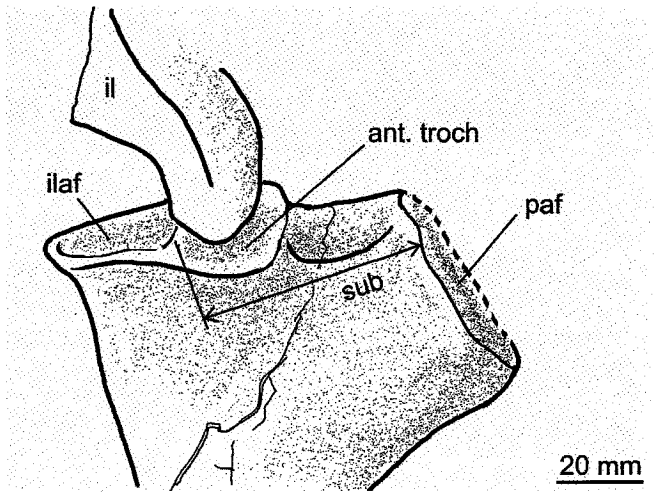

Figure 5.8: Proximal portion of the right ischium of GF13-I in lateral view.
The ichial peduncle of the ilium (il) has disarticulated from the articular facet on the ischium (ilaf) and now overlies the antitrochanter (ant. troch). The medial edge of the pubis articular facet (paf) remains covered in matrix and is shown in a dashed line. The subacetabular region of the ischium (sub) is 60 mm in length.

GF13-II

The two ischia of GF13-II remain fused together and were in near articulation with the right ilium; however the distal portions were extensively crushed during preservation (Figure 5.9). The ischial length (measured on right side) is 260 mm, and is seven times the transverse width of a single ischial blade (37 mm) at mid-length. The broadness is certainly exaggerated due to the extreme dorsoventral crushing. The left ischial blade has also been strongly compressed mediolaterally. The distal ends are thickened dorsoventrally (15 mm), especially along the medial edge.

The right ilial articular facet is 36 mm wide, and the antitrochanter measures 65 mm in length. The pubic articular surface is 55 mm deep and 15 mm wide. The left ilial articular facet appears of to be of similar proportions, although it currently remains covered by matrix. On the left side, a 40 mm long concave depression separates the antitrochanter from the anterior edge, and with the 65 mm long antitrochanter exposed on the right side, the subacetabular region of the ischium is estimated at 105 mm. The ischium therefore occupied nearly 85% of the subacetabular region, which is more than that of GF13-I (63%) and similar to that expected for GF13-III (90%). Therefore, all

specimens from the bone bed have pubis subacetabular lengths much less than the ischium subacetabular lengths.

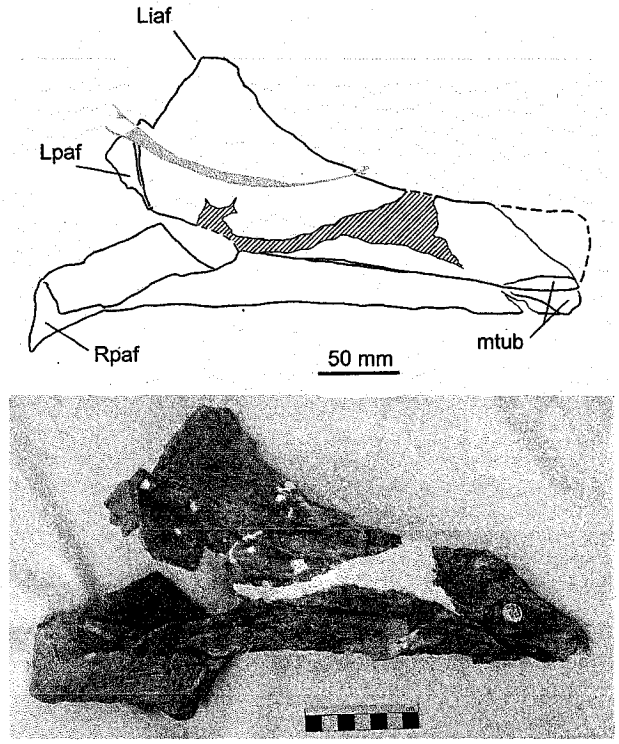

Figure 5.9: The articulated right and left ischia of GF13-II in ventral view.
The distal blades are flattened due to compression, and a rock-saw cut and missing portion has been reconstructed with plaster (cross-hatching). The left ilial articular surface (Liaf) and pubic articular surface (Lpaf) are well preserved, although an oblique fault (grey line) deforms the proximal blade between the two facets. The distal end of the left side has been reconstructed, but the dorsoventral thickening of the distal end is clearly restricted to the medial edge, resulting in medial tuberosities (mtub).

GF13-III

No ischium is articulated or located adjacent to the pelvic girdle of GF13-III. Although it remains possible that the ischium collected among the material of GF9 associates with the specimen, the ischium of GF9 is shorter than that expected and therefore likely represents a separate specimen.

GF9

The right and left ischia (FGM998GF9.19) remain articulated, although the proximal end of the distal blades are slightly separated (Figure 5.10). The right ischium is nearly complete, but the proximal end has several small fault displacements and the

distal end has been severed by a rock-saw cut. The left ischial proximal end was fractured and separated prior to burial, but it was recovered near by (GF9.15) and only a small missing section prevents the reattachment of these portions. The distal end of the left ischium is currently missing.

Like all of the ischia from the bone bed, the distal blades are mediolaterally wider than dorsoventrally deep. The right ischium, from ilial facet to the distal tip of the blade, is 210 mm long, and the mid-shaft width of a single blade is 30 mm. Therefore the ischium is of similar proportions (width equals 14% length) but only 80% the length as the ischium of GF13-II.

The posterior edge of the ilial facet is missing due to a rock saw cut, and the preserved portion is relatively narrower than the facet of GF13-I and GF13-II, but this is likely due to mediolateral crushing. Located anterior to the ilial articular facet, the ischial component of the antitrochanter is directed anterolaterally.

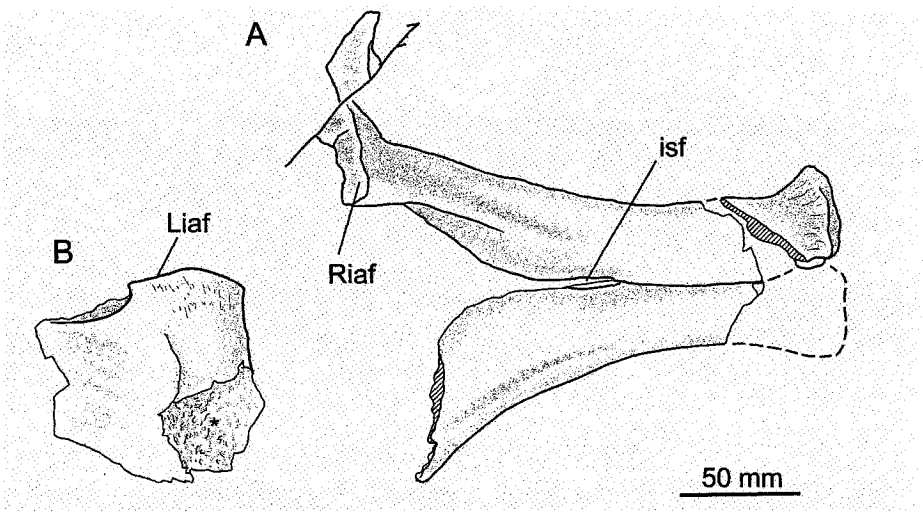

Figure 5.10: The articulated right and left ischia of GF9 (A) and the proximal portion of the left side (B) that was fractured and separated from the rest of the ischium prior to burial, in dorsal (A) and lateral (B) views.
The right proximal plate is deformed by an offset fault (grey line), but the right (Riaf) and left (Liaf) articular facets for the ilium are well preserved. An intersymphyseal foramen (isf) appears to be present, although somewhat difficult to confirm due to the slight separation of the distal blades. Intercortical bone surface (*), and sharp fracture surfaces are evident on the left lateral plate, demonstrating the taphonomic breakage of the ischium occurred prior to final burial.

The right and left ischia have shifted slightly along the medial suture, however an interischial foramen remains identifiable along the symphysial margin, about one quarter of the way from the proximal margin of the symphysis (Figure 5.10). The ischial blades

are narrower along the lateral edge, similar to the sharp lateral edges of *Anchisaurus* (YPM 208, see Yates 2004, Fig. 2). As demonstrated on the right side, the distal end is robustly expanded 26 mm deep dorsoventrally and slightly laterally, compared to the depth at mid-length (12 mm), which is similar to GF13-II and GF69.

The subacetabular length of the ischium cannot be reliably determined. The left side is incomplete due to broken and missing bone. The right side is deformed by several faults, and may also be missing a portion anteriorly. The minimum subacetabular length is 70 mm, measured on the right side. If the ischium of GF9 does associate with GF13-III, it is expected to have a subacetabular length of 100 mm (110 – 10 mm of pubis). Based on this smaller subacetabular length and overall small size of the ischium it is unlikely GF9 should be referred to GF13-III; rather this ischium most likely represents a separate (fifth) specimen.

GF69

Both the right and left ischia remain in articulation with the pelvis, but the proximal ends of the ischia were truncated by the large fault cutting through the block and by many other small transversely oriented faults. The ischial length was at least 210 mm. The long axis of the ischial distal blades was parallel to the bedding surface, which resulted in mediolateral compression and the extreme narrowness of the blades. The distal ischial blades exhibit medially positioned dorsoventral thickened tuberosities, similar to GF13-II and GF9.

Pubis

Similar to the two iliac morphs (long or blunt postacetabular processes), the two right pubes recovered from the bone bed also suggest the presence of two distinct morphs; one pubic morph with a narrow distal apron (16% pubis length), and the other morph with a broad distal apron (26% pubis length) and relatively shorter subacetabular component. The pubis with the broad distal apron was in close association with the pelvis of GF13-III, an elongate ilial morph. The narrow pubis was disarticulated, and based on the length of the subacetabular component and its different morphology, this pubis likely associates with specimen GF13-I (blunt ilial morph).

GF13-I?

A disarticulated right pubis (FGM998GF13.130) was recovered in a block with an isolated left femur (FGM998GF13.128), near the dorsal vertebrae, left coracoid and other pectoral girdle elements of GF13-II. While the pubis and femur were recovered one metre from the sacrum and pelvic girdle of GF13-II (Chapter 3), and two metres from the similar structures of GF13-I, associating the pubis to GF13-II based on proximity is not supported by other evidence. Based on size, the pubis could be referred to either GF13-I or GF13-II. However, the pubic subacetabular length (40 mm) is only slightly longer than that expected for the (unknown) pubis of GF13-I (35 mm), but is much longer than that expected for (unknown) pubis of GF13-II (25 mm)

A small portion of the pubis that bordered the ventral edge of the obturator foramen was broken prior to preservation. The foramen was circular, with a diameter of 22 mm. However, the missing portion gives the obturator foramen an oval shape (with a length of 45 mm and width of 22 mm). Regardless of the size and shape, the foramen is only partially visible in anterior view. The presence or absence of a pubic tubercle cannot be determined; the lateral surface of the proximal plate was damaged during collection (Figure 5.11).

As preserved, the longitudinal axis of the pubic apron is convex dorsally in lateral view, but this is due to plastic deformation after burial and subsequent faulting. The length of the pubis measured from the articular facet for the ilium to the distal end is at least 380 mm and the maximum transverse width of the apron is 60 mm, or 16% of the total length.

The ilial articular surface is 63 mm long and 25 mm wide. The subacetabular length is 40 mm, and the ischial articular facet is narrow (15 mm) and 56 mm deep (dorsoventrally). These proportions are consistent with the related features of the ischium of GF13-I and support the association of the pubis to this specimen. The referral of the pubis to GF13-I suggests the ischial length (estimate of 260 mm) would represent only 68% of the pubic length, and therefore differs from *Anchisaurus* that has an ischial length more than 90% of the pubic length (Galton and Upchurch 2004).

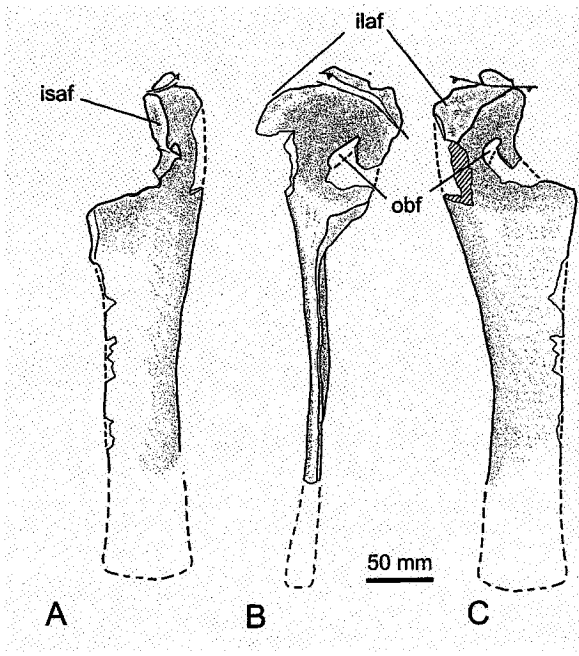

Figure 5.11: A disarticulated right pubis FGM998GF13.130, that likely associates with GF13-I, in posterior (A), medial (B), and anterior views (C).
The distal 80 mm was strongly fault offset and has been reconstructed (dashed lines). The obturator foramen (obf) is only partially visible in anterior view. The dorsal portion of the articular facet for the ischium (isaf) is offset by a small fault (grey line) but the articular facet for the ilium (ilaf) is well preserved.

The pubic apron blade is teardrop shape in cross-section; the deepest portion (14 mm) near the mediolateral midline of the blade, with the medial portion narrow (3 mm) and the lateral edge rounded and only 9 mm deep. The anteroposterior depth of the pubic distal expansion is 25 mm. In anterior view, the lateral edge is concave, recessed 11 mm from the straight line that joins the laterodistal corner to the proximal lateral edge, a feature currently only identified in members of Massospondylidae (*Massospondylus Lufengosaurus*) and *Riojasaurus* (Yates 2004).

GF13-III

The right pubis (FGM998GF13.73) remained in an appropriate orientation and position for articulation with the right ilium, although the ilium became disarticulated prior to final burial. The ventral surface of the posterior dorsals remain in contact with the anterior surface of the pubic distal apron. Most of the pubis was collected along with the dorsal vertebrae in the summer of 2000, and the distal 50% of the blade was collected four years later, but no material was lost along this break surface. The proximal portion

was damaged by several rock saw cuts during collection. The distal third is only exposed in posterior view.

The ilial articular facet is 39 mm wide posteriorly, 42 mm in length along the lateral edge, and narrows to a point on the anterolateral corner. The subacetabular portion of the pubis is short; the vertical articular facet for the ischium is located only 10 mm from the posterior edge of the ilial articular surface. The region between the articular facets is occupied by a recessed surface that extends from the medial to lateral surfaces. The ischial articular facet is at least 50 mm long and 23 mm wide along the dorsal margin, narrowing to a point on the ventromedial edge. The small (22 mm diameter) obturator foramen is fully enclosed by bone within the subacetabular plate, and is only partially visible in anterior view.

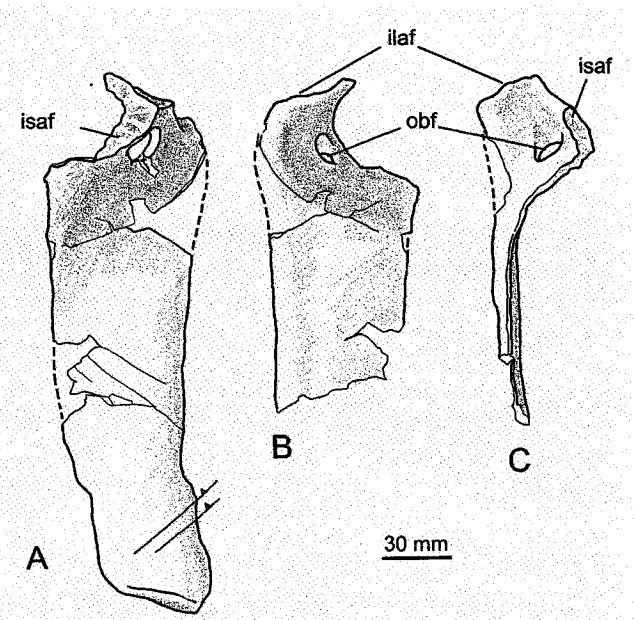

Figure 6.12: Right pubis (FGM998GF13.73) of GF13-III in posterior (A), anterior (B), and medial (C) views.
The obturator foramen (obf) is only partially visible in anterior view (B), and while the articular facets for the ischium (isaf) and ilium (ilaf) do not appear deformed, the subacetabular length of the pubis is very short (10 mm). The distal end is only visible posterior view, the anterior surface remains covered by matrix.

The pubic plate is broad (85 mm wide at mid-length), and represents 26% of the total pubic length (330 mm). The distal end is dorsoventrally expanded compared to the dorsoventral depth at mid-length, 24 mm and 9 mm respectively. The median symphysis

appears to have not extended to the distal end of the pubis, as the medial edge of the distal pubis is inflected. Alternatively this inflection may be due to small fault displacements in this area.

The lateral expanse of the iliac peduncle from the sagittal midline is 110 mm; therefore the pubic apron width (85 mm) is 80% of the expanse of the ilial peduncles, and differs from that of *Anchisaurus*, which has a narrow pubic apron, only 40% of the expanse of the ilial peduncles (Yates 2004).

GF69

Only the proximal portions of the right and left pubis are preserved. However, each is badly deformed by displacement faults, including several that displace the proximal most ends dorsally in relation to the more distal portions, and a large fault that displaced the proximoventral portion posterodorsally 13 cm. The right proximal pubis is partially visible in lateral view (Figure 5.6), and remains tightly articulated with the pubic peduncle of the ilium. The anterodorsal portion of the obturator foramen is still visible, suggesting a diameter of 13 mm, but the remainder of the foramen has been truncated by the 130 mm fault and cannot be reconstructed. The dorsoventral depth of the proximal pubis was approximately 90 mm deep (dorsoventrally), although two displacement faults make a confident assessment impossible. The distal apron was apparently obliterated by the large displacement fault.

Discussion

The specimens from the McCoy Brook Formation can now be confidently distinguished from *Anchisaurus*. The smallest specimen from the bone bed (GF69) is of similar size to the largest specimen of *Anchisaurus* (=*Ammosaurus*) (YPM2 208); the metatarsals of GF69 are only 106% larger than those of YPM 209 (see Chapter 5). The Nova Scotia specimens differ from *Anchisaurus* in lacking an elongate preacetabular process, a relatively long ischial subacetabular length, relatively shorter ischial total length, obturator foramen that is only partially visible in anterior view and a relatively broad pubic plate (over 80% of lateral expanse between iliac articular facets). The ischial

blades are also somewhat similar to the coplanar blades of *Anchisaurus*. Although the blades meet at an angle, it appears to be rather shallow. The significance of these morphological features will be considered within a broader phylogenetic context (see Chapter 8).

Of the elements shared among the bone bed specimens, the ilium provides the strongest evidence for multiple morphs preserved within the bone bed; one morph with a short postacetabular blade (GF13-I), and a second morph with an elongate postacetabular blade (GF13-II and GF13-III). The short postacetabular morph (GF13-I) also has a relatively deeper preacetabular process. The smallest ilium (GF69) appears to have an elongate postacetabular blade, although this remains somewhat uncertain due to incomplete preparation (left) and deformational damage (right). The unique and elongate postacetabular blade cannot be reconciled with deformational distortion, being represented by three different ilia, each exposed to different preservational deformation forces.

Two right pubes of similar length have different relative pubic apron widths; a difference that does not appear to be attributable to incompleteness or deformation. Although the association of the narrow pubis is uncertain, it is considered likely that the pubis associates with GF13-I. Thus associated, the pubis with the broad pubic apron (GF13-III) also differs from that of GF13-I in that the symphysis does not appear to extend to the distal end of the apron, and also has a relatively longer subacetabular component.

As mentioned, the pelvic morphological variation exhibited by the two morphs is not attributable to deformational distortion. Also, as is apparent from the other postcranial skeletal elements, GF13-I and GF13-II are similar based on other postcranial proportions (see following chapters); therefore the morphological differences are not likely attributable to ontogenetic variation. The morphological variation exhibited by the ilia is particularly striking. But consideration of whether the difference represents taxonomic or possibly sexual variation will be considered only after the description of the other postcranial material, and within the proper phylogenetic context.

Chapter 6 – Axial Skeleton Morphology of Specimens within the Lower Jurassic Bone Bed

Abstract

All recovered vertebrae have been distorted by compression deformation and fault displacements during preservation. However, the axial skeletal material provides additional evidence of minor morphological variation among four of the specimens recognized by associated (articulated) material (GF69, GF13-I, GF13-II, GF13-III). The centra of the posterior dorsal vertebrae of GF13-II are longer than tall, whereas those of GF13-I and GF13-III are tall as they are long. The sacrum of GF69 appears to be composed of three vertebrae, whereas the sacra of GF13-I, GF13-II and GF13-III include four vertebrae (by addition of a caudosacral) that contacted the medial surface of the ilium. There is also variation within the morphology of the caudal vertebrae; the centra of the proximal caudal vertebrae of GF13-I are much taller than long but the centra of GF13-II are longer than tall, and the first chevron occurs on the first caudal of GF13-II but the third caudal vertebra of GF13-I.

Introduction

The recovery of an elongate cervical vertebra (PU222126) from Wasson Bluff in 1976 provided evidence the disarticulated skeletal remains represented a 'prosauropod' dinosaur, which was then referred to cf. *Ammosaurus* (Olsen and Gore 1989). The pelvic girdle elements discovered during the current study demonstrate the occurrence of at least two morphs within the bone bed (Chapter 4). Therefore each specimen will continue to be considered separately when describing the various regions of the axial skeleton (cervical, dorsals, sacrals, caudals).

In all but one specimen (GF13-II) the total number of dorsal vertebrae cannot be reliably determined. To accommodate the uncertainty in the total number of dorsal vertebrae, the dorsal vertebrae are identified by their posterior position and increasing (anterior) distance away from the sacrum. The posterior-most dorsal (pD1) lies

immediately anterior to the sacrum, and the preceding dorsal is the second posterior dorsal (pD2). The posterior-most dorsal (pD1) and the first caudal (C1) do not fuse or contact the medial surface of the ilium.

Also, while each of the sacral vertebrae can be identified based on their relative position from anterior to posterior (S1, S2, S3, S4, ect.), the identity of the sacrals can be further determined based on morphological features (Novas 1996, Galton 1999, Moser 2003, Langer 2004). Two sacral vertebrae are plesiomorphic for Dinosauria (SI, SII) , with subsequent vertebrae added anteriorly from the dorsal vertebrae (dorsosacrals, dS) or posteriorly from the caudal vertebrae (caudosacrals, cS). The increase in number of sacral vertebrae within Sauropodomorpha occurs during ontogeny (Mook 1917, Galton 1999) as well phylogenetically (Galton and Upchurch 2004, Upchurch et al. 2004).

Ten cervical vertebrae remain articulated to the skull and dorsal vertebrae of GF13-II, although the posterior cervical vertebrae have been badly deformed by a large fault. While several disarticulated and poorly preserved cervical vertebrae are also associated with GF69, no other specimen from the bone bed has associated cervical vertebrae. Therefore, the cervical vertebrae are considered separately, together with the cranial material of GF13-II (see Chapter 7). Terminology of vertebrae lamination follows that of Wilson (1999) (Figure 6.7).

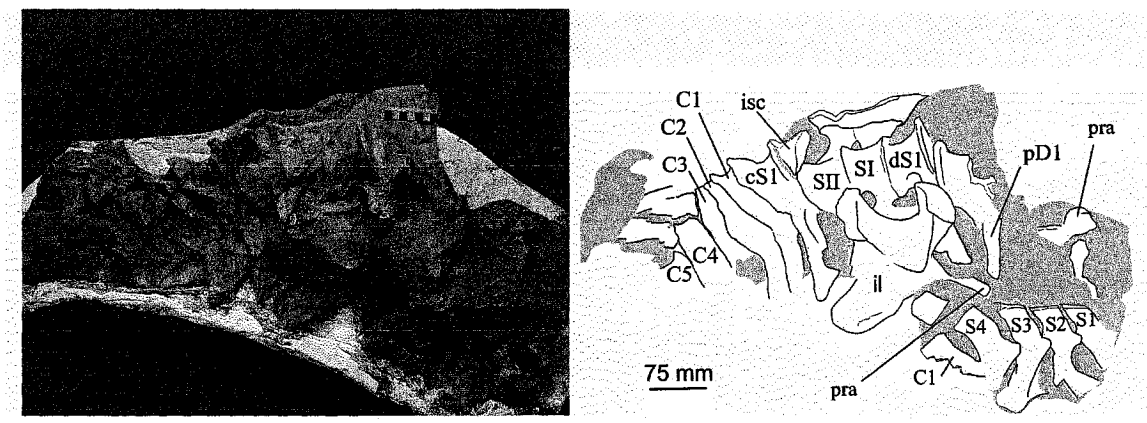

Figure 6.1: Posterior dorsal (pD1), sacral (dS1, SI, SII, cS1) and caudal vertebrae (C1-C5) of GF13-I and the sacral (S1-S4) and first caudal (C1) vertebrae of GF13-III.
The pelvis and associated vertebrae of GF13-I directly overly the left ilium and sacral vertebrae of GF13-III. The distal end of the left rib of the posterior dorsal vertebra (pD1) is medial, and close to the preacetabular process (pra) of the ilium of GF13-I (il).

Description

Dorsal Vertebrae

The posteriormost dorsal vertebrae are represented in all four articulated skeletons (GF69, GF13-I, GF13-II and GF13-III). Many are badly deformed by compression and faulting, which limits the ability to recognize definite morphological differences between specimens. However, as will be demonstrated, the second posterior rib of GF13-I is relatively longer than that of GF13-II, and the centra of GF13-II are also proportionally longer, compared to those of GF13-I and GF13-III.

Table 1: Centrum and neural spine measurements of posterior dorsal vertebrae of specimens GF13-I, GF13-II and GF13-III.
All measurements in millimetres; underlined values are estimates and dashes represent demarcate measurements that could not be determined due to deformation or missing elements.

		13-I	13-II	13-III
1pD	Centrum length (anteroposterior)	52	70	45
1pD	Centrum height (to neural canal edge)	65	50	53
1pD	Neural Spine length (anteroposterior)	44	-	45
1pD	Neural spine height (to dorsum lateral process)	41	-	-
2pD	Centrum length	53	70	45
2pD	Centrum height	68	50	-
2pD	Neural Spine length	-	65	60
2pD	Neural spine height	-	40	40
3pD	Centrum length	-	75	45
3pD	Centrum height	-	50	-
3pD	Neural Spine length	-	66	53
3pD	Neural spine height	-	43	43

GF13-I

Only the two posteriormost dorsal vertebrae were articulated to the sacrum and can therefore be confidently associated with the specimen. The second posterior dorsal vertebra, 98GF-13.31 (Figure 6.2), is completely prepared from the matrix. Both centra are taller than long (Table 1), amphicoelous, and have oval articular surfaces that have a maximum width of 45 mm at mid-height. The right lateral surfaces of the centra were compressed medially during preservation, but the left sides remains reasonably

undeformed. The dorsal half of the central lateral surface is occupied by a shallow pleurocoel fossa, which has a maximum depth of 7 mm (Figure 6.2B).

The neural spines of pD1 and pD2 are partially exposed on the underside of the block; the left side of the neural spines rest against the ilium of GF13-III. The spine of pD1 is only slightly taller (44 mm) than it is long (41 mm), although the anterodistal corner of the spine is displaced anteroventrally 23 mm by a fault. The posterior edge of the neural spine is concave in lateral view, and the distal end is thickened, exhibiting a strong rugose texture. The neural spine of the second posterior dorsal vertebra (GF13.31) is truncated by a fault and was further damaged during collection by a rock-saw, but is similar in proportions to that of pD1.

Each parapophysis of the posterior dorsals is located on the anterior edge of the neural arch, only slightly ventral to the diapophysis (Figure 6.2) and connected to the latter by a short paradiapophyseal lamina. The diapophysis is also ventrally supported by a posterior centrodiapophyseal lamina, which is the posterior boundary of a deep fossa under the lateral process. The circumference of the parapophysis has a thin ridge of bone, especially well developed along the posterior margin.

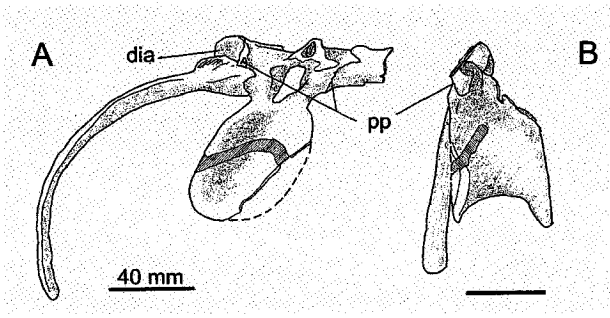

Figure 6.2: Second posterior dorsal vertebra (FGM998GF13.31) associated with specimen GF13-I, in anterior (A), and left lateral view (B).
The amphicoelous vertebral centrum is higher than it is long, and the parapophysis (pp) is nearly level with the diapophysis (dia). Broken and missing bone represented by crosshatch.

The prezygapophyses of pD2 were severed by a rock-saw cut and lost during collection. The prezygapophyses of the pD1 as well as the postzygaposphyses of pD2 require additional preparation; therefore the hyposphene depth cannot be evaluated. The complete left and proximal portion of the right ribs remain attached, and appear fused, to the posterior-most dorsal (pD1). The left rib is 90 mm in length, and the distal end is located medial to the right pubic peduncle (Figure 6.1). The close proximity of the rib to

the preacetabular process is exaggerated due to disarticulation; the centrum of pD1 is displaced from the anterior sacral, shifted dorsally and toward the right side. The complete right rib is articulated with the diapophysis of pD2 (Figure 6.2A) and measures 170 mm in length, which is considerably longer than the second posterior rib of GF13-II. The ribs of both pD1 and pD2 have longitudinal depressions along the posterior edges, especially proximally. The distal end of the pD2 right rib is 150% wider (anteroposteriorly) than the middle of the rib, but this increase is attributed to transverse crushing; the deformation is aligned with the compression on the right side of the centra.

GF13-II

The complete dorsal series of GF13-II was recovered in articulation with both the sacrum and cervical vertebrae, and with all dorsal ribs articulated (Figure 4.2 and Figure 6.3). Several of the anterior dorsals are difficult to identify due to extreme deformation from a large displacement fault, and it is unclear if there are 14 or 15 dorsal vertebrae. The three posterior-most dorsals are partially exposed in right lateral and in ventral left-lateral (Figure 6.3B) views. These vertebrae were split by a parasagittal crack that propagated through the block during collection and preparation.

The **first posterior dorsal** centrum is at least 70 mm long. The anterior portions of the centrum, neural spine and lateral processes were displaced ventrally in relation to the rest of the vertebra, and are located within a small block that connects to the anterior portion of the sacrum (Figure 6.4). The distal tips of the postzygapophyses are separated from the rest of pD1 and remain articulated to the first-sacral prezygapophyses. The spinopostzygapophyseal lamina terminates 3 mm from the distal end of each postzygapophyses and a fragment of hyposphene extends ventrally 14 mm.

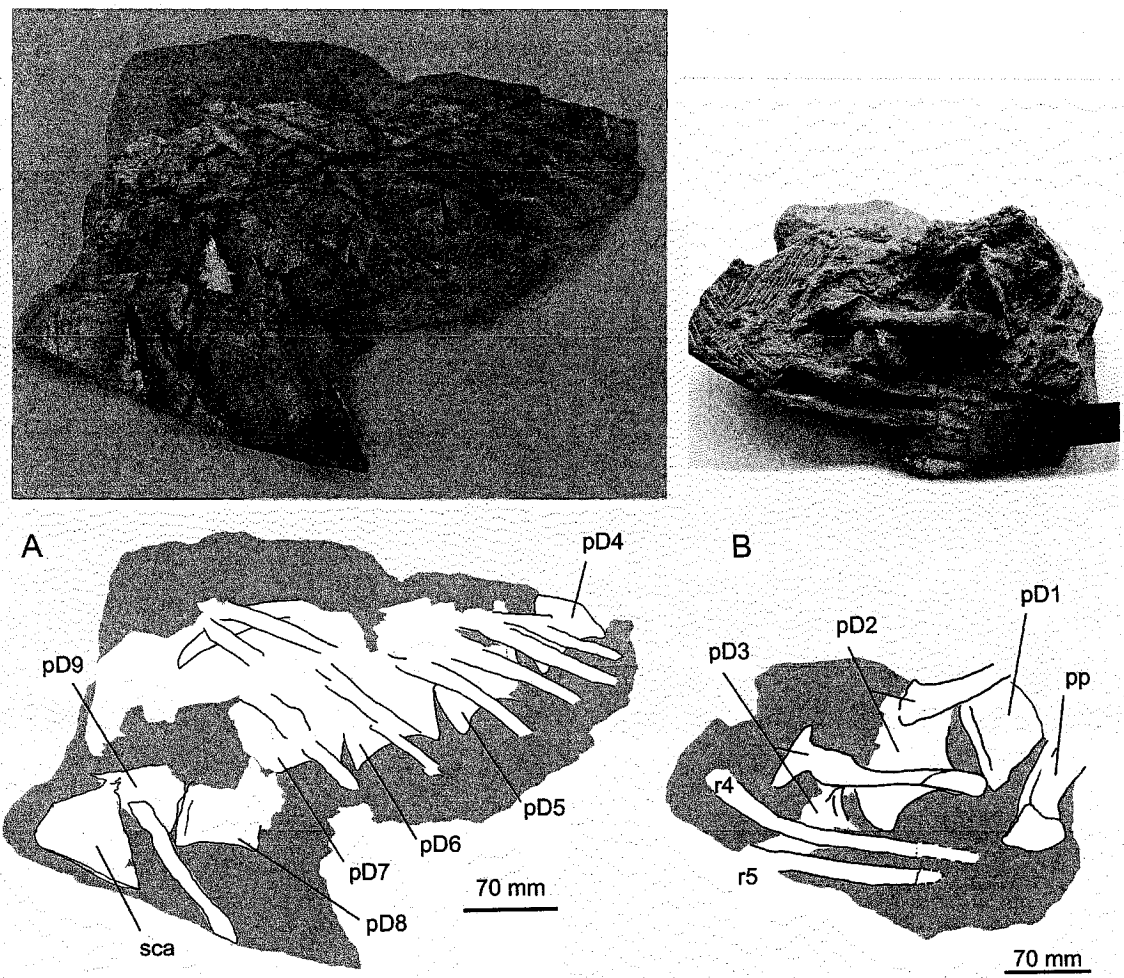

Figure 6.3: Dorsal vertebrae (pD1-pD9) of GF13-II are partially prepared from the sandstone matrix (grey shading) and visible in ventral left-lateral view.
The anterior and mid-dorsal vertebrae are deformed by several faults (A) and remain covered by the left ribs and portions of the left scapula (sca). The posterior dorsal vertebrae (B) are only partially prepared but are clearly longer than tall. The pubic peduncle of the ilium (pp) and the first posterior dorsal are truncated by a fault.

The right rib is of similar length to GF13-I (90 mm long), with the distal end preserved 45 mm anterior to the right ilium preacetabular process. While there appears to have been enough room on the medial edge of the ilium anterior process to accommodate the distal end of the rib, the medial edge of the anterior process remains covered by matrix, so it cannot be determined if a scar is present. Deformation and displacement during preservation rotated the transverse axis of the other posterior dorsal vertebrae counter clockwise (approximately 20°) in dorsal view, which would be consistent with the rib having been located medial to the preacetabular process. While the rib was

apparently not fused to the ilium, the distal end of the rib was positioned close to the preacetabular process.

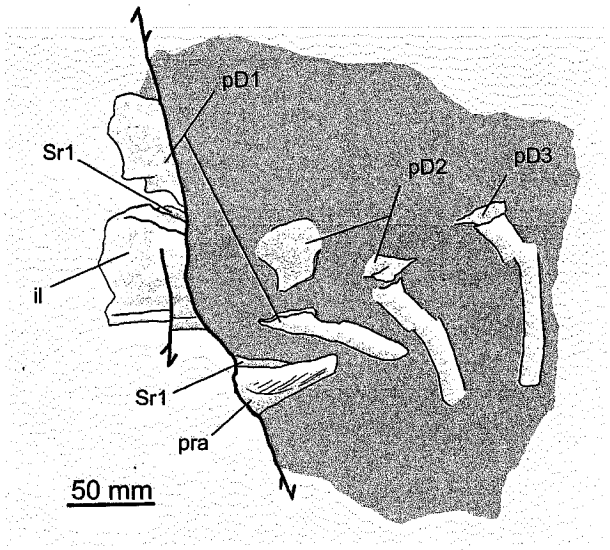

Figure 6.4: Posterior dorsal vertebrae (pD1-3) and ribs in right lateral view.
The preacetabular process of the ilium (pra), pD2-3 and rib of pD1 were offset ventrally by a 120 mm fault. The dorsal portion of the rib of sacral rib 1 (Sr1) can be seen articulated to the medial portion of the preacetabular process, and the rib of the short first posterior dorsal is immediately anterior to the process.

The **second posterior dorsal** vertebra is nearly complete. The centrum is clearly longer than tall (Table 1) and therefore differs from pD2 of GF13-I, which is taller than long. The ventral edge is anteroposteriorly concave in lateral view, recessed 15 mm at mid-length. The centrum appears to be amphicoelous although matrix still covers much of the articular facets.

The neural spine is contained in a separate block, but it can be reattached cleanly to the broken surfaces on the centrum. The neural spine is longer than high and nearly as long as the centrum (Table 1). In lateral view the spine has a concave posterior edge and convex anterodorsal profile. Matrix obscures the postzygapophyses, but a deep fossa is partially visible on the posteroventral edge of the neural spine. The ribs remain articulated to the 35 mm long lateral processes; the right rib has a small offset fault at mid-length but measures 90 mm in total length. Compared to the rib of GF13-I, which is 3.0 times the centrum length, the rib of GF13-II is considerably shorter (1.3 times centrum length), although the specimen appears to be of similar size based on metatarsal lengths (see Chapter 6). The complete third posterior dorsal rib is 110 mm long.

The **other dorsal vertebrae** are only partially exposed (Figure 6.3A) and offer limited additional information. All of the ribs (left and right) remain articulated to the axial skeleton, and unfortunately cover many of the details of the lateral surface of the vertebrae. Several faults have also deformed the ribs and underlying vertebrae. Similar to the posterior dorsals, based on the exposed surfaces the mid-dorsal centra appear to be slightly longer than tall.

GF13-III

The four posteriormost dorsal centra were recovered in articulation with the sacrum of GF13-III but these vertebrae were deformed dorsoventrally. Listed from posterior to anterior the vertebrae are: 98GF13.57 (pD1), 98GF13.90 (pD2), 98GF13.89 (pD3), 98GF13.72 (pD4). Two additional vertebrae recovered immediately anterior to the articulated series are not dorsoventrally deformed; one (98GF13.60) represents pD5, while the other (98GF13.62) is a more anterior dorsal (likely D3) based on the anteroposteriorly short and dorsoventrally tall neural spine.

Each of the four articulated posterior dorsal centra are 45 mm long. Due to the dorsoventral compression, height and width measurements for the articular surfaces of the centrum cannot be determined. Likewise, the lateral surfaces of the centra offer little useful information. Although affected by fault deformation, the components dorsal to the neural arch have not been strongly affected by the dorsoventral compression. As with GF13-I and GF13-III, all vertebrae lack spinodiapophyseal laminae.

The **first posterior dorsal** neural spine is missing, having been broken during collection and is currently missing. Based on the preserved proximal portion, the neural spine anteroposterior length is as long as the centrum (Table 1). The other posterior dorsal neural spines are also as long as the respective centra and this does not appear to be due to deformation; the long neural spines are a result of the strongly developed spinopostzygapophyseal laminae. The posterior portion of the postzygapophyses were severed by a rock-saw cut, but the distal tips remain articulated to the anterior sacral prezygapophyses. The posterior portions of the hyposphene was lost during preparation, yet the proximal portion of the hyposphene extends at least 12 mm from the ventral surface of the postzygapophyses articular surfaces, which are planar and oriented

horizontally. The lateral edges of the postzygapophyses span 40 mm, and are therefore nearly as wide as the centrum is long. The postzygadiapophyseal lamina is embayed along the posterior margin of the dorsoventrally thin lateral process. The prezygapophyses remain obscured by matrix and the overlying postzygapophyses of pD2, and the distal ends of the diapophyses are missing.

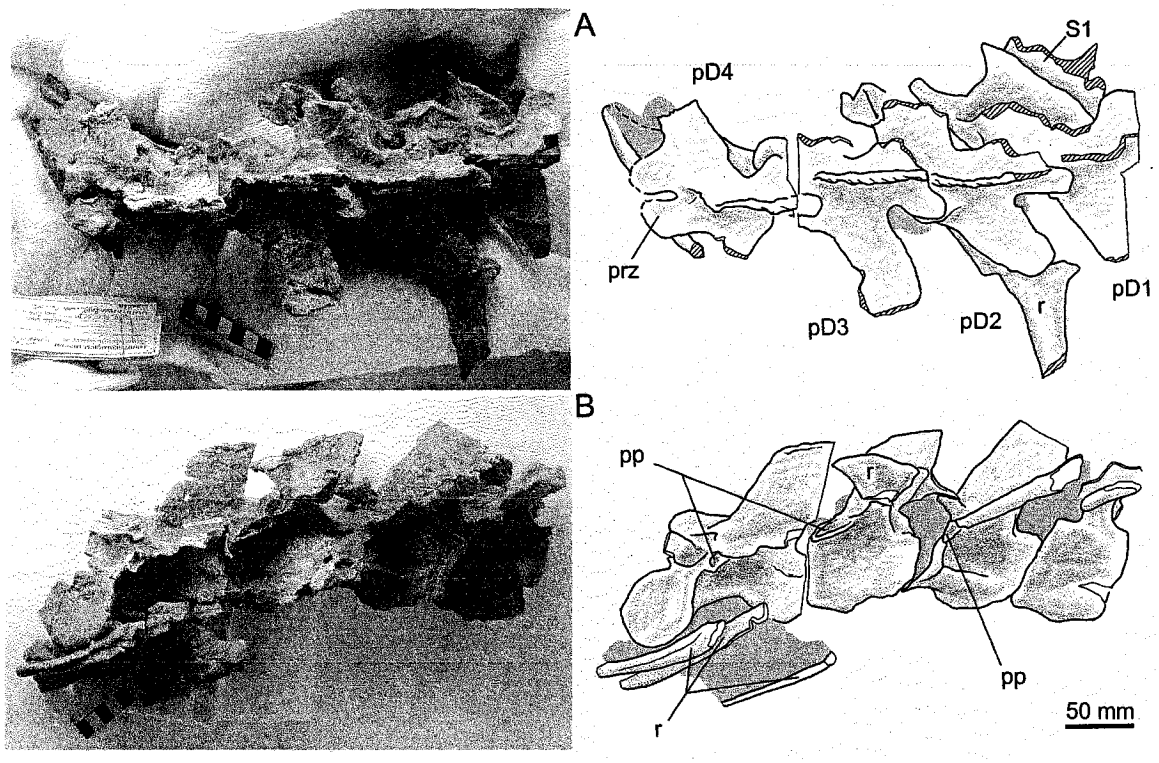

Figure 6.5: Posterior four dorsal vertebrae (pD1-pD4) of GF13-III in dorsal (A) and lateral (B) views. The lateral surfaces of the centra are collapsed due to strong dorsoventral crushing. The parapophyses (pp) are horizontally adjacent to the lateral processes. The anterior portion of the centrum of the anterior sacral (S1) remains attached to the dorsals. Although damaged during collection and preparation, the ribs (r) had remained articulated.

As a result of dorsoventral crushing, the posterior face of the centrum is wider than tall; 67 mm and 53 mm respectively. As the central length is 45 mm, the centrum was certainly taller than long. The fourth posterior dorsal (98GF13.72) is also wider than tall (61 mm versus 47 mm) due to dorsoventral compression, and considering the centrum length is 51 mm the centrum was at least as tall as long. As the other posterior dorsal centra remain tightly articulated, the heights of the other centra cannot be determined. The proportions of the centrum (taller than long) are therefore similar to GF13-I. The

elongate nature of the posterior centra of GF13-II is not attributable to deformation. Therefore the relative lengths of the posterior dorsals differ between two specimens that have an elongate postacetabular ilium (GF13-II and GF13-III).

The **second posterior dorsal** neural spine was longer than tall (Table 1), although the posterodorsal tip of the neural spine was broken off during collection and has not yet been recovered. The posterior edge of the neural spine (spinopostzygapophyseal lamina) is concave in lateral view, and overhangs the intercentrum space. The proximal portions of the right and left ribs remain articulated to the diapophyses and parapophyses, but the distal portions have been lost. The parapophysis is horizontally aligned with the diapophysis.

The neural spine of the **third posterior dorsal** is also long compared to its height above the postzygadiapophyseal lamina and the length of the centrum (Table 1), as in GF13-II; the condition of GF13-I cannot be evaluated. The spinopostzygapophyseal laminae extend to the end of the postzygapophyses and bound a deep fossa on the posterior margin of the neural spine. The parapophyses are located directly under (not behind) the prezygapophysial articular surfaces of pD3 and pD4. The parapophyses are obliquely oriented ovals, the posterior edge dorsoventrally taller than the anterior edge, with well developed margins. The posterior centrodiapophyseal lamina is present but not strongly developed, similar to the other posterior dorsals.

The **fifth posterior dorsal** (Figure 6.6) is one of the best preserved vertebra recovered from the bone bed. Although this vertebra was not directly articulated to pD4, it was located immediately anterior to it, and is of appropriate proportions to suggest it can be reliably associated. The centrum is nearly as long (57 mm) as it is tall (55 mm). The vertebra is slightly deformed obliquely, with the right side displaced anteriorly. The posterior edge of the left lateral process is parallel to the posterior face of the centrum, suggesting that prior to deformation the process was directed laterally. Two small (5 mm) displacement faults offset the right portion of the anterior centrum articular facet and anterior portion of the right parapophysis toward the right side, and the right lateral face of the centrum shows some collapse distortion. An oblique rock-saw cut traverses through most of the centrum, and is now filled with plaster.

The amphicoelous and oval articular facets of the centrum are taller (55 mm) than wide (45 mm). A small convex dimple located in the centre of the otherwise concave anterior face may be a preservation artefact, as it is not noted in other vertebrae. The dorsal margins of the articular facets are straight and represent the ventral edges of the neural canal.

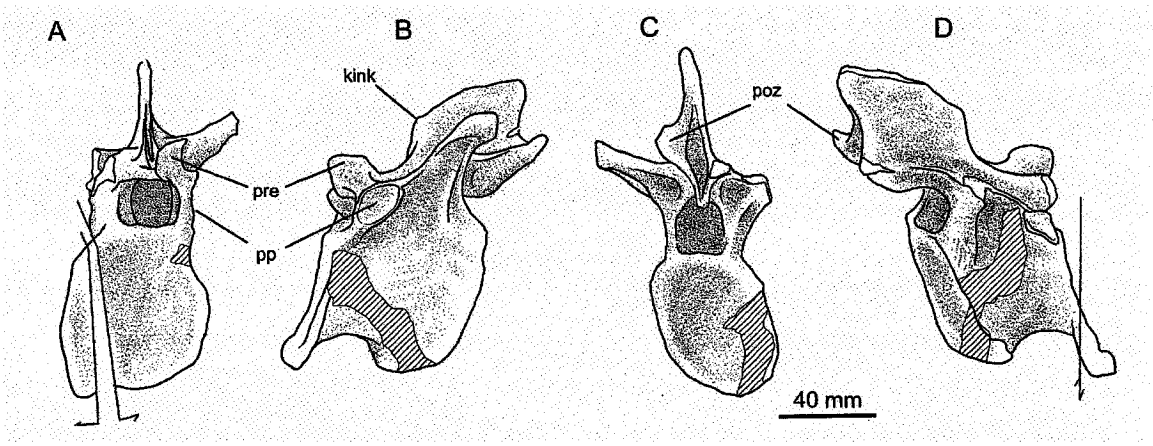

Figure 6.6: The fifth posterior dorsal of GF13-III in anterior (A), left lateral (B), posterior (C) and right lateral (D) views.
The anterior edge of the neural spine has a small tuberance (kink) at about mid-height, likely representative of an tendon or ligament insertion point. An oblique rock-saw cut through the centrum has been filled with plaster (crosshatching). The anterior centrum facet has been offset by a small fault (grey lines). Other Abbreviations: prezygapophyses (pre), postzygapophyses (poz) and parapophysis (pp).

The parapophysis is entirely on the neural arch and is posterior to the articular surface of the prezygapophysis. The oval parapophysis has a long axis (19 mm) directed posterodorsally from the anterior edge of the centrum, and a circumference composed of a well developed but thin ridge of bone. The paradiapophyseal lamina contacts the posterodorsal margin of the parapophysis, and together with the posterior centrodiapophyseal lamina bounds a deep fossa that underlies the diapophysis. The prezygapophysial ventral buttress contacts the anterodorsal margin of the parapophysis. Postspinal laminae extend nearly the full length of the postzygapophyses, and each borders a deep fossa on the ventral posterior edge of the neural spine. Spinoprezygapophyseal laminae are directed posterodorsally, from the prezygapophyses and enclose the rugose prespinal lamina on the anteroventral surface of the neural spine. The prespinal lamina is recessed 13 mm from the posterior margin of the hypantrum. As

in most sauropodomorphs other than some derived sauropods (Yates 2003a), prezygadiapophyseal laminae are not present; due at least in part to the dorsal positions of the parapophyses.

The hypantrum is recessed 19 mm from the distal tips of the prezygapophyses. The hyposphene reaches 11 mm ventrally from the articular facets of the postzygapophyses, and is shorter than the neural canal height (19 mm). With the ventral edge of the neural canal oriented horizontally, the neural spine is inclined posterodorsally, and tallest posteriorly (32 mm). The anterior margin of the neural spine appears to have an anterior kink, or knob, posterior to which the dorsal edge is inclined posterodorsally. A similar morphology is seen in dorsal 11 of *Plateosaurus* (von Huene 1926, Plate II, Fig. 15). The neural spine of the fifth dorsal of GF13-III is 44 mm long, with a concave posterior edge in lateral view and that overhangs the posterior centrum articular facet.

A disarticulated **anterior dorsal vertebra** (98GF13.62, Figure 6.7) is assumed to also associate with GF13-III, as it was located immediately adjacent to the other posterior dorsals. The centrum is 45 mm long, with concave articular facets that are much taller (56 mm) than wide (33 mm). The ventral portion of the anterior articular facet is missing due to a rock-saw cut. The left parapophysis was damaged by erosion prior to burial, and the left lateral process is missing the distal portions and is crushed dorsoventrally. The following description is based largely on the well preserved right side.

The neural spine is tall (47 mm) and anteroposteriorly short (30 mm). Based on the short morphology of the neural spine (Yates 2003c), this vertebrae likely represents the third dorsal vertebra. The dorsal edge of the spine is notably thickened (laterally) with extensively rugose anterior surface, and the posterior edge is concave in lateral view. The spinopostzygapophyseal laminae are prominent, with the dorsal edge of each reaching two-thirds of spine height and offset onto the lateral surface of the spine, away from the posterior edge.

The large parapophysis is 30 mm tall (dorsoventrally) and 11 mm wide (anteroposteriorly), and strongly constricted dorsally. Most of the articular facet is located on the lateral surface of the centrum, with only a small (dorsal) portion located on the neural arch. The circumference of the parapophysis is surrounded by a thin ridge of

bone. The strongly developed anterior and posterior centrodiapophyseal laminae enclose a fossa located directly dorsal to the parapophysis. Two additional fossae are located dorsal to the centrodiapophyseal laminae; the anterior fossa bound dorsally by the prezygadiapophyseal lamina, and the posterior fossa is bound dorsally by the postzygadiapophyseal lamina. The posterior fossa is also bound posteriorly by a centropostzygapophyseal lamina, which extends dorsally from the posterior border of the neural arch. The broad postzygapophyses together have a lateral expanse (45 mm) wider than the width of the centrum. The postzygapophyses have concave articular facets, and join medially to form a rudimentary hyposphene that is 3 mm tall and located immediately behind the centropostzygapophyseal laminae. The rudimentary hyposphene is much shorter (dorsoventrally) than the neural canal height (14 mm). Spinoprezygapophyseal laminae are present, and border the rugose prespinal lamina along the anterior margin of the neural spine. Spinodiapophyseal laminae are not present.

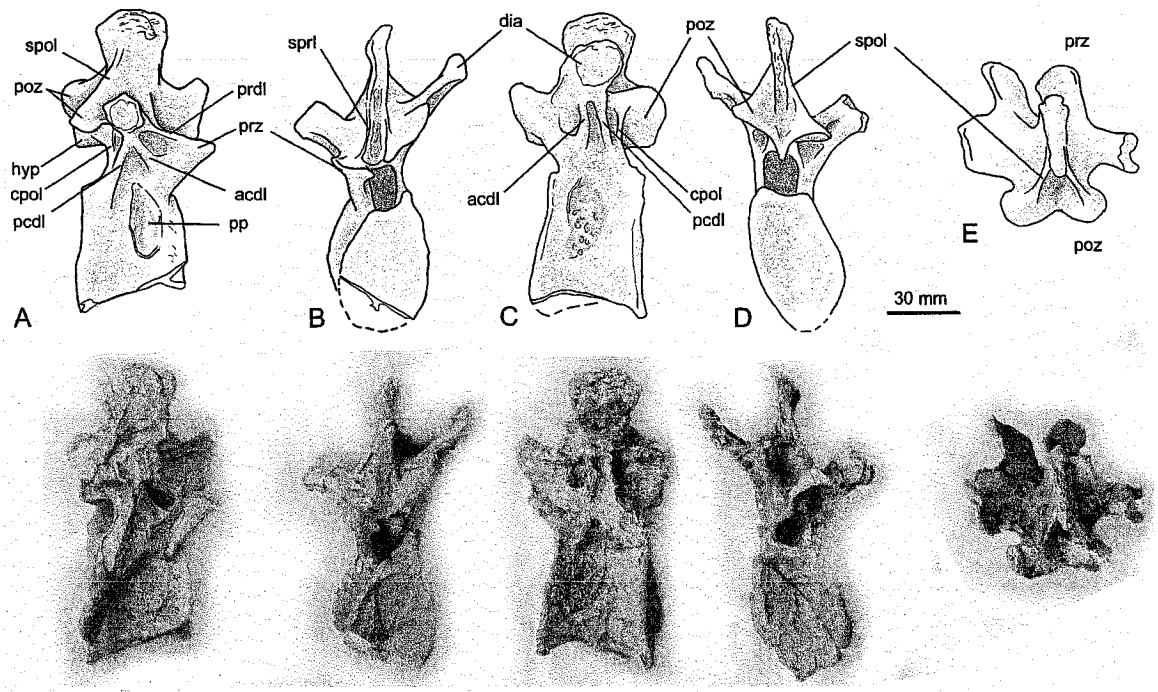

Figure 6.7: Anterior dorsal vertebra (D3) in left lateral (A), anterior (B), right lateral (C), posterior (D), and dorsal (E) views.
Abbreviations: acdl, anterior centrodiapophyseal lamina; cpol, centropostzygapophyseal lamina; dia, diapophysis; hyp, hyposphene; lat, lateral process; pcdl, posterior centrodiapophyseal lamina; poz, postzygapophysis; pp, parapophysis; prdl, prezygadiapophyseal lamina; prz, prezygapophysis; spol, spinopostzygapophyseal lamina; sprl, spinoprezygapophyseal lamina.

GF9

Two dorsal vertebrae were collected near the appendicular hind limb elements and were accessioned with GF9; FGM998GF9.5 is an anterior dorsal vertebra, and FGM998GF9.12 is a mid or posterior dorsal. Due to disarticulation, these isolated elements cannot be confidently associated with the hind limb elements, and the size discrepancy between the hind limb elements and isolated radius and ulna (Chapter 6) provide evidence that the material represents more than one individual. However, the morphology of the anterior dorsal vertebra does demonstrate features which are consistent with the cervicals of GF13-II, such as a strongly developed keel on the anteroventral edge of the centrum, and the lateral expansion of the anterior edge of the neural spine (Figure 6.8). The vertebra is identified as a dorsal based upon the large parapophysis, located slightly anterior to the middle of the centrum, and the short but well developed lateral process supported by the anterior and posterior centrodiapophyseal laminae, as well as the presence of the prezygadiapophyseal and postzygadiapophyseal laminae. The lateral processes are directed slightly posteriorly and are wing-like.

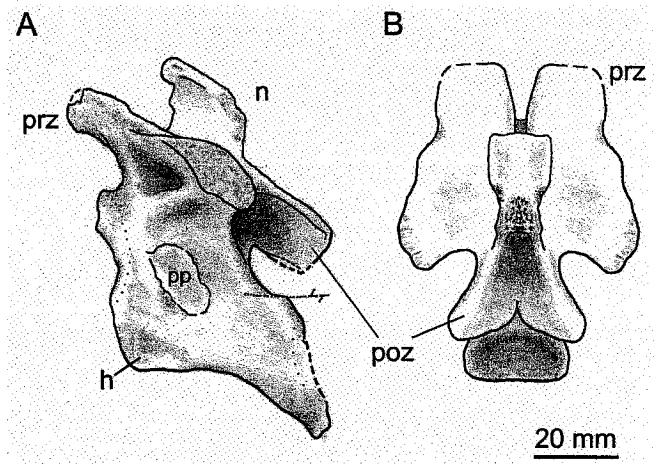

Figure 6.8: Anterior dorsal vertebra (FGM998GF9.5) in left lateral view (A) and a reconstruction in dorsal view (B).
The prezygapophyses (prz) are much wider than the postzygapophyses (poz), the anterior edge of the neural spine (n) is laterally expanded, and the anteroventral edge of the centrum has a strongly developed keel.

GF69

The posterior-most dorsal vertebra of GF69 is exposed only in dorsal view (Figure 6.9). The posterior left lateral portion of the centrum is visible, and appears to be

25 mm high. The length of the centrum cannot be determined because the anterior portion remains unprepared. Only the proximal portion of the neural spine is preserved. The right lateral process and rib are displaced dorsolaterally by two faults. However, the distal end of the rib was located slightly anterior to the preacetabular process and did not contact its medial surface.

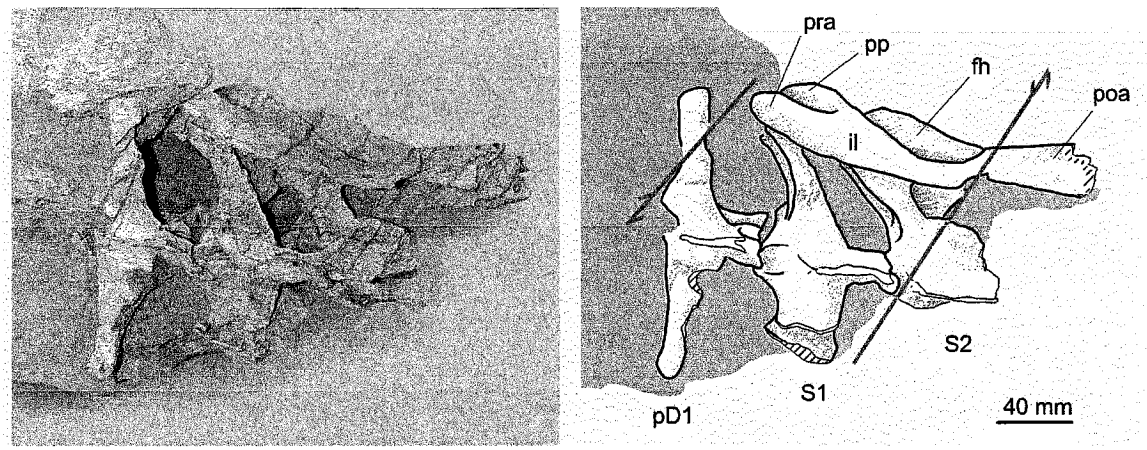

Figure 6.9: Posterior dorsal (pD1) and anterior two sacral vertebrae of 94GF69 in dorsal view. The right rib of pD1 is located anterior to the preacetabular process (pra). A fault (grey line) displaces the posterior left lateral portion of the second sacral vertebrae (S2) and ilium postacetabular process (poa). Additional abbreviations are femur head (fh), and pubic peduncle (pp). Note a small portion of the postacetabular blade is missing; broken bone surface is represented by cross hatching.

The left lateral process and rib are damaged, but the suture between the rib and lateral process can still be identified. The lateral process is 28 mm wide proximally, and the distal end of the rib extends 72 mm from the sagittal mid-line and is 16 mm wide (anteroposteriorly). Although not well exposed or preserved, the spinopostzygapophyseal laminae extend to the ends of the postzygapophsyses.

Sacral Vertebrae

Comparative Context

Designation of vertebrae as sacrals implies sutural contact or fusion with the medial surface of the ilium. The plesiomorphic sacrum for Dinosauria is composed of two sacral vertebrae (SI and SII), such as is in the basal archosauromorphs *Marasuchus* and *Lagerpeton* (Novas 1996). Yates (2003b) and Galton (1999) demonstrated the basis for identifying the two plesiomorphic sacrals in a sauropodomorph sacrum composed of

three or more vertebrae. Galton recognized that the plesiomorphic sacral centra often fuse together early in maturity and the others fuse progressively with increasing skeletal maturity. Yates (2003b) demonstrated several succinct morphological characters used to identify the plesiomorphic vertebrae, which are also similar to the features used by Langer (2003) in describing the sacrum of the basal sauropodomorph *Saturnalia*. In the first pleisiomorphic sacral, the anterior edges of the lateral process and sacral rib are joined by a thin vertical sheet of bone, resulting in a "C" shaped articular surface for the ilium in left lateral view. Similarly, the second plesiomorphic sacral vertebra has a sheet of bone joining the posterior edges of the lateral process and sacral rib, which typically defines an inverted "C" shape in left lateral view. Additionally, the lateral process of this vertebra is directed posterolaterally in dorsal view. Other methods for identifying the plesiomorphic vertebrae rely on the position where the sacral ribs articulate with the ilium (Nova 1996, Welles 1984), and attained similar conclusions. Welles (1984) also observed sacrals I and II have the dorsoventrally tallest ribs, which are located low on the centrum. Moser (2003) proposed many alternative characters for identifying the plesiomorphic sacrals that resulted in rather unconventional interpretations of sauropodomorph sacra, and which is not followed here.

Following the identification of the two plesiomorphic sacrals, the other sacral vertebrae can be recognized as either having been incorporated from the dorsal (dS, dorsosacral) or caudal (cS, caudosacral) vertebral series. Previous studies have demonstrated that the third sacral vertebrae is a dorsosacral in *Riojasaurus* (Novas 1996, Galton 1999), *Massospondylus, Lufengosaurus, and Yunnanosaurus* (Galton 1999), as well as *Efraasia* (Yates 2003) and *Saturnalia* (Langer 2003, Galton and Upchurch 2004), but the third sacral is a caudosacral in *Plateosaurus* (Galton 1999, Yates 2003b).

Several studies (Galton 1976, 1999, Galton and Upchurch 2004) have proposed the posteriormost sacral vertebra of *Anchisaurus* (YPM 208) is a caudosacral, which demonstrates an unusual large fenestra that pierces the sacral rib. However, Yates (2004) reinterpreted the posterior-most sacral vertebra as the second sacral (SII), demonstrating *Anchisaurus* has a dorsosacral, sacrum of three vertebrae.

Cooper (1981) proposed that *Massospondylus* has a four vertebrae sacrum (dS2, dS1, SI, SII). However, subsequent authors (Galton 1999, Yates 2004) have

demonstrated *Massospondylus* had a three vertebral sacrum (dS1, SI, SII); the potential second dorsosacral postulated by Cooper is considered too far forward to contact the ilium. Indeed, Cooper's suggestion of a second dorsal vertebra being incorporated into the sacrum seems to have been the premise for a "postulated cartilaginous extension of the anterior iliac spine" (1981, Fig 85), a suggestion for which there seems to be no evidence (Langer 2003).

Sauropodomorph taxa with four sacral vertebrae include *Melanorosaurus*, *Kotosaurus*, *Barapasaurus*, *Shunosaurus* and perhaps *Vulcanodon* (Upchurch et al. 2004). The sacrum of *Melanorosaurus* includes a dorsosacral and caudosacral (DS1, S1, S2, CS) , while the remaining four taxa have sacra that include two caudosacrals (S1, S2, CS1, CS2) (Galton *et al.* 2005).

Langer (2003) provided a detailed description of the pelvis of *Saturnalia*. While there are four vertebrae between the two ilia, the sacrum is composed of two plesiomorphic sacrals and a caudosacral. The first plesiomorphic sacral contacts the medial surface of the ilium coincident with the supracetabular crest, from immediately behind the anterior notch to the anterior edge of the ischial peduncle. The second sacral contacts the ilium posteriorly, from the midline of the ischial peduncle, tracing the posteroventral surface of the postacetabular process up to mid-height. Scarring on the medial surface of the ilium immediately behind the second sacral and on the posterior edge of the second sacral rib suggests a caudosacral was present.

The ribs and lateral processes of sacral vertebrae are usually indistinguishably fused into a single unit, referred to here as the sacral rib-complex. The sacral rib-complex is composed of a horizontal dorsal platform (lateral process) and a ventral platform (sacral rib), that are usually joined by a thin sub-vertical buttress. Based on typology, the vertical buttress may represent a reconfigured anterior or posterior centrodiapophyseal lamina.

GF13-I

Visible in ventral view, there are at least four sacral vertebrae in GF13-I that contact the medial surface of the ilium. Nothing can be said about the neural spines from the sacrals, as they remain largely unprepared at the time of this description. The sutural

boundaries amongst the anterior three vertebrae are closed but remain visible, while the posterior-most centrum remains completely separate. The anterior sacral ribs are partially disarticulated from the right ilium; the first sacral rib is separated from the ilium by the largest gap (15 mm), and the fourth sacral remains in contact with the ilium. The partial disarticulation of the ilium is consistent with the orientation of the skeleton during preservation, with the dorsal margin of the right ilium and sacral neural spines obliquely contacting the bedding surface, and a downward compressive force that shifted the right ilium ventrally and laterally in relation to the sacrum and other pelvic elements.

Table 2: Dimensions of sacral vertebrae from the bone bed specimens.
All measurements are in mm; '? 'represents data currently unavailable or unprepared, '-' signifies data that cannot be determined due to missing or damaged material and 'NA' is an abbreviation for not applicable.

		GF69	13_I	13_II	13_III
S1	Centrum length (anteroposterior)	45	58	62	60
S1	Pre-Post zygapophysis length	?	-	75	?
S1	Neural spine prox. length (anteroposterior)		-	43	?
S1	Neural spine height (to lateral process)	-	-	?	?
S2	Centrum length	?	61	67	55
S2	Pre-Post zygapophysis length	-	-	82	?
S2	Neural Spine prox. length	-	-	45	?
S2	Neural spine height	-	-	50	?
S3	Centrum length	?	66	85	55
S3	Pre-Post zygapophysis length	?	-	85	?
S3	Neural spine prox. length	?	-	60	?
S3	Neural spine height	?	-	67	?
S4	Centrum length	NA	48	50	40
S4	Pre-Post zygapophysis length	NA	-	90	?
S4	Neural spine prox. length	NA	-	50	?
S4	Neural spine height	NA	-	82	?

The rib-complex of the first (anterior) sacral vertebra contacts the ilial medial surface at the anterior proximal edge of the pubic peduncle and along the posterior portion of the preacetabular process. The second sacral rib is centered above the

acetabulum and the third rib contacts the medial surface of the ilium on the posterior portion of the ischial peduncle. A fourth sacral contacts the posteriormost aspect of the postacetabular process.

The anterior (first) sacral centrum of GF13-I is 58 mm long. The rib-complex originates from the anterior edge of the centrum, and the ventral surface is narrow medially, directed posterolaterally, and the distal end is expanded anteroposteriorly. Anterior to this distally broadening ventral surface, the anterior edge of the rib-complex is dorsoventrally expanded and inclined slightly anteriorly. The anterodistal corner of the rib-complex extends beyond the anterior articular face of the centrum, and the posterodistal edge of the rib-complex reaches the anteroposterior mid-point of the second sacral centrum. The dorsal surface of the rib-complex is not exposed.

The **second sacral centrum** is deformed by an oblique fault (Figure 6.10), displacing the right lateral and posterior portion of the centrum anteriorly and slightly laterally. The centrum length (61 mm) was measured on the right lateral edge, all of which was displaced by the fault. The rib-complex originates from the anterior edge of the centrum and articulates with the ilium directly above the acetabulum. The ventral and posterior surface of the rib-complex is composed of a posterolaterally directed ridge. The ridge is elaborated anteriorly as a fan like structure, which is inclined anterodorsally and in ventral view is concave both mediolaterally and anteroposteriorly. The anterior distal edge extends well beyond the anterior face of the centrum, to reach a position level with the mid-length of the first sacral. At this anterodistal point, the rib-complex remains attached to the posterodistal edge of the rib-complex of the first sacral. No foramen is present in the ventral surface of the rib-complex of the second sacral (unlike *Anchisaurus* Yates 2004). The rib-complex reaches 70 mm from the sagittal midline of the centrum.

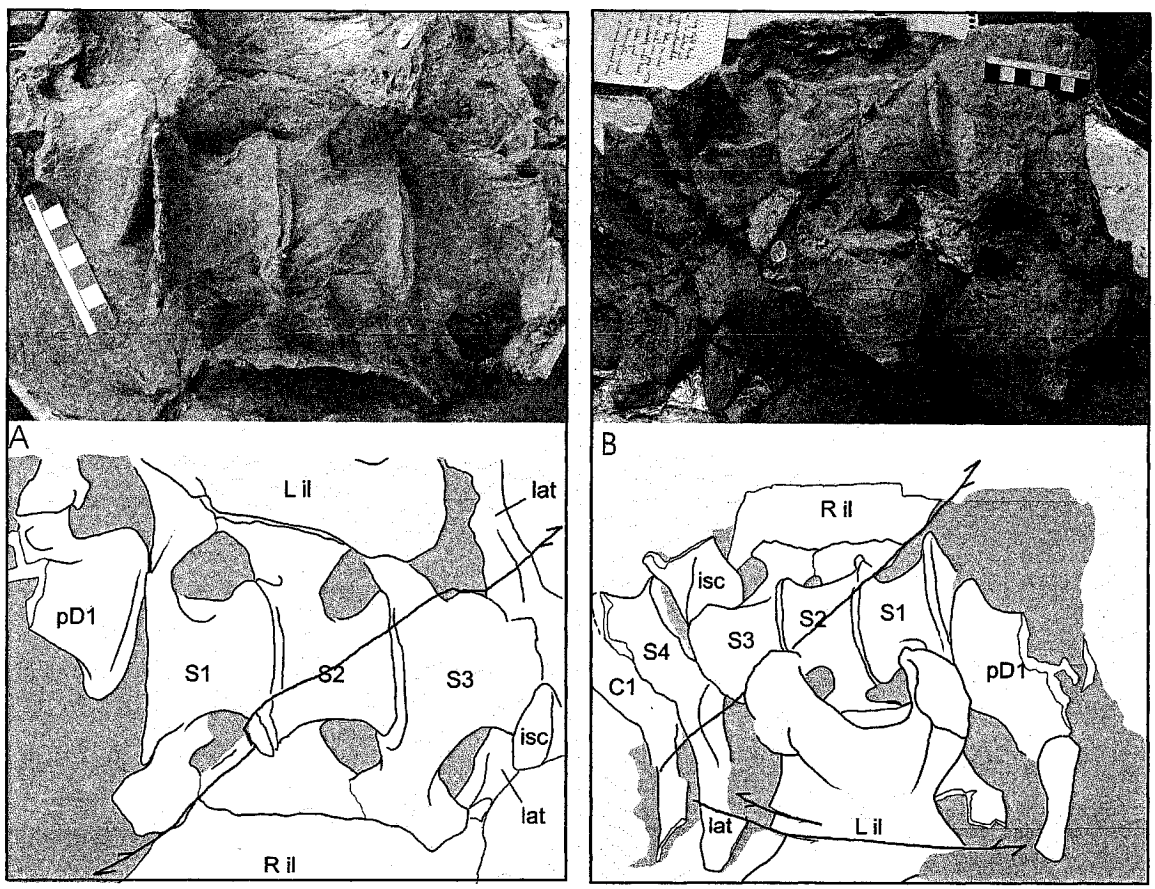

Figure 6.10: Posterior dorsal (pD1) and sacral vertebrae (S1-S4) of GF13-III in ventral (A) and ventrolateral (B) views.
The lateral process (lat) of the fourth sacral vertebra (S4) remains in contact with the right ilium (R il), but not the left, due to fault displacement of the left ilium (Lil). A portion of the proximal right ischium (isc) is located posterior to the third sacral centrum.

The **third sacral** centrum is the longest of the sacrum (66 mm), and has an anterior facet that is considerable wider than the posterior articular facet. At mid-length the centrum width is 58 mm, which is much broader than the widths of the first and second sacral centra (41 and 45 mms respectively).

The ventral surface of the rib-complex is directed laterally, the distal end expanded anteroposteriorly, but the posterodorsal edge does not extend beyond the posterior articular facet of the centrum. Similar to the second sacral, the rib-complex extends anteriorly beyond the anterior articular facet – to contact and fuse with the posterior edge of the preceding rib-complex. The rib-complex contacts the ventral edge of the postacetabular process, immediately caudal to the ischial peduncle.

An obliquely oriented vertical buttress that extends from the posterior edge is only partially exposed due to incomplete preparation. However, based on the size of the centrum, and presence of a posterior vertical buttress on the rib complex, the third sacral is certainly the second plesiomorphic sacral (SII). Thus, the two anterior sacrals represent a dorsosacral and the first plesiomorphic sacral (SI).

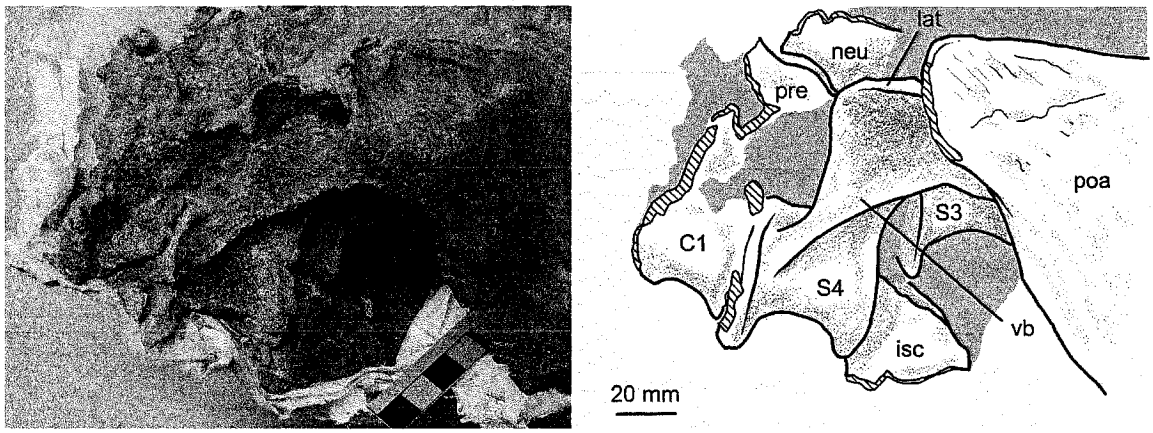

Figure 6.11: Posterior sacral vertebrae (S3, S4), proximal portion of the right ischium (isc), postacetabular process of the right ilium (poa) of the right ilium of GF13-I. The postzygaposphysis of the fourth sacral vertebrae does not extend beyond the posterior limit of the neural spine (neu). The prezygapophysis (pre) of the first caudal (C1), and the neural spine of the fourth sacral are displaced anteriorly due to a small fault. The ventral butress (vb) and the horizontal platform of the lateral process (lat) of the fourth sacral both contact the medial surface of the ilium.

The centrum of a **fourth (caudo) sacral** is 48 mm long and 58 mm in height (posteriorly) and is not fused to the centrum of the third sacral. The ventral surface of the centrum is anteroposteriorly concave, recessed 12 mm at mid-length, and has a longitudinal sulcus consistent with its origination from the caudal series.

The left lateral process was deformed during preservation, bent dorsally and displaced by several small faults. However, the right lateral process is well preserved and remains in contact with the medial surface of the ilium (Figure 6.10A, 5.9). The process extends laterally 75 mm from the base of the neural spine, and is composed of a dorsoventrally thin horizontally oriented platform and an obliquely oriented, anteroposteriorly thin, ventral buttress. The horizontal portion expands in length (anteroposteriorly) toward the distal end; the proximal and distal lengths measuring 29 mm and 35 mm long respectively. In lateral view, the ventral buttress is inclined 45°

with the ventral edge projected farther anteriorly than the dorsal edge. In ventral view, the buttress supports the dorsal lateral process obliquely, attached to the anterior edge distally but the posterior edge proximally. The ventral buttress divides into two thin laminae proximally, one directed anteroventrally and the other posteroventrally, which together define a shallow fossa. The single buttress element immediately under the lateral process likely represents a composite of the anterior and posterior centrodiapophyseal laminae, which remain as discrete laminae bounding the fossa. The diapophyseal laminae are not found on anterior caudal vertebrae of *Plateosaurus* and *Lufengosaurus* (Wilson 1999), and their presence and composite structure may represent autapomorphic characters.

Both the ventral buttress and the horizontal platform (lateral process) articulate with the medial surface of the ilium. The ventral buttress contacts a ridge on the ventral edge of the ilium, representing the medial border of the brevis fossa, and the horizontal platform articulates near the dorsal edge of the ilium.

The neural spine and postzygapophyses are offset anterodorsally by a small fault. The height and length of the neural spine cannot be determined; the distal end of the neural spine is currently in a separate block that remains unprepared.

GF13-II

The sacral vertebrae of GF13-II remain fused to the medial surface of the right ilium (98GF13.86), and were in articulation with the posterior dorsals and proximal caudal vertebrae (Figure 6.12). There are four sacral vertebrae; a possible fifth located posteriorly is interpreted as the displaced anterior caudal vertebra. The two anterior sacral centra have been deformed such that the ventral portions of the centra are displaced anteriorly (and perhaps dorsally); the first-sacral anterior articular face is inclined 30°, the ventral margin displaced considerably anterior to the dorsal margin.

The **first sacral** centrum is 62 mm long, with a transversely flat but longitudinally concave ventral surface. The vertebra currently lacks a neural spine, having been severed by a rock-saw cut and not yet located during preparation. The anterior base of the neural spine is present, as well as spinoprezygapophyseal laminae that originate from the medial edges of the prezygapophyses and surround a rugose prespinal lamina. Based on the

exposed cut edge, the neural spine was 43 mm long anteroposteriorly. After accounting for the anterior displacement of the ventral portions of the centrum, the posterior edge of the neural spine does not appear to extend beyond the posterior articular facet of the centrum.

The small prezygapophyses have limited anterior extension and the dorsomedially directed articular facets are only slightly raised above, and separate from, the anterior edge of the lateral process. The distal ends of the postzygapophyses of the posterior dorsal remain articulated with the prezygapophyses.

The sacral rib-complex is composed of a dorsoventrally thin dorsal platform and a vertical buttress inset from the anterior margin of the dorsal platform, which also fuses indistinguishably to the anterior edge of a horizontal ventral platform. The dorsal platform is directed anterolaterally; the distal end is located laterally adjacent to the prezygapophyses and contacts the posterior 30 mm of the preacetabular process. In dorsal view the anterior edge is mildly concave and the posterior edge is convex, the proximal point of the latter originates from the mid-length of the neural spine. The proximal end of the dorsal platform is 40 mm long (anteroposteriorly) and the platform extends 55 mm from the sagittal mid-line. The vertical buttress has a concave anterior surface, which may have been accentuated by the anterodorsal compression of the ventral portion of the centrum. Proximally, the height of the sacral complex anterior edge is only 20 mm, however this has also likely been reduced due to compression. The ventral platform originates from the anterior portion of the centrum, and expands to 60 mm long anteroposteriorly at the distal end. The posteroventral portion of the horizontal platform is under-lapped (ventrally) by the anterodistal edge of the second sacral rib-complex.

The posterior portions of the sacral rib-complex are missing on the left side due to damage during collection. The distal articular facet (for the ilium) is located above the ventral margin of the centrum. As preserved, the long axis of the facet is horizontal and is dorsoventrally tallest anteriorly, although at least some of the posterodorsal portion is broken and missing. The articular facet is directed ventrolaterally and contacts the medially inflected rim of the acetabulum immediately posterior to the anterior notch on the proximal portion of the pubic peduncle.

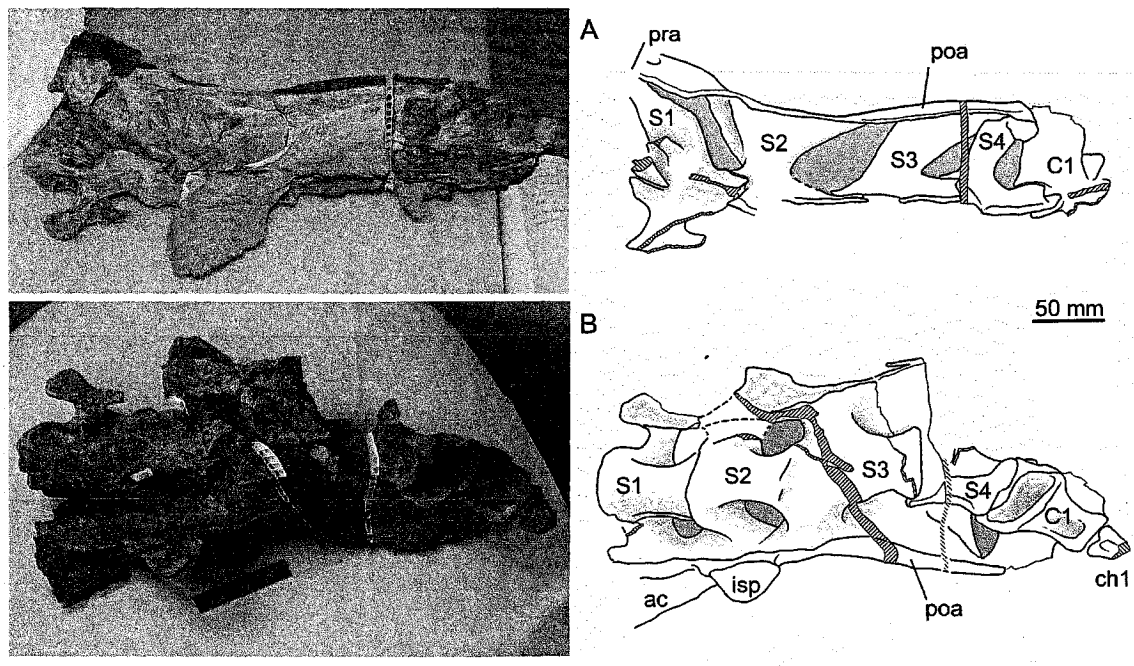

Figure 6.12: Sacral vertebrae (S1-S4), right ilium and proximal caudal vertebra (C1) of GF13-II in dorsal (A) and ventral (B) views.
Other Abbreviations: ac, acetabulum; ch1, chevron of first caudal vertebra; isp, ischial peduncle; pra, preacetabular process; poa, postacetabular process.

The **second sacral** centrum is 67 mm long with a flat but anteroposteriorly concave ventral surface. The neural spine is 50 mm tall (above the lateral process), 45 mm long proximally, and 50 mm long distally. The short postzygapophyses extend only slightly beyond the posterior limit of the neural spine. The anterior edge of the neural spine is partially obscured by matrix, and although spinoprezygapophyseal lamina are partially visible it cannot be determined if they surround a rugose anterior prespinal lamina, as in the first sacral.

The rib-complex of the second sacral is also composed of horizontal dorsal and ventral platforms, which are proximally joined by an oblique vertical buttress along their anterior margins. At the mid-length of the dorsal platform, the vertical buttress ends and the dorsal and ventral platforms appear to be separate, although matrix still fills much of this area. A distal gap in the vertical buttress is also present on the second sacral of GF69 and has been noted in *Melanorosaurus* (Galton et al. 2005). The dorsal platform is directed laterally and slightly anteriorly. The proximal portion of the posterior edge was damaged by a rock-saw cut. The distal end of the dorsal platform was not damaged,

although the posterodistal corner does not contact the ilium. A similar gap is notable in GF13-III, GF69 and other sauropodomorphs (Yates 2003b). The configuration of the sacral rib-complex demonstrates the vertebra represents the first plesiomorphic sacral (SI), therefore the preceding sacral (S1) is a dorsosacral.

The anterodistal portion of the dorsal platform contacts the medial surface of the ilium 15 mm ventral to the ilia; dorsal edge and directly above the anterior portion of the ischial peduncle. The ventral platform originates on the anterior edge of the centrum, is directed laterally, and expands in length distally. As seen on the right side, the ventral platform has extensive contact with the posterior edge of the first sacral rib-complex, and is ventrally under-lapped by the anterior portion of the third sacral rib-complex; although the later boundaries are difficult to determine with certainty as a result of the small faults visibly affecting the ventral surface. The left sacral rib-complex was severed at mid-length by a rock-saw cut and some portions were lost during collection, apparently including the entire distal articular surface.

The postzygapophyses are not elaborately developed; the base of the posterior neural spine is simply expanded and surrounded by the prezygapophyses of the third sacral. The joint between these processes is tight and may be fused. Similarly, the prezygapophyses are tightly appressed with the postzygapophyses of the first sacral.

The ventral boundary between the second and **third sacral** centra is difficult to identify with any certainty, as the two centra have undergone extensive fusion. Only a small raised ridge demarcates the centra edges, and this area has been affected by several small distortion faults. The posterior articular facet of the centrum is partially damage by a rock-saw cut, but the centrum is approximately 85 mm long. In ventral view, the posterior edge of the centrum is narrower than the anterior edge; similar to GF13-I.

The neural spine is 67 mm tall and 60 mm long (anteroposteriorly); being only poorly mildly distinguished from the zygapophyses, the anterior edge gently transitions into the prezygapophyses.

The right sacral rib-complex is exposed in dorsal and ventral views, but the posterior portion of the left sacral rib-complex is located in a separate small block that is only partially prepared. The dorsal platform of the sacral rib-complex is directed posterolaterally approximately 45°. Proximally, the posterior edge of the dorsal margin

is posterior to the spine mid-length. The dorsal platform expands distally, to reach 74 mm wide where it contacts the medial surface of the ilium postacetabular blade. The ventral component of the sacral rib-complex originates from the anterior portion of the centrum, is directed laterally, and expands a small amount anteriorly as well as strongly posteriorly at the distal end. In ventral view, the anteroventral margin of the sacral rib-complex is concave, and under laps the posterodistal portion of the ventral horizontal platform of the second rib-complex. The posterior edge of the rib-complex is inclined dorsally, and merges indistinguishably into the dorsal horizontal component. The rib-complex thus resembles an inverted "C" shape in lateral view, and demonstrates the vertebra represents the second plesiomorphic sacral (SII).

Although the specific boundary between the third and **fourth sacral** centra was damaged by a rock-saw cut, the two centra were clearly not fused. The anteroventral edge of the centrum is missing, but the length was approximately 50 mm based on the preserved right portion of the centrum. The posterior portion of the ventral surface does not exhibit a deep ventral sulcus, as is present on the ventral surface of the fourth sacral of GF13-I. The centrum is 48 mm high (posteriorly) and is therefore as long as tall.

The neural spine was damaged during collection and preparation, but it is 82 mm tall, 50 mm long above the postzygapophyses, and the posterior edge slightly overhangs the centrum posterior face. The postzygapophyses are situated at the base of the neural spine and extend only slightly posteriorly, with the articular facets directed ventrolaterally. The (right) lateral process is currently 40 mm long, but this appears to be due to compression; there is some evidence of telescopic compression visible on the dorsal surface, and the left lateral process is at least 75 mm long. The ventral surface of the left lateral process has only a low ventral buttress, which differs from the strong buttress of GF13-I. However, the ventral buttress may be reduced due to dorsoventral compression.

The transverse process of a fifth vertebra contacts the medial surface of the ilium and the posterior edge of the fourth sacral (Figure 6.12). This contact can be attributed to the deformation affecting the vertebra, therefore this does not represent a fifth sacral vertebra but rather is the first caudal. The four vertebra sacrum of GF13-II includes a dorsosacral and a caudosacral (dS1, SI, SII, cS1), similar to GF13-I.

GF13-III

The sacral vertebrae of GF13-III are exposed in dorsal (Figure 6. 13) and ventral (Figure 6.14) views, and remain articulated to the left ilium. The right ilium (98GF13.46, see Chapter 4) was disarticulated from the sacral series prior to burial. The distal ends of the right sacral ribs are severed by a rock-saw cut, and those of the left side have been displaced posteriorly by a 30 mm fault (Figure 6. 13).

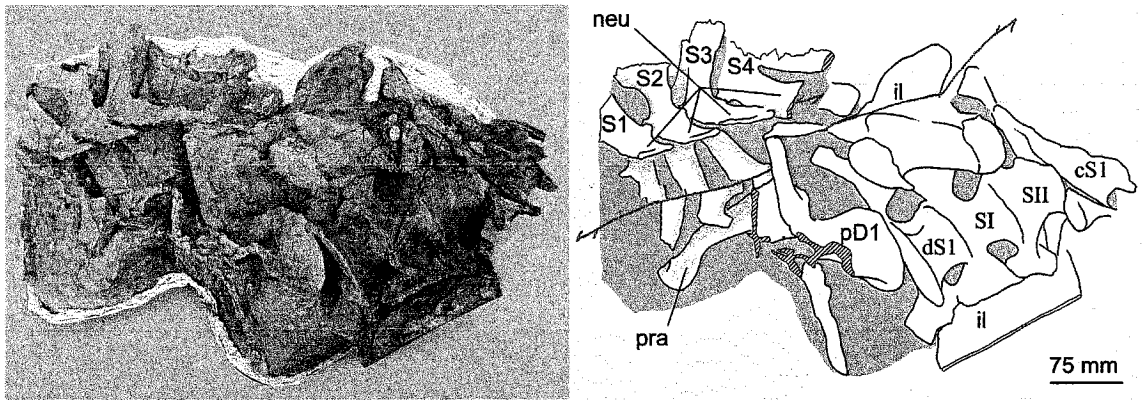

Figure 6. 13: The sacral vertebrae (S1-S4) and preacetabular process (pra) of GF13-III, which are located underneath the four sacral vertebrae (dS1, SI, SII, cS1), ilia (il), and posterior dorsal vertebra (pD1) of GF13-I.
The distal ends of the rib-complexes from the sacrals of GF13-III are offset posteriorly by a fault (dark grey). The neural spines (neu) are tall and anteroposteriorly short.

Four sacral vertebrae are visible in ventral view, although the fourth (caudo) sacral is not attached to the ilium. Similar to GF13-II, the dorsal platform of the third sacral rib-complex is directed posterolaterally and has an anteroposteriorly expanded distal end. This lateral process does not reach the posterior limit of the postacetabular process, and there is sufficient room for the articulation of a fourth sacral vertebra. The long lateral process of the fourth sacral would have reached the medial surface of the ilium, although apparently this contact was not firmly fused.

The dimensions of the sacrals of GF13-III (Table 2) are slightly shorter than both GF13-I and GF13-II, which is consistent with the dimensions of the dorsals and ilia. The neural spines of dS1, SI and SII are nearly complete, laterally thin, tall, and anteroposteriorly shorter than the caudal neural spines (Figure 6. 13). However, they are currently inaccessible for measurement.

The **first sacral** centrum was severed by a rock-saw cut, but the anterior portion of the centrum remains attached to the block containing the posterior dorsals. The left ilium and first sacral vertebra are also deformed by several faults, limiting the information available. After realigning the anterior portion of the centrum (and posterior dorsals) with the posterior portion that remains articulated to the sacrum (Figure 6.14), the centrum length is estimated at 60 mm. The ventral portion of the sacral rib-complex originates from the anterior edge of the centrum, and the dorsal portion of the left rib-complex contacts the medial surface of the preacetabular process (Figure 6.1).

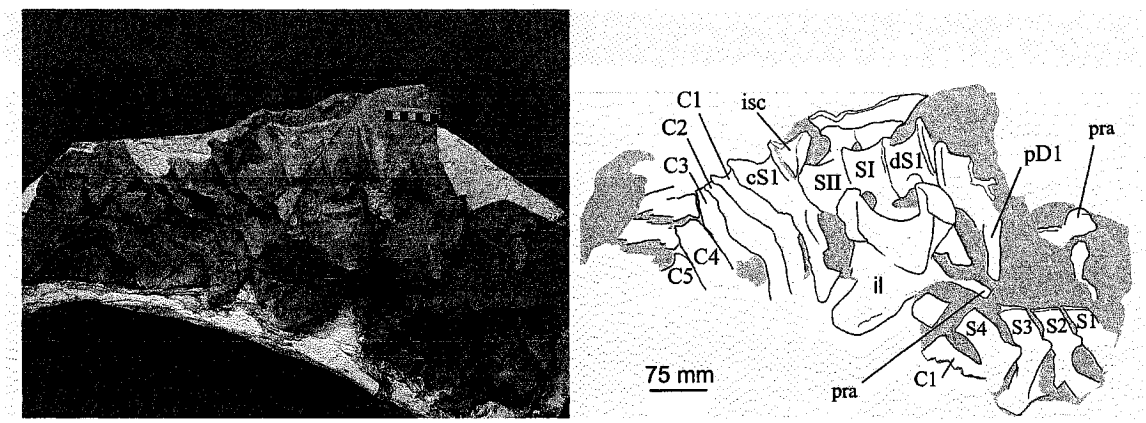

Figure 6.14: Posterior dorsal (pD1-pD3) and four sacral vertebrae (S1-S4), and left ilium (il) of GF13-III in ventrolateral view.
The ilium of GF13-I directly was preserved overlapping the pelvis of GF13-III; this view is the underside of the block.

The **second sacral** rib-complex also originates from the anterior edge of the centrum. It articulates to the medial surface of the ilium above the posterior portion of the acetabulum and the ischial peduncle. Similar to all other specimens from the bone bed, and differing from *Anchisaurus* (Galton 1976, Yates 2004), there is no foramen present in the ventral surface of the second sacral rib-complex.

The length of the **third sacral** centrum is compressed due to an oblique fault, which offsets the right rib-complex and right anteroventral corner of the centrum posterolaterally approximately 15 mm. Regardless, the centrum is short (estimate 55 mm) and broad, especially in comparison to the third sacral of GF13-II (Table 2). The rib-complex occupies the anterior two-thirds of the centrum. The posterior facet of the centrum is concave and is not fused to the fourth sacral centrum.

The ventral surface of the rib-complex is directed laterally. The posterior edge is inclined posterodorsally and becomes expanded (anteroposteriorly) at the distal end. The ventral portion of the rib-complex articulates with the medial surface of the ilium immediately posterior to the ischial peduncle, and the inclined posterior edge of the complex follows the ventral edge of the postacetabular blade. Similar to GF13-II but differing from GF13-I, the posterior edge of the rib-complex extends well beyond the posterior face of the centrum; the posterodistal corner is located adjacent to the mid-length of the following centrum.

The **fourth sacral** centrum remains articulated to the proximal caudal and is slightly disarticulated from the third sacral centrum. The ventral edges of the anterior and posterior facets of the centrum are offset posteriorly by a fault, but the centrum is 40 mm long. The ventral surface of the centrum remains covered by matrix.

The left lateral process extends 75 mm from the lateral surface of the centrum, and is exposed on the underside of the block containing the sacrum (Figure 6.14). The distal edge is covered by rugose texture, suggestive of strong ligamentous attachment. A mild ridge remains on the ventral surface of the lateral process, although this ridge is not a strongly developed buttress as occurs on the fourth sacral of GF13-II. As preserved the left lateral process does not contact the medial surface of the ilium; however, the process is long enough to contact the ilium and there was sufficient room on the posterior edge of the ilium. As mentioned, the centrum is slightly disarticulated from the centrum of the third sacral. The lateral process certainly would have contacted the medial surface of the ilium, but it was apparently not firmly fused, perhaps attributable to skeletal immaturity.

As preserved, the right lateral process is directed posterolaterally, and partially overlaps the lateral process of the first caudal vertebra. The first caudal vertebra has a sharply defined groove on the dorsal surface of the lateral process; however this groove is attributed to deformation rather than an articular surface for the lateral process of the fourth sacral vertebra.

GF69

The **first sacral vertebra** of GF69is well exposed in dorsal view (Figure 6.9). The centrum is 45 mm long based on the exposed dorsal margins of the centrum. The

neural spine measures only 15 mm tall, however this shortness is due to compression deformation. The second sacral neural spine and dorsal rim of the ilium postacetabular blade are similarly deformed, and all are consistent with dorsoventral compression.

The dorsal surface of the rib-complex is proximally 36 mm wide (anteroposteriorly) and is directed anterolaterally (120°), resulting in the distal end of the rib-complex being located laterally adjacent to the prezygapophyses. The posterior edge of the dorsal platform is gently convex, the anterior edge is concave, although the latter has been exaggerated by preparation damage. Mediolaterally directed rugose ridges located at mid-length on the dorsal surface of the rib-complex are in a similar location as the rib/lateral process suture of the posterior dorsal vertebra.

There is a vertical buttress 20 mm deep (dorsoventrally), partially inset from the anterior edge of the dorsal platform. The anterior surface of the vertical buttress is dorsoventrally concave. The ventral horizontal platform extends posteriorly from this vertical buttress, and expands (anteroposteriorly) distally. The distal end of the vertical buttress is continuous with the ilial anterior notch. The ventral platform contacts 28 mm of the ilial medial surface, from the anterior notch to the anterodistal edge of the second sacral rib. The dorsal platform articulates with 17 mm of the anterior medial surface of the preacetabular process.

On the left side the dorsal portion of the sacral rib-complex has been damaged and is not preserved beyond mid-length. The distal portion of the ventral platform remains fused to a small portion of the left ilium, likely a proximal fragment of pubic peduncle. These elements have been truncated by the strong oblique fault that offsets the third sacral and left ilium.

The left rib-complex of **the second sacral vertebra** has also been truncated by the large oblique fault through the pelvis, and the posterior portion of the right side is displaced laterally by a series of smaller faults. The right side of the centrum is currently not exposed in ventral view, so the length of the centrum cannot be determined. The neural spine is very short due to dorsoventral compression.

The dorsal platform of the rib-complex has a buttress supporting its proximal anterior edge. This buttress also contacts the anterior edge of the ventral platform, but does not extend beyond mid-length, similar to the second sacral of GF13-II. The dorsal

platform is directed anterolaterally, and contacts the medial surface of the ilium for 28 mm immediately posterior to the anterior notch, and 14 mm below the dorsal edge of the ilium. The distal end of the dorsal platform contacts a well developed ridge extending from the medial surface of the ilium, and a suture remains visible along this contact. Similar to GF13-II and GF13-III, there is a gap on the posterodistal edge of the dorsal platform. Therefore this vertebra represents the first plesiomorphic sacral (SI), and the anterior-most sacral is a dorsosacral.

The ventral platform originates from the anterior edge of the centrum and expands in width distally. The anterior edge is directed anterolaterally, and the posterior edge of the ventral platform is directed posterolaterally. Incomplete preparation prevents identification of the specific posterior boundary of the horizontal platform, but the platform articulates with the medial surface of the ilium for at least 50 mm. The anterodistal edge of the horizontal platform is attached to the posterodistal edge of the first sacral rib-complex.

The right sacral rib-complex of the **third sacral vertebra** is also truncated and displaced by the large oblique fault, but the left side of this vertebra and its articulation with the medial surface of the left postacetabular process are well preserved in the block on the other side of the fault. The dorsal horizontal platform is directed posterolaterally and contacts the ilium for at least 65 mm. Preparation of this important vertebra is ongoing but incomplete upon at the time of publishing this report.

Based on the orientation and morphology of the second and third sacral rib-complexes, these vertebrae represent the first and second plesiomorphic sacral vertebrae (SI, SII). The first sacral vertebra then represents a dorsosacral (dS1). The presence of a caudosacral cannot be evaluated at this time, as the area remains unprepared. The rib-complex of the third sacral extends to nearly the posterior edge of the postacetabular process, but it remains possible the following vertebra lateral process did contact the rib complex and/or corner of the postacetabular blade.

Caudal Vertebrae

The proximal caudal vertebrae are preserved in four specimens, but the caudals are badly faulted in GF13-I, partially dislocated in GF13-III, and currently unexposed in

94GF69, effectively limiting the useful comparisons that can be made between these specimens.

GF13-I

Currently eight proximal caudal vertebrae are partially exposed in GF13-I in left lateral view. The four proximal-most caudals are preserved in a small block that was separated from the sacrum during preparation, and the other caudals are located within the (left) pes block. The vertebrae are distorted by numerous fault displacements.

The **first proximal caudal** is reasonably well preserved and exposed (Figure 6.1). The anterior portion of the neural spine and the prezygapophyses remain in the block containing the sacrum, with the prezygapophyses tightly articulated to the fourth sacral vertebrae. The right lateral process is not exposed and the majority of the neural spine is located in a small block that was separated from the sacrum block during preparation; the distal two-thirds of the neural spine is currently missing and likely lost during collection. The centrum is 40 mm long (at mid-height), and although the concave anterior face is only partially exposed, it is at least 60 mm tall. Therefore the centrum is much taller than it is long. The ventral surface of the centrum is partially exposed, is mediolaterally thin, and a ventral sulcus is not present. There is no chevron facet on the posteroventral edge of the first or second caudal; the first chevron is located on the third caudal vertebra.

Similar to the first caudal, the second caudal centrum is short, 35 mm in length, and is of similar height (60 mm). Only the left lateral surface is exposed; the lateral process and the neural spine remain unprepared. Little else can be said of the other caudal vertebrae at this time; they are poorly preserved, with several fault displacements, and are only partially prepared.

GF13-II

The vertebra in GF13-II that remains posteriorly articulated with the fourth sacral vertebra is interpreted as the **first caudal**. The lateral process contacts the posterior edge of the ilium and the lateral process of the fourth sacral, but this contact is attributed to rotational displacement. The vertebra is obliquely deformed; the right side has been

displaced anterior relative to the left. The complete centrum, prezygapophyses, and proximal portion of the neural spine are articulated to the fourth sacral.

Differing from GF13-I, the first caudal centrum is as long as tall (Figure 6.12); the centrum height is approximately 60 mm and the length at mid-height is 57 mm. The ventral surface of the centrum is only 42 mm long, due to a facet for the first chevron located on the posterior edge of the centrum. The ventral surface of the centrum has a deep ventral sulcus that remains partially filled with matrix. The prezygapophyses extend slightly beyond the anterior face of the centrum. The distal portion of the neural spine was severed by a rock-saw cut and remains in the small block that contains the second caudal vertebrae. The distal end extends at least 88 mm posterodorsally, to a height of 68 mm above the dorsal surface of the lateral process.

The **second caudal** vertebra is obliquely deformed; the left side is displaced posteriorly relative to the right. The centrum is 42 mm tall and 58 mm long at mid-length, but only 45 mm long ventrally due to a well developed chevron facet. There is a well developed ventral sulcus, but the depth is unknown as matrix still fills the depression.

The neural canal is 10 mm tall anteriorly. The neural spine is located on the posterior half of the centrum, directed posterodorsally, and is 42 mm long above the postzygapophyses. The neural arch is 20 mm in length (below the postzygapophyses) and is therefore considerably shorter than the neural spine. The left lateral process distal end was truncated by a rock-saw cut. The lateral process is oriented in line with the deformed posterior centrum face; therefore prior to deformation it was directed laterally. The process extends at least 50 mm from the lateral surface of the centrum, and is proximally 40 mm wide (anteroventrally). The right lateral process is located in a separate block (2000NS02-50) and remains unprepared.

The anterior portion of the centrum of the **third caudal** vertebra was severed by a rock-saw cut and remains articulated to the second caudal centrum. It has a deep (9 mm) ventral sulcus and a concave anterior articular surface. The distal tips of the prezygapophyses do not extend beyond the anterior articular facet of the centrum. The prezygapophysial articular facets are directed dorsomedially and are concave. The

remainder of this vertebra and additional (unexposed) posterior caudals are located in the block under the left pes of GF13-I, which remains unprepared.

GF13-III

Eleven caudal vertebrae of GF13-III remain articulated to the sacrum. The proximal five caudals have been deformed by several small displacement faults that strike through the neural arch and spines.

The **first caudal** centrum is 53 mm long and at least 60 mm tall; the anterior centrum face is only partially exposed. The posteroventral edge of the centrum has been offset by a fault and severed by a rock-saw cut, therefore it cannot be determined if a chevron articulated to the anterior-most caudal, as in GF13-II.

The neural spine was severed obliquely dorsal to the postzygapophyses and ventral to the prezygapophyses, and the majority of the neural spine and prezygapophyses are located in the block containing the sacrum and left ilium. The neural spine was nearly vertical and is at least 75 mm tall; the distal end was truncated by a fault and is currently not exposed. The lateral process extends 55 mm from the lateral surface of the centrum and is proximally nearly as wide as the centrum is long, but narrows distally. The dorsal surface has a longitudinal groove inset from the anterior edge, but this is considered a deformational artefact.

The **second caudal** centrum is 44 mm long at mid-height and approximately 41 mm high based on the small exposure of the concave anterior face. The posteroventral edge of the centrum is recessed to suggest an articular facet for a chevron. If a chevron did remain articulated, it was severed by a rock-saw cut and apparently lost during collection.

The neural arch and spine are offset anteriorly by several displacement faults. The neural spine is directed posterodorsally approximately 30°, is at least 110 mm tall (from dorsal surface of lateral process) and is 48 mm long (anteroposteriorly) above the postzygapophyses. The prezygapophyses are relatively short, as long as they are tall, with articular facets that are directed medially and only slightly dorsally, although this orientation may be accentuated by preservational crushing. The lateral process was

directed laterally, although it is currently directed posterolaterally due to deformation. The lateral process extends 65 mm from the lateral surface of the centrum.

The right lateral surface of the **third caudal** centrum was taphonomically damaged. The surface is rugose; a pattern that is not consistent with erosion, which would tend to expose a porous pattern of (trabecular) bone, and would not be limited to a single vertebra. The vertical line of the rugose patterning is also found on the anteroproximal edge of the neural spine, immediately posterior to the prezygapophyses. Based on these features, the surface rugosity is likely due to a localized pathology. The lateral process and neural arch are badly deformed by fault displacements. Although the neural spine is also faulted at mid-length, it is directed posterodorsally at approximately 45°.

The **fourth caudal** vertebra is missing the anteroventral portion of the centrum due to a rock-saw cut, but the lateral process was not damaged by faulting. The lateral process is as wide (anteroposteriorly) as the centrum at mid-height (55 mm). The lateral process extends laterally the same distance, and narrows toward the distal end, where it measures only 33 mm long anteroposteriorly.

Discussion

The vertebrae recovered from the bone bed are nearly all deformed due to compression or fault displacements. The vertebrae were particularly susceptible to deformation because they are delicate structures with thin processes and the porous trabecular cores. Regardless of the abundant deformational damage, the vertebrae demonstrate several sauropodomorph features, as well as some additional evidence in support of two distinct morphs present among the recognized specimens.

Each mid-dorsal vertebrae lacks a prezygadiapophyseal lamina, which provides the referral to Sauropodomorpha (Wilson 1999, Yates 2003c), and the posterior edge of the neural spine is concave in lateral view, a feature that is typical of prosauropods (Yates 2003c). None of the vertebrae possess spinodiapophyseal laminae, a lamina that is found only in sauropods more derived than *Shunosaurus* (Wilson 1999, Yates 2004).

The ribs of the posteriormost dorsal vertebrae of GF69, GF13-I, GF13-II and GF13-III also have a typical prosauropod morphology, as they are short and each distal end is located medial to the medial edge of the preacetabular process. The posterior dorsal (D15) of *Plateosaurus* also has a short rib with the distal end located close to the medial edge of the preacetabular process (von Huene 1926, Plate II, Fig 8). Cooper (1981) proposed that the short posterodorsal rib of *Massospondylus* contacted the preacetabular process, but this would have involved a cartilaginous anterior extension of the preacetabular process, a situation that is not widely accepted (Galton 1999, Langer 2003).

The posterior-most rib of GF69 certainly did not contact the preacetabular process, but the situation of GF13-I and GF13-II is somewhat less certain. At this time all that can be confidently determined is that the distal end of the posterior-most dorsal of GF13-I and GF13-II was located medial, and very close to, the preacetabular process.

The posterior dorsal centra are generally longer than tall in prosauropod taxa, except for *Camelotia, Euskelosaurus, Jingshanosaurus* and *Lufengosaurus*, in which the posterior dorsals are taller than long (Galton and Upchurch 2004). There is variation between the specimens of the bone bed in the proportions of the posterior dorsal centra; the centra of GF13-II are notable longer than tall, whereas the inverse proportion (taller than long) occurs in the posterior dorsals of GF13-I and GF13-III. The variation is not consistent within the two ilial morphs, as GF13-II and GF13-III share the elongate postacetabular blade but differ in the proportions of the posterior dorsal centra. These two specimens also differ in the relative length of the third sacral centrum; GF13-II having a much longer third sacral centrum. The lengths of pD1 and S3 of GF13-III are both 64% the comparable lengths of GF13-II, whereas the ilium of GF13-III is estimated to be 86% the size of GF13-II. The variation in vertebra proportions does not appear to be due to deformation, and remains a disparity between two specimens that possess an elongate ilium.

Consistent with the recognition of two ilia morphs, GF13-I appears to differ from GF13-II and GF13-III in the development of the ventral buttress on the lateral process of the fourth sacral vertebra. The ventral buttress of GF13-I is strong but less developed in GF13-II and GF13-III. It remains possible this difference may be due to dorsoventral

compression of the lateral processes in the later two specimens. Representatives of the two ilia morphs also differ in the relative length of the rib of the second posterior dorsal; the rib is much longer in GF13-I than in GF13-II.

The four vertebra sacra of GF13-I, GF13-II and GF13-III each contain the two plesiomorphic sacrals as well as a dorsosacral and caudosacral. The only other sauropodomorph with a similar sacra composition is *Melanorosaurus*, from the Upper Triassic (Lower Elliot Formation) of South Africa. The morphology of these three specimens differ from that of *Melanorosaurus*; the dorsosacral rib-complex is directed strongly anterolaterally, not laterally as in *Melanorosaurus*, and the rib-complex originates from the anterior centrum edge, not at mid-length as with *Melanorosaurus* (Galton et al. 2005). Also, the third sacral of *Melanorosaurus* is not strongly backswept in dorsal view (Galton et al. 2005, Figure 1.4H), but the third sacral is backswept in GF13-II and GF13-III, which is the typical morphology of the second plesiomorphic sacral of sauropodomorph taxa (Yates 2003b). Similar to *Melanorosaurus*, the second sacral (=SI) rib-complex has a dorsal and ventral platform that are distally separate, and not joined by a vertical buttress.

The fourth sacral centrum of each of the Nova Scotia specimens is not fused to the centrum of the third sacral, and the lateral process was apparently not strongly sutured to the medial surface of the ilium. Therefore, the caudosacral was the last to join the sacral complex, and smaller (younger) specimens would be expected to have only three vertebra sacra each composed of a dorsosacral and the two plesiomorphic sacrals, such as is the case with the smallest specimen (GF69). The posterior portion of the sacrum of GF69 is not completely available for study. However, based on the left side there appears to only be three vertebrae that contact the ilium.

The rib-complex of the third sacral vertebra (SII) of both GF13-II and GF13-III reaches farther posteriorly (to the mid-point of the following centrum) than other basal sauropodomorphs, such as *Massospondylus* (Cooper 1981), *Lufengosaurus* (Young 1947), *Plateosaurus*, and *Efraasia* (Yates 2003b). The third sacral rib-complex of GF13-I is incompletely exposed.

The short length of the first caudal centrum (height greater than length) is an unambiguous derived character for Sauropodomorpha (Yates 2004), with several

reversals to the more elongate ancestral state. The anterior caudal centra of GF13-I are much taller (170%) than long, especially when compared to those of GF13-II and GF13-III, which have anterior caudal centra longer than tall. Cooper (1981, pg. 717) states that a "larger" specimen of *Massospondylus* (QG38) has an anterior caudal centrum much taller than long, while the smaller specimen (QG1159, Cooper 1981, figs. 13-14) has an anterior caudal centrum that is longer than tall. The phylogenetic significance of the proportions of the anterior caudal centra may therefore be confounded by intra-specific (ontogenetic, individual and/or sexual) variation. Likewise, the more distal position of the first chevron in GF13-I compared to GF13-II and GF13-III may also reflect intra-specific variation.

The identification of at least two morphs within the bone bed is further supported by evidence from the dorsal, sacral and caudal vertebrae. As with the pelvic morphology, the significance of this variation will be considered more fully elsewhere (see Chapter 10) within a broader phylogenetic context.

Chapter 7 – Comparative Descriptions of the Appendicular Skeletal Elements from the McCoy Brook Formation Bone Bed

Introduction

The pelvic and axial skeletal elements demonstrate a limited amount of morphological variation between the specimens recovered from the bone bed. To maintain consistency with the previous chapters, the morphology of the appendicular skeleton of specimens will again be evaluated individually, after considering the preservational state and obvious structural deformations exhibited by each specimen. Comparisons will be made between specimens and relevant taxa where possible, in order to consider the extent of morphological variation within the bone bed. The description of the forelimb elements associated with GF13-II, GF69, and GF9 are followed by the description hind limb elements (femur, tibia/fibula, tarsus and pes) recovered from the bone bed.

Description

Pectoral Girdle and Forelimb

Based on size and unique (left) coracoids (Table **3**), there were at least four specimens represented. However, only the partial right coracoid of GF69 can be confidently associated with an individual recognized by articulated elements. Similarly, only the scapulae of GF13-II and GF69 can be associated with certainty. The utility of these pectoral elements for discriminating between possible morphs is therefore limited. Description of the material is provided for phylogenetic analyses considered in Chapter 8.

GF13-II

The dorsal (distal) end of the left scapula of GF13-II remains associated with the ribs and dorsal vertebrae, although it is separated from the ventral portion of the scapula by a large (>10 cm) fault, so a reliable scapular length cannot be measured. The ventral portion of the left scapula was recovered in a separate block and directly overlies the ventral portion of the right scapula and the (unprepared) articulated right coracoid. A left

coracoid (GF13.129), recovered 40 cm from the scapula, has a small posteroventral portion of a scapula still attached to the suture and is therefore referred to GF13-II. The right clavicle is adjacent to the anterior edge of the scapula blade, and the right humerus and both sternal plates were also only slightly disarticulated (Figure 7.1) from the scapulae and coracoids.

Table 3: Listing of scapulae and coracoids that have been recovered from the bone bed, and their determined or possible (?) associations with specimens.

Associated Specimen	Scapula	Coracoid
GF13-I	- -	- -
GF13-II	R and L	?-98GF13.129 (L)
GF13-III	- -	- -
GF9	- -	?-98GF9.16 (L)
GF69	R	R
Unknown ?	98GF13.34 (L) 98GF13.43 (R)	98GF13.34 (L)

The dorsal end of the left **scapula** (98GF13.52) is 116 mm wide anteroposteriorly, and slightly expanded due to the extension of the posterior corner; the shaft near mid-length measures only 60 mm in width. The ventral portion of the scapula is poorly preserved, with the glenoid region apparently damaged prior to preservation.

The left **coracoid** (GF13.129, Figure 7.2B) is now completely removed from the matrix, and has a fragment of the scapula that remains attached immediately above the glenoid articular surface. In shape, the coracoid is an elongate semicircle with a dorsoventral height of 175 mm and maximum width through glenoid of 91 mm. Assuming the scapular articular surface was directed posterodorsally, the glenoid faces posteroventrally and is 42 mm long and 20 mm wide. The anteroventral corner of the coracoid is mediolaterally thickened, and is referred to here as an 'anterior tuber'. Externally, the coracoid foramen opens toward this anterior tuber, and is centered above the glenoid and at the mid point of the scapular articular facet. The scapula-coracoid suture deviates (anteriorly) immediately adjacent to the coracoid foramen.

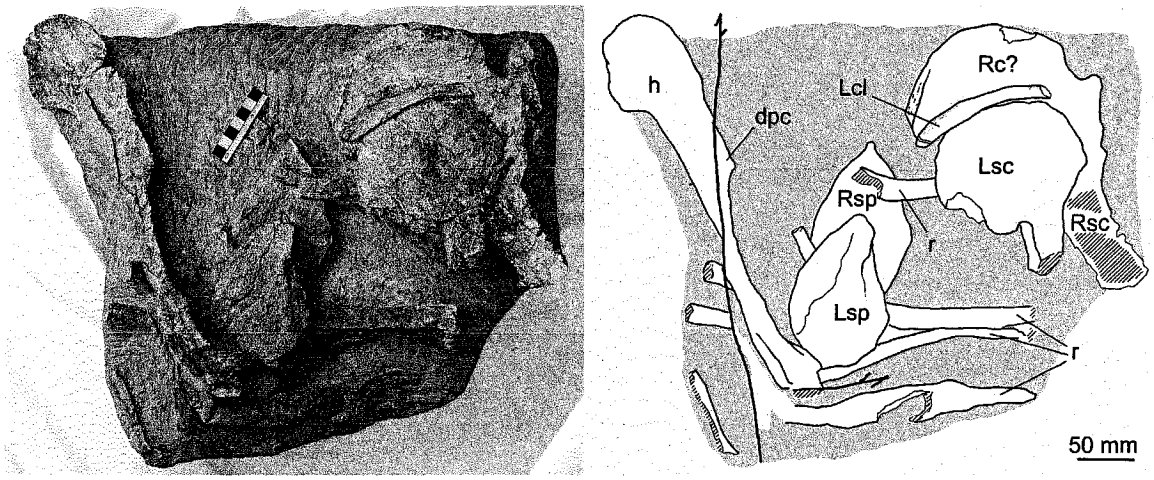

Figure 7.1: The pectoral girdle and fore limb elements of GF13-II.
The proximal (ventral) ends of the left (L) and right (R) scapula (sc) and distal end of the right humerus (Rh) are truncated by a large fault, and the right humerus is also deformed by a fault that traverses the distal end of the deltopectoral crest (dpc). The right coracoid (c) remains articulated to the scapula and the right and left sternal plates (sp) are slightly disarticulated and surround portions of several dorsal ribs (r). The left clavicle (cl) is located adjacent to the left scapula. Broken and faulted bone surface is denoted by cross-hatching.

The **right humerus** and both sternal plates were slightly disarticulated, and the humerus has been rotated away from the glenoid joint. The preservation of the humerus is poor, due to the faulting as well as internal cortical shrinkage; the distal portion of the humerus, including the distal edge of the deltopectoral crest, is displaced 40 mm (posterodistally) by an oblique fault, and a large transverse fault has truncated the ends of the distal condyles. Accounting for these faults, the humerus length is estimated at 285 mm and the distal end of the deltopectoral crest is 165 mm from the proximal end of the humerus. Therefore the deltopectoral crest extended well beyond the mid-length of the humerus.

The proximal anteroposterior width is 52 mm. The proximal end of the humerus is composed of a internal tuberosity that is directed posteromedially, an anteroposteriorly thickened humeral head located centrally, and the proximal portion of the deltopectoral crest (Figure 7.3A, B). In general proportions, the humerus is less robust than that of *Lufengosaurus* (Young 1941).

Both the right and left **sternal plates** are preserved (Figure 7.1, 7.2). The left sternal plate has been completely removed from the block, and is tear drop shaped; the narrow end directed dorsally. The plate is thin (4 mm), except for the dorsolateral edge,

which is thickened (20 mm) for articulation with the coracoid, near the anterior tuber. The left sternal plate is only exposed in anterior view, and is overlain by two ribs.

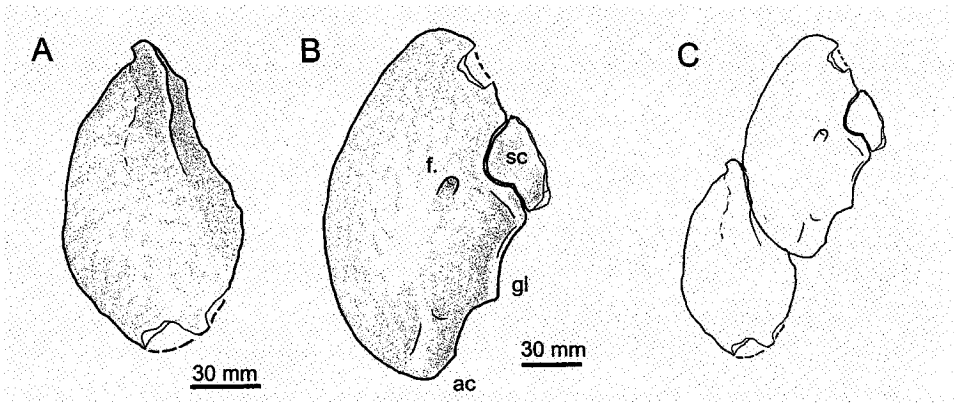

Figure 7.2: Left sternal plate (A) and coracoid GF13.129 (B) attributed to GF13-II, and proposed articular relationship (C).
A fragment of scapula (sc) remains attached to the coracoid immediately above the elongate glenoid (gl) of the coracoid. A long concave embayment separates the glenoid from the anterior tuber (ac).

A short, rod-like **clavicle** is located along the anteroventral edge of the left scapula (Figure 7.3C). It is 120 mm long, as 5 mm of the medial end was lost during collection. The clavicle is 17 mm wide near the medial end, and narrows in width distally. The anteromedial surface is covered by fine linear rugose striations. In general form, the clavicle is similar to that recently described for *Massospondylus* (Yates and Vasconcelos 2005).

GF69

A right **scapula** (GF69) and articulated coracoid fragment (Figure 7.4A, B) were reconstructed (by P. Olsen and others) from broken fragments collected as float in 1992. The dorsal end of the blade is missing. However, the scapula was at least 150 mm long, and 100 mm from the suture with the coracoid the shaft is 39 mm wide. The glenoid facet of the scapula is 27 mm in length, and the width across the ventral portion of the scapula is at least 106 mm.

The **coracoid** is only represented by a small fragment that remains attached to the scapula. The glenoid area of the coracoid is only partially preserved, thus the length of the coracoid glenoid facet is unknown, although was at least 11 mm in length.

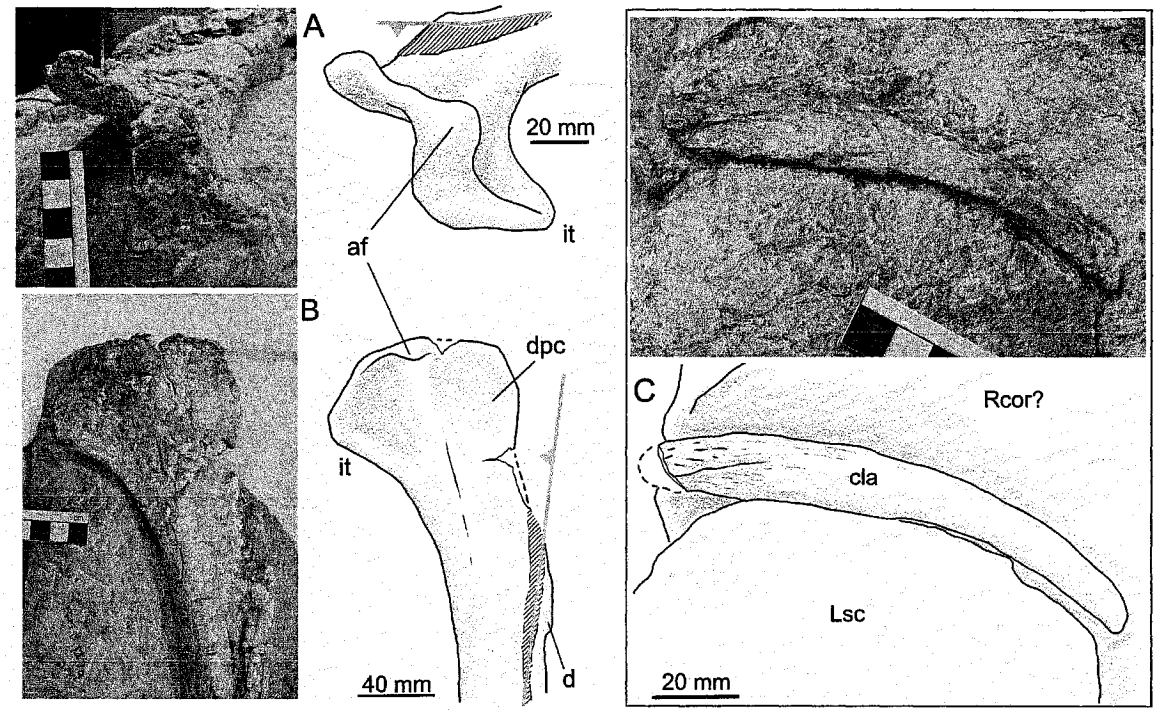

Figure 7.3: Disarticulated right humerus of GF13-II in proximal (A) and lateral (B) views, and the left clavicle (cla) still associated with the left scapula (Lsc) in lateral view.
A fault (grey line and crosshatching) offsets the distal end (d) of the deltopectoral crest (dpc). Other Abbreviations: af, articular facet fon head of humerus; it, internal tuberosity; Rcor?, right coracoid? (or scapula?) in medial view.

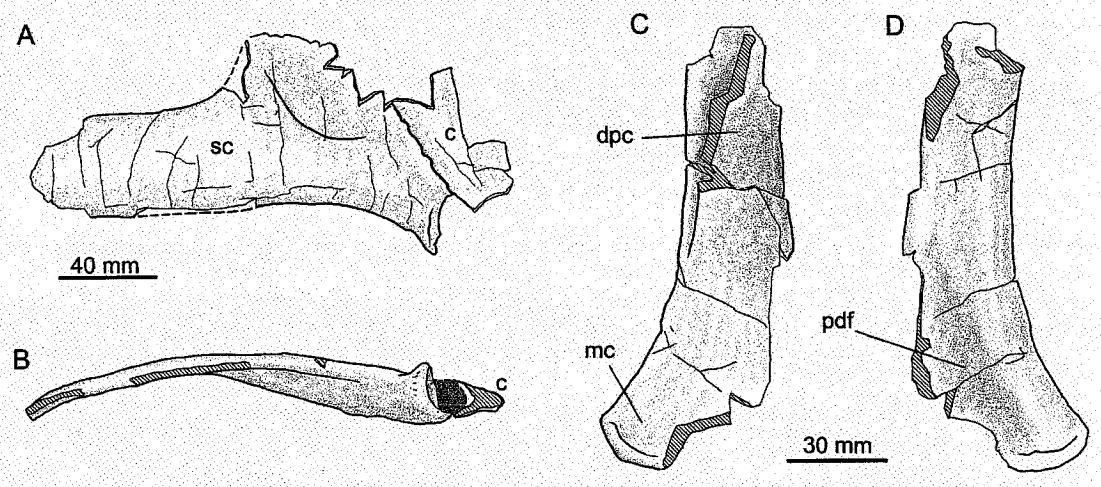

Figure 7.4: Right scapula (sc) and articulated coracoid (c) fragment in lateral (A) and ventral (B) views and the distal end of the left humerus in anterior (C) and posterior (D) views.
The distal end of the scapula blade, dorsal portion of the acromion process and majority of the coracoid were not recovered, and a small portion of sandstone remains in the glenoid fossa (grey.). The deltopectoral crest (dpc) and medial condyle (mc) are partially preserved, and a shallow fossa on the posterior distal surface of the humerus (pdf) does not appear to be a deformational artefact. The broken bone surfaces are denoted by cross-hatching.

The distal 130 mm of the left **humerus** (Figure 7.4C, D) was recently rebuilt from pieces collected during 1992 and 1994. However, the lateral (radial) condyle as well as the proximal portion of the shaft and deltopectoral crest could not be located. It appears as though the distal flexor fossa (Yates 2004) was present on the anterior distal surface, although the definition of the proximal edge has been obscured somewhat by anteroposterior crushing. Due to crushing, the anteroposterior length is reduced (only 9 mm) compared to the mediolateral width of 30 mm. The posterior distal surface between the two condyles is mildly concave but this is at least partially attributable to crushing. The preserved portion of the ulnar condyle is rather anteroposteriorly thin, with a well rounded articular surface (convex) anteroposteriorly as well as transversely.

The articulated right manus was isolated from the right radius/ulna by a fault, and is also deformed by several small faults, but is otherwise well preserved and important because it is the only manus represented among the bone bed specimens. The medial edge of the first digit has been truncated by a fault, unfortunately obscuring many of the details of this important digit. The ungual is incomplete distally.

Table 4: Measurements of the right manus of GF69.
The metacarpal (mc) and phalangeal (p) lengths are in millimetres; underlined values represent estimates due to faulting or distortion, and when preceded by a '+' sign represent minimum estimates. Ungual phalanges are denoted by an asterisk.

	mc	p1	p2	p3	p4
Digit 1	40	22	+30 *		
Digit 2	48	20	24	+35 *	
Digit 3	47	19	17	16	+15 *
Digit 4	?	13	+7		
Digit 5	25				

The second metacarpal is 15 mm wide proximally and at least 14 mm wide distally. The mediodistal edge of the second metacarpal and the proximomedial edge of the third metacarpal are displaced (or crushed) laterally by a fault. The phalanges of all digits are offset laterally by a separate fault, perhaps due to crushing. The unguals of digits I and III are missing significant portions distally. The distal half of the fifth metacarpal is offset dorsally by a fault, but the estimated length is 25 mm, or approximately 50% of the length of the third metacarpal.

The second digit is 137 mm long. The length of the right radius has an estimated length of 110 mm, but only the distal 130 mm of the right humerus is preserved, so the

relative length of the manus (digit 2) compared to the combined lengths of the humerus and radius cannot be reliably determined. *Anchisaurus* and derived sauropods each have a manus less than 38% of the combined humerus and radius length, whereas *Massospondylus*, *Plateosaurus* and *Lufengosaurus* have larger mani (45 to 38%) (Yates 2004).

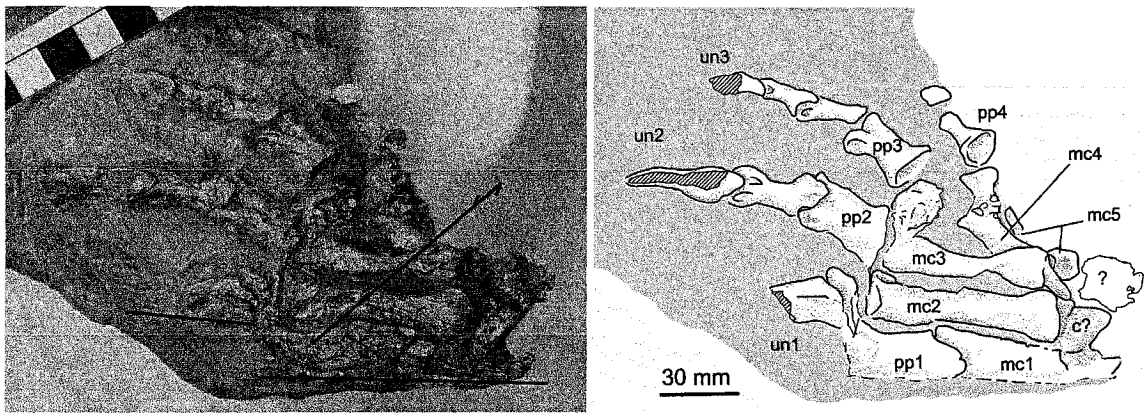

Figure 7.5: The only preserved manus from the bone bed, the left manus of 94GF69, in dorsal view. The first metacarpal (mc) and proximal phalanx (pp) and ungual (un)of digit 1 are truncated by a fault, and a second fault offsets the shafts of mc2-mc5 (photo). The phalanges of the digits are also offset laterally by a fault (not labelled). A poorly defined carpal (c?) appears to be present on the proximal end of mc2, and the fractured remains of a second carpal (?) appear to be located more laterally.

GF9

A left radius and ulna (Figure 7.6), and left coracoid (Figure 7.7) were recovered with the femora and other rear limb elements. The radius is missing portions of the proximal and distal ends, and the ulna is missing the proximal end of the olecranon process due to a rock-saw cut. The radius is currently 120 mm, but was approximately 135 mm in length. The ulna measures 108 mm, from the proximal articular surface to the distal condyle, the length from the distal condyle to the tip of the olecranon process was approximately 135 mm. The radius is similar in size and proportions to the partial right radius preserved with GF69. As the material associated together as GF9 is disarticulated and may combine elements of more than one individual, it remains possible that the left radius and ulna associated with GF69, a specimen that includes the distal end of a left humerus.

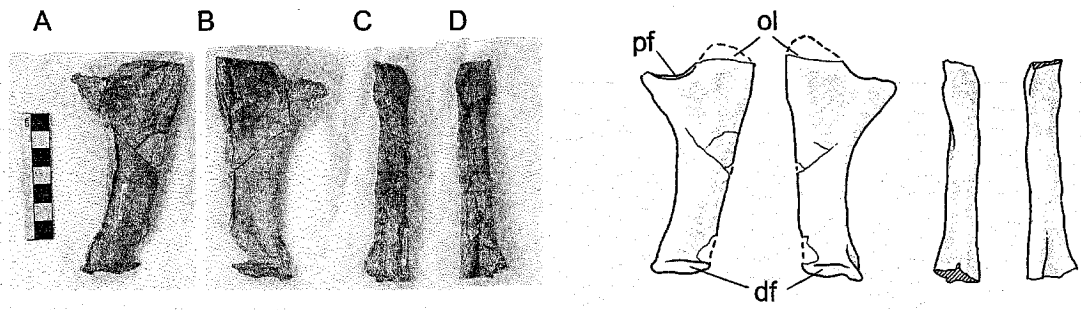

Figure 7.6: Left ulna (A, B) and radius (C, D) collected with GF9 in lateral (A, D) and medial (B, C) views.
The olecranon process (ol) was severed by a rock-saw cut, immediately proximal to the proximal articular face t (pf) for the humerus. The distal arcticular facet (df) is slightly compressed (mediolaterally) but is still somewhat rounded. The radius is missing the proximal and distal ends (cross hatching).

The left coracoid is nearly complete, and the anterior-half is offset medially 5 mm due to a fault. The coracoid foramen is located anterior to the mid-length of the scapular facet, and is level with the centre of the glenoid. Externally, the foramen is directed toward the anteroventral corner of the coracoid, and internally it exits the medial surface of the coracoid along the dorsal edge of the scapula coracoid suture. The glenoid articular facet is widere (mediolaterally) than long, 32 mm and 24 mm respectively. With the scapular articular facet oriented posterodorsally, the glenoid facet of the coracoid faces posteroventrally. Immediately anterior to the glenoid, the ventral surface is embayed, especially the medial edge, separating the glenoid from the anterior tuber, located at the anteroventral corner of the coracoid. This embayment is mediolaterally wider than anteroposteriorly long, especially compared to the coracoid of GF13-II. Considering the relatively deep glenoid, and the short and deep embayment, the coracoid was likely compressed anteroposteriorly. The embayed area separates the glenoid from another 'anterior tuber' that is another mediolaterally expanded area.

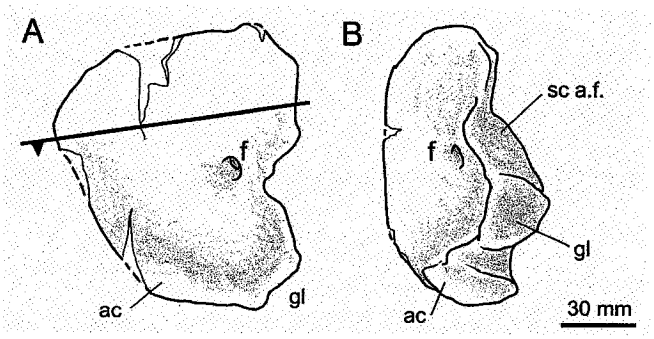

Figure 7.7: Left coracoid associated with GF9 elements, in lateral (A) and posteroventral (B) oblique view.
The dorsal portion of the coracoid has been offset (anteriorly) by a fault. Abbreviations: ac, anterior tuber; f., foramen; gl, glenoid; sc a.f., scapula articular facet.

The ventral edge of the scapular articular facet is as deep as the glenoid, but the facet narrows rapidly dorsally, becoming as thin as the more anterior portion of the coracoid. Similar to the coracoid of GF13-II, the scapula coracoid suture deviates anteriorly immediately adjacent to the coracoid foramen. A similar deviation of the scapula coracoid suture toward the coracoid foramen is well developed in *Lufengosaurus* (Young 1941, Figure 8) and *Massospondylus* (Cooper 1981, Figures 16a, 22), and present but less developed in *Plateosaurus* (von Huene 1932, Moser 2003). However, the scapula coracoid suture is not deviated in *Thecondontosaurus* (Benton et al. 2000, Figure 11C) or derived sauropodomorphs such as *Shunosaurus* (Zhang 1988) or *Omeisaurus* (Upchurch 1998).

Other

An articulated left scapula and coracoid (GF13.34) were collected near an isolated right ilium (GF13.46) that has been attributed to GF13-III. It cannot be determined if the scapula and coracoid associate with GF13-I, GF13-III, or perhaps another skeleton. The scapula was collected in several pieces while channelling around the block containing the left pes of GF13-I, and the dorsal end was poorly preserved due to cortical shrinkage after collection. The mid-length shaft proportions are similar to another isolated (right) scapula (GF13.43), and it remains possible these are collateral elements. The coracoid is strongly deformed due to anteroposterior compression. The coracoid foramen cannot be identified.

The other isolated (right) scapula (GF13.43) was located underneath the proximal-half of an isolated left femur, GF13.42. The scapula blade is deformed by four faults, displacing the blade into a series of staircase like fragments. The scapular proximal end was severed by two rock-saw cuts during collection. The acromion depression is visible on the posteroventral edge of the lateral surface, but most of the ventral edge has been damaged. The medial surface of the ventral end has a well developed longitudinal ridge that extends from the coracoid suture to about one-third scapula length. A similar ridge is present on the medial surface of 98GF13.34, although somewhat obscured by crushing and deformation. As a consequence of faulting the scapular length can only be estimated at 266 mm along the anterior edge. The shaft at mid-length is 57 mm long (anteroposteriorly), and the dorsal end is slightly expanded, measuring 75-80 mm. The dorsal end of the blade appears to have been rather square with mildly rounded corners, rather than having an extended posterodorsal corner as in GF13-II; although this is difficult to confirm due to faulting.

Femur

The presence of at least five different skeletons (Table **3**) can be identified based on complete right femora (GF13-1, GF13-II and GF69), the proximal end of a right femur (PU-22126), and the distal end of a different right femur (GF9.10b). Most femora from the bone bed exhibit compression distortion due to the collapse of the large medullar cavity during preservation, greatly limiting the amount of information that can be determined from the femora. For example, the sigmoid curvature in lateral or anterior views that is common for many 'prosauropods' (Galton and Upchurch 2004) cannot be evaluated in any of the bone bed femora due to compression, or missing portions.

GF13-I

The right femur (98GF13.13) is well represented from the proximal end to the distal edge of the fourth trochanter. Beyond this point the shaft is extensively damaged due to multiple left lateral faults. The proximal half of the femur is deformed due to crushing and the femur head is offset dorsally by a small fault.

The lesser trochanter is well preserved as a longitudinally oriented muscle scar, which is inset medially from the lateral edge of the femur shaft. The lesser trochanter is therefore not visible in posterior view, similar to *Massospondylus* (Cooper 1981), *Lufengosaurus* (Young 1947) and *Yunnanosaurus* (Young 1951), and differing from *Melanorosaurus* (Galton et al. 2005). A shallow longitudinal depression adjacent to the medial edge of the lesser trochanter proximally, bends medially near the distal limit of the trochanter. A similar shallow longitudinal depression is also present on PU22196, and 98GF13.128, the only other specimens which are adequately preserved.

Table 5: The number and portions of femora associated with various specimens within the bone bed.

Based on the number of unique right femora, there are at least five individuals represented within the bone bed.

Specimen #			Comments
GF13-I	-	R	Proximal end, to below fourth trochanter.
GF13-II	-	R	Complete but fault deformed right.
GF13-III	-	-	
GF9	L	R	Complete left, distal 1/2 of right.
GF69	L	R	Complete left, telescopically crushed right.
PU22126	-	R	Proximal end of right
GF13.42	L	-	Proximal end of left, many faults.
GF13.128	L		Complete left, anteroposteriorly flattened.

The proximal end of the lesser trochanter is nearly level with the distal edge of the head of the femur, similar to *Euskelosaurus, Lufengosaurus, Massospondylus* and *Yunnanosaurus* (Galton and Upchurch 2004), and all other femora from the bone bed (GF13-II, 98GF13.128, GF9, PU22126, and possibly 98GF13.42)

In posterior view, there is a well-developed depression (sulcus) immediately lateral to the femoral head. The lateral border of the sulcus is defined by an anteroposteriorly thickened tuberosity ('medial tuber', Langer 2001), which is a narrow oval with the long axis oriented dorsoventrally. The medial tuberosity is located at the mid-width of the proximal end. Lateral to the medial tuberosity, the rugose proximal edge becomes visible in posterior view; the proximal surface becomes directed posterolaterally and represents the greater trochanter.

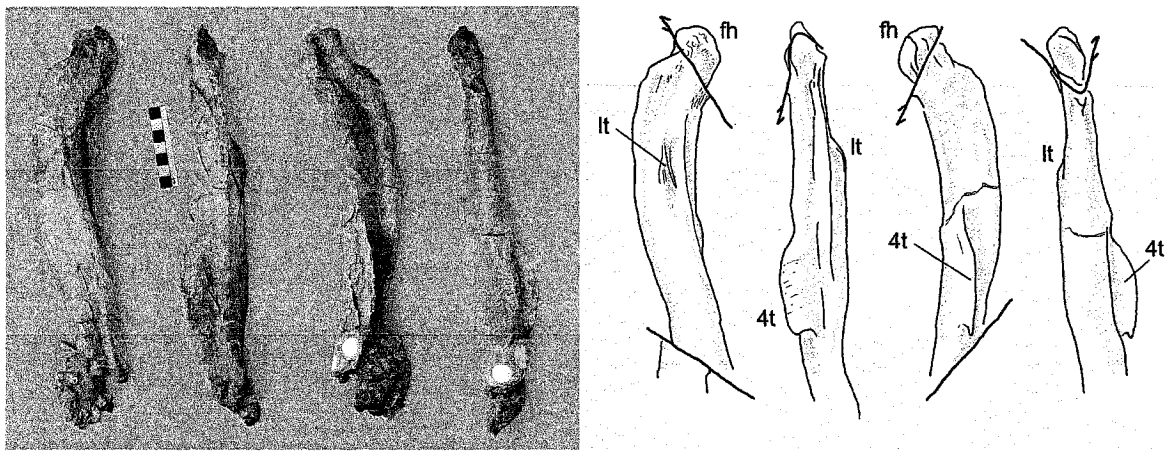

Figure 7.8: Proximal-half of the right femur of GF13-I in anterior (A), lateral (B), posterior (C), and medial (D) views. Abbreviations: fh, femoral head; lt, lesser trochanter; 4t, fourth trochanter.

The fourth trochanter is pendant, with a concave distal margin in lateral view (Figure 7.8). The distal edge is 220 mm from the proximal end. The shaft is faulted distally and incompletely preserved, but the length is greater than 400 mm. The trochanter is parallel to the long axis of the femur, and inset slightly laterally from the medial edge of the shaft. The position of the fourth trochanter is offset laterally from the medial edge of the femur in many sauropodomorph taxa, including Massopondylidae, and the fourth trochanter is pendant in *Massospondylus*, and at least some individuals of *Lufengosaurus* and *Yunnanosaurus* (Galton and Upchurch 2004).

GF13-II

The complete right femur was only slightly dislocated from the acetabulum. The longitudinal axis of the femur shaft was oriented obliquely through the bedding plane, and the downward post-burial compression force sheared and mediolaterally compressed the medial portion of the femur shaft, and also obliquely flattened the distal shaft and condyles. Most morphological details are obscured by this complex crushing as well as deformation from numerous displacement faults.

The femur head narrows sharply proximally and no medial tuberosity is identifiable due to compression deformation. Although now subtle due to deformation, the posterior surface immediately lateral to the femur head exhibits longitudinal furrows. Similar striations are also well developed in 98GF13.42. Although similar in overall size, the preserved structures of the proximal femur (GF13-II) cannot be easily related to

PU22196. The articular surface of the femoral head appears to be directed more medially and the thin proximally tall posterior surface produces a proximal surface directed anteriorly, not posteriorly as in PU22196.

The proximal 60 mm of the femur are displaced by a large fault, truncating the proximal end of the lesser trochanter. The fourth trochanter is symmetrical, without a well developed distal prong. The distal edge is straight, but the extremely deformed nature of this area of the femur reduces the significance of these features, which may represent a deformational artefact.

GF9

The left femur (FGM998GF9.10.1) is complete, 490 mm in length, but deformed by several faults and anteroposteriorly compressed. The lesser trochanter is a longitudinal ridge, the proximal edge located level with the distal edge of the femoral head. The anterior edge is deformed by crushing and folded over laterally. The distal end of the femur head narrows sharply toward the distal edge. The medial tuberosity (Langer 2004) is well developed and positioned similarly as in GF13-I, near the mid-width of the proximal end. As preserved, the greater trochanter is located toward the anterior edge of the proximolateral surface. Based on the bone texture lateral to the tuberosity, this area appears to have been eroded slightly prior to collection.

The fourth trochanter is large and sheet-like, with a well developed distally directed tip and concave ventral edge, and is inset from the medial edge of the shaft. The apex of the fourth trochanter is located 240 mm from the proximal end, and is therefore located within the proximal half of the femur, similar to most basal sauropodomorphs (Galton and Upchurch 2004). The shaft of the left femur is dramatically crushed at mid-length, the posteromedial edge displaced laterally to expose anterior portion of the cortical bone as a sharply defined surface (Figure 7.9C).

The distal end of the right femur (Figure 7.10) was located adjacent to and appressed against the left femur. This fractured shaft was taphonomically broken; a sharply defined splinter fracture is located 230 mm from the distal condyles and immediately below the fourth trochanter based on comparison with the left femur. The shaft has not been compressed, because the large medullar cavity was filled with sand

prior to final burial, providing additional structural support during preservation. The maximum diameter of the (uncrushed) right femoral shaft below the fourth trochanter is 46 mm (anteroposteriorly). The medullar cavity at this same location is 35 mm in diameter, or 76% of the shaft width.

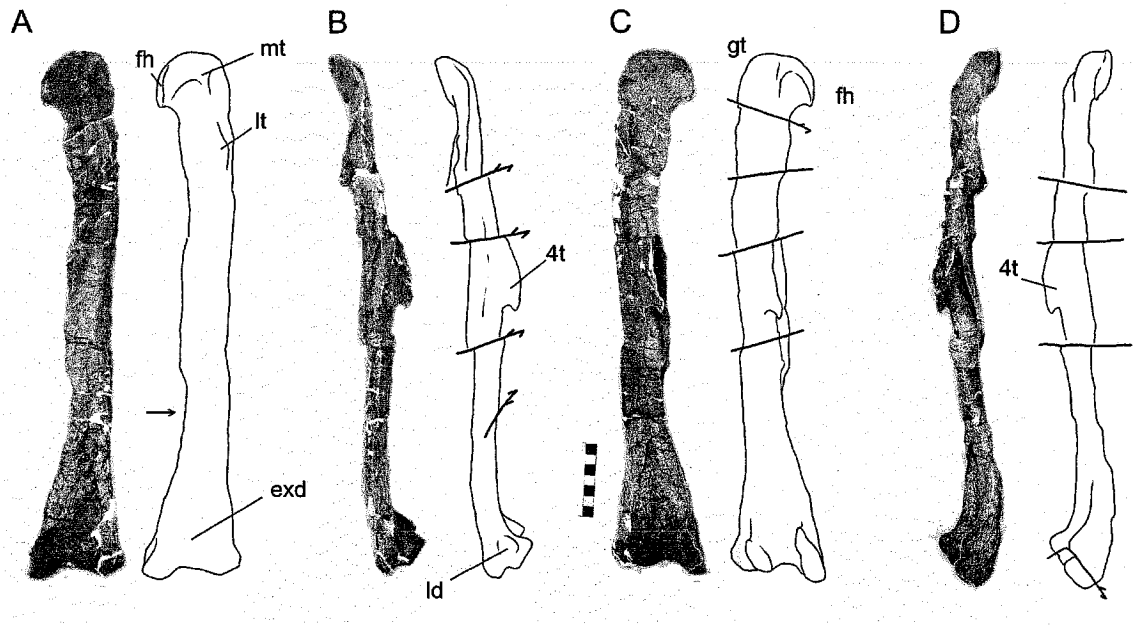

Figure 7.9: Complete left femur FGM998GF9.10.1, in anterior (A), lateral (B), posterior (C), and medial (D) views. Abbreviations: exd, extensor depression; fh, femur head; ld, lateral depression; lt, lesser (anterior) trochanter; mt, medial tuberosity; 4t, fourth trochanter.

The orientation of the distal condyles with the more proximal portion of the femur may be distorted by the numerous fault offsets. However, assuming the anteroposterior axis of the femur is oriented with the long axis of the medial condyle (Hutchinson 2001a), the femoral head is directed anteromedially. The medial distal condyle is mediolaterally broader than the lateral condyle. There is a depression on the lateral surface of the lateral condyle (Figure 7.9B). The lateral condyle is divided by a groove into a distal component and a smaller, posteriorly directed ectocondylar tuber (Welles 1984). The extensor depression on the anterodistal surface of the femur is still visible, although the area was mildly flattened by anteroposterior compression.

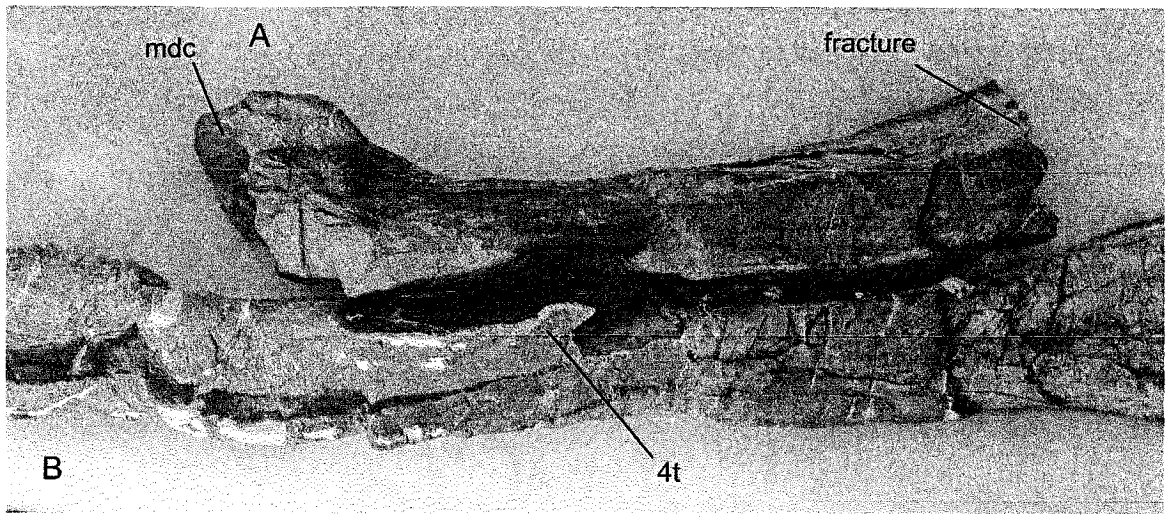

Figure 7.10: The distal end of the right femur (A) appressed against the mid-shaft of the left femur (B), as oriented during preservation. The shaft of the right femur is fractured. The distal end of the left femur (B) is outside of the frame, on the right side of the photo. Abbreviations: 4t, fourth trochanter; mdc, medial distal condyle of right femur.

GF69

The right and left femora of GF69 are preserved, although the right is so badly deformed by telescopic shortening and faulting it would likely not be recognized as a femur except for it remains in articulation between the pelvis and tibia. The left femur is complete, but extensively crushed mediolaterally, and the proximal end remains unprepared within the acetabulum of the left ilium. The lesser trochanter is visible on the proximalmost exposed edge, but the proximal edge of the trochanter is located on the unprepared section within the acetabulum of the left ilium. The fourth trochanter is approximately 62 mm in length, and located 215 from the distal end. However, the length of this distal portion of the femur appears to be exaggerated due to the deformational crushing.

The lateral distal condyle has a distal component and a posterior component, which are separated by a shallow concave edge and oriented perpendicular to each other. The medial distal condyle is directed posterodistally, and is broader (mediolaterally) than the lateral distal condyle. The two condyles (medial and lateral) are separated by a deep sulcus posteriorly, that extends half way up to the distal end of the fourth trochanter. The lateral condyle has a shallow depression on the lateral surface, again similar to GF9.

Other

The proximal 277 mm of a robust right femur (**PU-22196)** were apparently broken obliquely during collection in the 1970's and the distolateral edge was offset slightly laterally and proximally when repaired. This misalignment gives the shaft an increased (artificial) width. This proximal fragment represents a distinct individual separate from GF9, which includes the distal portion of the right femur. The fourth trochanter of GF9 left femur is 240 mm from the proximal end, whereas in PU-22126 the fourth trochanter is only 210 mm distal to the proximal end. Also, the fourth trochanter is located along the medial edge of the shaft, not inset laterally as in the left femur of GF9.

Similar to GF13-I the lesser trochanter is a longitudinal oriented ridge, inset from the lateral edge of the femur, with a shallow longitudinal depression located medially. The proximal end of the lesser trochanter is approximately level with the distal edge of the head of the femur. The distal-half of the fourth trochanter is missing; therefore the shape of the distal edge cannot be determined.

The proximal half of another isolated (**left**) femur, 98GF13.42, is badly deformed by both transverse and longitudinal oriented faults. Immediately distal to the fourth trochanter the shaft is truncated with sharp edged splinter fractures. The femur may associate with either GF13-I, GF13-II, or GF13-III, or PU22126. The fourth trochanter is offset posteriorly by an oblique transverse fault, but the distal end is well preserved and is concave, with a slight posterodistal projection (hook). The lesser trochanter is not visible in posterior view, and is well developed with a sharply defined (anterior) edge.

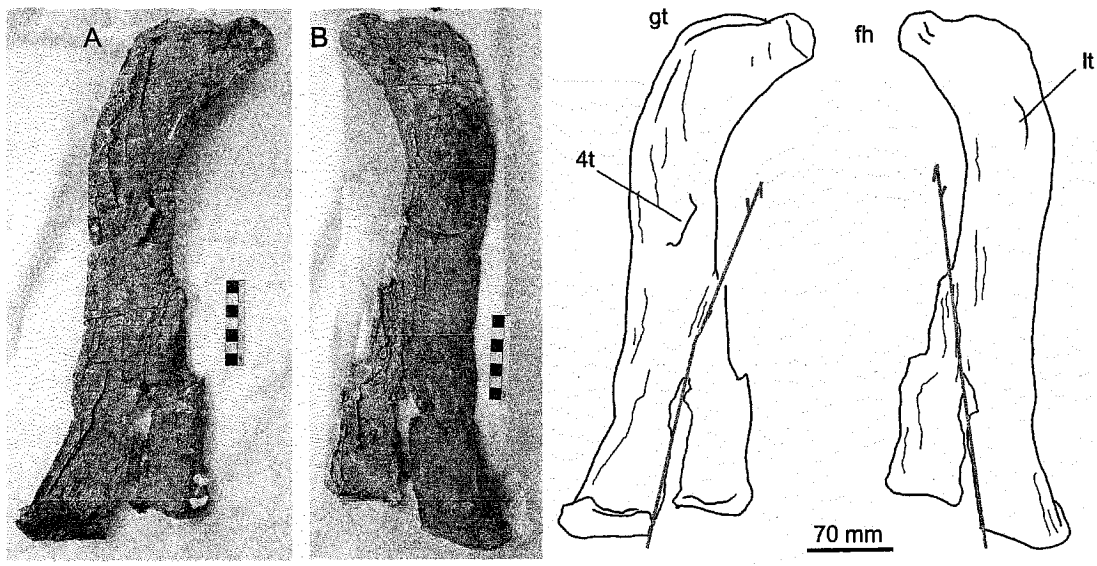

Figure 7.11: An isolated left femur (98GF13.128) in posterior (A) and anterior (B) views, which is anteroposteriorly flattened due to compression, and the medial distal condyle is offset by a fault. Abbreviations: fh, femur head; gt, greater trochanter; 4t, fourth trochanter; lt, lesser trochanter.

A complete **left** femur (98GF13.128, Figure 7.11) near the disarticulated pectoral girdle may associate with GF13-I, GF13-II or GF13-III. The femur has been anteroposteriorly flattened due to compression. The femoral shaft is only 17 mm in length anteroposteriorly but is 82 mm wide mediolaterally. The current length is approximately 425 mm, but this also includes a small amount of expansion due to crushing. An oblique fault offsets the medial distal condyle as well as the medial portion of the femoral head. As preserved, the fourth trochanter is short and the distal end is 180 mm from the proximal end, and inset from the medial edge of the shaft.

Tibia/Fibula

GF13-I

The **right** tibia and fibula of GF13-I were articulated with the right femur, but both are in poor condition; having fractured into small fragments due to erosion damage while exposed at the cliff surface prior to collection. The proximal anterolateral edge (cnemial crest) of the right tibia was crushed and displaced posteriorly during preservation, and the lateral (fibular) condyle and anteromedial portion of the tibia were damaged during collection; this was the first portion of the specimen discovered in 1998.

The length of the tibia is approximately 340 mm and the mediolateral width of the anterior distal process is 85 mm.

Based upon the appropriate orientation and location, a **left** tibia, fibula and partial pes are also referred to GF13-I, the proximal tibia is directed toward and located a reasonable distance (350 mm) from the acetabulum of GF13-I. The association is also supported by the similar sizes of the referred left tibia and the articulated right tibia. The distal mediolateral width of the left tibia is also 85 mm, and although the left tibia has been shortened by several oblique faults, it appears to have been of similar length to the right tibia.

The left tibia is damaged by compression, especially on the proximal end. The posterolateral rim of the proximal articular surface is flared strongly laterally as a consequence of the medial displacement of the posterolateral tibia surface due to crushing and the collapse of the medullar cavity. The crushing of the proximal portion of the tibial shaft was oblique, in a posteromedial and anterolateral direction. Deformation expanded the anteroposterior length while decreasing the width of the proximal shaft, and displaced the fibular condyle anteriorly from the more midline location it likely occupied prior to deformation. The proximal articular surface is an elongate oval, 147 mm long and 55 mm wide mediolaterally, although again this has been deformed by oblique compression. The posterior edge of the cnemial crest is bordered by a well developed ridge on the anterolateral portion of the tibia, which is the deformed remnant of the fibular condyle. The fibula was slightly disarticulated from this ridge, but a groove in the proximomedial surface of the fibula corresponds well with the proportions of the ridge that represents the fibular condyle.

In general, the lateral condyle (ridge) is in a similar position as the fibular condyle of the left tibia of GF69 and GF13-II. However the mid-line (to slightly anterior) position of the fibular condyle differs from that of GF9, in which the condyle is along the posterolateral margin of the tibia.

The anteroposterior length of the distal portion of the tibia has been reduced slightly due to compression, but the mediolateral width of the distal articular facets for the astragalus (30 mm) are appropriate for the preserved widths of articular surfaces on the proximal surface of the astragalus. The anterior distal process of the tibia is extended

distally as far as the posterior distal process, and is not recessed from the distal end as in other basal sauropodomorphs (Galton and Upchurch 2004). Therefore, the anterior distal process covers the anterior surface of the ascending process. This distal extension of the anterior distal process represents the pre-deformational shape. All six tibia from the bone bed exhibit a distally expanded anterior distal process, regardless of their differing deformational histories and orientations. Aslo, a unique and large (2 mm) foramen on the articular surface of the anterior distal process of GF13-I aligns with the fossa at the anterior base of the ascending process, which would accommodate the distal extension of the anterior process, and not be expected if the process was recessed proximally.

GF13-II

Another isolated **left** tibia and fibula are located under the left pes of GF13-I, although only the proximal ends are currently exposed. The association of this tibia and fibula to GF13-II is based on the appropriate orientation, and reasonable distance from the acetabulum (450 mm) of this specimen. If the tibia and fibula were prepared from the underside of the block, it is likely that an articulated left foot (if preserved) would not be extensively deformed by faults.

The **right** tibia remains in partial articulation with the femur, fibula and pes, although it has been offset and deformed by several very large displacement faults that limit the ability to measure the length with any accuracy. The proximal 125 mm of the tibia and fibula were severed by two rock saw cuts during collection. The estimated length is 380 mm, based on the sum of lengths of the faulted components (Figure 7.12), which is similar to the tibia length of 98GF9.

The femur was apparently buried obliquely, with the long axis of the shaft oriented at approximately 45° to the bedding plane, and resting on the mediodistal edge of the medial condyle. With this orientation the lateral edge of the lateral condyle was directed upwards, and downward compressive force was directed obliquely on the shaft and condyles. The convex lateral edge of the shaft was flattened and displaced slightly posteroventrally, and the lateral condyle was flattened dorsoventrally.

The right tibia and fibula were slightly dislocated from the femur but are oriented similar to the long axis of the femur; 45° to the bedding plane. The fibula was slightly

dislocated from the fibular condyle of the tibia (shifted anterolaterally) and oriented with the posterolateral edge directed upwards. This orientation resulted in the anteroposterior deformation of the fibula due to the downward compression force of the overlying sediment; the medial surface of the fibula is now strongly embayed on account of this compression. The tibia lateral condyle is located at the midpoint of the proximal lateral surface of the tibia. Immediately posterior to the fibular condyle, the proximolateral surface is gently recessed, and has likely been expanded in anteroposterior length due to the oblique compression. The anterior edge of the cnemial crest is deformed posterolaterally, resulting in a sharply defined and deep cavity. Fine rugose striations are visible on the anteromedial surface of the proximal tibia; offset distally 50 mm from the proximal edge. Also, an oblique ridge from the middle of the proximomedial edge, which is directed anterodistally, meets the rugose striations on the anteromedial edge and does not appear to be due to deformation.

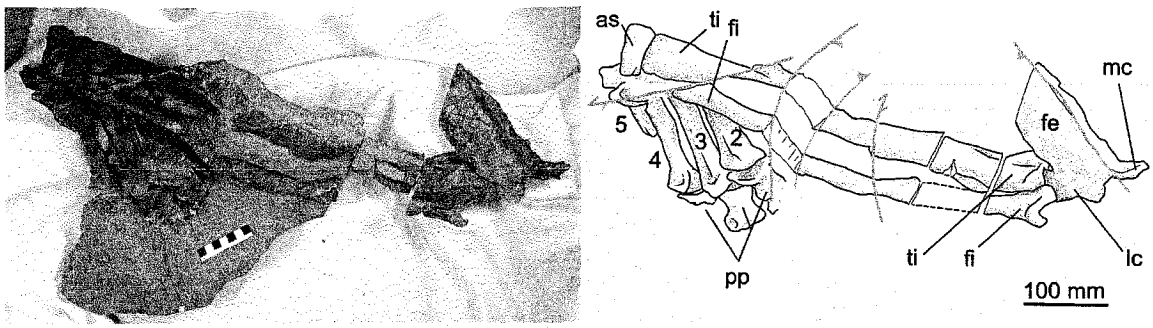

Figure 7.12: The badly faulted (grey lines) right hind limb of GF13-II in posterolateral view; including the femur (fe), tibia (ti), fibula (fi), astragalus (as), and metatarsals (2-5) and proximal phalanges (pp).

The proximal articular surface of the tibia is rugose and 100 mm long (anteroposteriorly); much shorter than the proximal surface of the tibia of GF13-I (147 mm), which was certainly expanded due to deformation. The distal end of the tibia is partially dislocated from the tarsus and pes, in a position of extreme dorsiflexion, and the astragalus is displaced distally 10 mm.

Similar to GF13-I, the anterior distal process covers the anterior face of the astragalar ascending process prior to deformation. It cannot be reliably determined if

there was a foramen on the articular facet of the tibial anterior distal process, as is present on the left tibia of GF13-I.

GF69

The **right** tibia and fibula of GF69 are articulated with the right tarsus, pes and the badly deformed right femur. The proximal end of the fibula and posterior corner of the proximal end of the tibia are offset posteriorly by several displacement faults, and the shafts of both the tibia and fibula are also shortened by an oblique fault that offset the distal ends anteriorly and proximally (Figure 7.13); as preserved the right tibia is only 190 mm in length.

The **left** tibia was deformed obliquely through the anteromedial and posterolateral edges, and the left fibula was compressed anteroposteriorly. The deformation lengthened the posterior portion of the tibia, displacing the condyle onto the anterior half of the lateral surface, whereas it was likely positioned more centrally prior to deformation. The proximal articular surface of the left tibia has sharply defined, crest like rugose texture, but the proximal fibular articular surface is gently rounded, both mediolaterally and anteroposteriorly.

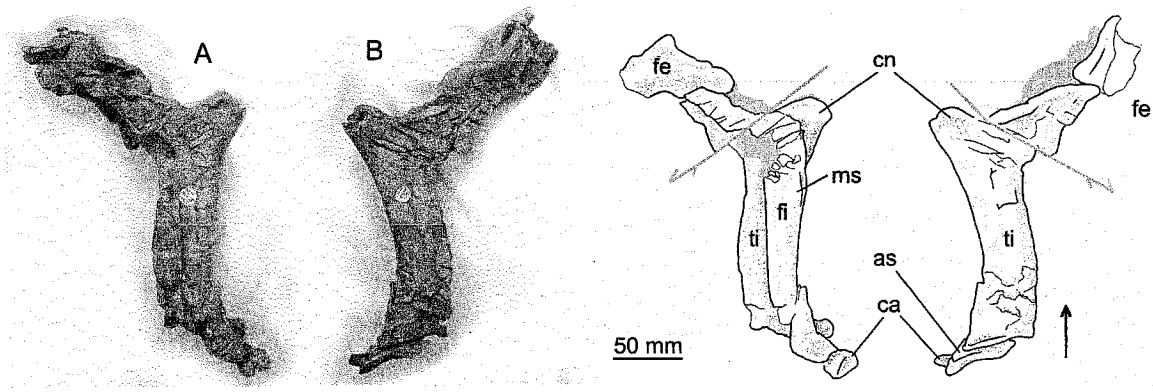

Figure 7.13: The distal end of the right femur (fe), and articulated tibia (ti), fibula (fi), astragalus (as) and calcaneum (ca) of GF69, in lateral (A) and medial (B) views.
The tibia and fibula are telescopically shortened by compression (arrow), and the proximal ends are offset by several faults (grey line). Fine rugose striations remain visible on the anterolateral edge of the cnemial crest (cn). The muscle scar (ms) for insertion of M. iliofibularis is present on the anterolateral edge, about 1/3 from the proximal end.

Based on the lengths of the faulted components, the estimated length of the left tibia is 285 mm,. The proximal anteroposterior width of the left tibia is 85 mm; the posterior edge of the proximal end of the right tibia is offset by faulting, and cannot be

reliably measured. As preserved, the fibular condyle is located within the anterior half of the proximolateral surface of the left and right tibia. While this has likely been exaggerated due to compression of the proximal end, the condyle was certainly located near, if not at the mid-point of the lateral proximal surface. The lateral condyle is 55 mm from the proximal posterior edge of the tibia. The cnemial crest extends 22 mm from the anterior edge of the fibular condyle on the left tibia, and is not notably expanded dorsally above the proximal articular surface. The medial surface of the cnemial crest is concave, and the anterior edge is directed anterolaterally. This concave depression on the lateral surface of the cnemial crest extends 45 mm distally along the anterolateral edge of the tibia (less than 1/3 tibia length), although the distal boundary is incompletely prepared. Posterior to the fibular condyle, the tibia rapidly narrows (mediolaterally) toward the posterior edge, which is consistent with compression. In lateral view, the posterior and proximal edges meet at an acute (~ 45°) angle.

Rugose linear striations are located on the anteromedial surface of the right and left tibia, extending posterodistally 30 mm from the anterior proximal edge. The anteroposterior width of the tibia tapers to 40 mm, 120 mm from the proximal end. The mediolateral width at this location is only 20 mm, although this is likely reduced due to mediolateral compression.

The distal ends of the tibia are somewhat obscured by crushing and displacement of the astragalus (Figure 7.19), but like GF13-I (and other tibia from the bone bed) the anterior distal process overlaps the ascending process of the astragalus. The anterior and posterior distal processes extend a similar amount laterally.

The anteroposterior width of the proximal end of the **fibula** is 40 mm on both the left and right side. The proximal fibular medial surfaces are mildly concave, but remain tightly appressed against the lateral condyle of the tibia. The shaft of the right fibula preserves a distinct muscle scar on the anterolateral surface (Figure 7.13A), positioned about 85 mm from the proximal end. The length of the left fibula is estimated at 245 mm, and therefore the muscle scar is located distally about one-third of the fibular length, which is the typical location for the insertion of M. iliofibularis (Langer 2001).

GF9

Association of the left tibia (FGM998GF9.11) and fibula (FGM998GF9.3 is well founded based on their close proximity. The tibia is 77% the length of the femur, which is a typical for Sauropodomorpha, which have a tibia slightly shorter (75-90%) than the femur (Benton et al. 2000).

The complete left tibia (FGM998GF9.11) was recovered in close proximity to the left femur, fibula, and distal end of the right femur. The proximal end of the tibia was collected in 1997 and the remaining distal portion was collected during the excavation in 2000. Although a small wedge of bone is missing from mid-length, the contact of the proximal and distal ends exists along the medial edge; therefore the preserved length is accurate. The anterior edge of the cnemial crest was damaged during collection, and two faults offset the proximal end. The proximal articular surface is displaced posteriorly by a transverse fault and an oblique fault displaces the entire proximal end anteriorly relative to remainder of the tibia. Anteroposterior compression of the tibia is also evident, with collapse structures on the lateral surfaces of the shaft.

Prior to being repaired, the cross-sections also demonstrated the nature of subduction that has occurred at mid-shaft. Approximately 14 mm of the medial surface is displaced centrally, resulting in the complete collapse of the medullar cavity. Sediment matrix inclusions are not found in the bone subduction zone, which demonstrates the medullar cavity was empty prior to structural collapse. Also the cross-sections show the cortex of the tibia at mid-shaft was 7 mm thick, and fine longitudinal cracks in the shaft can be seen in cross section to extend 1.5 mm into the cortex, suggestive of subaerial drying.

The lateral condyle of the tibia is on the posterior edge of the proximal medial surface, and this posterior position is not due to deformation. The anterior edge of the proximal tibia (cnemial crest) was damaged during collection, and the specific anterior extent is unknown. Fine longitudinally oriented striations are visible within the concave surface on the anterolateral surface of the tibia, and this lateral surface of the cnemial crest is concave (anteroposteriorly). A low ridge appears to have emanated distally from the anterior edge of the fibular condyle, but anteroposterior crushing of the tibia shaft complicates the interpretation of the structure.

The tibia length is 390 mm, and the shaft is notably flexed in medial and lateral views (Figure 7.9). However, the flexion is at least partially a consequence of deformation. The posterolateral process extends laterally slightly beyond the anterolateral process of the distal tibia. Similar to other tibia from the bone bed, the anterior distal process is not recessed from the proximal end, but rather extends as far distally as the posterior process. The posterior distal process has a well developed and nearly horizontal articular facet, but the anterior distal process articular facet is inclined posteriorly.

The ratio of radius to tibia length is 0.50 for *Lufengosaurus* (Young 1947). Assuming a similar ratio for GF9, the projected radius length would 245 mm. The length of the radius associated with GF9 is only ~135 mm, notably shorter than expected. However, the radius and ulna are an appropriate length for association with GF69, which has a tibia length of ~285 mm, which suggests the material included in GF9 likely represents multiple individuals.

The **left fibula** (FGM998GF9.3) is nearly complete, with an estimated length of 340 mm. The distal end is truncated by a displacement fault. The proximal end is anteroposteriorly long, 45 mm. A collapse fracture on the medial surface of the fibula shaft demonstrates significant anteroposterior compression, and the proximal third of the fibula is offset posteriorly due to a small displacement fault.

A longitudinal concave boss is centrally located on the proximal medial surface, has several longitudinal rugose striations. Anterior and posterior to this relatively raised area, the proximal medial surface is concave. A longitudinal low boss is also present on the medial proximal surface of the fibula of *Massospondylus* (Cooper 1981, Fig 69A), separating the anterior and posterior concave depressions. A groove on the mediodistal surface is flanked by two thin ridges, and is suggestive of an articulation with the lateral surface of the ascending process of the astragalus. The greatest distal width (25 mm) is oriented mediolaterally, before being truncated by a fault. Therefore, the distal end is twisted 90° relative to the proximal end.

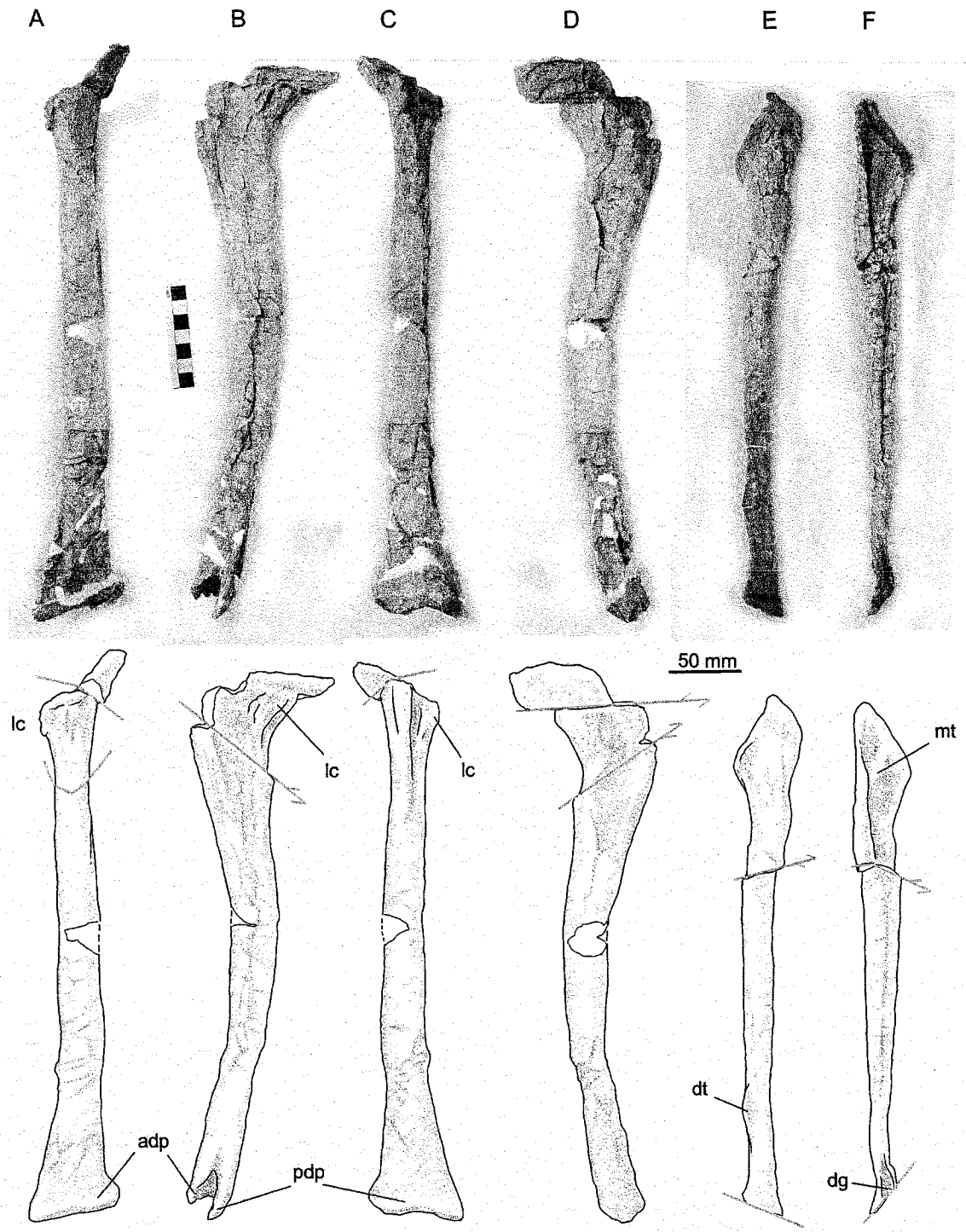

Figure 7.14: The left tibia (A-D) and fibula (E-F) of GF9, in posterior (A), lateral (B, E), anterior (C) and medial (D, F) views.
Abbreviations: adp, anterior distal process; dg, distal groove of fibula; dt, distal tubercle on fibula; lc, lateral condyle; mt, medial tuberosilty; pdp, posterior distal process.

A unique, strongly developed muscle scar is located distally on the anterolateral surface, 270 mm from the proximal end, or ¾ fibula length. While a distal scar cannot be identified on the right fibula of GF13-II, at least one specimen of *Massospondylus* (NMR5403) has a similarly positioned feature on the distal anterolateral surface of the fibula (Cooper 1981, Fig. 69B), which Cooper described as an "interrupted lateral carina".

Tarsus

Only three specimens (GF69, GF13-I, and GF13-II) include associated tarsal elements. The astragalus of GF3-I is completely prepared and well preserved, and the calcaneum of 13_II and GF69 are deformed but demonstrate the relative size and articular relationships of these elements.

GF13-I

The right astragalus and calcaneum were eroded and lost prior to collection the specimen. However, the left astragalus (Figure 7.15) and distal tarsals are well preserved and exposed. The left astragalus was disarticulated from the calcaneum prior to preservation. The (unexposed) calcaneum likely remains attached to the distal end of the fibula. The astragalus was broken during preparation. However, no material was lost during the fracture and the lateral half is now free from direct articulation with the tibia, providing the ability to examine these surfaces and articulations in detail. The astragalus is displaced anteriorly 13 mm in relation to the distal end of the tibia and has been slightly compressed proximodistally. The astragalus was also dislocated from the distal tarsals, with the distal tarsals and pes displaced anteriorly. The astragalus and pes were preserved on top of the left lateral surface of the articulated caudal series of GF13-I, and a small distal fragment of the right lateral process from the eighth caudal vertebra of GF13-I remains attached to the distal surface of the astragalus.

In distal view, the astragalus is tear-drop shaped, with a narrow lateral edge. The posterior edge is 90 mm wide (mediolaterally), and the medial edge is roughly perpendicular to this surface, 37 mm long and gently convex. The anterior edge is sub-parrallel to the posterior edge. At approximately the mediolateral midpoint of the

astragalus the anterior edge becomes directed sharply posterolaterally, resulting in the strong lateral constriction. This mediolateral mid-point is also were the astragalus is the longest (anteroposteriorly). The articular facets for the calcaneum are well preserved at the apex of the lateral edge. The anterior edge of the astragalus underlapped the ventral surface of the calcaneum, and immediately posterior to this finger like projection is a deep articular facet for a reciprocal process from the calcaneum. A third facet on the posterolateral edge of the astragalus would have contacted the posterior edge of the calcaneum, thus the two elements would have been in tight articulation prior to preservation.

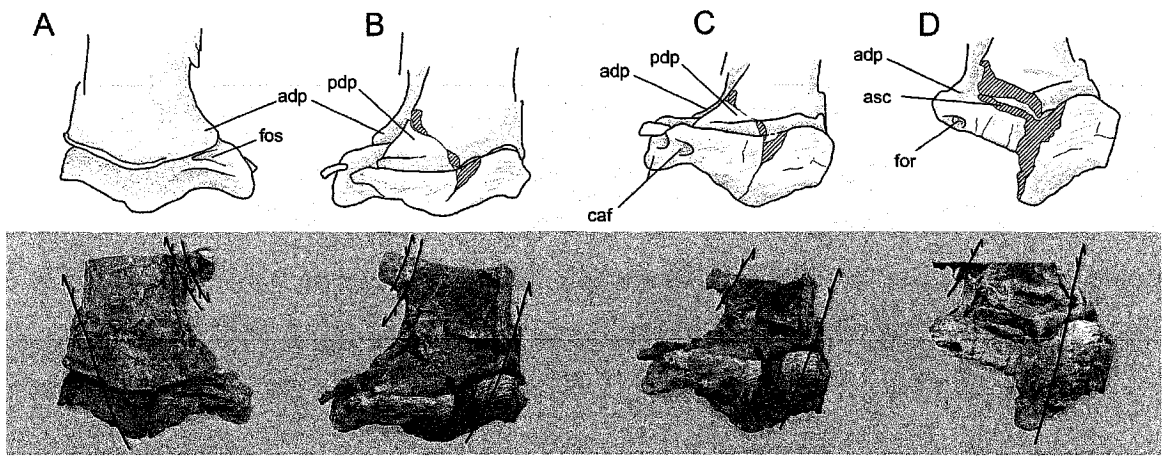

Figure 7.15: The left distal tibia and articulated astragalus, in anterior (A), posterior (B), and posteroventral (C,D) views.
The lateral portion of the astragalus and posterior distal process can be removed due to a break in the bone (D) exposing the ascending process of the astragalus (asc) and a foramen (for) located on the articular facet of the anterior descending process of the tibia. A deep fossa at the anterior base of the ascending process of the astragalus (asc), aligns with the foramen (for) on the anterior distal process of the tibia (adp). The anterior distal process extends distally nearly as far as the posterior distal process (pdp), and thus covers the anterior surface of the ascending process of the astragalus. The articular facets for the calcaneum (caf) are visible in posteroventral view (C). Broken bone surfaces are shown with cross-hatching, and faults offsets are labelled on the photographs.

The distal articular surface of the astragalus is covered with many delicate rugose ridges, oriented obliquely (posterolaterally) from the medial edge. The medial third of the distal surface appears to have had a convex, rounded surface, which contacted the medial portion of the proximal surface of metatarsal-II and the proximal surface of metatarsal-I.

The ascending process originates from the posterolateral edge of the astragalus and is inset from the posterior margin of the astragalus. The process is 64 mm wide (mediolaterally) along its base, and has a maximum height of 23 mm from the medial surface of the astragalus. The astragalus dorsoventral height currently measures 3-5 mm, and accounting for dorsoventral crushing may have had a maximum depth of 10 mm, which would suggest the ascending process is tall in comparison to astragalus body.

A deep fossa (Figure 7.15A) is developed at the anterior base of the ascending process, and aligns with a 5 mm foramen present in the anterior descending process of the tibia (Figure 7.15D). While a similar fossa has been noted in other sauropodomorphs (Wilson and Sereno 1998), the association with a foramen in the tibia is unique and provides additional evidence that the distally extended anterior distal process is not a deformational artefact.

The ascending process is perpendicular to the distal articular surface of the astragalus, and the distolateral edge remains in contact with the posterodistal edge of the anterior distal process of the tibia. The medial surface of the fibula appears to have contacted the lateral edge of the ascending process. The horizontal portion of the anterior edge of the astragalus extends slightly beyond the anterior distal process of the tibia.

Rather than being a broad element that contacts the anterior, recessed surface of the tibia, the ascending process is thin and is surrounded both anteriorly and posteriorly by the distal processes of the tibia. The astragalus of *Saturnalia* (Langer, Fig. 6) and *Massospondylus* (Cooper, Fig. 70) are subrectangular (the lateral edge at least 70% the length of the medial edge), whereas the astragalus of GF13-I and GF69 are pinched laterally, and therefore tear-drop in shape. The ascending process of the astragalus is also anteroposteriorly narrower than the ascending process of *Saturnalia* (Langer 2003, Fig 6).

GF13-II

The morphology of the astragalus of GF13-II is confounded by deformation. The right astragalus was displaced only 12 mm from the distal end of the tibia, but a large fault displaced the lateral portions of the astragalus (and distal tibia), and a smaller (2 mm) fault also displaces the posterolateral edge.

Similar to GF13-I, the distal articular surface of the astragalus has long but delicate rugose ridges oriented obliquely, from the posteromedial corner to the anterolateral corner, especially along the posterior edge. The posterior edge is incomplete (laterally), truncated 59 mm from the medial edge by the large fault. The medial edge is mildly convex, perpendicular to the posterior edge, and 45 mm long (anteroposteriorly). The anterior edge is at least 62 mm long before being truncated by a fault, and is sub-parallel to the posterior edge.

The anterior medial edge of the astragalus is17 mm deep. The ascending process of the astragalus is tall and fits into the groove on the distal lateral surface of the tibia.

GF69

The right and left astragalus and calcaneum of GF69 are preserved, although each has been deformed in different ways. The right proximal tarsals have been deformed by dorsoventral crushing and a small fault, but on the left side the tarsals have been crushed anteroposteriorly and displaced by two faults. The left calcaneum is also disarticulated but remains adjacent to the astragalus, making the lateral extent of elements appear wider (mediolaterally) than both the articulated right proximal tarsals or the reconstruction of the proximal articular surface of the metatarsals.

The mediolateral width of the articulated right astragalus and calcaneum is 66 mm. The astragalus and calcaneum are 48 mm and 26 mm wide respectively, with an 8 mm overlap. The calcaneum is wide (54% of the astragalus width), compared to *Saturnalia* (50%), *Coloradisaurus* (44%), *Anchisaurus* (28%), and sauropods (<30%) (Yates 2004). Although the left astragalar mediolateral width has been exaggerated due to anteroposterior crushing, preventing the measurement of a precise width, the relative proportions confirm the wide calcaneum observed in the right calcaneum.

The distal (ventral) articular surface of the astragalus is marked by numerous obliquely oriented striations, especially on the posterior and medial edges. The astragalus is anteroposteriorly widest along the medial edge, and the width tapers rapidly from the mediolateral mid-point to the lateral edge, resulting in a tear-drop shape in ventral view. The medial edge of the right astragalus is 56 mm (~50 mm accounting for faulting). In distal view the calcaneum overlaps a semicircular facet on the anterolateral surface of the

astragalus, and a short finger-like extension on the posterolateral margin of the astragalus wraps around, and dorsally overlaps, the posterolateral surface of the calcaneum.

Two distal tarsals are also preserved; an oblong medial tarsal that is longest (30 mm) anteroposteriorly, and a tear-drop shaped lateral tarsal that is 30 mm wide along the medial edge and tapers laterally, to a width of 13 mm along the lateral edge. The two tarsals are slightly displaced in the left pes, but a groove on the lateral edge of the lateral tarsal demonstrates they were in tight contact. The medial distal tarsal appears to have been located within a shallow depression visible in the lateral half of the articular surface of the second metatarsal and the medial edge of the third metatarsal. The lateral distal tarsal articulated with the lateral portion of the proximal end of metatarsal three and the proximal surfaces of metatarsals 4 and 5. The dimensions correspond well to the dimensions of the proximal surfaces of these digits demonstrating the tarsals are not affected by dramatic deformation, although the lateral tarsal is offset by a small fault through the midline.

Pes

The right and left pes of GF69 are fully articulated and well preserved. Only two other specimens (GF13-I and GF13-II) include articulated pedal elements, both of which are approximately 120% larger in linear dimensions than GF69 but are poorly preserved and incomplete. All pedes from the bone bed are only partially prepared, and badly faulted. The length of the metatarsals can only be estimated for most specimens. Therefore the ability to compare specimens based on the metatarsal dimensions is limited.

Table 6: Metatarsal (mt) dimensions of specimens recovered from the bone bed.
The relative sizes of metatarsals 1, 2, and 3 are similar, and the sum of metatarsal lengths (excluding mt-4 due to incomplete data) provides a relative size metric. Underlined values are those that could only be estimated due to faulting or distortion.

		mt-1	mt-2	mt-3	mt-4	mt-5	mt2/mt1	mt3/mt1	∑ 1,2,3,5
GF13-I	L	104	152	170	>105	85	1.46	1.63	511
left	Wp	15	42	?	>50				
	Wm	24	26	?					
	Wd	50	-	?					
GF13-II	L	65	135	145	130	80	2.08	2.23	425
right	Wp	36				48			
	Wm								
	Wd								
GF69	L	85	115	120	105	65	1.35	1.41	385
right	Wp			27		33			
	Wm								
	Wd								
GF9	L					89			
left	Wp					40			
	Wm								
	Wd								

GF13-I

The right pes of GF13-I was lost due to erosion prior to specimen collection. The left pes and articulated tibia/fibula were close enough in the bone bed to suggest association with GF13-I, suggesting this specimen was sprawled and lying on it back prior to burial. The pes is currently exposed in dorsal view, and deformed by a series of complex faults (Figure 7.16). Only the proximal most phalanges of digits I, II and V are preserved; the others having been disarticulated prior to final burial or displaced due to faulting. The fibula, phalanges, and metatarsal V are noticeably flattened due to dorsoventral compression.

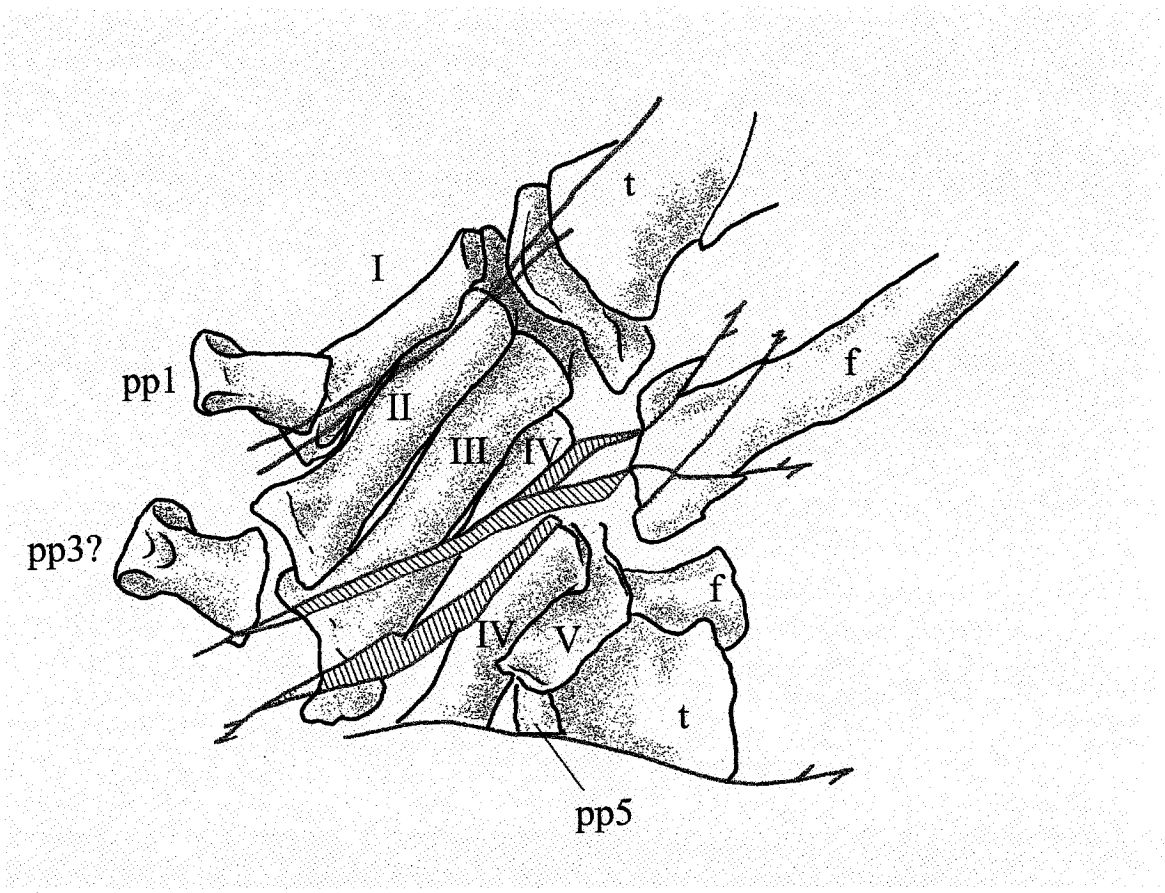

Figure 7.16: The preserved portions of the left distal tibia (t), fibula (f), and pes, referred to specimen GF13-I. Several faults displace the elements, particularly the third and fourth metatarsals (crosshatched area).
The proximal ends of another articulated tibia and fibula are under the foot, adjacent to the fifth metatarsal. Proximal phalanges (pp) are preserved on digits I, III?, and V.

The oblong proximal articular surface of the **first metatarsal** has the long axis directed anteroposteriorly (36 mm) and is 15 mm wide (mediolaterally). The proximal length to width ratio is therefore greater than that of *Anchisaurus*, which has a ratio of only 0.25 (Galton and Upchurch 2004). The proximal articular surface contributes to the tarsus, as is typical for sauropodomorphs. The distal articular surface is twisted approximately 45° laterally in relation to the proximal end, resulting in the distal articular surface of metatarsal-I being oriented obliquely in comparison to the distal end of metatarsal-II. Two small (6 mm) faults offset the lateral edge of the distal end. Accounting for these offsets the length of the lateral edge is approximately 104 mm. The medial edge is 98 mm long and the distal condyles are therefore inflected medially. A shallow depression on the distal dorsum surface of metatarsal-I represents an extensor depression. The greatest width across the distal condyles is 29 mm.

In proximal view, the **second metatarsal's** medial and lateral edges are concave, and accommodate a tight articulation with metatarsals one and three. The lateral edge of the proximal end is offset by two small faults, but the proximal articular surface is 46 mm long anteroposteriorly, and is 35 mm wide both dorsally and ventrally. The proximal dorsal surface of metatarsal-II overlaps the lateral edge of metatarsal-I and the medial edge of metatarsal-III. The lateral distal condyle extends farther (distally) than the medial condyle, 152 mm and 140 mm respectively. Therefore, like metatarsal-I, the distal condyles of metatarsal-II are directed slightly medially. The second metatarsal also has a shallow extensor depression on the distal dorsal surface.

The distal portion of the **third metatarsal** is offset by two oblique displacement faults (Figure 7.16). However, the length can be reasonably estimated at 170 mm. Thus, the third metatarsal is the longest of the pes and is 59% the length of the tibia.

The **fourth metatarsal** is deformed by several faults, and truncated distally 105 mm from the proximal end. Therefore, the complete length cannot be determined. The proximolateral edge of metatarsal-IV overlaps the dorsal surface of metatarsal-V. The **fifth metatarsal** is anteroposteriorly flattened due to compression, and as a consequence of slight dislocation, the distal end of mt-V is lateral and slightly dorsal to the lateral edge of mt-4. The dislocation can be attributed to this area of the foot overlying the proximal end of the left tibia and fibula referred to GF13-II. The metatarsal is at least 85 mm long, but the metatarsal is extensively faulted so the proximal width cannot be determined.

The **proximal phalanges** of digit I and II are flattened dorsoventrally, but the distal ends still preserve the deep lateral pits. The first proximal phalanx of digit 1 is 58 mm long medially and 51 mm laterally. The proximal phalanx for digit 3 is 59 mm long, 59 mm wide proximally, and ~ 45 mm wide distally, and a shallow depression on the distal dorsal surface likely represents a shallow extensor depression. The fifth digit preserves at least one phalanx, which is at least 20 mm long, but the distal end is truncated by a fault.

A disarticulated phalanx (98GF13.30, Figure 7.17) was collected separately while channelling around the block that contains the pes. The proximal articular surface is pathologically deformed, with porously textured and rugose bone.

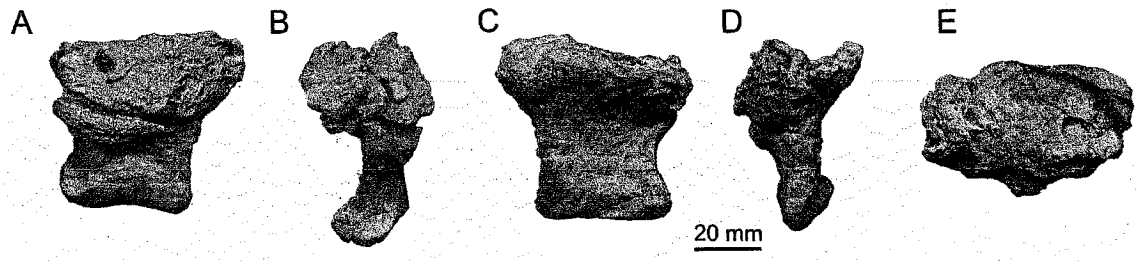

Figure 7.17: An isolated phalanx located near the pes of GF13-I, in dorsal (A), lateral (B), ventral (C), medial (D) and proximal (E) views, which shows pathologically deformed bone on the articular surface

GF13-II

The left pes of Gf13-II is not exposed but is likely articulated to the left tibia and fibula on the underside of the block containing the pes of GF13-I. The right pes is badly deformed by numerous faults, particularly the proximal ends of the metatarsals and phalanges. Therefore, the pes of this specimen offers limited information.

The right pes remains in articulation with the tibia and fibula. The proximal ends of metatarsals 1-4 are displaced ventrally by a fault. The proximal 20 mm of the first metatarsal is articulated with the second metatarsal, contributed to the tarsus, and has a proximal articular surface that is 36 mm long (anteroposteriorly) and approximately 15 mm wide (mediolaterally). The proximal phalanx is articulated to the distal end of metatarsal-I, but is faulted, and most of the other phalanges are not exposed. The phalanges of digits 1-4 are located under the caudal vertebrae of GF13-III, and offset dorsally by the 65 mm fault affecting this area. The proximal portion of the ungual of digit-1 is under the centrum of the eleventh caudal vertebra (GF13-III).

The proximal surface of metatarsal-II is hour-glass shaped, with concave medial and lateral edges. The proximal end is faulted (ventrally), so the length can only be estimated at 135 mm. The distal end of the fifth metatarsal is crushed anteroposteriorly, due to compression deformation. The proximal end is partially disarticulated from the lateral surface of metatarsal-IV. The proximal articular surface for metatarsal-IV is concave, and the lateral edge is thick and convexly rounded. The proximal end of metatarsal-V is flattened due to compression; the proximal width is 60% of the length, but this is certainly exaggerated due to deformation.

GF69

GF69 is the only specimen that includes both the right and left pedes. They are articulated and reasonably complete; therefore they represent the best pes specimens from the bone bed. The right leg and pes were under the body prior to burial, causing the central digits to be hyperextended and dislocated. A small block containing portions of the distal phalanges of the left pes had been separated during collection, and fragments joining this block to the metatarsals cannot be located. However, the small block containing the distal phalanges can be aligned with the metatarsal block based upon an impression of the proximal phalanx from digit-3 and the broken surfaces of metatarsal-IV. These two pedes demonstrate the importance of considering crushing and fault deformations for the bone bed specimens, as the morphology of the pedes are different depending upon the direction of crushing deformation and occurrences of fault displacements.

The proximal surface of the **first metatarsal** contributes to the articular surface for the tarsus, with a narrow facet, which is at least twice as long (anteroposteriorly) as it is wide. The proximal end of the left mt-1 is faulted slightly, but was 9 mm wide (mediolaterally) and 24 mm deep (anteroposteriorly). The proximal end of metatarsal-I is mediolaterally compressed when compared to the width of the shaft (14 mm) immediately distal to the articular surface. It is similar to *Lufengosaurus* (Young 1941), but different from *Saturnalia* (Langer 2001) in being proportionally deeper, and nearly as long anteroposteriorly as the other metatarsals. The medial and lateral edges of the proximal articular facet are gently convex. The lateral edge has a short lip anteriorly that wraps around the anteromedial edge of metatarsal-II, which may be deformational artefact. As observed on the left pes (Figure 7.19B), the palmar surface of the proximal end is marked by a longitudinal rugose scar that is also found on the adjacent proximal end of metatarsal-II. These scars likely represent the origins of a strong inter-metatarsal ligament.

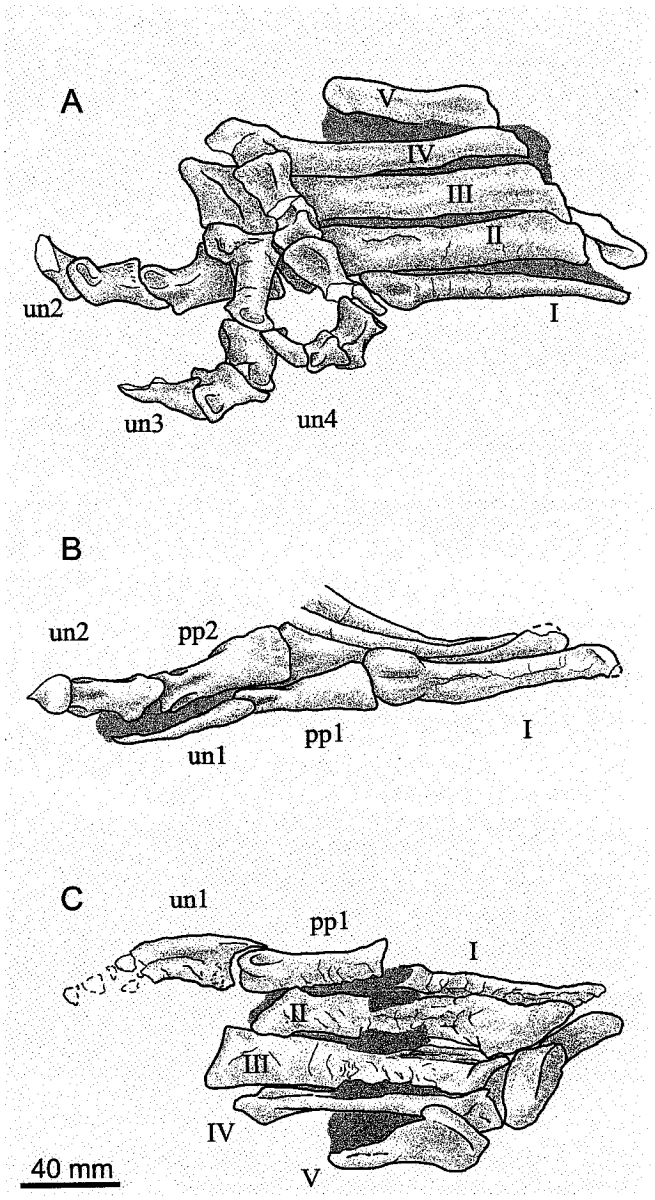

Figure 7.18: Right pes of FGM994GF69, in dorsal (A) , medial, (B) and ventral (C) views. Abbreviations: I-V, metatarsals 1-5; pp, proximal phalanx; un, ungual phalanx.

The length of metatarsal-I is difficult to determine with certainty. The right metatarsal medial edge appears to be extended due to deformation, measuring 100 mm in length, but the lateral edge has been crushed significantly. The length of the first metatarsal of the right pes can only be estimated at 85 mm; the distal end was displaced by a fault. The right metatarsal is also rotated, with the medial edge now directed dorsally in relation to the other metatarsals. The articular facets of the distal condyles are directed medially due to rotation of the metatarsal, but prior to preservation they most

likely were directed ventrally, and only slightly distally. Unfortunately, the orientation of the distal surface of the left metatarsal-I cannot be reliably determined due to a displacement fault. The articular facets of the distal condyles are separated by a medial furrow. A deep collateral extensor pit is visible on the distal medial surface (Figure 7.18C).

The proximal articular surface of **metatarsal-II** is hour-glass shaped, 30 mm long anteroposteriorly, with concave medial and lateral edges. The anterior and posterior proximal edges are of similar mediolateral width, 25 mm on the left pes; the posterior edge of the right metatarsal has been elongated due to crushing of the lateral edge. The distal articular surface is 29 mm wide mediolaterally, and in both pedes the lateral condyle extends further distally than the medial condyle. The metatarsal length is 115 mm along the medial edge, and 107 mm along the lateral edge (measured on the right pes).

The length of **metatarsal-III** is difficult to determine, although it was certainly the longest of the pes. The ventral surface of the right metatarsal-III measures 122 mm in length along the lateral edge, and 111 mm along the medial edge. The left metatarsal-III is at least 130 mm in length, but it is offset by a fault near the proximal end. The third metatarsal length is therefore at least 45 % of the tibial length.

The proximal articular surface of metatarsal-III is only partially exposed on both the left and right sides. The proximal surface is sub-triangular; the dorsal side 27 mm long mediolaterally, the convex medial edge is 34 mm deep and meets the concave ventrolateral edge forming a rounded corner. The proximal end is overlapped medially by metatarsal-II and laterally it overlaps the medial edge of metatarsal-IV.

In both the right and left pedes, the **fourth and fifth metatarsals** appear to have remained articulated as a unit but rotated counter clockwise in proximal view relative to the rest of the pes. This rotation resulted in the lateral edge of the fifth metatarsal being oriented dorsally (anteriorly). The rotation of these lateral digits is supported by the orientation of the phalanges that remain attached to metatarsal-IV and the tight articulation of metatarsal5.

The distal articular surface of the right fourth metatarsal has been crushed proximodistally, especially the dorsal-most portion, which has been displaced proximally.

As preserved, the length of the right metatarsal-IV is approximately 105 mm. The lateral extensor pit has been shortened due to compression (Figure 7.18A). A longitudinal groove on the proximal ventral surface accommodated the fifth metatarsal. Immediately distal and lateral to this groove, there is a second groove in the shaft, which may have accommodated an unpreserved proximal phalanx, or alternatively represents a ligament or muscle scar. The proximal articular surface of metatarsal-IV is wedge shaped, widest medially and narrowing sharply toward the lateral edge. The surface currently directed dorsally is interpreted as the lateral edge, which is approximately 20 mm deep. The distal articular surface is 21 mm wide.

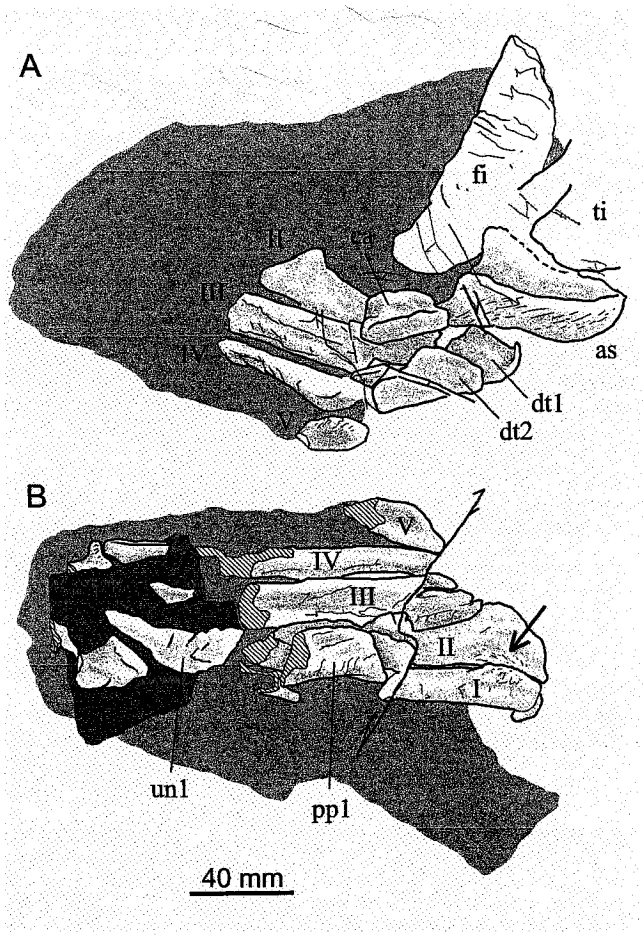

Figure 7.19: Left pes of FGM994GF69 in posterodorsal (A) and ventral (B) views. The ungual phalanx of digit 1 (un1) and phalanges of digits 2-4 are located in a small piece (dark grey) that connects to the underside of the block. Abbreviations: as, astragalus; ca, calcaneum; dt, distal tarsal; fi, fibula; pp, proximal phalanx; ti, tibia; I-V, metatarsals 1-5.

The proximal articular surface of metatarsal-V is mediolaterally wide and anteroposteriorly thin, 33 mm and 9 mm respectively. The fifth metatarsal is 64 mm

long; therefore the width is equal to or slightly greater than 50% of the length. The distal palmar surface is rounded and slightly rugose and dorsoventrally deeper than mediolaterally wide, 16 mm and 9 mm respectively. The long axes of the proximal and distal ends are therefore perpendicular to each other. The fifth metatarsal of GF69 closely resembles the morphology of the isolated metatarsal from GF9, although it is only 71% as long.

The phalangeal formula is 2,3,4,5,?; there is currently no phalanges for the fifth digit, but it remains possible there was one present prior to burial and preparation. Several of the proximal phalanges have extensor depressions on their distal dorsal surfaces. The second proximal phalanges have a proximally elongate (extensor) process on the dorsal proximal surface; the second phalanx of digit-2 is 46 mm in length along the dorsum surface and only 33 mm long ventrally.

The proximal phalanx of digit-1 is 60 mm long, 19 mm wide proximally and 16 mm wide distally. The phalanx has been compressed mediolaterally, but the length is not expected to have increased significantly due to this compression. The proximal phalanx of digit-2 is 58 mm long, and the extensor depression on the dorsal distal surface is well developed, corresponding with the extension on the dorsal proximal end of the second proximal phalanx of this digit. The proximal phalanx of digit-3 is crushed, especially on the proximal end, but was at least 38 mm in length. Phalanges on the left foot are not well preserved or exposed (Figure 7.18).

The ungual of the right digit-1 is at least 55 mm (measured to centre of articular facet) or 70 mm (measured to dorsal edge of the articular facet). The distal tip of the ungual has been displaced by several faults, therefore the absolute length cannot be determined. Only the proximal portions of unguals of digits 2-4 were collected; the lengths cannot be estimated.

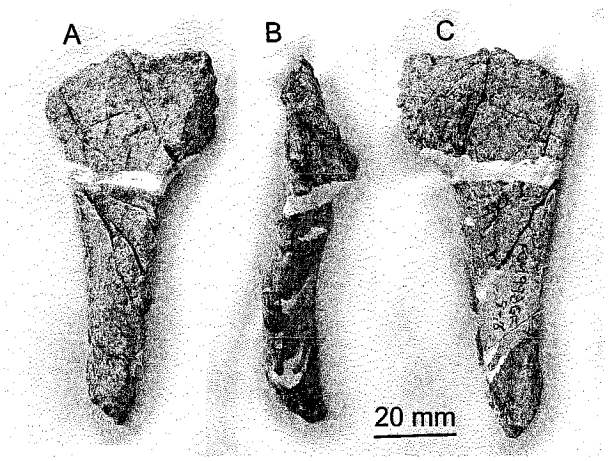

Figure 7.20: The left fifth metatarsal of GF9 in dorsal (A), lateral (B) and ventral (C) views.

GF9

An isolated left metatarsal-V (FGM998GF9.16) was recovered among the disarticulated material of GF9. The proximal surface is widest laterally and narrows to a thin plate medially. The plantar surface is concave from the proximal end to mid-length. The entire dorsal surface of the proximal end was overlaid by metatarsal-IV. At about mid-length, the fifth metatarsal would be visible in dorsal view. The distal dorsal surface has longitudinal rugose ridges, which also partially extend onto the plantar surface at the distal end. The proximal width is slightly less than 50% of metatarsal length; the transverse width of the proximal end is 41 mm and the length is 89 mm. The metatarsal was cut by a rock-saw, 30 mm from the proximal end, and this (predictable) gap has been filled with plaster.

The fifth metatarsal of *Massospondylus* is proximally broad, 54-58 % metatarsal length (Cooper 1981; Fig 16 B, Fig. 77 A-D). This is also true for the fifth metatarsal of *Plateosaurus* (Huene 1926, Plate VI, Fig.11 A-F), width is 56% length (contra Yates 2004). However, the fifth metatarsal of *Plateosaurus* has a deep depression on the dorsal surface near the distal end that separates two pronounced ridges. The proximal end of the fifth metatarsals from most specimens are slightly wider than 50% the metatarsal length. Therefore, it seems likely the fifth metatarsal of GF9 is elongate, especially the proximal end, due to compression.

Discussion

In general, the appendicular skeletal elements within the bone bed are poorly preserved, and are therefore of limited value for evaluating the morphological, and possible taxonomic, variation within the bone bed. For example, while femora are associated with every specimen except GF13-III. However, unless the shaft was broken and the large medullar cavity (75 % of shaft diameter) was filled with matrix and thus structurally reinforced during burial and preservation, the femur became dramatically crushed as the medullar cavity collapsed. A similar collapse of the tubular nature of the diaphysis occurred in all tibia, fibulae and to a lesser degree the metatarsals. The morphological details of these elements have therefore been obscured by preservational deformation, as well as due to the fault deformation that affects nearly all skeletal elements within the bone bed. As a result of the extreme deformation that resulted as the 'open' structure of the medullar cavity became 'closed' from structural collapse, the distinctions of morphological variation between specimens is limited. Regardless of these problems, some important details are observable within individual specimens.

The lesser (anterior) trochanter of all femora is a well developed and longitudinally oriented muscle scar, the proximal end of which is nearly level with the distal edge of the femur head. When adequately preserved, the fourth trochanter is pendant, with a concave distal margin in lateral view that results in a distally directed edge. The lateral condyle on the proximal end of the tibia is positioned at or near the mid-width in all specimens except GF9, where it is on the posterior edge, although it remains unclear at this time if this is a true feature or a preservational artefact. All specimens exhibit a unique, distally expanded anterior distal process of the tibia that anteriorly overlaps a tall ascending process of the astragalus, rather than being recessed from the proximal edge as in other basal sauropodomorphs. A unique foramen is also present on this expanded distal process in at least one specimen (GF13-I), which aligns with the anterior fossa in the base of the ascending process of the astragalus. Also, a groove in the mediodistal edge of the fibula likely accommodated the lateral most edge of the ascending process.

A radius and ulna collected among the disarticulated elements accessioned as GF9 are of similar size and therefore most certainly associated. However, these elements are

short in comparison to the hind limb elements. They are an appropriate size for association with GF69, suggesting that the material of GF9 represents more than one individual. The hind limb elements of GF9 were adjacent to each, are of a similar size to confirm they do associate together, and the relative length of the tibia compared to the femur (77%) is similar to other basal sauropodomorphs. Due to the incomplete and deformed state of the articulated pedes associated with GF13-I, GF13-II, and GF9, it is not possible to consider morphological variation between the specimens among these elements. The details of appendicular skeletal elements are also used in a phylogenetic analysis (Chapter 8) of the specimens from the bone bed.

Chapter 8 – Cervical Vertebrae and Skull Recovered from the Bone Bed Specimens

Introduction

The following description focuses upon the articulated cervical vertebrae series and the partially articulated cranial elements associated with the most complete specimen from the bone bed (13-II). It also includes supplemental information from the cervical vertebrae of GF69 and two isolated cervical vertebrae. These morphological details are used in a subsequent analysis (Chapter 8) of the phylogenetic relationships of this specimen and the other specimens within the bone bed to other basal sauropodomorphs. The skull and anterior cervical vertebrae have been deformed by both large and small fault displacements, and as these elements are only partially prepared, there many details that remain inaccessible at this time. Regardless, the material represents the first sauropodomorph skull discovered from the McCoy Brook Formation in more than thirty years of research, and provides substantial new information for assessing these important specimens.

The anterior six cervical vertebrae and majority of the skull elements are contained in a single large block. The cervical vertebrae are exposed in left lateral view, the surface that was directed upwards during preservation. A large (150 mm) fault severed the fourth cervical vertebra, and displaced the anterior portion of the vertebra ventrally relative to the posterior portion. Many smaller faults, oriented obliquely nearly perpendicular to the large fault, displace the anterior three cervical vertebrae and nearly all cranial elements.

To be consistent with previous chapters and other authors (Sues et al. 2004), anterior and posterior will be used for directional terminology. The adopted terms avoid the use of similar terms for both anatomical structures and anatomical directions. Also as in previous chapters, vertebra lamination terminology follows Wilson (1999); see Figure 6.7 for reference.

Description

Cervical Vertebrae

GF13-II

The entire cervical series was articulated together and in direct contact with the posterior cranial elements and anterior dorsal vertebrae. The anterior cervical vertebrae are exposed in left lateral view, which limits the measurements that can be determined at this time. A basalt boulder (~30 cm in diameter) was located on top of the sixth cervical vertebra, which along with the underlying cervicals was cut by a rock-saw during collection. The prezygapophyses of the seventh cervical vertebra remain in the skull block, but the posterior portions of the vertebra were collected separately (NS02 90, 102-106). Unfortunately, a large fault had displaced and deformed the posterior cervicals (7-10), and morphological details of these vertebrae cannot be reliably determined; Therefore, the description focuses upon the anterior six cervical vertebrae.

The anterior six cervical centra do not have obvious neurocentral sutures, although most lateral surfaces are well preserved; therefore, the cervical neurocentral sutures are well fused and suggestive of skeletal maturity (Brochu 1996).

Table 7: Dimensions of the anterior six articulated cervical vertebrae of GF13-II, and two isolated cervical vertebrae, FGM998GF13.47.
All measurements in millimetres, underlined values are estimates, and values proceeded by a '+' sign are minimum estimates.

	GF13-II					98GF13.47	
	Axis	C3	C4	C5	C6	C4?	C5?
Centrum ventral length	70	112	100	128	122	-	121
Centrum dorsal length	-	108	-	120		-	115
Centrum posterior height	-	30	35	31	30	35	29
Centrum posterior width	-	-	-	-	-	-	30
Centrum anterior height	-	29	-	+25	-	-	33
Centrum anterior width	-	-	-	-	-	-	-
Prezygapophyses length	-	24	-	34	-	-	17
Centrum-spine height	56	41	-	41	51	-	52
Neural spine length	60	-	-	65	+64	-	75
Neural spine height	20	-	-	-	22	22	19
Epipophyses lateral span	-	-	-	33	-	30	36
Cervical rib length	75	100	145	195	101	-	-

Although the anterior edge of the centrum is poorly exposed, the axis centrum (Figure 8.1) is approximately 70 mm long. The right and left ribs remain articulated to the axis, are 75 mm long, 4.5 mm wide, and taper to a sharp point distally. The neural spine is tallest toward the anterior end, and the anterior edge is concave in lateral view that results in an anteriorly projected dorsal edge. The neural spine morphology differs from the axial neural spine of *Plateosaurus* (Galton 1985a), *Massospondylus* (pers. obser. BP/I/5241), and *Anchisaurus* (pers. obs., YPM 1883), which have spines that are tallest at mid-length and are reduced in height anteriorly. The axial neural spine of *Plateosaurus* is uniform in height but marginally taller at mid-length, and the postzygapophyses overhang the posterior centrum face (von Huene 1926, Plate II, Fig. 1, Galton 1985a, Plate 4, Figs. 5 and 9).

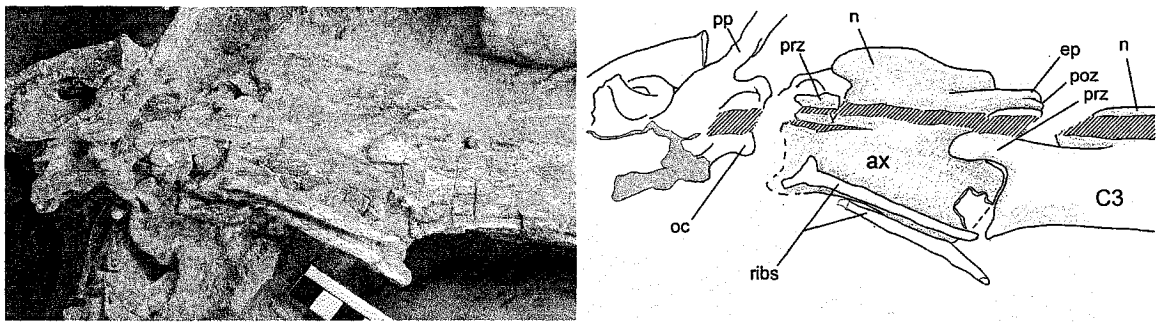

Figure 8.1 Occipital region of the skull, axis (ax) and anterior half of the third cervical vertebra (C3) of GF13-II.
The occipital region of the skull, represented here by the occipital condyle (oc) and right paroccipital process (pp), was rotated 90° in relation to the cervical vertebrae; therefore the axis and third cervical are exposed in left lateral view and the occipital region is exposed in dorsal view. Faults offset the dorsal portion of the axis and third cervical neural spines; the crosshatched area denotes exposed fault surface. Other abbreviations: ep, epipophysis; n, neural spine; poz, postzygapophysis; prz, prezygapophysis. Broken bone surface is depicted by solid grey shading.

The prezygapophyses are offset by small faults, but originate from the anterior edge of the centrum. The postzygapophyses overhang the posterior centrum face (Figure 8.1). Although the posterior centrum face of the axis of *Anchisaurus* (YPM 1883) is poorly exposed (Galton 1976, Figure 15D), the posterior limit of the postzygapophyses did extend beyond the posterior face of the centrum (as proposed by Yates 2004).

The left lateral surface of the **third cervical** centrum was separated during collection and remains in two small counterparts. The neural spine is short (10 mm tall),

and is displaced laterally (to the right) by small faults along with the dorsal surface of the postzygapophyses. The centrum is proportionally long; length is 3.7 times the height of the posterior centrum face. The prezygapophyses are also elongate. The anterior extension equal to the height of the anterior centrum face.

The **fourth cervical** centrum is truncated by a 160 mm fault offset. Twenty mm of the anterior centrum is articulated with the third cervical, but the posterior 82 mm of the centrum is offset dorsally and remains articulated with the more posterior cervical centra. The length of the fourth cervical centra is estimated to be 100 mm. The posterior face of the centrum is 14 mm from the anterior face of the fifth cervical centrum, which likely represents the intercentral space of the neck in full dorsal flexion. The zygapophyseal articulations are in natural articulation. The postzygapophyses and neural spine are exposed in dorsal view. The epipophyses overhang the posterior edge of the postzygapophyses by 3 mm. The postzygapophyses extend 20 mm beyond the posterior face of the centrum. Because the neural arch is embayed anteriorly 20 mm, the postzygapophyses extend 40 mm from the posterior edge of the neural arch. The neural spine is tallest anteriorly. Although it is slightly damaged on the left side due to a crack that runs through the block, the anterodorsal edge appears to have been mediolaterally expanded (similar to the fifth and sixth cervical neural spines).

The ventral length (127.8 mm) of the **fifth cervical centrum** is slightly more than the dorsal centrum length (119.7 mm). The height of the posterior centrum face is 31 mm, demonstrating the centrum is extremely elongate, with a length to height ratio of 4.1. Among sauropodomorph dinosaurs this elongation has only otherwise been reported for derived sauropods (Wilson and Sereno 1998). The anterodorsal edge of the neural spine is expanded laterally by thin, anteriorly directed projections offset 4 mm laterally and 3 mm behind the anterior edge. *Melanorosaurus* has a laterally expanded anterodorsal edge of the cervical neural spine (Galton et al. 2005), but the lateral expansion of the cervicals of GF13-II is specific to the short, well-defined tubercle like processes. The anterior edge of the neural spine is concave in lateral view, making the anterodorsal corner appear expanded anteriorly. The prezygapophyses are long.

The fifth left cervical rib remains articulated to the parapophysis, which is located on the anteroventral corner of the centrum. The rib is at least 195 mm long, and has a 12

mm long anterior extension from the anteroventral edge of the parapophyseal articulation. The anterior half of the extension is displaced laterally by a 6 mm fault. The posterior centrodiapophyseal lamina originates from the mid-length of the centrum, and terminates (anteriorly) in a short, slightly thickened articular surface for the tuberculum, 20 mm from the anterior face of the centrum and immediately above the posterior edge of the parapophysis.

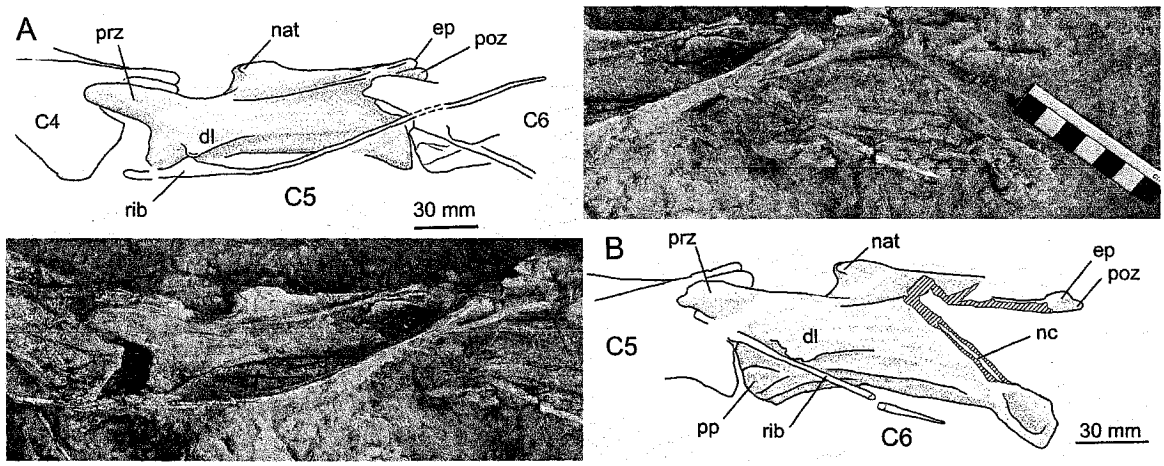

Figure 8.2: Fifth (A) and sixth (B) cervical vertebra in left lateral view.
Both cervical vertebrae possess well developed but small tubercles on the anterodorsal corner of the neural spine lateral surface (neural spine anterior tubercles, nat). The left postzygapophysis (poz) and posterior portion of the neural arch of the six cervical are missing due to a rock saw cut (cross-hatching). Other abbreviations: dl, posterior centrodiaphyseal lamina; ep, epipophysis; nc, neural canal; pp, parapophysis; prz, prezygapophysis.

The **sixth cervical vertebra** was obliquely cut by a rock saw through the neural spine and dorsal portion of the posterior facet of the centrum; the left and medial portions of the right postzygapophyses are missing. The posterior face of the centrum is concave and oriented obliquely to the long axis of the centrum, facing posterodorsally. Along with articular facets of the fifth centrum, this is suggests a natural angulation in this region of the neck. The diapophyseal lamina is level with the ventral border of the neural canal posteriorly. The anterior-most portion of the diapophyseal lamina is deformed, appressed flat against the lateral surface of the centrum. The left cervical rib has become dissarticuated, and is appressed against the deformed anterior portion of the diaphyseal lamina. The rib is 101 mm long, tapering to a sharp point, and is therefore shorter than the centrum length.

The parapophysis is located on the anteroventral edge of the centrum. The posterior centroparapophyseal lamina originates from the ventral edge of the parapophysis. This lamina is parallel to the posterior centrodiapophyseal lamina but becomes deflected ventrally and extends toward to the posterior edge of the centrum. The centrum has a pronounced but thin sagittal ridge (keel) that extends along the full length of the ventral surface of the centrum. The anterior end is well exposed in ventral view.

GF69

Portions of several cervical vertebrae (GF69) have been assembled from broken fragments (float) that were collected near the surface of the cliff in 1992. It represents some of the first material of this specimen located at the site. The skull, if it remained in articulation after burial, would have been lost due to erosion only a short time before discovery. The cervicals are poorly preserved, mediolaterally compressed and incomplete due to their breakage prior to discovery.

The most complete cervical (Figure 8.3) articulates with fragments of the anteriorly and posteriorly adjoining cervicals. The left epipophysis is missing a portion distally, but extended slightly over the posterior edge of the postzygapophysis. The neural spine and posterior facet of the centrum are missing. The length of the centrum can only be estimated at 70 mm, but in appearance the cervicals appear elongate, and of similar proportion to GF13-II.

A sagittal keel is present on the ventral surface of the centrum, especially anteriorly. The keel diminishes in depth at centrum mid-length but then increases in depth again more posteriorly. Again, the morphology of the sagittal keel is similar to those of the cervicals of GF13-II.

Other

A nearly complete cervical vertebra (FGM998GF13.47) and the posterior-half of the adjacent anterior cervical were isolated and may associate with GF13-I, GF13-II, or another unidentified specimen. The anterior most centrum is truncated by a large fault,

and the prezygapophses were severed by a rock-saw and recovered as separate pieces while channelling around the small block during collection.

The nearly complete centrum is well preserved and provides the opportunity to document the laminae present on the lateral and ventral surfaces of the centrum (Figure 8.4). The ventral surface of the centrum has a sharp sagittal ridge anteriorly. Another lamina extends posteriorly from the ventral edge of the parapophysis, and more dorsally the diaphyseal lamina extends posteriorly from the articular surface for the tuberculum to beyond mid-length of the centrum. The cervical ribs are not articulated, although a dorsal rib is under the right side of the centrum.

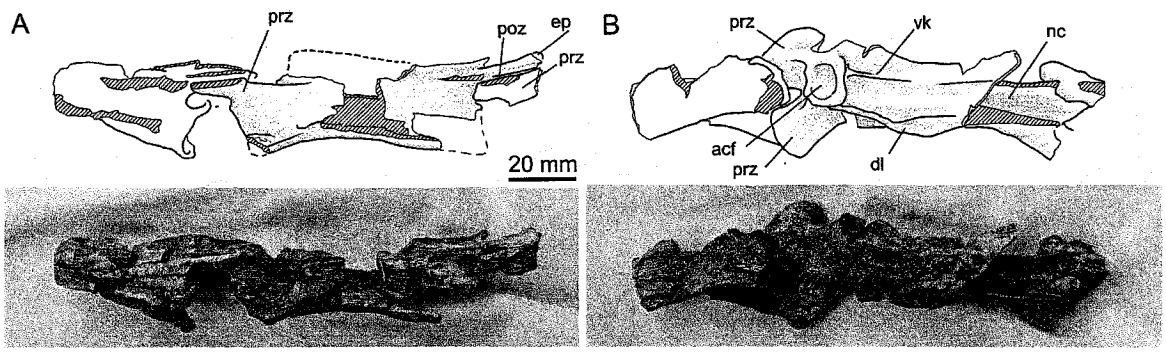

Figure 8.3: Three articulated but fragmentary cervical vertebrae assembled from float collected in 1992, the first fragments of FGM994GF69 discovered in the field; in left lateral (A) and ventral (B) views.
The most complete cervical is shaded and labelled, and remains articulated to the prezygapophysis of the posterior cervical as well as the larger portion of the anterior cervical. The ventral surface of the centrum exhibits a well defined, thin ventral keel (vk) that diminishes in size at mid-length, but again increases in size toward the posterior end. Other abbreviations: acf, anterior centrum facet; dl, posterior centrodiapophyseal lamina; ep, epipophysis; nc, dorsal surface of neural canal; poz, postzygapophysis; prz, prezygapophysis. Broken, missing bone surface is demarcated by crosshatching.

The centrum is amphicoelous, 121 mm long (ventrally) and the posterior intervertebral articulation is 29 mm tall and 30 mm wide. The anterodorsal edges of both neural spines were damaged during collection or preparation; splinter fractured surfaces were exposed during preparation.

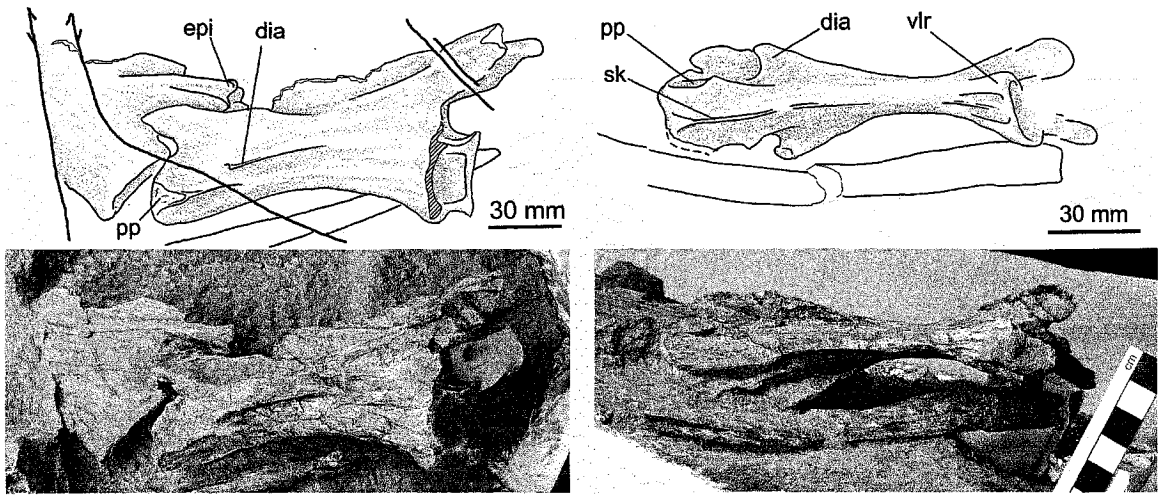

Figure 8.4: Two isolated cervical vertebrae (C4-C5) in left lateral view (A), and the ventral view of C6(B).
Abbreviations: dia, diapophysis; epi, epipophysis; pp, parapophysis; sk, sagittal keel; vlr, ventrolateral ridge.

The diapophyseal lamina originates posteriorly at about the mid-length of the centrum. The lamina extends laterally 11.6 mm from the lateral surface of the centrum, and a thickened articular process remains preserved on the right side, located 10 mm from the posterior edge of the parapophysis. The distal end of the left diaphyseal lamina was damaged. Linear rugose ridges cover the lateral and ventral surfaces that surround the articular surfaces of the centrum. A sharp sagittal keel is located on the ventral surface of the centrum. It is strongly developed anteriorly, diminishing (but still present) at mid-length and remains visible as a small ridge to the posterior edge of the centrum. The posteroventral edge of the centrum is recessed, as a result of the development of ventrolateral ridges on the posterior half of the centrum (Figure 8.4). The sagittal keel is present but only weakly developed between the ventrolateral ridges.

The neurocentral suture is fused but visible on the well preserved right lateral surface. The postzygapophyses are displaced laterally (to the right) at mid-length. The epipophyses of the more anterior cervical vertebra are level with the postzygapophyses, and a shallow groove is present on the dorsal surface of these epipophyses.

Comparing the length to height ratio with the cervicals of GF13-II, the complete centrum is likely to be the sixth cervical, and therefore the more anterior partial centrum represents the fifth cervical vertebra. Similar to GF13-II, the cervical centra are elongate; with the length to height ratio of the sixth cervical centrum being (4.2).

A single, isolated cervical vertebra (PU22126, Figure 8.5) was among the first dinosaur elements discovered in the McCoy Brook Formation in the mid-1970's (by P. Olsen and others). The anterior and posterior portions of the centrum were lost, as well as the anterodorsal corner of the neural spine and the distal end of the left postzygapophysis. The centrum is compressed mediolaterally, and slightly obliquely. The epipophyses extend to the posterior edges of the postzygapophyses but not beyond. Based on proportions, this cervical is similar to C4 or C6 of GF13-II, the prezygapophyses are not as elongate as in the fifth cervical. The length can only be estimated, due to the missing anterior and posterior ends of the centrum. However, the length was approximately 105 mm, and the centrum appears to have been as elongate those of GF13-II.

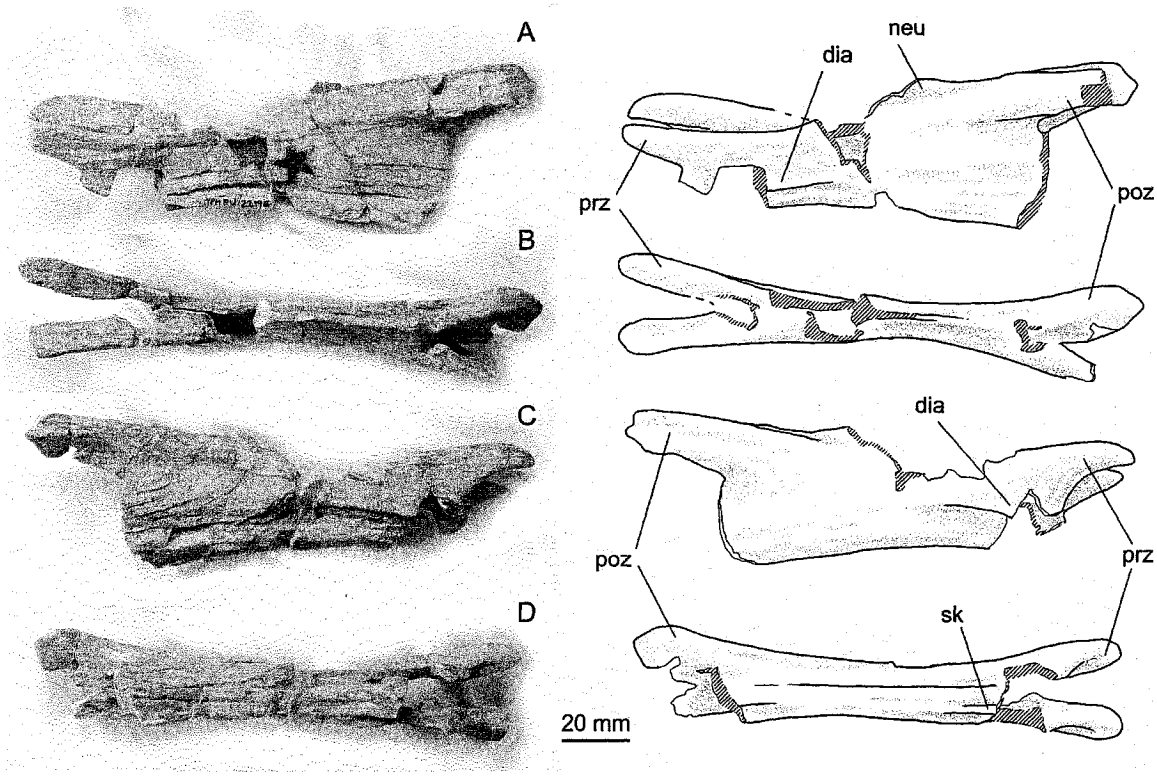

Figure 8.5: Isolated cervical vertebrae collected in the mid-1970's (PU 22196), in left lateral (A), dorsal (B), right lateral (C), and ventral (D) views.
Abbreviations: dia, diapophsyis; neu, neural spine; poz, postzygapophysis; prz, prezgyapophysis; sk, sagittal keel.

Skull

Occipital Region

There are several faults that strike parasagitally through the occipital region of the skull but longitudinally through the dorsal parts of the anterior cervicals. These faults have displaced the right side of the occipital condyle ventrally by 20 mm. The occipital condyle and right paroccipital process are rotated 90° in relation to the cervical vertebrae, as a consequence of displacement and disarticulation of the other cranial elements.

The dorsal surface of the basioccipital (posterior floor of the braincase) is visible, but distorted by faulting. The foramen magnum is 13 mm wide mediolaterally. The posterior edge of the right exoccipital is partially exposed, but the foramina for cranial nerve XII are not currently exposed.

Parabasisphenoid

The cultriform process is visible in dorsal and right lateral view. The exposed portion was not affected by the parasagital displacement faults of the occipital region. The lateral edges are tall (3.5 mm), but become lower anteriorly. The length from the distal tip to the posterior edge of the occipital condyle is 90 mm. The basisphenoid and basipterygoid processes are not currently exposed.

Maxilla

The tripartite maxilla is composed of an extended anterior ramus that underlies the posterior portion of the external naris, a dorsal ramus that borders the anterior edge of the antorbital fenestra and a posterior ramus that contacts the jugal posteriorly and the lacrimal dorsally. The right maxilla is visible in dorsal and lateral views it appears to be complete, although it is deformed by several displacement faults (Figure 8.7) and the posterior end is not currently exposed. The anterior ramus of the maxilla is long (25mm) and rounded in lateral view. A pointed and rugose process extends from the anteromedial edge of the anterior ramus, similar to the "anteromedial process" of *Plateosaurus* (Galton 1984, 1985a).

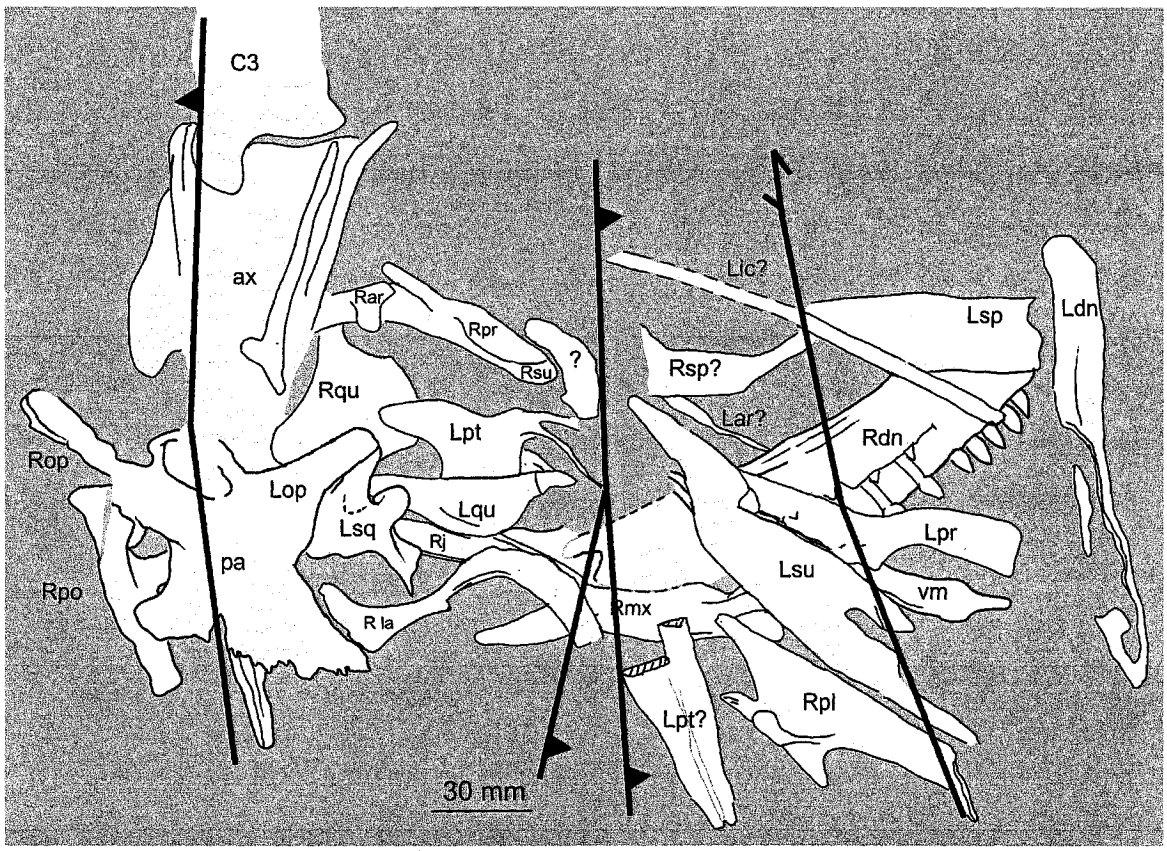

Figure 8.6: Schematic drawing of the axis (ax), third cervical (C3) and the disarticulated cranial elements within the skull block and related counterparts.
Abbreviations: ar, articular; dn, dentary; ic, intercoronoid; j, jugal; la, lacrimal; mx, maxilla; op, opisthotic; pa, parietal; pl, palatine; po, postorbital; pr, prearticular; pt, pterygoid; qu, quadrate; sp, splenial; sq, squamosal; su, surangular; vm, vomer. Elements are also designated with a prefix to designate as either left (L) or right (R).

The dorsal process of the maxilla was located in a counterpart to the skull block that was separated during collection; however, it has since been prepared free of the matrix and now articulates well with the main body of the maxilla. The tip of the dorsal process is offset slightly by a displacement fault. The process measures 38 mm in height and is therefore much taller (2.7 x) than the height of the maxillar lateral edge (14 mm). The proportional length of the dorsal process is similar to members of Massospondylidae; *Massospondylus* height of the dorsal process is 2.3 – 2.9 the lateral maxillar height (Sues et al. 2004, Figs. 5 and 1), and the ratio for *Lufengosaurus* is approximately 2.4 (Barrett et al. 2005, Figs. 1-2). The lateral edge of the dorsal process of *Plateosaurus* is slightly taller, 3.1 times the height of the main ramus of the maxilla.

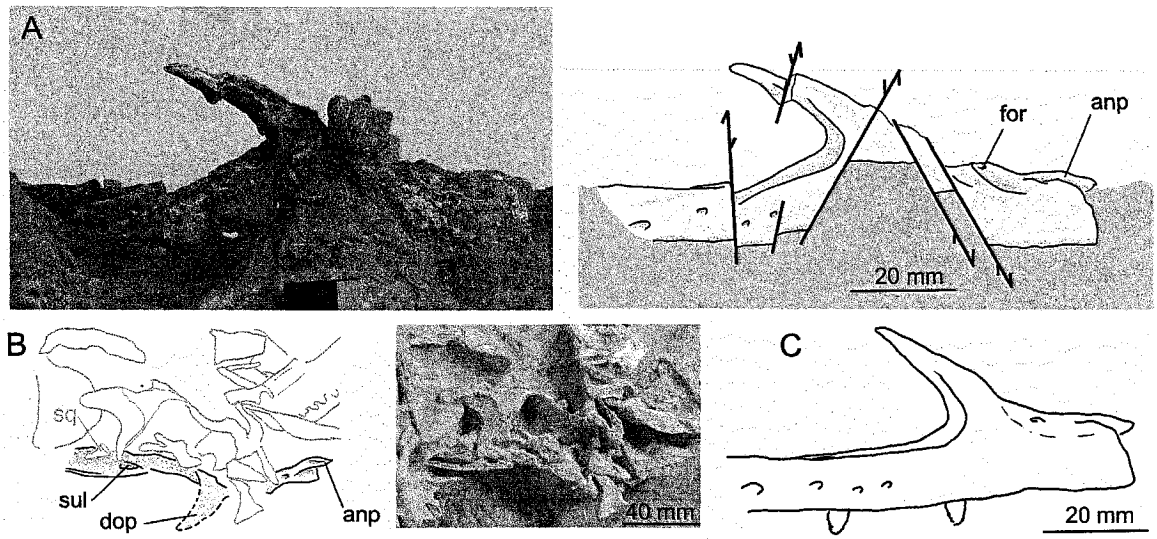

Figure 8.7: Right maxilla as preserved, in left lateral (A) and dorsal (B) views, and the reconstruction (C) in lateral view. The maxilla is deformed by five separate faults (A).
A deep sulcus (sul) is present on the dorsal surface of the posterior ramus, and the dorsal process (dop) was located in a separate block, and is not visible in the dorsal view (B), but has since been removed and can be temporarily reattached (A). The anterior process (anp) is well exposed in dorsal view, as is the foramen (for) at the anterior base of the dorsal process.

The dorsal process of the maxilla of GF13-II does not have a low boss on the lateral edge, the presence of which is an autapomorphy for *Lufengosaurus* (Barrett et al. 2005). Similar to *Massospondylus*, *Lufengosaurus* and *Anchisaurus* (Yates 2004), but different from *Plateosaurus* (Galton 1984, 1985a), the medial sheet of the maxilla does not extend far posteriorly, making the dorsal edge of the antorbital fenestra strongly emarginated (concave). The base of the dorsal process has a shallow depression on the anterior edge that represents the corner of a shallow fossa surrounding the external naris (Sues et al. 2004). A foramen is medial to this fossa, within the posteroventral corner of the external naris as in *Massospondylus* (Sues et al. 2004) and *Lufengosaurus* (Barrett et al. 2005). The dorsal process is anteroposteriorly longer than dorsoventrally tall.

At least three small foramina are visible on the lateral surface of the posterior ramus of the maxilla, as well as a larger foramen located posteriorly. These foramina are aligned linearly; the posterior-most one is the largest and opens posteriorly. The exposed lateral surface of the tooth bearing portion of the maxilla is taller than the lingual side; the roots of erupted maxillary teeth are partially exposed in lingual view, similar to *Lufengosaurus*. Tthe lateral extension is considered different from the 'lateral plate'

exhibited by derived sauropods (Upchurch 1998), following Barrett et al. (2005) who suggest the 'lateral plate' morphology of derived sauropods is unevenly expressed along the length of the maxilla. Similar to the dentary, triangular interdentary plates are located mesial and distal to the bases of the tooth crowns. Two maxillary teeth and four empty aveolae are within the 40 mm of the maxilla posterior to the base of the dorsal process, and are exposed in lingual view.

The dorsolateral edge of the posterior ramus extends slightly above the more medial portion due to the presence of a shallow groove on the posterior ramus, representing a neurovascular canal for the maxillary nerve and associated vasculature (Witmer 1997, Yates 2003a). Gow et al. (Gow *et al.* 1990) noted a similar foramen in *Massospondylus*. Although no mention was made by a recent study of *Massospondylus* (Sues et al. 2004), one is clearly visible in BP/I/5241 (pers. obs.).

Lacrimal

The dislocated right lacrimal is within the counterpart of the skull block (Figure 8.1), adjacent to the right squamosal and quadrate. The ventral end is appressed against the anterior edge of the parietal. The ventral arm of the lacrimal is offset by a small fault at mid-height. Dorsally, the lacrimal bends anteriorly, and this anterior ramus projects 25 mm, up to a fault offset, beyond which the length is unknown. The anterior ramus would have bordered the dorsal edge of the antorbital fenestra. At mid-height, the lacrimal is mediolaterally wider (5 mm) than anteroposteriorly long (3 mm). A hole in the anterior ramus is due to preparation damage.

Prefrontal

The disarticulated right prefrontal was located dorsal to the neural spine of the third cervical, but has since been completely removed from the matrix. The prefrontal is composed of a thin but broad, subrectangular dorsal portion and a ventral ramus that extends from the anteroventral edge, which appressed against the posteromedial edge of the lacrimal. Most of the ventral ramus is broken and missing, except for a short portion of the proximal end, which is offset 3mm anteromedially by a fault.

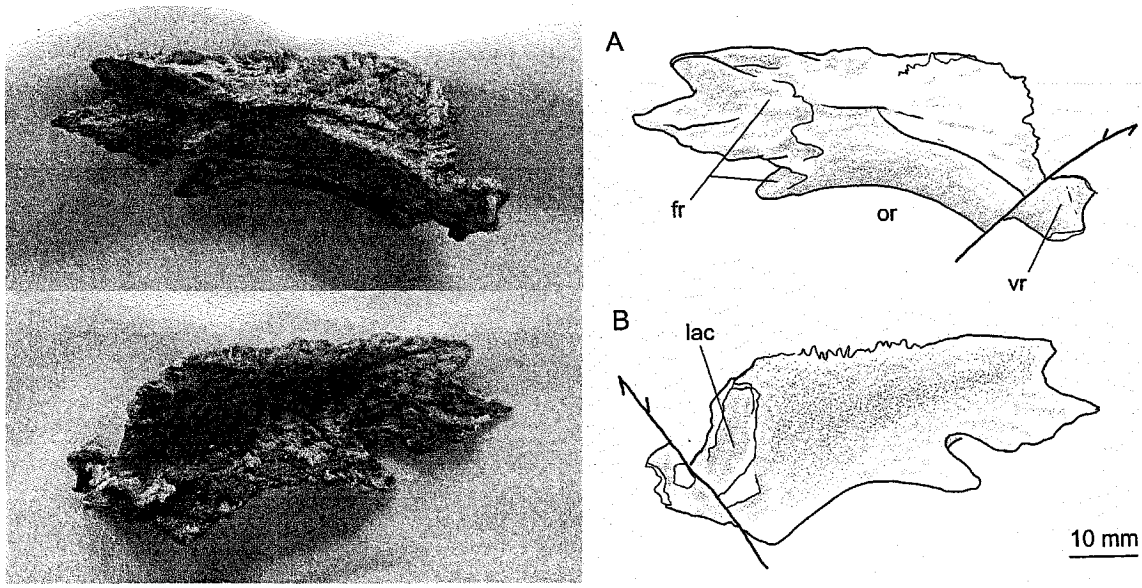

Figure 8.8: Right prefrontal of GF13-II in dorsal (A) and ventral (B) views.
Abbreviations: fr, articular surface for frontal; lac, articular surface for lacrimal; or, orbital margin; vr, base of ventral ramus.

The dorsal surface of the broad, sheet like dorsal portion of the prefrontal is mediolaterally convex. The ventrolateral edge represents the anterodorsal corner of the orbital margin. Rugose sutural surfaces are located along the anteromedial edge and posterior portion of the dorsal surface, for contact with the nasal (anteriorly) and the frontal (posteriorly). A short finger like projection of the posterior orbital margin of the prefrontal overlapped the anterolateral edge of the frontal, and medial to this point the prefrontal was overlapped by the frontal.

A deep depression in the anteroventral surface of the prefrontal represents the surface for the posterolateral edge of the lacrimal. As seen in ventral view (Figure 8.8), the structural integrity of the prefrontal is damaged by shrinkage fracturing of the internal bone structure. The ventral surface is mediolaterally concave, as well as slightly anteroposteriorly. The medial edge of the ventral surface has fine interdigitated suture, apparently for the anterolateral edge of the frontal

Frontal

Only the most posterior edge of the left frontal was preserved as a fragment attached to the parietal, and is only partially visible in ventral view within the counterpart that includes the posterior portion of the skull (Figure 8.9).

Parietal

The parietals remain in contact, and are visible only in ventral view. The preparation of the dorsal side has not been completed. As with the other elements preserved in this area, the right side of the parietals has been offset downward by small faults. The distal end of the right anterolateral process, which has several fine (rugose) ridges, represents the contact surface for the anterior ramus of the postorbital and posterolateral corner of the frontal.

Postorbital

The right postorbital is well preserved but disarticulated and rotated counter-clockwise. This results in the ventral process being directed anteriorly, and underlying the anterolateral process of the parietal (Figure 8.6). A fault displaces the anterior-most portion of the anterior process dorsally 7 mm. At its mid-point, the ventral processes anteroposterior length (11 mm) is much longer than the mediolateral width (2.5 mm), which differs from those of *Anchisaurus* and Neosauropoda, where it is mediolaterally wider than it is long (Yates 2004).

Measured from the dorsal margin of the postorbital, the ventral process is 40 mm long. The distal end of the ventral process is markedly rounded and broad, compared to the pointed distal end of *Massospondylus* (Sues et al 2005) and *Plateosaurus* (Galton 1984). In medial view, the posterior edge of the anterior ramus forms a sharp ridge that extends partially onto the ventral ramus. The ridge represents the supratemporal fossa that extends onto the posterior surface of the anterior process, which is typical for sauropodomorph taxa (Galton 1985a, Wilson and Sereno 1998, Sues et al. 2004).

Squamosal

The left squamosal is visible in ventral view within a counterpart to the skull block (Figure 8.9). A fault offsets the lateral portion posteriorly by 2 mm. The dorsal end of the left quadrate is only slightly disarticulated from the cup-like articular recess on the ventral surface of the squamosal. The distal portion of the quadratojugal ramus of the squamosal was separated during collection but a small fragment remains in the main

block near the posterodorsal edge of the maxilla. The preserved portion of the ventral ramus is broad and short. Therefore the ventral ramus was likely fractured during disarticulation, and the distal end is lost. The dorsolateral edge of the anterior process has a deep groove to accommodate the posterior ramus of the postorbital. The squamosal overlapped the posterior ramus of the postorbital dorsomedially.

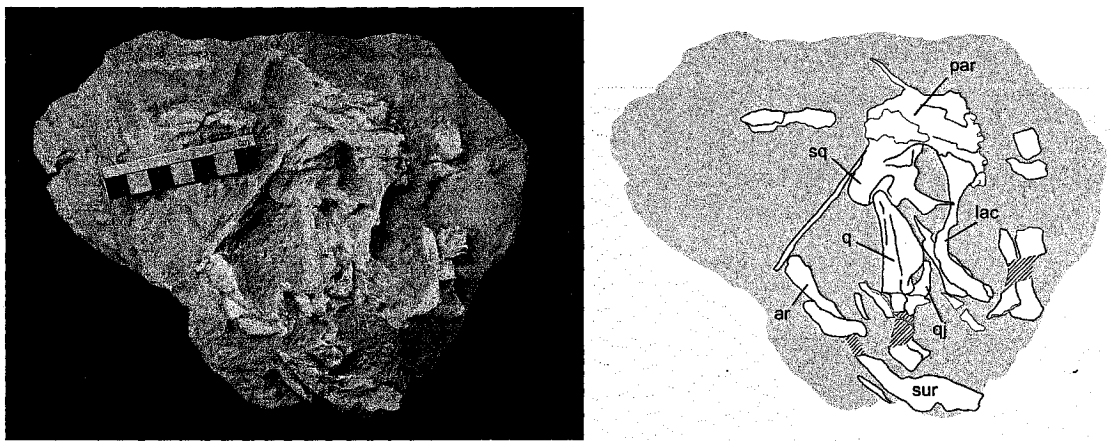

Figure 8.9: A counterpart to the skull block that contains the posterodorsal portion of the skull and associated elements.
The parietals (par) are exposed in ventral view and the right side is displaced ventrally due to small faults. Faulted surface of the left quadrate (q), quadratojugal (qj) and other elements is demarcated by crosshatching. Other abbreviations: ar, right articular; lac, right lacrimal; sq, left squamosal; sur, right surangular.

Quadrate

The quadrate is composed of a large anteromedial flange and a smaller laterally directed flange, which are nearly perpendicular to each other and meet along the posterior edge. Ventral to these flanges, the quadrate narrows into a rod-like process, the ventral end of which is composed of a medial and lateral condyle, which articulate with the mandibular facet on the articular.

The right quadrate is exposed in medial view on the left side of the skull. It was disarticulated from the right squamosal and displaced along with the right mandible toward the left side during burial. The height of the quadrate, from medial condyle to posterodorsal corner, is 60 mm (Figure 8.10). The ventral end of the left quadrate was displaced by a fault and is not exposed.

A small (2 mm) fault displaces the posterior portion of the anteromedial flange ventrolaterally. The anteromedial flange of the right quadrate is semi-circular in outline.

However, this outline differs from *Plateosaurus* (Galton 1984) and *Massospondylus* (Sues et al. 2004), in which the flanges are widest along the ventral margin and tapersdorsally. The shape of the anteromedial flange of the left quadrate is difficult to evaluate due to breakage. The right anteromedial flange is 42 mm tall (dorsoventrally) and thus occupies 70% of the quadrate, which is a similar proportion to *Massospondylus* (Sues et al. 2004) but much less than *Thecodontosaurus caducus,* which is 76% quadrate height (Yates 2003a, figure 5A). The ventral end of the anteromedial flange is 21 mm wide anteroposteriorly. The medial condyle of the right quadrate is mediolaterally thinner, and extends 11 mm further ventrally than the lateral condyle. The medial condyle is 2 mm wide mediolaterally, and at least 17.5 mm wide anteroposteriorly.

The dorsal end of the left quadrate is only slightly displaced from its articulation within a recessed cup like articular surface on the posteroventral portion of the left squamosal. The left quadrate also remains in contact with the posterolateral flange of the left pterygoid, although the lateral flange of the pterygoid has rotated counter-clockwise 90° in lateral view. The ventral portion, including the articular condyles, is offset downward within the block by a fault and remains unexposed.

The presence of the foramen incised into the ventral edge of the posterolateral flange cannot be evaluated on the left quadrate, and this area of the right quadrate is not exposed. The anteromedial flange of the left quadrate was fractured during collection, separated from the rest of the quadrate, and remains a loose fragment that also includes a portion of the left pterygoid.

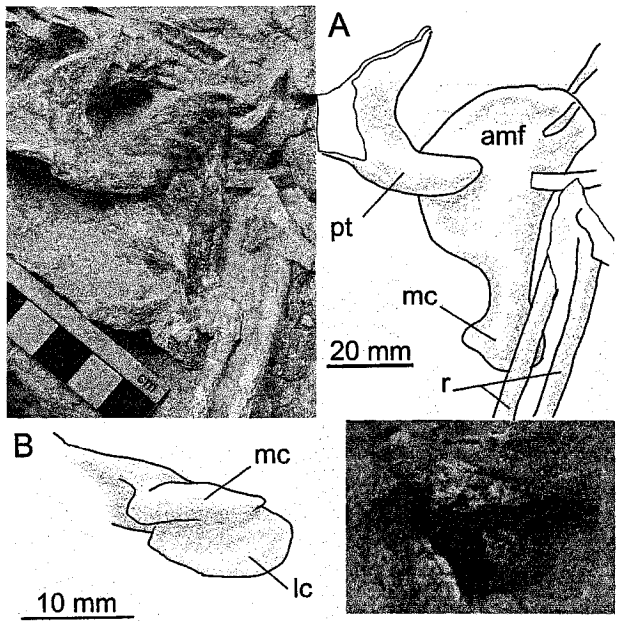

Figure 8.10: Right quadrate of GF13-II in medial view (A), and distal condyles in distal view (B). Abbreviations: amf, anterior medial flange of quadrate; lc, lateral condyle of quadrate; mc, medial condyle of quadrate; pt, dorsal quadrate flange of the pterygoid; r, cervical ribs of axis.

Quadratojugal

A portion of the anterodorsal arm of the left quadratojugal (Figure 8.9) lies underneath the left quadrate, but little can be said of the morphology because most of the quadratojugal was truncated by a fault and remains unexposed.

Pterygoid

The complex structure of the pterygoid is interpreted through comparison to the pterygoid of *Plateosaurus* (Figure 8.11), which is well exposed in multiple specimens and views (Galton 1984). The pterygoid is composed of a lateral and posterodorsally directed quadrate flange, a lateral process ('pterygoid flange', Galton 1984), a posteromedially directed facet for articulation with the basipterygoid process, and an anteriorly directed palatal ramus (Galton 1984, Sues et al. 2004). A small 'epipterygoid process' at the base of the quadrate flange is overlapped laterally by the base of the epipterygoid.

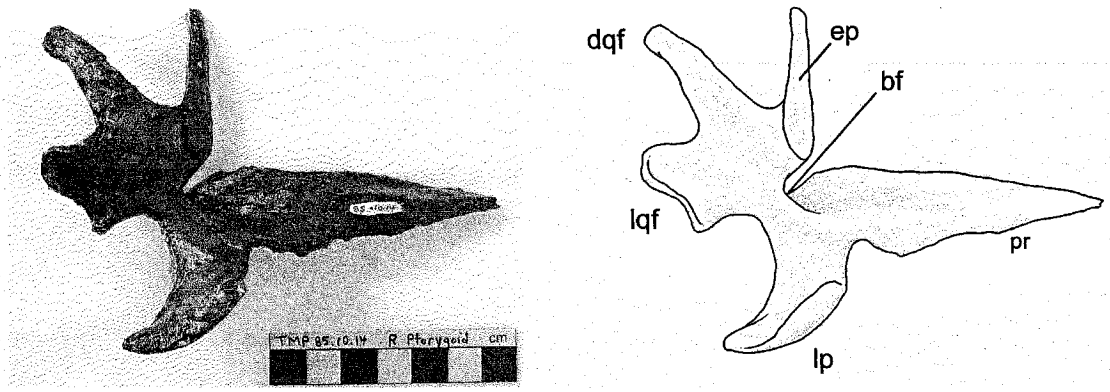

Figure 8.11: Cast (Tyrell specimen number 85.10.14) of the right quadrate and epipterygoid (ep) of *Plateosaurus* (AMNH 6810) in lateral view.
Abbreviations: bf, articular facet for basipterygoid process; dqf, dorsal component of quadrate flange; lp, lateral process; lqf, lateral component of the quadrate flange; pr, palatal ramus.

The quadrate flange and epipterygoid process of the left pterygoid is exposed in anterolateral view, but the more anterior components of the pterygoid have been truncated by a fault, displaced downwards and are not exposed. The lateral quadrate flange remains appressed against the medial edge of the left quadrate. The dorsal arm of the quadrate flange (Figure 8.10B) is mediolaterally wide along the anterior edge. Unfortunately, due to the fragmentary and faulted condition of the pterygoid, little else can be said about the morphology of this complex element.

Palatine

The right palatine is exposed in dorsal view (Figure 8.12), and has been displaced anteriorly in comparison to the right maxilla. A dorsally directed process (Figure 8.12, dp), with a transversely compressed suture on the dorsal end, is approximately at mid-length of the lateral edge. The dorsally directed process likely contacted the medial and ventral portion of the lacrimal, as in *Plateosaurus* (Galton 1985a: pg 122, Plate 3), although a similar process was not visible on Massospondylus material studied by Sues et al. (2004).

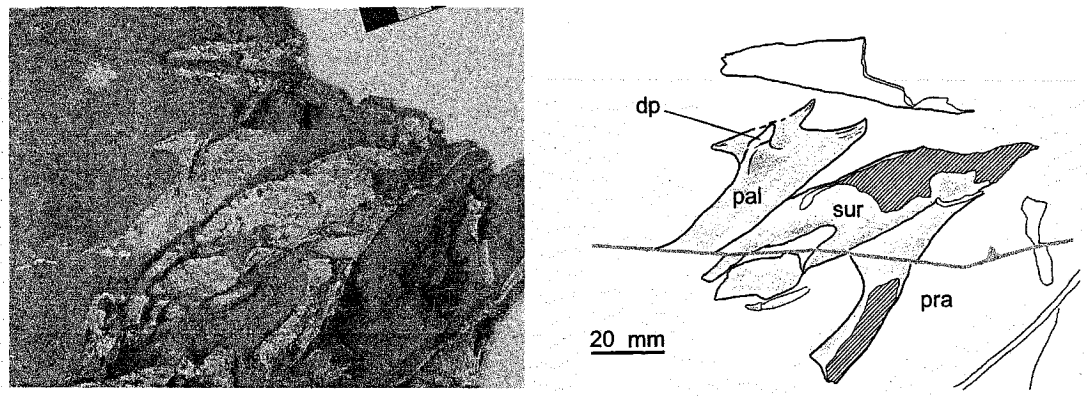

Figure 8.12: Right palatine (pal), left surangular (sur) and prearticular (pra) of GF13-II, exposed on the counter part from the block containing the skull.
A tall, dorsal process (dp), is inset from the lateral edge.

The anterior and posterior ends of the lateral edges resemble sharply pointed processes as a consequence of the anterior and posterior edges of the palatine being strongly embayed. The deeply incised anterior and posterior edges more closely resemble the condition of *Massospondylus* (Sues et al. 2004) and *Plateosaurus* (Galton 1985a), than that of *Thecondontosaurus* in which these edges are straight (Yates 2003a). The two processes on the lateral edge are covered with fine rugose ridges, apparently relating to the contact with the medial surface of the maxilla.

Vomer

The disarticulated right vomer is located under and adjacent to the right palatine, which has been displaced anteriorly. The vomer was broken into two pieces during collection of the skull. The anterior half is exposed in dorsal view within a counterpart to the skull block, and the posterior half is located in the main skull block and exposed in ventral view. It is 92 mm long, and narrow (7 mm) at mid length, and appears more similar to *Lufengosaurus* (Barrett et al. 2005, Figure 4). The posterior end narrows sharply to accommodate the suture with the anterior edge of the palatine. The lateral and medial edges of the anterior end are constricted. The lateral edge apparently contacted the medial edge of the anterior process of the maxilla.

Dentary

Both the right and left dentary were preserved, but are only partially exposed. The anterior 30 mm of the right dentary is exposed in lateral view and an additional 95 mm is exposed in medial view. The posterior end of the right dentary is offset (upwards) by a fault, and is also exposed in medial view. The posterior end is embayed, producing a dorsal and ventral arm that surround the anterior edge of the external mandibular fenestra. The ventral arm of the dentary extends farther posteriorly than the dorsal arm.

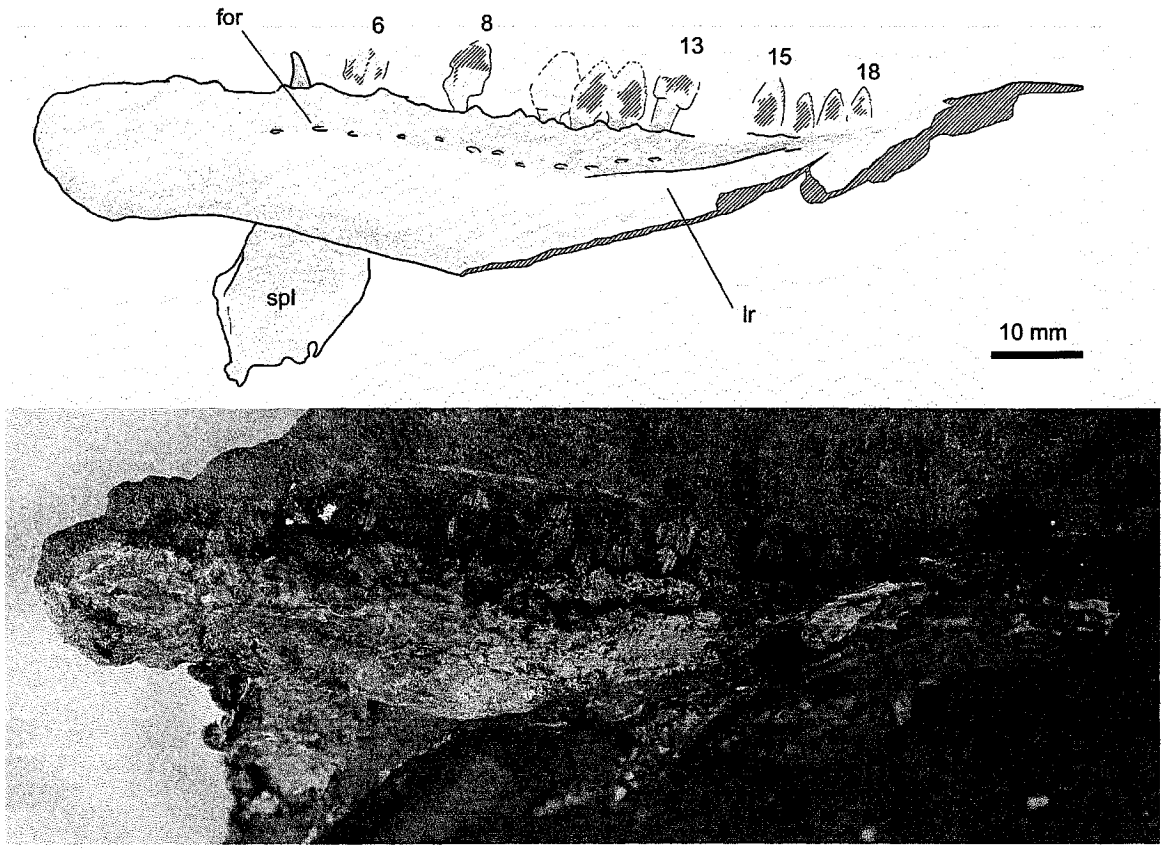

Figure 8.13: Anterior portion of the right dentary (GF13-II) in lateral view. Eighteen tooth positions can be identified based on the exposed buccal surfaces of the dentary teeth shown here, as well as the lingual view (Figure 8. 14). Abbreviations: for, small vascular foramina; lr, lateral ridge of dentary; spl, disarticulated splenial. Damaged enamel and missing bone surface noted with cross-hatched pattern.

In lateral view, the anterior (symphyseal) edge of the right dentary is not perpendicular to the tooth row, but is directed slightly ventrally (Figure 8. 14). In lateral view the ventral edge of the dentary is shallowly concave at the anterior end, creating a slightly downturned symphyseal end, similar to *Massospondylus* (Sues et al. 2004) but

less than in *Plateosaurus* (Galton 1984, figure 1A). The height of the anterior tip of the dentary is 25 mm (below the first tooth).

The labial edge of the dentary extends much farther dorsally than the lingual edge. Therefore, the roots of the teeth are exposed 8.5 mm in lingual view, in both the left and right dentary. While this condition seems similar to the 'lateral plate' of derived sauropods (Upchurch 1995), a similar condition on the maxilla of *Lufengosaurus* was distinguished from the lateral plate based on the uneven depth of the latter (Barrett et al. 2005). Although it seems strikingly similar, at this time the distinction is followed until further clarification of the distribution and differences can be established with additional analysis.

The dorsal labial edge of the dentary has strongly developed concave facets that surround the tooth at the base of the crown. Quadrangular interdentary plates are located along the lingual edge of the dentary, in front of and behind the base of the tooth crowns. The base of each interdentary plate is slightly incised and the plates are therefore connected to the dentary only by a thin bridge of bone. A deep groove on the medioventral edge of the dentary, from the posterior edge to the fifth tooth position, is also present on the dentary of *Plateosaurus* (Galton 1984), representing the contact for the ventral edge of the splenial.

The length of the tooth bearing portion of the (left) dentary is 100 mm, which (like the quadrate) is similar in size to the *Massospondylus* specimen BP/I/4934 . The left dentary is well exposed in lateral view, although it is missing the anteroventral and posteroventral edges; the height of the left dentary below the first tooth is only 18 mm, compared to 25 mm on the right dentary.

A ridge on the lateral surface of the dentary, from the posterior end of the tooth row diminishes in depth until it disappears completely below the eighth tooth position. Numerous vascular foramina are present between this lateral ridge and the base of the tooth crowns. The foramina are distributed approximately every 8 mm. The presence of the ridge and foramina has been used to suggest the presence of shallow 'cheeks' in *Plateosaurus* (Galton 1985a).

Articular

The right articular has a medial process behind the glenoid, but rather than being stout (Yates 2004), the process is rather thin and rectangular. A medial embayment does appear to be present behind the glenoid. However, due to incomplete preparation at this time, little else can be said about this region.

Surangular

The right mandible was only slightly disarticulated from the articular condyles of the right quadrate, although both the right mandibular ramus and quadrate have been dramatically displaced (in a medial direction) beyond the left side of the skull. The posterior portion of the right surangular has been removed from the skull block. The posterior surangular foramen (Wilson and Sereno 1998) is positioned along the dorsal edge of the surangular, similar to those of *Plateosaurus* (Galton 1984, Fig. 3 X) and *Massospondylus* (Sues et al. 2004). The anterior portion of the surangular (Figure 8.12) is exposed in lateral view, and deformed by several faults.

Prearticular

The left prearticular has become slightly displaced (ventrally) from the left surangular, is currently visible in medial view (Figure 8.6, 8.12), and is on the bottom of the counterpart to the skull block. Little can be said about the morphology of this incomplete and disarticulated element.

Splenial

The disarticulated left splenial is within a counterpart to the skull block. Due to displacement, it is rotated 90° relative to the left dentary and is on top of the symphyseal surface of the right dentary. The lateral surface, which contacted the medial surface of the dentary, is exposed on the upper surface of the counterpart to the skull block, and is dorsoventrally concave. The posterior edge of the splenial is strongly embayed, with the ventral edge extending farther anteriorly than the dorsal edge (Figure 8.6 and 14A).

Teeth

Terminology for describing tooth directions and positions follows that of Smith and Dodson (2003); labial, lingual, mesial and distal are the preferred terms to describe directions within the dentition, and location of a tooth is identified as associated with the maxilla, premaxilla, or dentary (pr, mx , d). The tooth position is described relative to the mesial-most tooth within the element and from the left (L) or right (R) side. For example, the anterior-most (mesial) left maxillary tooth is Lmx1. Empty aveolae are easily recognized and common due to tooth loss or replacement, and these are counted as temporarily empty tooth positions.

The tooth crowns are extremely fragile; the internal structure of the dentine shrank as the specimen dried after collection, leaving the thin enamel (less than 0.2 mm thick) largely unsupported medially, in a fragile state. The right and left premaxillae have not been located and were likely lost prior to collection. However, at least some of the isolated teeth that were found disarticulated among and around the cranial elements appear to represent premaxillary teeth.

Table 8: The dimensions and presence/absence of dentary teeth in the left dentary and anterior portion of the right dentary.
A tooth is either exposed (*) in lingual (Ln) or labial (Lb), not present or perhaps is unprepared ('-') or has not fully erupted (n) and is only visible in lingual view. The crown fore-aft basal width (W) and crown height (H) dimensions are listed in millimeters when measurement was possible.

	Ld1	3	4	5	6	7	8	10	11	12	13	14	15	16	17	18	Rd2	3	4
Ln	*	*	n	n	*	n	*	*	*	*	*	*	-	-	-	-	-	-	-
Lb	-	-	-	-	*	-	*	*	*	*	*	-	*	*	*	*	*	*	*
W		6.7			5.9			5.0	5.0	5.0							5.8		
H		8.2			8.6		8.9	8.6	8.5								9.7	8.4	8.8

The largest known adult *Massospondylus* skull (BP/I/4934) has 26 dentary tooth positions (Sues et al. 2004) occupying approximately 110 mm of the dentary. *Plateosaurus* has 22 dentary tooth positions (Galton 1984) and *Lufengosaurus* has an uncertain number, but the teeth have no ridges, furrows or ornamentation of the enamel (Barrett et al. 2005). The number of teeth in the maxilla of *Massospondylus* increases with size (age); 15 teeth in the maxilla of the small skull (BP/1/4376) and 22 in the largest skull (BP/1/4934) (Sues et al. 2004). A similar pattern would be expected for the dentary as well as for other sauropodomorph taxa.

The complete dentary tooth row of 18 tooth positions is exposed on the left side and occupies 100 mm of the dentary. Only five empty aveolae and eight teeth are present in the anterior 85 mm of the right dentary. The anterior five teeth are exposed in labial view and three teeth are exposed in lingual view. Therefore, an additional 5 tooth positions remain unexposed on the posterior portion of the right dentary.

The first dentary tooth is inset from the symphyseal edge by one tooth width (5 mm), with the serrated carinae directed labiolingually, rather than mesiodistally as with the more distal teeth. The labial (anterior) surface of the first tooth crown is strongly convex and the lingual surface is mildly concave. Five serrations on the distal carinae are somewhat rounded in comparison to the unerupted teeth, which have sharper denticles. The mesial carinae of Ld1 is missing and currently is not exposed on Rd1, so the presence or number of denticles cannot be determined. There is a prominent longitudinal depression adjacent to the distal carina, and the enamel exhibits fine textured patterning.

The anterior four dentary tooth crowns are about 9 mm tall (Table 8), and crown height gradually decreases posteriorly; tooth crown height of the last dentary tooth is 7.8 mm. The average tooth width is 5.5 mm,, based on those teeth that could be measured (Table 8), which is further supported by the average tooth position fore-aft width (total length of tooth bearing portion / number of teeth), which is also 5.5 mm. For comparison, the mid-dentary tooth crowns of *Massospondylus* (BP/I/4934) have a fore-aft width of 4.0 mm wide and a height of 8.0 mm, which is again consistent with the fore-aft width of the average tooth position (4.2 mm); the tooth bearing portion of the dentary is 110 mm and contains 26 tooth positions.

Generally the denticles are restricted to the distal half of the carinae, but the denticles of one tooth (Figure 8.15) extend beyond the mid-point of the carinae. The distribution of the denticles is asymmetrical because all teeth have fewer denticles on the distal carinae. The carinae of exposed teeth have denticle densities of 3-4 denticles per 2 mm. At least one tooth (Rd2) has no denticles along the mesial edge, although six serrations extend to crown mid-height on the distal carinae of Ld2. One isolated tooth (98GF13.40.14) has no serrations on the exposed edge or the partially buried edge. The tooth has obvious enamel wrinkling on both the labial and lingual surfaces. The anterior most dentary teeth have at least some serrations. Therefore this likely represents a

premaxillary tooth with a fore-aft crown width of 5.6 mm, a height of 10.0 mm, and a tapering tooth root 18.7 mm long.

The lingual surfaces of the dentary teeth each have a centrally located convex ridge bordered by longitudinal concavities. The mesial and distal depressions of the lingual surface provide for the overlapping (twisted) arrangement of the teeth (Figure 8. 14).

The unerupted Ld5 is partially exposed in lingual view, and has a double row of serrations on the mesial carinae (Figure 8. 14). This is the only tooth to exhibit this unique morphology so the double row of denticles is interpreted as a pathology, and appears similar to the pathologies reported for theropod serrations (Abler 1997).

All dentary and maxillary teeth have a convex labial surface with a central longitudinal furrow (Figure 8. 14), whereas the teeth of *Massospondylus* have a centrally located longitudinal ridge on the convex labial surface (Sues et al. 2004). Many teeth also exhibit several longitudinal furrows adjacent to the centrally located (and deeper) furrow. The lingual surface is concave on the distal half and bulbously convex toward the base. The distal portion of the teeth are slightly recurved lingually. The maxillary teeth appear to have a ridge on the lingual surface, and are concave on each side of the ridge. The dentary teeth of *Massospondylus* (Sues et al. 2004) and *Plateosaurus* (Galton 1985a) are situated lingual to the maxilla and premaxillary teeth when the mandibular rami are adducted, and the same situation is expected for the GF13-II.

At least twenty isolated teeth are scattered around the skull elements (10 remain in block, 10 have been removed). Two short (5 mm) tooth crowns (98GF13.40.17) are likely from the posterior portion of the maxilla or dentary as a similar size of tooth can be seen in the posterior portion of the left dentary. The tooth serrations are asymmetrical. One tooth has four serrations on one side and five on the other side slightly farther down the crown.

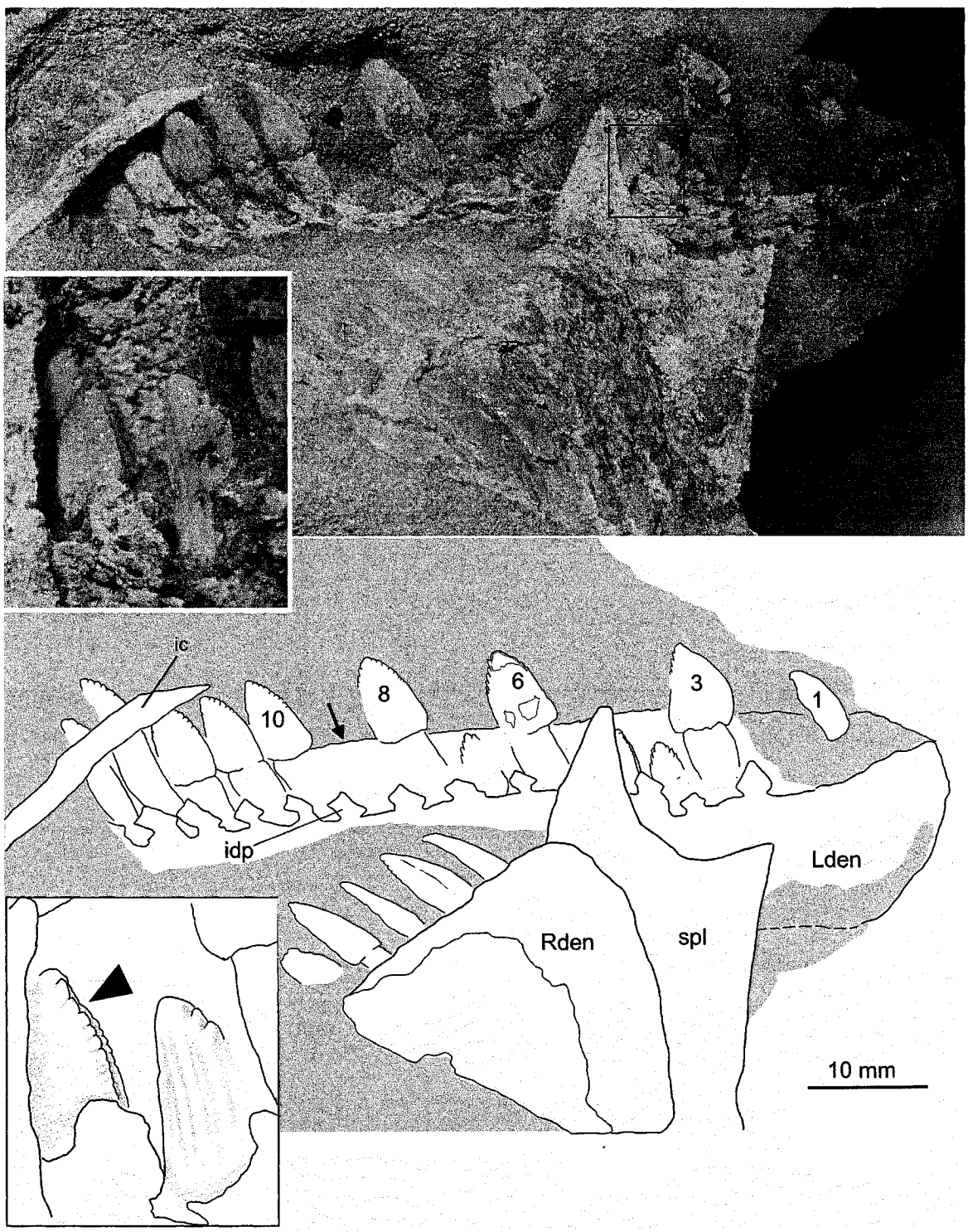

Figure 8. 14: The anterior end of the right (Rden) dentary in buccal view and the left dentary (Lden) in lingual view.
Abbreviations: ic, intercoronoid; idp, interdentary plate; spl, splenial. The lingual edge of the dentary is lower than the lateral edge (arrow). The fifth tooth of the left dentary (inset, arrow head) exhibits a pathological, double set of serrations on the mesial carina. Sandstone matrix is demarcated in grey.

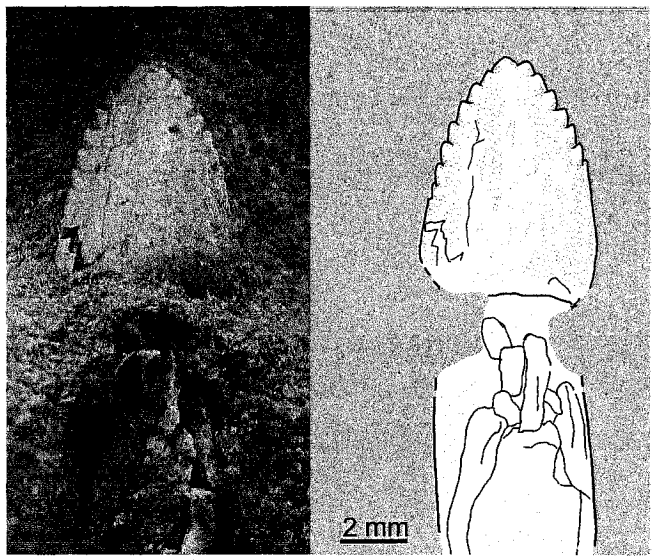

Figure 8.15: A disarticulated dentary tooth, located immediately below the right dentary, in buccal view.
Note the serrations that extend beyond the distal half of the tooth crown, and the fine texture of the enamel surface. The tooth root has shrunk and broken into many pieces while drying, shortly after collection. Seven denticles are located on either side of a central denticle, although the denticles extend further toward the base on one side (distal?). The crown is 6.6 mm tall and the fore-aft basal width is 5.3 mm.

Ceratobranchials

Several thin elongate elements were found dispersed among the disarticulated cranial material, especially in the caudal regions of the skull. Some are thicker than others, the thicker likely being the hyoid elements. The thinner elements present may represent other elements of the hyoid apparatus. One thin element currently overlies the medial surface of the right quadrate.

Discussion

The elongation index (Upchurch 1998), the ratio of cervical centrum length compared to the width of the posterior centrum surface, cannot be used to evaluate the cervical elongation of GF13-II. The posterior central facets for all (but one?) cervical vertebrae are not exposed. The cervical vertebrae of *Lufengosaurus hueni* (Young, 1941) demonstrate it is unreasonable to use the height as a proxy for centrum width. Although Young did not provide measured dimensions, the relative length was provided as a length to height ratio. The ratios for the third and fifth cervical vertebrae are 3.3 and 2.5

respectively. However, the illustrations provided by Young (1941, Fig. 6), demonstrate the posterior central face of each cervical vertebra is wider than tall in most cervical vertebrae. Wilson and Sereno (1998) used the relative centrum length compared to the height of the posterior centrum face as a metric for cervical vertebrae elongation. They noted that extreme elongation (when length to height ratio > 4.0) occurs three times among Sauropoda; *Plateosaurus* was used as the 'prosauropod' outgroup and does not exhibit this extreme elongation (4.0 > central length > 3.0).

The fifth cervical vertebra has the greatest length to height ratio (4.13) of the cervicals for GF13-II. The cervical vertebrae from other specimens (GF69, 98GF13.47 and PU22196) also exhibit elongate cervical vertebrae. The morphology of the cervical vertebrae and cranial elements that have been identified from the skull provide important data with which to consider the phylogenetic relationships of the bone bed specimens.

The identification of a pathological double row of serrations on the mesial carina of the fifth dentary tooth suggests that the distinction between serrations of theropod dinosaurs and denticles of basal sauropodomorphs may not be as significant as is typically accepted (Galton 1985c, Abler 1992). The other dentary teeth of GF13-II are relatively broad, especially compared to the teeth of *Massospondylus*, and have well developed denticles that at least on some teeth extend beyond the distal half of the carinae.

As in the postcranial material, the cranial material can also be used to demonstrate the McCoy Brook specimens are not referable to cf. *Ammosaurus*. In particular the ventral arm of the postorbital of GF13-II is not medialaterally wider than anteroposteriorly long, and therefore differs from that of *Anchisaurus* (=*Ammosaurus*, Chapter 2).

The palatine of GF13-II possesses a unique dorsal process slightly inset from the lateral margin, which may have articulated with or against the ventral portion of the lacrimal. A similar feature has been reported for *Plateosaurus*, but not as yet for *Massospondylus*, perhaps due to the lack of appropriately exposed material.

Chapter 9 –Phylogenetic Analyses and Significance of the Sauropodomorph Specimens from the McCoy Brook Formation

Introduction

Evaluation of the new prosauropod material collected from the McCoy Brook Formation (Chapters 5-8) found the material represents at least five individuals, includes the first cranial material from the McCoy Brook, and can now be confidently differentiated from *Anchisaurus (=Ammosaurus)*. Furthermore, the most complete specimen (GF13-II) possesses several unique features that demonstrates it represents a new taxon. The identification of this new taxon and its phylogenetic relationships are considered, as well as the morphological variation exhibited by the specimens from the McCoy Brook bone bed.

Phylogenetic Analysis

The specimens described in the previous chapters were coded within the matrix of Chapter 2, which represents a matrix from Yates (2004) updated with information from the new analysis of *Anchisaurus* (Chapter 2) and the recent study of *Massospondylus* (Sues et al 2004). The matrix includes 205 characters (Appendix 1) and 17 ingroup taxa other than the Nova Scotia specimens. As in the analyses of Yates (2004) and Chapter 2, two outgroup taxa were used (Theropoda, and *Herrerasaurus*). The use of two alternative outgroup taxa (proposed by Yates 2004), Ornithischia and Theropoda (including *Herrerasaurus*), produces similar results. The revised data were analyzed using PAUP 4.0 beta version (Swofford 2002). Multi-state characters were treated as polymorphic, and the shortest, most parsimonious trees were found using branch and bound search algorithms.

Three separate analyses were considered; the first included the most complete specimen (FGM998GF13-II), which represents the holotype of the new taxon *Fendusaurus eldoni*. The second analysis included only data available from FGM998GF13-I, the specimen with the short bladed ilium. The third analysis combined

all specimens as a 'Combined' dataset, including all the four specimens from the bone bed that include articulated material (GF13-I, GF13-II, GF13-III, GF69, and GF9).

The initial analysis of FGM998GF13-II resulted in two equally most parsimonious trees of 451 steps. The two trees differed only in the placement of GF13-II within Massospondylidae, either as a sister taxon to *Massospondylus* + *Lufengosaurus* or more closely related to *Lufengosaurus*. The result is robust, with a bootstrap of 62% (based on 1000 replicates).

Due to the close relationship proposed with *Lufengosaurus*, the results of a recent redescription of the skull of *Lufengosaurus* (Barrett et al. 2005) was incorporated to revise the matrix. As suggested by Barrett et al. (2005), the following changes were made to the original matrix of Yates (2004) for *Lufengosaurus*: character 7 (2 to ?); characters 8, 65 and 66 (1 to ?); characters 10, 17, 55, 59 and 60 (0 to ?); characters 2 and 40 (0 to 1); characters 21 and 25 (1 to 0); character 44 (1 to 2); characters 19, 20, 28, 35, 36, 46, 51 and 63 (? to 0); characters 49 and 56 (? to 1).

Systematic Palaeontology

DINOSAURIA Owen, 1842

SAURISCHIA Seeley, 1887

SAUROPODOMORPHA von Huene, 1932

PROSAUROPODA von Huene, 1920

MASSOSPONDYLIDAE von Huene, 1914

***Fendusaurus* gen. nov.**

Derivation of name: From *fendu*, French for 'split', in reference to the origin of the name for the Bay of Fundy, derived from an English corruption of the original name for Cape Split (Cape Fendu); and *saurus*, Latin for lizard.

Type Species: *Fendusaurus eldoni*

Diagnosis: A prosauropod with a four vertebra sacrum, that includes a dorsosacral and a caudosacral; teeth are proportionally wide with finely textured enamel and longitudinal furrows; elongate cervical vertebrae (>4.0 times longer than tall); posterior dorsals with well-developed suprapostzgyaposphyseal laminae; anterior caudal

vertebrae with long neural spines; well developed brevis fossa on posteroventral edge of ilium; anterior distal process of tibia overlaps the anterior surface of the ascending process of the astragalus.

Fendusaurus eldoni sp. nov.

Derivation of Name: In recognition of Eldon George, a fossil enthusiast from Parrsboro, Nova Scotia, who has done much to promote the local area and palaeontological research.

Holotype: FGM998GF13-II in the collection of the Fundy Geological Museum, Parrsboro, Nova Scotia. A nearly complete specimen, including a disarticulated skull, complete axial skeleton (except distal caudal vertebrae), pectoral and pelvic girdles, right humerus, and the right ilium, femur, tibia, fibula and pes.

Referred Specimens: FGM998GF13-I, sacrum with articulated ilia and ischia, right hind limb, left tibia, fibula and pes, two posterior dorsal vertebrae and anterior caudal vertebrae: FGM998GF13-III, sacrum with articulated left and associated right ilium, articulated right pubis, posterior dorsal vertebrae and anterior caudal vertebrae; FGM994GF69, sacrum with articulated pelvic girdle, right and left hind limbs, posterior dorsal vertebrae and anterior caudal vertebrae, anterior cervical vertebrae, ribs, gastralia, right radius? and manus: FGM998GF9, material from more than one individual, including a left femur, tibia, fibula, and distal end of right femur, ischium, fifth metatarsal, two dorsal vertebrae, a portion of cervical vertebra, radius and ulna.

Type horizon and locality: Lower Jurassic (Hettangian) McCoy Brook Formation, Wasson Bluff, Cumberland County, Nova Scotia; approximately 53 meters up section from the 'fish bed' Scots Bay Member.

Diagnosis: As for genus; currently only known species.

Discussion

The revised matrix did not affect the typology of the two resulting trees, which again differed only in the placement of GF13-II, although the tree lengths were slightly larger (456 steps). The placement of GF13-II remains robust, the bootstrap was unchanged (62%), and three additional steps (resulting in 115 most parsimonious trees) were required to pull GF13-II out of Massospondylidae, at which point the resolution among the entire tree falls apart.

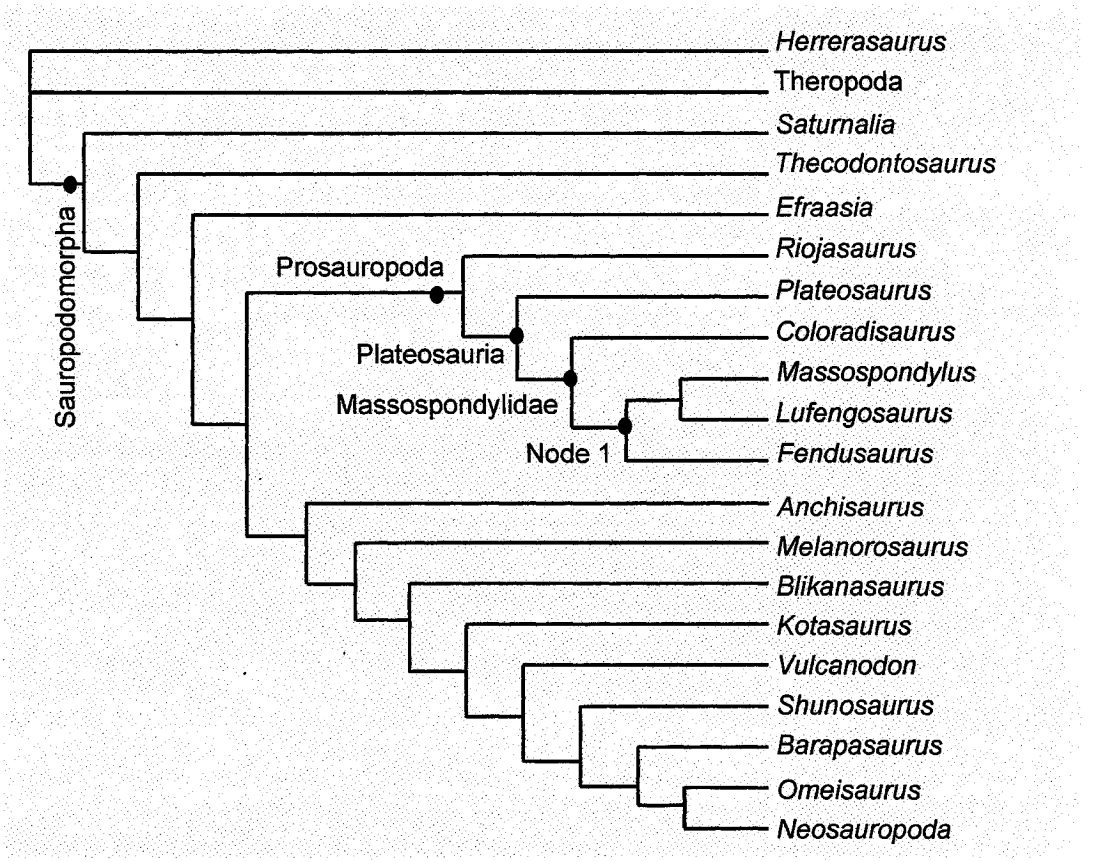

Figure 9.1: Tree-1 of two most parsimonious trees that resulted from the phylogenetic analysis of the new prosauropod specimens from the McCoy Brook Formation.

In order to consider the importance of the morphological variation exhibited by the specimen with a short bladed ilium, GF13-I was included in the matrix (without GF13-II). A single tree of 449 steps results, which places GF13-II as the sister taxon to *Lufengosaurus* (Figure 9.2). When GF13-II and GF13-I are both included within an analysis, they are placed as a dichotomy in the two resulting trees, again either more closely related to *Lufengosaurus* or as the immediate outgroup to *Massospondylus* +

Lufengosaurus. The dichotomy of the GF13-I and GF13-II is not surprising, as they only differ in two codings; relative lengths of the caudal centra (103) and shape of the posterior end of the ilium (156).

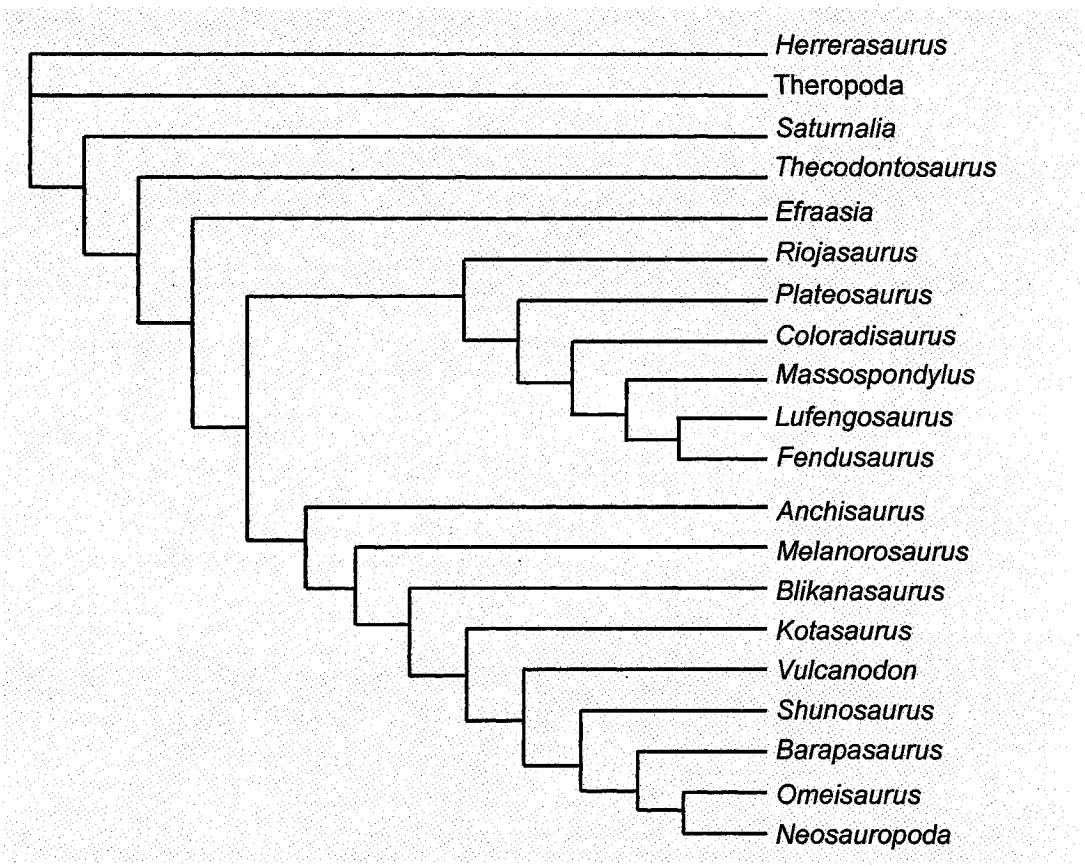

Figure 9.2: Tree-2 of two most equally most parsimonious trees that result from the analysis of the McCoy Brook Formation specimens, which differs from Figure 9.1 only in the placement of *Fendusaurus*.

All other specimens (GF13-III, GF69, GF9) do not differ in any codings when compared to the most complete specimen (GF13-II). These other specimens provide additional information that is not available in GF13-II alone, especially GF69, which includes the only preserved manus, as well as both pedes. In order to maximize the amount of data available for the phylogenetic analysis, all of the Nova Scotia bone bed specimens were included in a single 'combined' taxon. For the three codings that differed between specimens, both alternatives were included as multi-state character.

Analysis of the 'Combined' data resulted in two most parsimonious trees of 456 steps (CI = 0.5746, HI = 0.5000), which varied only in the placement of the 'Combined' specimen in the same configuration as previous analyses (Figure 9.1, Figure 9.2). The

similar configuration of the most parsimonious trees demonstrates that the morphological diversity within the bone bed is not extreme on a phylogenetic level. The results from the 'Combined' analysis where used to consider specifically how the two trees differ. The diagnostic characters of each node differ slightly between the two trees, and also depending upon which optimization criteria is used (ACCTRAN versus DELTRAN). Characters that are found in both ACCTRAN and DELTRAN optimization are considered unambiguous. The characters in several nodes are considered below.

Prosauropoda:
Unambiguous: 17, 63, 87, 99, 131, 154, 156
ACCTRAN: 51, 53 (*Tree 2*), 99 (*Tree 1*), 121, 157
DELTRAN: 14, 15, 24, 44, 52, 118, 129, 130, 136

Massospondylidae:
Unambiguous: 47, 81, 115, 166, 169, 198, 202
ACCTRAN: 40, 47, 76, 114 (*Tree 2*), 134, 140, 157
DELTRAN: 7, 197

The unambiguous characters of Prosauropoda are the same as in Yates (2004), except that 99 is only ACCTRAN in Tree 1, character 53 is a new DELTRAN character (in Tree 2 only), and 48 is no longer found to be a DELTRAN character. The unambiguous characters of Massospondylidae remain the same, but both 22 and 25 are no longer found to be ACCTRAN characters of this clade.

Node 1 - (*Massospondylus* + *Lufengosaurus*) + *Fendusaurus*:
Unambiguous: 17, 48, (*Tree 2*), 154
ACCTRAN: 48 *(Tree 1)*, 74, 163 (*Tree 1*)
DELTRAN: 134 (*Tree 2*), 140 (*Tree 2*), 190

In considering the character states that define the relationships of the three terminal taxa of Massospondylidae (Node 1: *Massospondylus*, *Lufengosaurus*, and *Fendusaurus*), the second tree is slightly better supported. However, character 48 (septum spanning the interbasipterygoid space) is currently unknown for the Nova Scotia taxon. Therefore, both of these trees remains equally likely based on the current data available.

The only unambiguous character of Node 1 in either tree for which there are data for *Fendusaurus* is the lack of a caudally projecting heel on the posterior edge of the ischial peduncle (154). The transversely wide distal ischial expansion (163) is an ACCTRAN character for Tree-1 and is observable in *Fendusaurus* specimens, but the isolation of the serrations on the distal half of the tooth (74) is polymorphic for GF13-II. For DELTRAN characters, a horizontal groove on the calcaneum is observable in GF69. Therefore, there are only several characters observable in *Fendusaurus* specimens that place this taxon within Node 1, but this congruity is strengthened by the character distributions of the taxa immediately below Node 1.

For placement among Massospondylidae, the dorsoventral depth of the parasphenoid rostrum (47), presence of ventral keels on the cervical centra (81), and the concave edges of the pubic apron (166) are three unambiguous characters for both trees that are also observable in *Fendusaurus*. Additional ACCTRAN characters observable in *Fendusaurus* include the overhanging axial postzygapophyses (76), notch of ischial obturator plate (157). The relatively wide proximal end of the fifth metatarsal (197) is a DELTRAN character for this node, and in all specimens except GF9, the metatarsal is wider than 50 % of length, similar to the other taxon within this node. The placement of *Fendusaurus* within Massospondylidae is well supported by characters that are documented within the specimens.

Plateosauria
Unambiguous: 5, 34, 49, 57, 62, 80, 87, 109, 120, 139, 163 (*Tree 2*)
ACCTRAN: 19, 122, 163 (*Tree 1*), 179
DELTRAN: 3, 6, 27, 51, 56, 75, 204

Five unambiguous characters for Plateosauria are observable in current specimens of *Fendusaurus*, including the strongly curved symphyseal end of the dentary (57), the relatively long retroarticular process (62), long third cervical centrum (80), presence of laterally expanded tables on the pectoral and cervical vertebrae (87), and presence of a ventral sulcus on caudal centra (109). Six characters (5, 34, 49, 120, 139, 163) were not coded due to missing data. Based on these missing characters, it would be of considerable interest to recover additional specimens of *Fendusaurus*, especially cranial

material that includes a well preserved braincase, as well as forelimb and articulated manus.

Sereno (1998) defined Massospondylidae as a stem based taxon, including all taxa closer to *Massospondylus* than to *Plateosaurus*. The placement of *Fendusaurus* among Masspondylidae is statistically well supported, but additional specimens will be of considerable interest to further confirm this placement. The placement of *Fendusaurus* among Plateosauria is more strongly supported, but again additional cranial material, including a well preserved braincase, would be of considerable importance to confirm this result.

Morphological Variation

The morphological variation within the *Fendusaurus* bone bed is currently attributed to intraspecific variation. While the morphology of the short bladed ilium (GF13-I) is different from that of the other specimens, there are only limited differences in the other postcranial material of this specimen. The location of additional cranial and forelimb material will be of interest for further clarifying the nature of this variation. It would be particularly useful if additional cranial material could be reasonably associated with a specimen that has the short-ilium morphology.

Previous studies of sexual dimorphism among prosauropod taxa have focused exclusively upon *Plateosaurus*, for which there is abundant material. These studies included consideration of morphological variation within the skull (Gow et al. 1990) and femora (Weishampel and Chapman 1990). However, the results of these two studies provided limited considertation of sexual dimorphism and produced contrary results, which led to the dismissal of the evidence for sexual dimorphism among *Plateosaurus* (Galton 1997). The variation was attributed to individual variation.

The occurrence of a rich bone bed of prosauropod dinosaurs in the McCoy Brook Formation provides the opportunity for the collection of additional specimens. These specimens are certainly contemporaneous, being articulated skeletons stacked on top of each other. Additional material present at the site will be useful in further considering the basis for the morphological variation. At this time, the morphological diversity of the ilium, and relative lengths of the dorsal and caudal vertebrae are attributed to intra-specific variation.

Chapter 10 – Conclusions

Previous work demonstrated the fragmentary sauropodomorph specimens from Arizona are not referable to the genus *Anchisaurus* (Yates 2004). Based on the new specimens recovered from Wasson Bluff, the small and somewhat enigmatic *Anchisaurus* is also absent from the McCoy Brook Formation. Due to the close proximity and temporal similarity between the Hartford and Fundy rift basins, it remains possible that specimens of *Anchisaurus* may yet be found in the Fundy Basin. However, with the new information about the Nova Scotia specimens, *Anchisaurus* is now geographically restricted to the Hartford Basin.

The new specimens from the McCoy Brook Formation provide clear evidence for at least one new taxon of massospondylid prosauropod, *Fendusaurus eldoni*. The identification of a massospondylid within the McCoy Brook Formation is consistent with other recent studies of the fragmentary sauropodomorph specimens in western USA (Yates 2004, Irmis 2005), which concluded the material represented an indeterminate massospondylid. Also, in an analysis of early Mesozoic biogeography (Shubin and Sues 1991) the presence of the family Anchisauridae and absence of Massospondylidae were two factors that distinguished the McCoy Brook Formation from the Lower Lufeng Formation (China), Upper Stromberg (South Africa) and Kayenta Formation (western USA). The identification of the massospondylid *Fendusaurus* within the McCoy Brook Formation removes these disparities, and increases the similarity of the faunas from these Lower Jurassic formations.

There is evidence of at least one other prosauropod taxon other than *M. carinatus*, within the *Massospondylus* range zone of the Upper Elliot Formation, South Africa, based on the morphological variation of the braincase and teeth of a recently described specimen (Barrett 2004). An increased appreciation of the diversity in the Upper Elliot Formation will provide further evidence with which to evaluate the morphological diversity of the McCoy Brook Formation bone bed, and vice versa.

While the diversity among the McCoy Brook Formation specimens remains somewhat uncertain, the most complete specimen demonstrates that at least one new taxon can be recognized. The new taxon, *Fendusaurus*, demonstrates several interesting

morphological features. All specimens within the bone bed preserve a four vertebrae sacrum that includes a dorsosacral and caudosacral. Also, all tibiae have an anterior distal process that overlaps the anterior surface of the ascending process of the astragalus, which is a unique morphology although somewhat similar to that exhibited by *Melanorosaurus* (Galton et al. 2005). The cervical vertebrae are elongate, to a degree that is only attained in three groups of more derived sauropodomorphs. Sereno and Wilson (1998) demonstrated that cervical elongation occurred independently three times, with *Omeisaurus*, *Brachiosaurus*, and some diplodocoids), and a similar result was recently obtained by Wedel (2006). The occurrence of this level of cervical vertebrae elongation among prosauropod dinosaurs is a novel and unexpected result.

Two ilium morphologies are present for the bone bed specimens - an elongate postacetabular blade (GF13-II, GF13-III) and a short bladed form (GF13-I). The elongate postacetabular blade is rather distinctive amongst sauropodomorph dinosaurs, although *Saturnalia* (Langer 2001) has a similarly elongate postacetabular blade. While this degree of morphological variation of the ilium has not been reported for other sauropodomorph taxa, the other postcranial material of GF13-I is similar to the other bone bed specimens and does not warrant recognition of a separate taxon at this time. Additional well preserved specimens are required to clarify the possibility of intraspecific (sexual?) variation of the ilium within these bone bed specimens.

The results of the phylogenetic analysis (Chapter 9) are consistent with other recent studies (Yates 2004, Barrett et al. 2005) that identify a clade Prosauropoda, composed of a restricted number of taxa. The new descriptions of the skull and braincase material of *Anchisaurus* resulted in a similar tree typology as proposed by Yates (2004). However, the robustness of the placement of *Anchisaurus* with the Sauropod clade is now much reduced due to the possibility of skeletal immaturity of the specimens. The McCoy Brook Formation can now be recognized as including the richest site in North America for prosauropod dinosaurs and the oldest dinosaur skeletal remains in Canada. The presence of additional specimens within the bone bed provides the possibility for future studies to clarify the skeletal morphology of *Fendusaurus*, and a basis for further consideration of the morphological variation within the bone bed.

Appendix 1 – Character Descriptions and Codings

The following character descriptions are taken directly from Yates (2004), and are provided for reference, but the character data for GF9, GF13-I, GF13-II, GF13-III and GF69 represents new data. The various codings for *Anchisaurus* marked in bold represent new data from Chapter 3, while the bold character codings for *Lufengosaurus* (Barrett et al. 2005) and *Massospondylus* (Sues et al. 2004) have been included for comparative purposes.

	Characters (from Yates 2004).	GF9	GF13_I	GF13_II	GF13_III	GF69	Combined	*Anchisaurus polyzelus*	*Lufengosaurus huenei*	*Massospondylus carinatus*
1	Skull to femur ratio: greater than (0), or less than (1), 0.5 (Gauthier, 1986).	?	?	1	?	?	1	1	1	1
2	Lateral plates, ventral extension of lateral maxilla surface that is uneven along the tooth bearing element (Barrett et al. 2005), appressed to the labial side of the premaxillary, maxillary and dentary teeth: absent (0) or present (1) (Upchurch, 1995).	?	?	?	?	?	?	0	**1**	0
3	Distal end of the dorsal premaxillary process: tapered (0) or transversely expanded (1) (Sereno, 1999).	?	?	?	?	?	?	?	?	1
4	Caudolateral process of premaxilla: present (0) or absent (1) (Sereno, 1999; referring to variation within theropods).	?	?	?	?	?	?	0	0	0
5	Dorsal profile of the snout: straight to gently convex (0) or with a depression behind the naris (1)	?	?	?	?	?	?	?	1	1
6	Elongate median nasal depression: absent (0) or present (1) (Sereno, 1999)	?	?	?	?	?	?	?	1	1
7	Relationship between caudolateral process of the premaxilla and the rostroventral process of the nasal: broad sutured contact (0), point contact (1) or separated by maxilla (2) (modified from Gauthier, 1986). Ordered.	?	?	?	?	?	?	?	**?**	2
8	Ratio of narial diameter to orbital diameter: less than (0), or greater than (1), 0.5 (Wilson and Sereno, 1998).	?	?	?	?	?	?	?	**?**	1
9	Narial position: near terminus of snout (0) or retracted caudodorsally so that the dorsal margin is level with the dorsal margin of the orbit (1) (Wilson and Sereno, 1998).	?	?	?	?	?	?	0	0	0
10	Profile of premaxilla: convex (0) or with an inflection at the base of the dorsal process (1) (Upchurch, 1995).	?	?	?	?	?	?	0	**?**	0
11	Anteroposterior length of the antorbital fossa: greater (0), or less (1), than that of the orbit (Yates, 2003a).	?	?	?	?	?	?	1	1	1
12	Anterior profile of the maxilla: slopes continuously towards the rostral tip (0) or with a strong inflection at the base of the ascending ramus, creating a rostral ramus with parallel dorsal and ventral margins (1) (Sereno et al., 1996; referring to variation within theropods).	?	?	1	?	?	1	1	1	1
13	Length of rostral ramus of the maxilla: less than (0), or greater than (1), its dorsoventral depth (Sereno et al., 1996; referring to variation within theropods).	?	?	1	?	?	1	1	1	0
14	Size of the neurovascular foramen at the caudal end of the lateral maxillary row: not larger than the others (0) or distinctly larger than the others in the row (1) (Yates, 2003a).	?	?	1	?	?	1	1	1	1
15	Direction that the neurovascular foramen at the caudal end of the lateral maxillary row opens: rostrally, ventrally, laterally (0) or caudally (1) (modified from Sereno, 1999).	?	?	1	?	?	1	1	1	1
16	Arrangement of lateral maxillary neurovascular foramina: linear (0) or irregular (1) (modified from Sereno, 1999).	?	?	0	?	?	0	?	0	0
17	Shape of the rostral margin of the antorbital fenestra: strongly concave, roughly parallel to the rostral margin of the antorbital fossa, creating a narrow antorbital fossa (0) or straight to gently concave creating a broad, subtriangular antorbital fossa (1) (Galton, 1985b)	?	?	0	?	?	0	0	**?**	0

18	Dorsally open neurovascular canal on the floor of the antorbital fossa: absent (0) or present (1) (Yates, 2003a).	?	?	1	?	?	1	1	?	1
19	Nasal contribution to the margin of the antorbital fenestra: absent (0) or present (1) (modified from Sereno, 1999).	?	?	?	?	?	?	?	0	1
20	Pointed caudolateral process of the nasal overlapping the lacrimal: absent (0) or present (1) (Sereno, 1999).	?	?	?	?	?	?	?	0	0
21	Dorsal exposure of the lacrimal: present (0) or absent (1) (Gauthier, 1986).	?	?	?	?	?	?	?	0	0
22	Length of the rostral ramus of the lacrimal: greater than (0), or less than (1), half the length of the ventral ramus (modified from Galton, 1990).	?	?	0	?	?	0	?	1	1
23	Extension of the antorbital fossa onto the ventral end of the lacrimal: present (0) or absent (1) (modified from Wilson and Sereno, 1998).	?	?	?	?	?	?	?	0	0
24	Length of the caudal process of the prefrontal: short (0), or elongated (1), so that total prefrontal length is equal to the rostrocaudal diameter of the orbit (Galton, 1985a).	?	?	?	?	?	?	1	1	1
25	Jugal contribution to the antorbital fenestra: absent (0) or present (1) (Holtz, 1994).	?	?	?	?	?	?	1	0	(01)
26	Shape of the anterior end of the jugal: blunt (0) or sharply tapered (1) (Rauhut, 2000).	?	?	?	?	?	?	1	1	1
27	Ratio of the minimum depth of the jugal below the orbit to the distance between the rostral end of the jugal and the rostroventral corner of the lower temporal fenestra: less than (0), or greater than (1), 0.2 (modified from Galton, 1985a).	?	?	?	?	?	?	1	1	1
28	Transverse width of the ventral ramus of the postorbital: less than (0), or greater than (1), its rostrocaudal width at mid shaft (Wilson and Sereno, 1998).	?	?	0	?	?	0	1	0	0
29	Position of the rostral margin of the lower temporal fenestra: behind the orbit (0), extends under the rear half of the orbit (1) or extends as far forward as the midlength of the orbit (2) (modified from Upchurch, 1995). Ordered.	?	?	?	?	?	?	?	1	1
30	Frontal contribution to the supratemporal fenestra: present (0) or absent (1) (modified from Gauthier, 1986).	?	?	?	?	?	?	0	0	0
31	Orientation of the long axis of the supratemporal fenestra: longitudinal (0) or transverse (1) (Wilson and Sereno, 1998).	?	?	?	?	?	?	0	0	0
32	Length of the quadratojugal ramus of the squamosal relative to the width at its base: less than (0) or greater than (1) four times its width (Sereno, 1999).	?	?	?	?	?	?	1	1	1
33	Squamosal-quadratojugal contact: present (0) or absent (1) (Gauthier, 1986).	?	?	?	?	?	?	?	0	0
34	Angle of divergence between jugal and squamosal rami of quadratojugal: close to 90° (0) or close to parallel (1).	?	?	?	?	?	?	?	1	0
35	Length of jugal ramus of quadratojugal: no longer than (0), or longer than (1), the squamosal ramus (Wilson and Sereno, 1998).	?	?	?	?	?	?	?	0	1
36	Shape of the rostral end of the jugal ramus of the quadratojugal: tapered (0) or dorsoventrally expanded (1) (Wilson and Sereno, 1998).	?	?	?	?	?	?	?	0	0
37	Rounded, heel-like caudoventral process of the quadratojugal: absent (0) or present (1).	?	?	?	?	?	?	?	0	0
38	Position of the quadrate foramen: on the quadrate-quadratojugal suture (0) or deeply incised into, and partly encircled by, the quadrate (1) (Rauhut, 2000).	?	?	?	?	?	?	?	?	1
39	Proportion of the length of the quadrate that is occupied by the *rostromedial lamina* (pterygoid wing): at least 70% (0) or greater than 70% (1) (Yates, 2003a).	?	?	1	?	?	1	?	?	1
40	Shape of jugal process of ectopterygoid: gently curved (0) or strongly recurved and hook-like (1) (Yates, 2003a).	?	?	?	?	?	?	0	1	0
41	Pneumatic fossa on the ventral surface of the ectopterygoid: present (0) or absent (1) (Sereno, et al., 1996).	?	?	?	?	?	?	?	1	0
42	Position of the maxillary articular surface of the palatine: along the lateral margin of the bone (0) or at the end of a narrow anterolateral process (1) (Wilson and Sereno, 1998).	?	?	0	?	?	0	?	0	0
43	Medial process of the pterygoid forming a hook around the basipterygoid process: absent (0), flat and blunt-ended (1) or bent upwards and pointed (2) (modified from Wilson and Sereno, 1998). Ordered.	?	?	?	?	?	?	?	1	0
44	Ridge formed along the junction of the parabasisphenoid and the basioccipital, between the basal tuberae: present with a smooth rostral face (0), present with a median fossa on the rostral face (1), or absent with the basal tuberae being separated by a deep caudally open U-shaped fossa (2) Unordered	?	?	?	?	?	?	2	2	1

45	Ossification of the extremity of the basal tuber: complete so that the basioccipital and parabasispenoid form a single rugose tuber (0), or unossified with the basioccipital forming a ventrally facing platform of unfinished bone that abuts a similarly unfinished, caudally facing wall of the parabasisphenoid (1).	?	?	?	?	?	?	1	0	0
46	Shape of basal tuberae: knob-like, with basisphenoidal component rostral to basioccipital component (0), or forming a transverse ridge with the basisphenoidal component lateral to the basioccipital component (1).	?	?	?	?	?	?	1	0	1
47	Dorsoventral depth of the parasphenoid rostrum: much less than (0) or about equal to the transverse width (1) (Yates, 2003a).	?	?	1	?	?	1	1	?	1
48	Deep septum spanning the interbasipterygoid space: absent (0) or present (1) (Galton, 1990).	?	?	?	?	?	?	1	0	0
49	Shape of the floor of the braincase in lateral view: relatively straight with the basal tuberae, basipterygoid processes and parasphenoid rostrum roughly aligned (0), bent with the basipterygoid processes and the parasphenoid rostrum below the level of the basioccipital condyle and the basal tuberae (1), or bent with the basal tuberae lowered below the level of the basioccipital and the parasphenoid rostrum raised above it (2) (modified from Galton 1990). Ordered	?	?	?	?	?	?	0	1	0
50	Length of the basipterygoid processes (from the top of the parasphenoid to the tip of the process): less than (0), or greater than (1), the height of the braincase (from the top of the parasphenoid to the top of the supraoccipital) (Benton et al., 2000).	?	?	?	?	?	?	1	0	0
51	Location of the posttemporal fenestra: between the parietal, the supraoccipital and the exoccipital-opisthotic complex (0) or fully enclosed by the suproccipital (1) (Yates, 2003a).	?	?	?	?	?	?	0	0	1
52	Fontanelle between the supraoccipital and the parietals: absent (0) or present (1).	?	?	?	?	?	?	1	?	1
53	Shape of the supraoccipital: diamond-shaped, at least as high as wide (0), or semilunate and wider than high (1) (Yates, 2003b).	?	?	?	?	?	?	1	0	0
54	Position of jaw joint: no lower than the level of the dorsal margin of the dentary (0) or depressed well below this level (1) (Sereno, 1999).	?	?	1	?	?	1	1	1	1
55	Shape of upper jaws in ventral view: narrow with an acute rostral apex (0) or broad and U-shaped (1) (Wilson and Sereno, 1998).	?	?	?	?	?	?	0	?	0
56	Caudal end of dentary tooth row medially inset with a thick lateral ridge on the dentary forming a buccal emargination: absent (0) or present (1) (Gauthier, 1986).	?	?	1	?	?	1	1	1	1
57	Orientation of the symphyseal end of the dentary: in line with the long axis of the dentary (0) or strongly curved ventrally (1) (Sereno, 1999).	?	?	1	?	?	1	?	?	1
58	Position of first dentary tooth: adjacent to symphysis (0) or inset one tooth's width from the symphysis (1) (Sereno, 1999).	?	?	1	?	?	1	0	?	1
59	Height: length ratio of the dentary: less than (0), or greater than (1), 0.2 (modified from Benton et al., 2000).	?	?	0	?	?	0	0	?	0
60	Dorsoventral expansion at the symphyseal end of the dentary: absent (0) or present (1) (Wilson and Sereno, 1998).	?	?	0	?	?	0	0	?	0
61	A stout, triangular, medial process of the articular, behind the glenoid: absent (0) or present (1) (Yates, 2003a).	?	?	?	?	?	?	1	1	1
62	Length of the retroarticular process: less than (0), or greater than (1), than the depth of the mandible below the glenoid (Yates, 2003a).	?	?	1	?	?	1	0	1	1
63	Strong medial embayment behind glenoid of the articular in dorsal view: absent (0), or present (1).	?	?	1	?	?	1	0	0	1
64	Orientation of the maxillary tooth crowns: erect (0) or procumbent (1) (modified Gauthier, 1986).	?	?	0	?	?	0	0	0	0
65	Orientation of the dentary tooth crowns: erect (0) or procumbent (1) (modified Gauthier, 1986).	?	?	0	?	?	0	0	?	0
66	Number of dentary teeth (in adults): less than 18 (0), 18 or more (1) (modified from Wilson and Sereno, 1998).	?	?	1	?	?	1	0	?	1
67	Teeth with basally constricted crowns: absent (0) or present (1) (Gauthier, 1986).	?	?	1	?	?	1	1	1	1
68	Tooth – tooth occlusion: absent (0) or present (1) (Wilson and Sereno, 1998).	?	?	0	?	?	0	0	0	0
69	Mesial and distal serrations of the teeth: fine and set at right angles to the margin of the tooth (0) or coarse and angled upwards at an angle of 45° to the margin of the tooth (1) (Benton et al., 2000).	?	?	1	?	?	1	1	1	1
70	Long axis of the tooth crowns distally recurved: present (0) or absent (1) (Gauthier, 1986).	?	?	1	?	?	1	1	1	1
71	Texture of the enamel surface: smooth (0) or finely wrinkled (1) (Wilson and Sereno, 1998).	?	?	1	?	?	1	?	0	0

72	Lingual concavities of the teeth: absent (0) or present (1) (Upchurch, 1995).	?	?	0	?	?	0	?	0	0
73	Longitudinal labial grooves on the teeth: absent (0) or present (1) (Upchurch, 1998).	?	?	0	?	?	0	0	0	0
74	Distribution of the serrations along the mesial and distal carinae of the tooth: extend along most of the length of the crown (0) or are restricted to the upper half of the crown (1) (Yates, 2003a).	?	?	(01)	?	?	(01)	1	?	1
75	Shallow, dorsally facing fossa on the atlantal neurapophysis: absent (0) or present (1).	?	?	?	?	?	?	1	?	1
76	Posterior margin of the axial postzygapophyses: overhang the axial centrum (0) or are flush with the caudal face of the axial centrum (1) (Sereno, 1999).	?	?	0	?	?	0	0	?	?
77	Dorsal excavation of the cervical parapophyses: absent (0) or present (1) (Upchurch, 1998).	?	?	0	?	?	0	?	0	0
78	Strong lateral compression of the cranial cervical vertebrae: absent (0) or present (1) (Upchurch, 1998).	?	?	?	?	?	?	?	0	0
79	Number of cervical vertebrae: 9 to 10 (0), 12-13 (1) or more than 13 (2) (Wilson and Sereno, 1998). Ordered.	?	?	0	?	?	0	0	0	0
80	Length of the centrum of the third cervical vertebra: less than (0), or more than (1), 2.5 times the height of its cranial face (modified from Sereno, 1999).	?	?	1	?	?	1	?	1	1
81	Ventral keels on cranial cervical centra: present (0) or absent (1) (modified from Upchurch, 1998).	?	?	0	?	0	0	0	0	0
82	Lamination of the cervical neural arches 4 to 8: well developed with a diapophyseal-postzygapophyseal lamina (0) or weakly developed with no diapophyseal-postzygapophyseal lamina (1) (Yates, 2003a).	?	?	1	?	1	1	1	1	1
83	Short cranially projected pedicels bearing axial prezygapophyses: absent (0) or present (1) (Sereno, 1999).	?	?	?	?	?	?	0	?	0
84	Epipophyses overhanging the rear margin of the postzygapophyses: absent (0), or present (1), in at least some postaxial cervical vertebrae (Sereno and Novas, 1993).	?	?	1	?	?	1	1	?	1
85	Caudal ends of cranial, postaxial epipophyses: with a free pointed tip (0) or joined to the postzygapophysis along their entire length (1).	?	?	0	?	?	0	0	?	0
86	Cervical centra: amphicoelous (0) or opisthocoelous (1) (Gauthier, 1986).	?	0	0	?	0	0	?	0	0
87	Lateral expanded tables at the midlength of the dorsal surface of the neural spines: absent in all vertebrae (0), present on the pectoral vertebrae (1) or present on the pectoral and cervical vertebrae (2). Ordered	?	?	2	?	?	2	0	?	2
88	Dorsoventral height of the hyposphenes: much less than (0), or equal to (1), the dorsoventral height of the neural canal.	?	?	0	?	?	0	0	0	0
89	Height of the dorsal neural spines: greater than (0), or less than (1), 1.5 times the length of the base of the spine (modified from Bonaparte, 1986).	1	?	1	?	?	1	1	1	1
90	Lateral surfaces of the dorsal centra: with at most a vague, shallow depressions (0), with deep fossae that approach the midline (1) or with invasive, sharp-rimmed pleurocoels (2) (Gauthier, 1986). Ordered	?	0	0	?	0	0	0	0	0
91	Diapo-prezygapophyseal lamina and associated anterior triangular fossa (chonos): present on all dorsals (0) or absent in mid dorsals (1) (Yates, 2003a).	?	?	1	?	?	1	1	1	1
92	Cross sectional shape of dorsal neural spines: narrow and elliptical (0) or broad and triangular (1) (Bonaparte, 1986).	?	?	0	?	?	0	0	0	0
93	Composite lateral spinal laminae on dorsal neural spines: absent (0) or present (1) (Wilson and Sereno, 1998).	?	?	0	?	?	0	0	0	0
94	Dorsal centra: entirely amphicoelous to amphiplatyan (0) first two dorsals are opisthocoelous (1), or cranial half of dorsal column is opisthocoelous (2) (Wilson and Sereno, 1998). Ordered.	?	?	0	?	?	0	?	0	0
95	Excavations of the cranial face of the dorsal neural arches, surrounding the neural canal; absent (0) or present (1).	?	?	0	?	?	0	?	0	0
96	Well developed suprapostzygapophyseal laminae: absent (0), present on the caudal dorsal vertebrae (1), present on all dorsal vertebrae (2). (Yates and Kitching 2003)	?	?	1	?	?	1	0	0	0
97	Supradiapophyseal laminae on dorsal vertebrae: absent (0) or present (1).	?	?	0	?	?	0	0	0	0
98	Accessory infrapostzygapophyseal lamina in dorsal vertebrae: present (0) or absent (1).	?	?	1	?	?	1	?	?	1
99	Last presacral rib: free (0) or fused to vertebra (1).	?	1	1	?	1	1	?	0	1
100	Caudosacral vertebra: absent (0) or present (1) (Galton and Upchurch, in press)	?	1	1	?	?	1	0	0	0

101	Number of dorsosacral vertebrae: none (0), one (1) or two (2) (modified Gauthier, 1986).	?	1	1	?	1	1	1	1	1
102	Strong constriction between the sacral rib and the transverse process of the first primordial sacral rib (and dorso-sacral if present) in dorsal view: absent (0) or present (1).	?	?	1	?	?	1	0	1	1
103	Length of first caudal centrum: less than (0), or greater than (1), its height (Yates, 2003a).	?	0	1	0	?	(01)	?	0	(01)
104	Length of base of the proximal caudal neural spines: less than (0), or greater than (1), half the length of the neural arch (Gauthier, 1986).	?	?	1	?	?	1	?	0	0
105	Position of postzygapophyses in proximal caudal vertebrae: protruding with an interpostzygapophyseal notch visible in dorsal view (0) or placed on either side of the caudal end of the base of the neural spine without any interpostzygapophyseal notch (1) (	?	?	0	?	?	0	?	0	0
106	A hyposphenal ridge on caudal vertebrae: absent (0) or present (1) (Upchurch, 1995).	?	?	?	?	?	?	?	?	0
107	Midcaudal chevrons with a ventral slit: absent (0) or present (1) (Upchurch, 1995).	?	?	?	?	?	?	?	0	0
108	Length of midcaudal centra: greater than (0), or less than (1), twice the height of their anterior faces (Yates, 2003a).	?	?	?	?	?	?	?	1	0
109	Longitudinal ventral sulcus on caudal centra: absent (0) or present (1) (Upchurch, 1995).	?	1	1	?	1	1	?	1	1
110	Length of the longest chevron: is less than (0), or greater than (1), the length of the preceding centrum (Yates, 2003a).	?	1	?	?	1	1	?	1	1
111	Longitudinal ridge on the dorsal surface of the sternal plate: absent (0) or present (1) (Upchurch, 1998).	?	?	0	?	?	0	?	0	?
112	Craniocaudal length of the acromion process of the scapula: less than (0), or greater than (1), one and a half times the minimum width of the scapula blade (Wilson and Sereno, 1998).	?	?	?	?	?	?	1	0	0
113	Minimum width of the scapula: is less than (0), or greater than (1), 20% of its length (Gauthier, 1986).	?	?	?	?	?	?	0	0	0
114	Scapula blade in lateral view: with a strap- shaped midsection that has straight, subparallel margins (0) or waisted with curved margins (1) (Sereno et al., 1993).	?	?	1	?	1	1	0	1	0
115	Caudal margin of the acromion process of the scapula: rises from the blade at angle that is less than (0), or greater than (1), 65° from the long axis of the scapula, at its steepest point (modified from Novas, 1992).	?	?	?	?	?	?	(01)	1	(01)
116	Flat caudoventrally facing surface on the coracoid between glenoid and coracoid tubercle: absent (0) or present (1).	1	?	1	?	?	1	?	1	1
117	Coracoid tubercle: present (0) or absent (1) (modified from Pérez-Moreno et al., 1994; referring to variation within theropods).	0	?	0	?	?	0	?	0	0
118	Length of the deltopectoral crest of the humerus: less than (0), or greater than (1), 50% of the length of the humerus (Sereno, 1999).	?	?	1	?	?	1	0	1	1
119	Deltopectoral crest of the humerus: is a tall, sharp-edged crest (0) or is a low, rounded ridge (1) (Wilson and Sereno, 1998).	?	?	0	?	?	0	0	0	0
120	Length of the humerus: less than 55% (0), 55-65% (1), or greater than 65% (2), of the length of the femur (modified from Gauthier, 1986). Ordered.	?	?	?	?	?	?	2	1	1
121	Craniolateral margin of the deltopectoral crest of the humerus: straight (0) or strongly sinuous (1) (Yates, 2003a).	?	?	?	?	?	?	0	1	0
122	Well-defined fossa on the distal flexor surface of the humerus: present (0) or absent (1).	?	?	?	?	0	0	1	0	0
123	Transverse width of the distal humerus: is less than (0), or greater than (1), 33% of the length of the humerus (Langer, 2001).	?	?	?	?	?	?	0	1	1
124	Length of the radius: less than (0), or greater than (1), 80% of the humerus (modified from Langer, 2001)	?	?	?	?	?	?	0	0	0
125	Deep radial fossa on proximal ulna: absent (0) or present (1) (Wilson and Sereno, 1998).	?	?	0	?	?	0	0	0	0
126	Olecranon process on proximal ulna: present (0) or absent (1) (Wilson and Sereno, 1998).	?	?	0	?	?	0	0	0	0
127	Maximum linear dimensions of the ulnare and radiale: exceed that of at least one of the first three distal carpals (0) or are less than any the distal carpals (1) (Yates, 2003a).	?	?	?	?	?	?	?	1	1
128	Transverse width of the first distal carpal: less than (0), or greater than (1), 120% of the transverse width of the second distal carpal (Sereno, 1999).	?	?	?	?	?	?	?	1	1
129	Lateral end of first distal carpal: abuts (0), or overlaps (1), second distal carpal (Yates, 2003a).	?	?	?	?	?	?	?	1	1
130	Proximal end of first metacarpal: flush with other metacarpals (0) or inset into the carpus (1) (Sereno, 1999).	?	?	?	?	?	?	1	1	1

131	Second distal carpal: does (0), or does not (1), completely cover the proximal end of the second metacarpal.	?	?	?	?	?	?	?	1	1
132	Length of the manus: greater than 45% (0), between 45 and 38% (1), or less than 38% (2), of the humerus + radius (modified from Sereno et al., 1993). Ordered	?	?	?	?	?	?	1	1	1
133	Proximal width of first metacarpal: less than (0), or greater than (1), the proximal width of the second metacarpal (modified from Gauthier, 1986).	?	?	?	?	?	?	1	1	1
134	Proximal width of the first metacarpal: less than 65% (0), between 65% and 80% (1), or greater than 80% (2), of its length (modified from Sereno, 1999). Ordered.	?	?	?	?	?	?	1	2	2
135	Strong assymetry in the lateral and medial distal condyles of the first metacarpal: absent (0) or present (1) (Gauthier, 1986).	?	?	?	?	?	?	1	1	1
136	Shape of the fifth metacarpal: longer than wide at the proximal end with a flat proximal surface (0) or close to as wide as it is long with a strongly convex proximal articulation surface (1) (Yates, 2003a).	?	?	?	?	1	1	1	1	1
137	Length of the fifth metacarpal: less than (0), or greater than (1), 75% of the length of the third metacarpal (Upchurch, 1998).	?	?	?	?	0	0	0	0	0
138	Deep distal extensor pits on the second and third metacarpals: present (0) or absent (1) (Novas, 1993).	?	?	?	?	1	1	1	1	1
139	Ventrolateral twisting of the transverse axis of the distal end of the first phalanx of manual digit one relative to its proximal end: absent (0), present but much less than 60° (1) or 60° (2) (Sereno, 1999). Ordered.	?	?	?	?	?	?	2	2	2
140	Length of manual digit one: less than (0), or greater than (1), the length of manual digit two (Yates, 2003a).	?	?	?	?	?	?	0	1	1
141	Length of the ungual of manual digit two: greater than the length of the ungual of manual digit one (0), 75-100% of the ungual of manual digit one (1), less than 75% of the ungual of manual digit one (2) or the ungual of manual digit two is absent (3) (modified from Gautheir 1986). Ordered	?	?	?	?	?	?	2	2	2
142	Shape of non-terminal manual phalanges: longer than wide (0) or as long as wide (1) (Yates, 2003a).	?	?	?	?	0	0	0	1	0
143	Phalangeal formula of manual digits four and five: greater than (0), or less than (1), 2-0, respectively (Gauthier, 1986).	?	?	?	?	?	?	1	1	1
144	Strongly convex dorsal margin of the ilium: absent (0) or present (1) (Gauthier, 1986).	?	0	0	?	0	0	0	0	0
145	Cranial extent of preacetabular process of ilium: does not (0), or does (1), project further forward than cranial end of the pubic peduncle (Yates, 2003a).	?	0	0	?	0	0	(01)	0	0
146	Buttress between preacetabular process and the supra-acetabular crest of the ilum: present (0) or absent (1) (Yates, 2003a).	?	1	1	?	1	1	1	1	1
147	Shape of the preacetabular process: blunt and rectangular (0) or with a pointed, projecting cranioventral corner and a rounded dorsum (1) (modified from Sereno, 1999).	?	1	1	?	1	1	1	1	1
148	Length of the postacetabular process of the ilium: greater than (0), or less than (1), 30% of the total length of the ilium. NOTE: how do you define extent of processes on ilium?	?	0	0	?	0	0	0	0	0
149	Depth of the preacetabular process of the ilium: much less than (0), or subequal to (1), the depth of the ilium above the acetabulum (modified from Gauthier, 1986).	?	0	0	?	0	0	0	0	0
150	Length of preacetabular process of the ilium: less than (0), or greater than (1), twice its depth.	?	0	0	?	0	0	1	0	0
151	Medial bony wall of the acetabulum: at least partially present (0) or absent (1) (Gauthier, 1986).	?	1	1	?	1	1	1	1	1
152	Well developed brevis fossa with sharp margins on the ventral surface of the postacetabular process of the ilium: absent (0) or present (1) (Gauthier, 1986).	?	1	1	1	?	1	0	0	0
153	Length of the pubic peduncle of the ilium: less than (0), or greater than (1), twice the craniocaudal width of its distal end (Sereno, 1999).	?	1	1	?	1	1	1	1	1
154	Caudally projecting 'heel' at the distal end of the ischial peduncle: absent (0) or present (1) (Yates, 2003b).	?	?	0	?	?	0	0	0	0
155	Length of the ischial peduncle of the ilium: similar to (0), or much shorter than (1), the pubic peduncle (Wilson and Sereno, 1998).	?	0	0	?	?	0	0	0	0
156	Shape of the caudal margin of the postacetabular process of the ilium: rounded to bluntly pointed (0), square ended (1) or with a pointed ventral corner and a rounded caudodorsal margin (2) (Yates, 2003b). Unordered	?	2	1	1	?	(12)	?	2	0

157	Notch separating caudoventral end of the ischial obturator plate from the ischial shaft: present (0) or absent (1) (Rauhut, 2000; referring to variation within theropods).	1	?	1	?	?	1	1	1	1
158	Elongate interischial fenestra: absent (0) or present (1) (Yates, 2003b).	1	?	?	?	1	1	1	1	1
159	Length of ischium: less than (0) or greater than (1) that of the pubis (Salgado et al., 1997).	?	0	0	?	?	0	?	0	0
160	Shape of the transverse section of the ischial shaft: ovoid to subrectangular (0) or triangular (1) (Sereno, 1999).	?	1	1	?	1	1	0	1	1
161	Orientation of the long axes of the transverse section of the distal ischia: meet at an angle (0) or are colinear (1) (Wilson and Sereno, 1998).	0	0	0	?	0	0	1	0	0
162	Depth of the transverse section of the ischial shaft: at least as great as (0), or much less than (1), the transverse width of the section (Wilson and Sereno, 1998).	?	1	1	?	1	1	1	0	0
163	Transverse width of the conjoined distal ischial expansions: greater than (0), or less than (1), their sagittal depth (Yates, 2003a).	0	0	0	?	0	0	0	0	1
164	Pubic tubercle on the lateral surface of the proximal pubis: present (0) or absent (1) (Yates, 2003a).	?	?	?	?	?	?	1	1	1
165	Width of the conjoined pubes: less than (0), or greater than (1), 75% of their length (Cooper, 1984).	?	0	0	?	?	0	0	0	0
166	Lateral margins of the pubic apron in cranial view: straight (0) or concave (1).	?	1	1	?	?	1	0	1	1
167	Orientation of the pubic blades: transverse (0) or twisted posteromedially (1) (Wilson and Sereno, 1998).	?	0	0	?	?	0	0	0	0
168	Minimum transverse width of the pubic apron: much more than (0), or less than (1), 40% of the width across the iliac peduncles of the ilium.	?	0	0	?	?	0	1	0	0
169	Craniocaudal length of the distal pubic expansion: less than (0), or greater than (1) 15% of the length of the pubis (modified Gauthier, 1986; referring to variation within theropods).	?	1	1	?	?	1	0	1	1
170	Length of the hindlimb: greater than (0), or less than (1), the length of the trunk (Gauthier, 1986).	?	?	?	?	?	?	1	1	1
171	Longitudinal axis of the femur in lateral view: strongly bent with an offset between the proximal and distal axes greater than 15° (0), weakly bent with an offset of less than 10° (1) or straight (2) (Cooper, 1984). Ordered.	?	?	?	?	?	?	0	0	0
172	Shape of the cross section of the midshaft of the femur: subcircular (0) or strongly elliptical with the long axis oriented mediolaterally (1) (Wilson and Sereno, 1998).	?	0	?	?	0	0	0	0	0
173	Height of the fourth trochanter: tall crest (0) or a low rugose ridge (1) (Gauthier, 1986).	?	0	0	?	0	0	0	0	0
174	Shape of the lesser trochanter: small rounded tubercle (0), elongate ridge that is oriented dorsoventrally (1) or absent (2) (modified from Gauthier, 1986). Unordered	?	1	1	?	?	1	1	1	1
175	Angle between the long axis of the femoral head and the transverse axis of the distal femur: about 30° (0) or close to 0° (1) (Carrano, 2000).	?	?	?	?	?	?	1	1	1
176	Shelf-like ridge associated with lesser trochanter: present (0) or absent (1) (Rowe and Gauthier, 1990).	?	1	1	?	1	1	1	1	1
177	Position of the fourth trochanter along the length of the femur: in the proximal half (0) or straddling the midpoint (1) (Galton, 1990).	?	0	0	?	0	0	0	0	0
178	Profile of the fourth trochanter of the femur: rounded and symmetrical (0) or asymmetrical with a steeper distal slope than the proximal slope and a distinct distal corner (1) (Langer, 2001).	?	1	1	?	1	1	(01)	1	1
179	Postion of fourth trochanter along the mediolateral axis of the femur: centrally located (0) on the medial margin (1) (Galton, 1990).	?	0	0	?	0	0	1	0	0
180	Tibia : femur length ratio: greater than 1.0 (0), between 1.0 and 0.6 (1) or less than 0.6 (2) (modified from Gauthier, 1986). Ordered.	?	?	1	?	1	1	1	1	1
181	Extensor depression on the distal femur: absent (0) or present (1) (Molnar et al., 1990; referring to variation within theropods).	1	?	?	?	1	1	1	1	1
182	Lateral margin of descending caudoventral process of the distal tibia: protrudes laterally at least as far as (0), or set well back from (1), the craniolateral corner of the distal tibia.	?	0	0	?	0	0	1	0	0
183	Transverse width of the distal tibia: subequal to (0), or greater than (1), its craniocaudal length (Gauthier, 1986).	?	1	1	?	1	1	1	1	1
184	A triangular rugose area on the medial side of the fibula: absent (0) or present (1).	0	0	?	?	?	0	?	0	0
185	Ossified distal tarsals: present (0) or absent (1) (Gauthier, 1986).	?	0	0	?	0	0	0	0	0

186	Depth of the medial end of the astragalar body in cranial view: roughly equal to the lateral end (0) or much shallower creating a wedge shaped astragalar body (Wilson and Sereno, 1998). NOTE: check wording	?	0	0	?	0	0	0	0	0
187	Shape of the caudomedial margin of the astragalus in dorsal view: forming a moderately sharp corner of a subrectangular astragalus (0) or evenly rounded with formation of a caudomedial corner (1) (Wilson and Sereno, 1998).	?	0	0	?	0	0	0	0	0
188	Dorsally facing horizontal shelf forming part of the fibular facet of the astragalus: present (0) or absent with a largely vertical fibular facet (1) (Sereno, 1999).	?	1	1	?	1	1	?	1	1
189	Vascular foramina set in a fossa at the base of the ascending process of the astragalus: present (0) or absent (1) (Wilson and Sereno, 1998).	?	0	0	?	0	0	?	?	0
190	A lateral horizontal groove on the calcaneum: absent (0) or present (1).	?	?	?	?	1	1	0	1	1
191	Mediolateral width of the calcaneum: greater than (0), or less than (1), 30% of the mediolateral width of the astragalus.	?	?	?	?	0	0	1	0	0
192	Length of the third metatarsal: greater than (0), or less than (1), 40% of the length of the tibia (Gauthier, 1986).	?	0	0	?	0	0	0	0	0
193	Proximal width of the first metatarsal: is less than (0), or at least as great as (1), the proximal width of the second metatarsal (modified from Wilson and Sereno, 1998).	?	0	0	?	0	0	?	0	0
194	Shape of the medial margin of the proximal surface of the second metatarsal: straight (0) or concave (1) (modified from Sereno, 1999).	?	1	1	?	1	1	?	1	1
195	Shape of the lateral margin of the proximal surface of the second metatarsal: straight (0) or concave (1) (modified from Sereno, 1999).	?	1	?	?	1	1	?	1	1
196	Transverse width of the proximal end of the fourth metatarsal: less than (0), or at least (1), twice the craniocaudal depth of the proximal end (modified from Sereno, 1999).	?	1	1	?	1	1	?	1	1
197	Transverse width of the proximal end of the fifth metatarsal: less than 25% (0), between 30 and 49 % (1), or greater than 50% (2), of the length of the fifth metatarsal (modified from Sereno, 1999). Ordered	1	2	2	?	2	2	1	2	2
198	Length of the ungual of pedal digit two: greater than (0), between 100% and 90% (1), or less than 90% (2), of the length of the ungual of pedal digit one (modified from Gauthier, 1986). Ordered.	?	?	?	?	?	?	1	2	2
199	Length of the first phalanx of pedal digit one: greater than (0), or less than (1) the length of the ungual of pedal digit one.	?	?	?	?	1	1	1	1	1
200	Minimum shaft diameters of third and fourth metatarsals: greater than (0), or less than (1), 60% of the minimum shaft diameter of the second metatarsal (Wilson and Sereno, 1998).	?	0	0	?	0	0	0	0	0
201	Shape of the ungual of pedal digit one: shallow, pointed, with convex sides and a broad ventral surface (0), or deep, abruptly tapering, with flattened sides and a narrow ventral surface (1) (Wilson and Sereno, 1998).	?	?	?	?	0	0	0	0	0
202	Size of the ungual of pedal digit three: greater than (0), or less than (1), 85% of the ungual of pedal digit two in all linear dimensions (Yates, 2003a).	?	?	?	?	?	?	0	1	1
203	Number of phalanges in pedal digit four: four (0) or fewer than four (1) (Gauthier, 1986).	?	?	?	?	0	0	0	0	0
204	Phalanges of pedal digit five: absent (0) or present (1) (modified Gauthier, 1986).	?	1	1	?	1	1	0	1	1
205	Pedal digit five: reduced, non-weight bearing (0), or large (fifth metatarsal at least 70% of fourth metatarsal), robust and weight bearing (1) (Wilson and Sereno, 1998).	?	0	0	?	0	0	0	0	0

Appendix 2- Stomach Stones and Canada's Oldest Dinosaurs

Manuscript Won the Nova Scotia Institute of Science
Graduate Student Writing Competition - 2006

Abstract

A dinosaur skeleton and associated gastroliths discovered in 1986 at Wasson Bluff, Nova Scotia (Lower Jurassic, McCoy Brook Formation) is re-examined and formally described for the first time. Contrary to previous reports, a partial sphenodontian dentary cannot be confidently demonstrated to have been included in the stomach contents of the dinosaur. Furthermore, two newly exposed sacral vertebrae suggest the skeleton cannot be referred to any currently known prosauropod dinosaur. It also differs from the other dinosaurs recently collected from the McCoy Brook Formation. Based on this new information, the specimen does not represent evidence for omnivory among prosauropod dinosaurs. The specimens from the McCoy Brook Formation represent the oldest known dinosaur skeletons in Canada, and the detailed study of these specimens provides important information about taxa that survived the dramatic mass extinction event that occurred at the Triassic-Jurassic boundary.

Introduction

Gastroliths (stomach stones) are commonly found in the stomachs of many extant terrestrial vertebrates, including crocodilians (Platt *et al.* 2002), birds, and marine mammals (Alonso *et al.* 2000). It is thought gastroliths aid in digestion, acting as an internal grind mill to process food within the stomach, or to counteract buoyancy of semi-aquatic vertebrates (Taylor 1993). It is often proposed that dinosaurs possessing simple shearing teeth that were incapable of oral processing (chewing) of food, used gastroliths to process plant matter (Upchurch et al. 2004). Alternatively, several recent studies have demonstrated that it remains difficult to confirm stones associated with dinosaur skeletons were true gastroliths found in the stomach prior to death (Lucas 2000, Wings

2005). The discovery of gastroliths in association with a dinosaur specimen collected in the Lower Jurassic sandstones of Nova Scotia provides the opportunity to further consider the challenges of studying these ancient digestive aids.

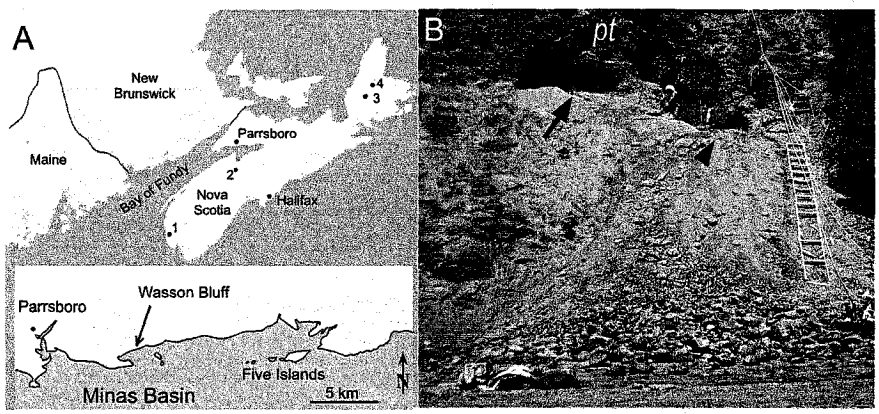

Figure 1: Location of Lower Jurassic site where a dinosaur skeleton and associated gastroliths were discovered at Wasson Bluff, along the northern shore of the Minas Basin, near Parrsboro, Nova Scotia. A – Several potential source rocks for the quartzite gastroliths include the Chegoggin Point deposit (1), the White Rock deposit (2), the Sky Mountain deposit (3) and the Hunters Mountain deposit (4). B – The skeleton and gastroliths were recovered from a quarry (arrow) excavated by a team from Harvard, while other small bone fragments were recovered from a second quarry (arrowhead) opened by the NSMNH one month later. Both quarries likely represent the same bedding plane, being located at the top of deposit of eolian sands, capped by large boulders representing palaeo-talus (pt). Note person in NSMNH quarry for scale.

The Triassic and Jurassic strata exposed along shoreline cliffs of the Minas Basin (Bay of Fundy) in Nova Scotia preserve rare vertebrate fossils from an important transition period of the Mesozoic Period. The Triassic-Jurassic boundary and a recently recognized iridium anomaly (Tanner and Kyte 2005) are located within sandstone strata approximately 30 cm below the lowest exposure of the North Mountain Basalt (Olsen *et al.* 2005). The Triassic-Jurassic boundary represents a period of dramatic mass extinction with a combined marine and terrestrial family extinction rate estimated at over 30% (Benton 1995).

The Lower Jurassic McCoy Brook Formation directly overlies the North Mountain Basalt Formation. The sedimentary deposits at the base of the McCoy Brook Formation, located at Wasson Bluff, near Parrsboro, Nova Scotia (Figure 1A) are estimated to have been deposited only 100,000 - 200,000 years after the Triassic-Jurassic boundary and mass extinction event (Olsen and Gore 1989). The vertebrate fossil record

of Wasson Bluff is therefore especially important due to its representation of vertebrate taxa that survived the Triassic-Jurassic mass extinction event.

Paul Olsen and others found the first dinosaur skeletons from Wasson Bluff in 1976. As the sediments at Wasson Bluff are dated at 200 million years old, the skeletons from this site represent the oldest dinosaurs in Canada. Based on an elongate cervical vertebra and a proximal femur fragment, these specimens were initially identified as c.f. *Ammosaurus* (Olsen et al. 1987).

The sauropodomorph dinosaur *Ammosaurus* was first discovered in Connecticut in the late 1800's in the fluvial sandstones of the Portland Formation, which is now recognized as nearly contemporary in age to the McCoy Brook Formation (Olsen and Gore 1989). Sauropodomorph dinosaurs include the gigantic long-necked sauropods such as *Apatosaurus* and *Diplodocus*, as well as the earlier and smaller taxa such as *Plateosaurus*, *Massospondylus,* and *Ammosaurus*. Often these earlier taxa are referred to as prosauropods, although there remains disagreement as to whether these taxa represent a true monophyletic group (Upchurch et al. 2004).

In 1986, additional fragmentary dinosaur bones with associated gastroliths were recovered from deposits that represent the base of an ancient cliff (Figure 1B), located at "Site N" of Olsen and Gore (1989). While this specimen was never described in detail, it was also attributed to c.f. *Ammosaurus* (Olsen and Gore 1989). Most recently, excavations from 1997-2005 have resulted in the identification of a rich bone bed containing at least five articulated dinosaur skeletons. They demonstrate that many of the Wasson Bluff specimens are not referable to c.f. *Ammosaurus*, but rather represent a new taxon (Fedak 2004). The description of the new taxon is considered elsewhere. However, the gastrolith specimen collected in 1986 is described here in some detail because of its inclusion in two recent studies (Barrett 2000, Whittle and Onorato 2000) related to sauropodomorph diet and ecology.

Whittle and Onorato (2000) included samples of the Wasson Bluff gastroliths in their scanning electron microscopy analyses that attempted to identify true fossil gastroliths by characterizing the number of pits, rilles, and surface smoothness. A second study (Barrett 2000) suggested the Wasson Bluff gastroliths provided evidence that basal sauropodomorphs (prosauropods) were at least opportunistically omnivorous. A partial

mandible of a sphenodontian lizard was reportedly associated with the gastroliths and used to suggest the lizard fragment had been in the stomach along with the gastroliths. The rare occurrence of authentic gastroliths with sauropodomorph skeletons and use of the Nova Scotia gastroliths in other important studies provides the current interest for the re-examination of the gastrolith specimen and associated skeletal material.

Specimen Description

Prior to the start of this study the location of the gastrolith specimen was unknown, however during a visit to the collections of the Nova Scotia Museum of Natural History (NSMNH), I located the specimen within a temporary specimen storage cabinet. Based on labels with the specimen and recent communications with the collectors, the material was excavated by Neil Shubin, Dan E. Lieberman (DEL) and others from Harvard University in July and August 1986.

Numerous fragments of matrix and bone were located with the specimen at the NSMNH, as well as separately within the collections of the Fundy Geological Museum (FGM). Field labels for these fragments included information such as "07/10/86 #1", "DEL gastrolith", "8/1 4xW.F. near dino", "Float East End Pro. b locality 8/1/86" and "DEL/FF 4-5 8/26". The inclusion of fragments marked as "float", as well as the range of collection dates suggests all of the material is not necessarily directly associated with the gastroliths and skeleton. The material that could be directly attached and thus confidently assignable to the specimen has been recently catalogued as museum number NSM005GF9.1. Additionally, two blocks that contain faulted and crushed dinosaur bones in the collection of the Fundy Geological Museum (catalogued as FGM000GF46) also represent elements from the same skeleton.

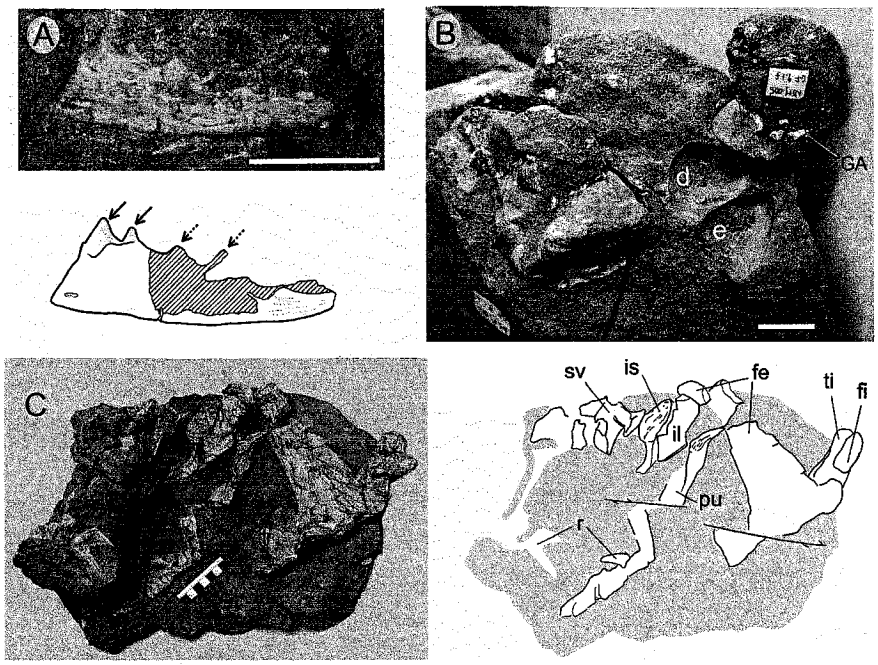

Figure 2: Fossil bones and stones recovered from the Harvard quarry in 1986. A – the partial sphenodontian dentary reported as found near the gastroliths exhibits two complete teeth (solid arrows) and two partial teeth (dashed arrows). B – the gastrolith clasts (NSM005GF9.1) still preserved within the sandstone matrix. The gastroliths analyzed by Whittle and Onorato (2000) were located at (d and e), and two gastralia rib fragments (GA) remain in direct association with the gastroliths. Abbreviations: fe – femur, fi – fibula, il – ilium, is = ischium, pu – pubis, r – rib, sv – sacral vertebra, ti - tibia. Scale bars A = 5 mm, B = 10 mm, C = 1 cm increments.

Gastroliths

The gastroliths (Figure 2B) vary in size, shape and source rock. The two samples (GF9.1 *d* and *e*) examined by Whittle and Onorato (2000) are white crystalline (quartz/quartzite) clasts. However, there are also two flat (2-3 mm) oblong clasts of non-igneous origin as well as several small basalt fragments. The presence of large quartzite clasts within the Wasson Bluff section of the McCoy Brook is extremely unusual; in over 10 years of fieldwork I have never observed similar clasts at the site. There are a total of 10-11 clasts (1 partially exposed in GF9.1*a*, 6-7 in GF9.1*b*, and 3 loose; GF9.1*d-f*) that are clearly associated.

Within the matrix surrounding the gastroliths there are several layers containing numerous small (< 2 cm) basalt clasts. Similar small basalt clasts are also found in the sediments directly under and around the associated skeletal material. The gastroliths can be distinguished from the basalt depositional clasts based on their mineralogy and close

association within the gastralia basket. However, the small basalt clasts demonstrate the sediment entombing the skeleton was heterogeneous. It includes sand and some gravel sized clasts, which is of importance to the reported association of a sphenodontian dentary with the gastroliths.

The quartzite clasts that compose the gastroliths have not been found within any other locations at the McCoy Brook Formation. The identification of the clasts as gastroliths is supported by their tight grouping, direct association with gastralia ribs (see below), as well as a previous study that examined their microsurface characteristics (Whittle and Onorato 2000). Interestingly, there are also several potential sources of Devonian-Silurian aged quartzite deposits (Figure 1A) in close proximity of the Fundy Basin (MacDonald 1988). Thus, the dinosaurs did not require an ecological range of more than 50 km to acquire appropriate clasts identified as gastroliths.

Associated Skeletal Material

The only skeletal samples within the gastrolith block are two small fragments of gastralia and a small portion of a vertebra. Unfortunately, no diagnostic information can be gathered from the vertebral fragment, with only a partial central body and prezygopophyses preserved. Gastralia, fine "ribs" located along the midline of the belly, are pleisiomorphic for archosaurs and occur widely among many theropod and prosauropod dinosaurs, but are not found in sauropod and ornithischian dinosaurs (Claessens 2004).

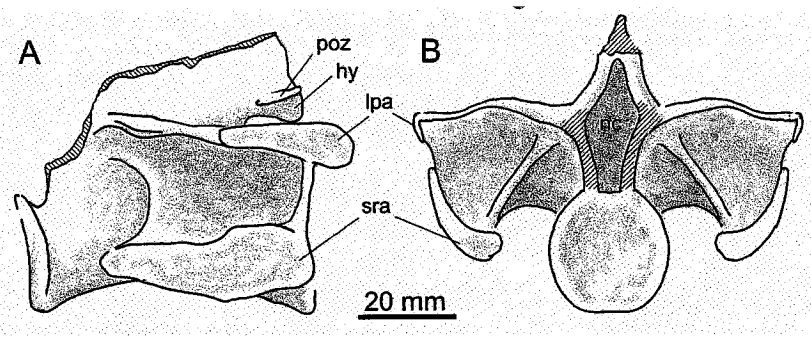

Figure 3: Sacral vertebra of FGM000GF46 in left lateral (A) and anterior (B) views, showing that the sacral rib originates from the posterior end of the centrum. The crosshatched areas represent broken (and missing) bone surfaces, and the missing right lateral process has been reconstructed based on the complete left side. Abbreviations: hy - hyposphene, lpa – lateral process articular surface for ilium, nc – neural canal, poz – postzygapophyses, sra – sacral rib articular surface for ilium.

Fortunately, two other blocks of sandstone (FGM000GF46) associated with the gastroliths contain more complete skeletal elements, although these are badly deformed and crushed. One block contains two or perhaps three vertebrae, which are so badly crushed they are barely recognizable as vertebrae. The second block (Figure 2C) contains more abundant and slightly better preserved material. However, this block was dropped and suffered significant damage and later repaired at the NSMNH in the early 1990s. The specimen has been on display at the Fundy Geological Museum since 1994 but was recently removed from display for this study. Several new skeletal elements were exposed after removing some of the sandstone matrix. Also, upon comparison with archival NSMNH photos of the block prior to its damage, it was evident several of the repaired pieces had been attached incorrectly. Several bags of fragments collected in 1986 were also located at the NSMNH and FGM; unpacking of this material resulting in discovering several fragments that directly attached to broken surfaces of bones in the block.

Based on the new study, the elements within the block (Figure 2C) can now be confidently identified and include a complete left pubis, proximal portion of the right ischium, the pubic peduncle of the left ilium, the head and distal shaft of the left femur, proximal portions of the left tibia and fibula, and two partial sacral vertebrae (Figure 3).

A detailed description and formal consideration of the taxonomic identity of the specimen is beyond the capacity of this paper. However the morphology of the most complete sacral vertebra (Figure 3) is of specific interest to the interpretation of the gastroliths.

The sacral vertebral centrum is elongate, being 60 mm long (ventrally) and 25 mm high anteriorly. The right lateral process, prezygapophyses and neural spine are missing. However, the left lateral process is directed posterolaterally, and a thin vertical lamina of bone connects the posterior edge to the posterior edge of the underlying sacral rib. The distal end of the lateral process exhibits a dorsoventrally short articular surface for the medial surface of the ilium. The sacral rib originates from the posterior half of the centrum and distally expands anteroposteriorly. The distal surface, which also articulated with the medial surface of the ilium, is dorsoventrally tallest posteriorly and directed ventrolaterally (45° to horizontal). The morphology of this sacral vertebra is not typical

for any known sauropodomorph dinosaur or the new dinosaur taxon being described from the Nova Scotia bone bed, as the centrum is elongate and the sacral rib originates from the posterior half of the centrum.

Sphenodontian Dentary

A partial sphenodontian dentary (Figure 2A), reportedly found among the gastralia (Barrett 2000), has been located within the drawer containing the gastroliths. The specimen is preserved with the long axis of the dentary parallel to a finely undulating bedding surface within a small sandstone fragment (approximate dimensions 6 x 6 x 4 cm). The dentary was truncated mesially prior to or during preservation by a straight line (perhaps due to a fault) and is missing sections posteriorly due to damage sometime after the specimen was excavated. Two complete and two partial dentary teeth are preserved, a foramen is adjacent to the truncated edge, and fine longitudinal lines are present on the distal surface.

After considerable effort, the matrix fragment containing the dentary could not be directly attached to any portion of the block containing the gastroliths. Therefore, while there is little reason to doubt the dentary was collected during the same time as the gastroliths, it cannot be reliably demonstrated the dentary fragment was in direct association with the gastroliths.

Disarticulated sphenodontian mandibles are commonly found in the aeolian sandstones at Wasson Bluff (Olsen and Gore 1989). The sandstone blocks containing the gastroliths and the dinosaur skeletal material also include numerous sedimentary layers containing small basalt gravel clasts. These clasts demonstrate the matrix preserving the bones and gastroliths was heterogeneous, and supports a hypothesis offered here that the sphenodontian dentary was loose within the sediment that entombed the gastroliths and associated skeleton. If the entombing matrix had been homogeneous, the dentary being deposited with the matrix during specimen burial would be less likely. The remaining exterior surfaces of the bone and teeth of the dentary are well preserved, with no pits from acid etching that might be expected if present within the stomach.

Conclusions

The block containing the dinosaur gastroliths (NSM005GF9) has been relocated, and is now re-associated with skeletal material collected from the same quarry (FGM000GF46). The recent cleaning and study of the associated skeletal material has resulted in the exposure of important new skeletal elements, including two sacral vertebrae that will be useful for future studies considering the taxonomic status of the specimen. The various elements within the block have also now been identified. Based on the morphology of the sacral vertebra, the skeleton associated with the gastroliths does not appear to represent any currently known sauropodomorph dinosaur, and also differs from the new sauropodomorph taxon recently discovered in the nearby bone bed.

Detailed examination of a sphenodontian dentary was unable to confirm its direct association with the gastroliths. Due to the presence of small gravel clasts around the skeleton, it remains possible that even if the dentary was collected in close proximity to the gastrolith specimen, the dentary fragment may have been mobilized within the sediments that eventually entombed the gastroliths and associated skeleton. Thus there is little evidence to show the dentary was part of the gut contents of the dinosaur, and therefore cannot confidently be used as evidence prosauropod dinosaurs may have been omnivorous.

The specimens from the McCoy Brook Formation represent the oldest dinosaur skeletons in Canada, and the detailed study of these specimens will provide important information about the taxa that survived the dramatic mass extinction event that occurred at the Triassic-Jurassic boundary. The detailed study of the specimen with gastroliths demonstrates that regardless of the fragmentary nature of these specimens, much can be learned.

References

Abler, W. L. 1992. The serrated teeth of tyrannosaurid dinosaurs, and biting structures in other animals. Paleobiology 18(2):161-183.

Abler, W. L. 1997. Tooth serrations in carnivorous dinosaurs. Pp. 740-743. *In* P. J. Currie, and K. Padian, eds. Encyclopedia of Dinosaurs. Academic Press, San Diego.

Allen, D. J. 2003a. Ontogenetic determination of a new specimen confirms *Terrestrisuchus* to be a junior synonym of *Saltoposuchus*. The Palaeontological Association Newsletter 53:72-73.

Allen, D. J. 2003b. When *Terrestrisuchus gracilis* reaches puberty it becomes *Saltoposuchus connectens*. Journal of Vertebrate Paleontology Supplement to 3:29A.

Alonso, M. K., E. A. Crespo, S. N. Pedraza, N. A. Garcia, and M. A. Coscarella. 2000. Food habits of the South American sea lion, *Otaria flavescens*, off Patagonia, Argentina. Fishery Bulletin 98(2):250-263.

Bambach, R. K. 1973. Tectonic deformation of composite-mold fossil bivalvia (Mollusca). American Journal of Science 273A:409-430.

Barrett, P. M. 2000. Prosauropod dinosaurs and iguanas: speculations on the diets of extinct reptiles. Pp. 42-78. *In* H. D. Sues, ed. Evolution of herbivory in terrestrial vertebrates: Perspectives from the fossil record. Cambridge University Press, New York, NY.

Barrett, P. M. 2004. Sauropodomorph dinosaur diversity in the upper Elliot Formation (*Massospondylus* range zone: Lower Jurassic) of South Africa. South African Journal of Science 100:501-503.

Barrett, P. M., P. Upchurch, and Wang Xiao-Lin. 2005. Cranial osteology of *Lufengosaurus huenei* Young (Dinosauria: Prosauropoda) from the Lower Jurassic of Yunnan, People's Republic of China. Journal of Vertebrate Paleontology 25(4):806-822.

Baumel, J. J., and L. M. Witmer. 1993. Osteologia. Pp. 45-132. *In* J. J. Baumel, A. S. King, J. E. Braeazile, H. E. Evans, and J. C. Vanden Berge, eds. Handbook of Avian Anatomy: Nomina Anatomica Avium. The Nuttall Ornithological Club, Cambridge, Massachusetts.

Behrensmeyer, A. K. 1978. Taphonomic and ecological information from bone weathering. Paleobiology 4(2):150-162.

Bellairs, A. d. A., and A. M. Kamal. 1981. The chondrocranium and the development of the skull in recent reptiles. Pp. 1-263. *In* C. Gans, and T. S. Parsons, eds. Biology of the Reptilia, Volume 11, Morphology F. Academic Press, Toronto.

Benton, M. J. 1995. Diversification and extinction in the history of life. Science 268:52-58.

Benton, M. J., L. Juul, G. W. Storrs, and P. M. Galton. 2000. Anatomy and systematics of the prosauropod dinosaur *Thecodontosaurus antiquus* from the Upper Triassic of Southwest England. Journal of Vertebrate Paleontology 20(1):77-108.

Bonaparte, J. F. 1971. Los Tetrápodos del Sector Superioir de la Formación Los Colardos,, La Rioja, Argentina. Opera Lilloana 22:1-183.

Bonaparte, J. F. 1978. *Coloradia brevis* n. g. et n. sp. (Saurischia Prosauropoda), dinosaurio Plateosauridae de la Formacion Los Colorados, Triasico Superior de La Rioja, Argentina. Ameghiniana 15:327-332.

Bonaparte, J. F. 1999. Evolution of the presacral vertebrae of Sauropodomorpha. Ameghiniana 36(2):115-187.

Bonaparte, J. F., and O. Mateus. 1999. A new diplodocid, *Dinheirosaurus lourinhanensis* gen. et sp. nov., from the Late Jurassic beds of Portugal. Revista del Museo Argentino de Ciencias Naturales 5(2):14-29.

Bonaparte, J. F., and M. Vince. 1979. El hallazgo del primer nido de dinosaurios Triasicos, (Saurischia, Prosauropoda), Triasico Superior de Patagonia, Argentina. Ameghiniana 16:173-182.

Bonnan, M. F. 2003. The evolution of manus shape in sauropod dinosaurs: Implications for functional morphology, forelimb orientation, and phylogeny. Journal of Vertebrate Paleontology 23(3):595-613.

Britt, B. B., and B. G. Naylor. 1994. An embryonic *Camarasaurus* (Dinosauria, Sauropoda) from the Upper Jurassic Morrison Formation (Dry Mesa Quarry, Colorado). Pp. 256-264. *In* K. Carpenter, K. F. Hirsch, and J. R. Horner, eds. Dinosaur Eggs and Babies. Cambridge University Press, New York, NY.

Brochu, C. A. 1992. Ontogeny of the postcranium in crocodylomorph archosaurs. M.A. Thesis. University of Texas, Austin, Texas.

Brochu, C. A. 1996. Closure of neurocentral sutures during crocodilian ontogeny: Implications for maturity assessment in fossil archosaurs. Journal of Vertebrate Paleontology 16(1):49-57.

Buffrénil, V. d., and J.-M. Mazin. 1990. Bone histology of the ichthyosaurs: comparative data and functional interpretation. Paleobiology 16:435-447.

Carpenter, K., and J. S. McIntosh. 1994. Upper Jurassic sauropod babies from the Morrison Formation. Pp. 265-278. *In* K. Carpenter, K. F. Hirsch, and J. R. Horner, eds. Dinosaur Eggs. Cambridge University Press, New York.

Carroll, R. L. 1988. Vertebrate Palaeontology and Evolution. W.H . Freeman and Company, New York.

Carroll, R. L., E. S. Belt, D. L. Dineley, D. Baird, and D. C. McGregor. 1972. Excursion A59: Vertebrate Paleontology of Eastern Canada. Pp. 1-113. XXIV International Geological Congress, Fieldtrip Guidebook. Montreal.

Casamiquela, R. M. 1980. La presencia del genero Plateosaurus (Prosauropoda) en el Triasico superior de la Formación El Tranquilo, Patagonia. Actas del Congreso Argentino de Paleontología y Bioestratigrafía 2(143-158).

Castanet, J., S. Croci, F. Aujard, M. Perret, J. Cubo, and E. de Margerie. 2004. Lines of arrested growth in bone and age estimation in a small primate: *Microcebus murinus*. Journal of Zoology 263:31-39.

Chatterjee, S., and Z. Zheng. 2005. Neuroanatomy and dentition of *Camarasaurus lentus*. Pp. 199-211. *In* V. Tidwell, and K. Carpenter, eds. Thunder-Lizards. Indiana University Press, Indianapolis.

Chiappe, L. M., L. Salgado, and R. A. Coria. 2001. Embryonic skulls of Titanosaur sauropod dinosaurs. Science 293:2444-2446.

Chiappe, L. M., J. G. Schmitt, F. Jackson, A. Garrido, L. Dingus, and G. Grellet-Tinner. 2004. Nest structure for sauropods: sedimentary criteria for recognition of dinosaur nesting traces. Palaios 19:89-95.

Chinsamy, A. 1993. Bone histology and growth trajectory of the prosauropod dinosaur *Massospondylus carinatus* Owen. Modern Geology 18: 319-329.

Chinsamy, A., and M. A. Raath. 1992. Preparation of Fossil Bone for Histological Examination. Palaeontologia Africana 29:39-44.

Chinsamy-Turan, A. 2005. The microstructure of dinosaur bone: Deciphering biology with fine-scale techniques. Johns Hopkins University Press, Baltimore, Maryland.

Claessens, L. P. A. 2004. Dinosaur gastralia; origin, morphology, and function. Journal of Vertebrate Paleontology 24:89-106.

Clark, J. M. 1986. Phylogenetic relationships of the Crocodylomorph Archosaurs. Dissertation. University of Chicago, Chicago, Illinois.

Colbert, E. H., and C. C. Mook. 1951. The ancestral crocodilian *Protosuchus*. Bulletin of the American Museum of Natural History 97:147-182.

Coombs, W., Jr. 1990. Dinosaur Paleobiology, Part I: Behavior patterns of dinosaurs. Pp. 32-42. *In* D. B. Weishampel, P. Dodson, and H. Osmólska, eds. Dinosauria. University of California Press, Berkeley.

Cooper, M. R. 1981. The prosauropod dinosaur *Massospondylus carinatus* Owen from Zimbabwe: Its biology, mode of life and phylogenetic significance. Occasional Papers of the National Museums and Monuments of Rhodesia, B, Natural Sciences 6(10):689-840.

Cope, E. D. 1870. Synopsis of the extinct Batrachia, Reptilia and Aves of North America. Transactions of the American Philosophical Society 14:1-252.

Currie, P. J. 2003. Allometric growth in tyrannosaurids (Dinosauria: Theropoda) from the Upper Cretaceous of North America and Asia. Canadian Journal of Earth Sciences 40:651-665.

de Ricqlès, A. 1983. Cyclical growth in the long limb bones of a sauropod dinosaur. Acta Palaeontologica Polonica 28:225-232.

de Ricqlès, A., F. J. Meunier, J. Castanet, and H. Francillon-Vieillot. 1991. Comparative Microstructure of Bone. Pp. 1-78. *In* B. K. Hall, ed. Bone. CRC Press, Boca Raton.

Dilkes, D. 2001. An ontogenetic perspective on locomotion in the Late Cretaceous dinosaur *Maiasaurua peeblesorum* (Ornithischia: Hadrosauridae). Canadian Journal of Earth Sciences 38:1205-1227.

Dodson, P. 1975. Functional and ecological significance of relative growth in *Alligator*. Journal of Zoology 175:315-355.

Durand, J. F. 2001. The oldest juvenile dinosaurs from Africa. Journal of African Earth Sciences 33:597-603.

Engelder, T., and R. Engelder. 1977. Fossil distortion and decollement tectonics of the Appalachian Plateau. Geology 5(8):457-460.

Erickson, G. M., K. Curry Rogers, and S. A. Yerby. 2001. Dinosaurian growth patterns and rapid avian growth rates. Nature 412(6845):429-433.

Fedak, T. J. 2000. Dinosaurs of Nova Scotia, Conservation Problems. P. 32. Society for the Preservation of Natural History Collections, 15th Annual Meeting. Halifax, NS.

Fedak, T. J. 2001. Locating Collection sites and a summary of Dinosaur Specimens from the Early Jurassic McCoy Brook Formation, Nova Scotia. Journal of Vertebrate Paleontology (Abstracts of Papers Supplement) 21(3):49.

Fedak, T. J. 2002. Recent vertebrate fossil discoveries from the (Hettangian) McCoy Brook Formation. Pp. 15-16. Atlantic Geoscience Society Colloquium and Annual General Meeting. Atlantic Geology, Antigonish.

Fedak, T. J. 2003. A new interpretation and description of the *Anchisaurus polyzelus* (Saurischia: Sauropodomorpha) braincase and its implications for prosauropod systematics. Journal of Vertebrate Paleontology 23:49A.

Fedak, T. J. 2004. New information on the Early Jurassic prosauropod dinosaurs of Nova Scotia. Atlantic Geology 40(1):139.

Fedak, T. J. 2005. Two heads are better than one: Considering *Anchisaurus* as a small sauropod. Journal of Vertebrate Paleontology 25(3):56A.

Fedak, T. J. 2006a. A rich bone bed of sauropodomorph dinosaurs in the Early Jurassic (Hettangian) McCoy Brook Formation. Journal of Vertebrate Paleontology 26:60A.

Fedak, T. J. 2006b. Using capillarity for determining and maintaining a polymer consolidant concentration after solution preparation. Collection Forum 20(1-2):108-112.

Fedak, T. J., A. Cole, B. K. Hall, W. Olson, and M. K. Vickaryous. 2003. Sutures joining ontogeny and fossils. Palaeontology Association Newsletter 52:29-32.

Franz-Odendaal, T. 2003. A fresh look at a developmental enamel defect in humans, mutant mice, and fossil giraffes: A contribution to evo devo. Developmental Biology 259(2):452-452.

Franz-Odendaal, T. 2004. Enamel hypoplasia provides insights into early systemic stress in wild and captive giraffes (*Giraffa camelopardalis*). Journal of Zoology 263:197-206.

Fraser, N. C., K. Padian, G. M. Walkden, and A. L. M. Davis. 2002. Basal Dinosauriform Remains from Britain and the Diagnosis of the Dinosauria. Palaeontology 45(1):79-95.

Galton, P. M. 1976. Prosauropod dinosaurs (Reptilia: Saurischia) of North America. Postilla 169:1-98.

Galton, P. M. 1984. Cranial anatomy of the prosauropod dinosaur *Plateosaurus* from the Knollenmergel (Middle Keuper, Upper Triassic) of Germany. I - Two complete skulls from Trossingen/Württ. with comments on the diet. Geologica et Palaeontologica 18:139-172.

Galton, P. M. 1985a. Cranial anatomy of the prosauropod dinosaur *Plateosaurus* from the Knollenmergel (Middle Keuper, Upper Triassic) of Germany. II - All the cranial material and details of soft-part anatomy. Geologica et Palaeontologica 19:119-159.

Galton, P. M. 1985b. Cranial anatomy of the prosauropod dinosaur *Sellosaurus gracilis* from the Middle Stubensandstein (Upper Triassic) of Nordürttemberg, West Germany. Stuttgarter Beiträge zur Naturkunde Serie B 118:1-39.

Galton, P. M. 1985c. Diet of prosauropod dinosaurs from the Late Triassic and Early Jurassic. Lethaia 18:105-123.

Galton, P. M. 1990. Basal Sauropodomorpha-Prosauropoda. Pp. 320-344. *In* D. B. Weishampel, P. Dodson, and H. Osmólska, eds. The Dinosauria. University of California Press, Los Angeles.

Galton, P. M. 1997. Comments on sexual dimorphism in the Prosauropod dinosaur *Plateosaurus engelhardti* (Upper Triassic, Trossingen). Neues Jahrbuch für Geologie und Paläontologie Monatshefte 11:674-682.

Galton, P. M. 1999. Sex, sacra and *Sellosaurus gracilis* (Saurischia, Sauropodomorpha, Upper Triassic, Germany) or why the character two sacral vertebrae is plesiomorphic for Dinosauria. Neues Jahrbuch für Geologie und Paläontologie - Abhandlungen 213:19-53.

Galton, P. M. 2005. Basal sauropodomorph dinosaur taxa *Thecodontosaurus* Riley & Stutchbury, 1836, *T. antiquus* Morris, 1843 and *T. caducus* Yates, 2003: their status re. humeral morphs from the 1834 fissure fill (Upper Triassic) in Clifton, Bristol, UK. Journal of Vertebrate Paleontology 25(Suppl. to Num. 3):61A.

Galton, P. M., and R. T. Bakker. 1985. The cranial anatomy of the prosauropod dinosaur *Efrassia diagnostica*, a juvenile individual of *Sellosaurus gracilis* from the Upper Triassic of Nordwürttemberg, West Germany. Stuttgarter Beiträge zur Naturkunde Serie B 117:1-15.

Galton, P. M., and M. A. Cluver. 1976. *Anchisaurus capensis* (Broom) and a revision of the Anchisauridae (Reptilia, Saurischia). Annals of the South African Museum 69:121-159.

Galton, P. M., and J. V. Heerden. 1998. Anatomy of the prosauropod dinosaur *Blikanasaurus cromptoni* (Upper Triassic, South Africa), with notes on the other tetrapods from the Lower Elliot Formation. Paläontologische Zeitschrift 72:163-177.

Galton, P. M., and P. Upchurch. 2004. Prosauropoda. Pp. 232-258. *In* D. B. Weishampel, P. Dodson, and H. Osmólska, eds. The Dinosauria. Berkeley.

Galton, P. M., J. Van Heerden, and A. M. Yates. 2005. Postcranial anatomy of referred specimens of the sauropodomorph dinosaur *Melanorosaurus* from the Upper Triassic of South Africa. Pp. 1-37. *In* V. Tidwell, and K. Carpenter, eds. Thunder-Lizards. Indiana University Press, Indianapolis.

Gauthier, J. 1986. Saurischian monophyly and the origin of birds. Pp. 1-55. *In* K. Padian, ed. The origin of birds and the evolution of flight. California Academic Society, San Francisco.

Gow, C. E. 1990. Morphology and growth of the *Massospondylus* braincase (Dinosauria Prosauropoda). Palaeontologia Africana 27:59-75.

Gow, C. E., J. W. Kitching, and M. A. Raath. 1990. Skulls of the prosauropod dinosaur *Massospondylus carinatus* Owen in the Collections of the Bernard Price Institute for palaeontological research. Palaeontologia Africana 27:45-58.

Hall, B. K. 1999. Evolutionary Developmental Biology. Klewer Academic Publishers, Boston.

Hitchcock, E. 1858. Ichnology of New England. A report on the sandstone of the Connecticut Valley, especially its fossil footprints. Commonwealth of Massachusetts.

Hitchcock, E., Jr. 1865. A supplement to the ichnology of New England. Wright and Potter, Boston.

Horner, J. R., A. de Ricqles, and K. Padian. 1999a. Variation in dinosaur skeletochronology indicators: implications for age assessment and physiology. Paleobiology 25(3):295-304.

Horner, J. R., K. Padian, A. de Ricqles, and Anonymous. 1999b. Osteohistology of some embryonic and perinatal archosaurs; phylogenetic and behavioral implications for dinosaurs. Journal of Vertebrate Paleontology 19:53.

Hubert, J. F., and K. A. Mertz, Jr. 1984. Eolian sandstones in Upper Triassic-Lower Jurassic red beds of the Fundy Basin, Nova Scotia. Journal of Sedimentary Petrology 54(3):798-810.

von Huene, F. 1906. Über die Dinosaurier der aussereuropäischen Trias. Geologische und Paläontologische Abhandlungen 8:97-156.

von Huene, F. 1914a. Nachträge zu meinen früheren Beschreibungen triassischer Saurischia. Geologische und Paläontologische Abhandlungen 13:69-82.

von Huene, F. 1914b. Saurischia et Ornithischia Triadica ('Dinosauria' Triadica). Pp. 1-21. Fossilium Catalogus. I: (Animalia) Part IV.

von Huene, F. 1926. Vollsändige osteologie eines Plateosauriden aus dem Schwäbischen Keuper. Geologische und Paläontologische Abhandlungen 15:129-179.

von Huene, F. 1932. Die fossile Reptil-Ordnung Saurischia, ihre Entwicklung und Geschichte. Monographien zur Geologie und Paläontologie. Series 1 4:1-361.

Hutchinson, J. R. 2001a. The evolution of femoral osteology and soft tissues on the line to extant birds (Neornithes). Zoological Journal of the Linnean Society 131:169-197.

Hutchinson, J. R. 2001b. The evolution of pelvic osteology and soft tissues on the line to extant birds (Neornithes). Zoological Journal of the Linnean Society 131:123-168.

Hwang, S. H. 2005. Phylogenetic patterns of enamel microstructure in dinosaur teeth. Journal of Morphology 266(2):208-240.

Irmis, R. B. 2005. A review of the vertebrate fauna of the Lower Jurassic Navajo Sandstone in Arizona. Mesa Southwest Museum Bulletin 11:55-71.

Jianu, C.-M., D. B. Weishampel, J. W. M. Jagt, P. H. Lambers, E. W. A. Mulder, and A. S. Schulp. 1999. The smallest of the largest; a new look at possible dwarfing in sauropod dinosaurs. Geologie en Mijnbouw 78:335-343.

Klein, N. F. 2001. Bone histology and its implications for the life history of the prosauropod *Plateosaurus*. Journal of Vertebrate Paleontology 21:68.

Kumbar, S. M., and K. Pancharatna. 2002. Annual Growth Layers in the Phalanages of the Indian skipper frog *Rana cyanophliycits* (Schn.). Copeia 3:870-872.

Langer, M. C. 2001. *Saturnalia tupiniquim* and the early evolution of dinosaurs. dissertation. University of Bristol, Bristol, U.K.

Langer, M. C. 2003. The pelvic and hind limb anatomy of the stem-sauropodomorph *Saturnalia tupiniquim* (Late Triassic, Brazil). Paleobios 23(2):1-30.

Langer, M. C. 2004. Basal Saurischia. Pp. 25-46. *In* D. B. Weishampel, P. Dodson, and H. Osmólska, eds. The Dinosauria. University of California Press, Berkeley.

Langer, M. C., F. Abdala, M. Richter, and M. J. Benton. 1999. A sauropodomorph dinosaur from the Upper Triassic (Carnian) of southern Brazil. C. R. Acad. Sci. (Paris): Sci. de la Terre 329:511-517.

Lehman, T. M., and A. B. Coulson. 2002. A juvenile specimen of the sauropod dinosaur *Alamosaurus sanjuanensis* from the Upper Cretaceous of the Big Bend National Park, Texas. Journal of Paleontology 76(1):156-172.

Lucas, S. G. 2000. The gastromyths of "*Seisomosaurus*", a Late Jurassic dinosaur from New Mexico. New Mexico Museum of Natural History and Science Bulletin 17:61-67.

Lull, R. S. 1912. The life of the Connecticut Triassic. American Journal of Science 4:397-422.

Lull, R. S. 1915. Triassic Life of the Connecticut Valley. Connecticut State Geological and Natural History Survey Bulletin 24:1-285.

Lull, R. S. 1953. Triassic life of the Connecticut Valley[Revised ed.]. Connecticut Geological and Natural History Survey Bulletin 81:1-331.

MacDonald, R. A. 1988. Silica in Nova Scotia : Information Circular 14. No. Information Circular ME 14. Nova Scotia Department of Mines and Energy, Halifax, Nova Scotia.

Maisano, J. A. 2002. Terminal fusions of skeletal elements as indicators of maturity in squamates. Journal of Vertebrate Paleontology 22(2):268-275.

Marsh, O. C. 1882. Classification of the Dinosauria. American Journal of Science 3:81-86.

Marsh, O. C. 1885. Names of extinct reptiles. American Journal of Science, Series 3 29:169.

Marsh, O. C. 1889. Notice of new American dinosaurs. American Journal of Science 3:331-336.

Marsh, O. C. 1891. Notice of new vertebrate fossils. American Journal of Science, Series 3 42:265-269.

Marsh, O. C. 1892. Notes on Triassic Dinosauria. American Journal of Science, Series 3 43:543-546.

Marsh, O. C. 1896. The dinosaurs of North America. United States Geological Survey 16th Annual Report:133-244.

Mook, C. C. 1917. Criteria for the determination of species in the Sauropoda, with description of a new species of *Apatosaurus*. Bulletin of the American Museum of Natural History 37:355-360.

Moser, M. 2003. *Plateosaurus engelhardti* Meyer, 1837 (Dinosauria: Sauropodomorpha) aus dem Feuerletten (Mittelkeuper; Obertrais) von Bayern. Zitteliana B24:1-188.

Motani, R. 1997. New technique for retrodeforming tectonically deformed fossils, with an example for ichthyosaurians specimens. Lethaia 30:221-228.

Mussell, J., and D. B. Weishampel. 2000. *Magyarosaurus* and the possible role of progenesis in sauropod development. Journal of Vertebrate Paleontology 20, Suppl.to 3:59-60A.

Nash, D. S. 1975. The morphology and relationships of a crocodilian, *Orthosuchus strombergi*, from the Upper Triassic of Lesotho. Annals of the South African Museum 67(7):227-329.

Nopsca, F. 1914. Uber das Vorkommen der Dinosaurier in Siebenburgen. Verh Zool Bot Ges 54:12-14.

Novas, F. E. 1996. Dinosaur monophyly. Journal of Vertebrate Paleontology 16:723-741.

Olsen, P. E. 1978. On the use of the term Newark for Triassic and Early Jurassic rocks of eastern North America. Newsletters on Stratigraphy 7:90-95.

Olsen, P. E., ed. 1980. A comparison of the vertebrate assemblages from the Newark and Hartford basins (early Mesozoic, Newark Supergroup) of eastern North America.

Olsen, P. E. 1986. A 40-million-year Lake record of Early Mesozoic orbital climatic forcing. Science 234:842-848.

Olsen, P. E., and P. M. Galton. 1977. Triassic-Jurassic tetrapod extinctions: Are they real? Science 197:983-986.

Olsen, P. E., and J. W. Gore. 1989. Tectonic, Depositional, and Paleoecological History of Early Mesozoic Rift Basins, Eastern North America. American Geophysical Union., Washington, D.C.

Olsen, P. E., A. McCune, and K. S. Thomson. 1982. Correlation of the early Mesozoic Newark Supergroup by vertebrates, principally fishes. American Journal of Science 282:1-44.

Olsen, P. E., and R. W. Schlische. 1990. Transtensional arm of the early Mesozoic Fundy rift basin: Penecontemporaneous faulting and sedimentation. Geology 18:695-698.

Olsen, P. E., N. H. Shubin, and M. H. Anders. 1987. New Early Jurassic Tetrapod Assemblages Constrain Triassic-Jurassic Tetrapod Extinction Event. Science 237:1025-1029.

Olsen, P. E., J. H. Whiteside, and T. J. Fedak. 2005. Field Trip A7: The Triassic-Jurassic faunal and floral transition in the Fundy Basin, Nova Scotia. Atlantic Geoscience Society, Halifax, Nova Scotia.

Ostrom, J. H., and J. S. McIntosh. 1966. Marsh's Dinosaurs. The collections from Como Bluff. Yale University Press, New Haven.

Owen, R. 1842. Report on British fossil reptiles. Report of the British Association for the Advancement of Science 11:60-294.

Padian, K., J. R. Horner, and A. De Ricqles. 2004. Growth in small dinosaurs and pterosaurs: The evolution of archosaurian growth strategies. Journal of Vertebrate Paleontology 24(3):555-571.

Peabody, F. E. 1961. Annual Growth Zones in Living and Fossil Vertebrates. Journal of Morphology 108:11-62.

Peczkis, J. 1994. Implications of Body-Mass Estimates for Dinosaurs. Journal of Vertebrate Paleontology 14:520-533.

Platt, S. G., T. R. Rainwater, and S. T. McMurry. 2002. Diet, gastrolith acquisition and initiation of feeding among hatchling Morelet's crocodiles in Belize. Herpetological Journal 12(2):81-84.

Reid, R. E. H. 1981. Lamellar-zonal bone with zones and annuli in the pelvis of a sauropod dinosaur. Nature 292:49-51.

Reisz, R. R., D. Scott, H.-D. Sues, D. C. Evans, and M. A. Raath. 2005. Embryos of an Early Jurassic prosauropod dinosaur and their evolutionary significance. Science 309:761-764.

Rhodin, A. G. 1985. Comparative chondro-osseous development and growth of marine turtles. Copeia 3:752-771.

Rieppel, O. 1993. Studies on skeletal formation in reptiles. V. Patterns of ossification in the skeleton of *Alligator mississippiensis* Daudin (Reptilia, Crocodylia). Zoological Journal of The Linnean Society 109:301-325.

Rogers, K. C. 1999. Ontogenetic histology of *Apatosaurus* (Dinosauria: Sauropoda): New insights on growth rates and longevity. Journal of Vertebrate Paleontology 19(4):654-665.

Rogers, R. R. 1994. Collecting taphonomic data from vertebrate localities. Pp. 47-58. *In* P. Leiggi, and P. May, eds. Vertebrate Paleontological Techniques. Cambridge University Press, Cambridge.

Salgado, L., R. A. Coria, and L. M. Chiappe. 2005. Osteology of the sauropod embryos from the Upper Cretaceous of Patagonia. Acta Palaeontologica Polonica 50(1):79-92.

Sander, P. M. 2000. Longbone histology of the Tendaguru sauropods: implications for growth and biology. Paleobiology 26(3):466-488.

Sankar, S. S. 1966. Study of fossil distortion caused by tectonic deformation in the Kashmir Himalayas (Liddar Valley). Current Science 13:341-343.

Seeley, H. G. 1887. On the classification of the fossil animals commonly named Dinosauria. Proceedings of the Royal Society of London 43:165-171.

Sereno, P. C. 1999. The evolution of the dinosaurs. Science 284:2137-2147.

Shubin, N. H., A. W. Crompton, H. D. Sues, and P. E. Olsen. 1991. New fossil evidence on the sister-group of Mammals and Early Mesozoic Fauna Distributions. Science 251:1063-1065.

Shubin, N. H., P. E. Olsen, and H. D. Sues. 1994. Early Jurassic small tetrapods from the McCoy Brook Formation of Nova Scotia, Canada. Pp. 242-250. *In* N. C. Fraser, and H. D. Sues, eds. In the Shadow of the Dinosaurs; Early Mesozoic Tetrapods. Cambridge University Press, Cambridge.

Shubin, N. H., and H. D. Sues. 1991. Biogeography of early Mesozoic continental tetrapods: patterns and implications. Paleobiology 17(3):214-230.

Smith, J. B., and P. Dodson. 2003. A proposal for a standard terminology of anatomical notation and orientation in fossil vertebrate dentitions. Journal of Vertebrate Paleontology 23(1):1-12.

Snover, M. L., and A. A. Hohn. 2004. Validation and interpretation of annual skeletal marks in loggerhead (*Caretta caretta*) and Kemp's ridley (*Lepidochelys kempii*) sea turtles. Fishery Bulletin 102(4):682-692.

Starck, J. M., and A. Chinsamy. 2002. Bone microstructure and developmental plasticity in birds and other dinosaurs. Journal of Morphology 254(3):232-246.

Sues, H. D., R. R. Reisz, S. Hinic, and M. A. Raath. 2004. On the skull of *Massospondylus carinatus* Owen, 1854 (Dinosauria : Sauropodomorpha) from the Elliot and Clarens formations (Lower Jurassic) of South Africa. Annals of Carnegie Museum 73(4):239-257.

Sues, H. D., N. H. Shubin, P. E. Olsen, and W. W. Amaral. 1996. On the cranial structure of a new protosuchid (Archosauria; Crocodyliformes) from the McCoy Brook Formation (Lower Jurassic) of Nova Scotia, Canada. Journal of Vertebrate Paleontology 16:34-41.

Swofford, D. L. 2002. PAUP *. Phylogenetic Analysis Using Parsimony (*and other methods), Version 4. Sinauer Associates, Sunderland, Massachusetts.

Tanner, L. H. 1994. Distribution and origin of clay minerals in the Lower Jurassic McCoy Brook Formation, Minas Basin, Nova Scotia. Sedimentary Geology 92:229-239.

Tanner, L. H., and J. F. Hubert. 1991. Basalt Breccias and Conglomerates in the Lower Jurassic McCoy Brook Formation, Fundy Basin, Nova Scotia: Differentiation of talus and debris-flow deposits. Journal of Sedimentary Petrology 61:15-27.

Tanner, L. H., and J. F. Hubert. 1992. Depositional facies, palaeogeography and palaeoclimatology of the Lower Jurassic McCoy Brook Formation, Fundy rift basin, Nova Scotia. Palaeogeography, Palaeoclimatology, Palaeoecology 96:261-280.

Tanner, L. H., and F. T. Kyte. 2005. Anomalous iridium enrichment at the Triassic-Jurassic boundary, Blomidon Formation, Fundy basin, Canada. Earth and Planetary Science Letters 240:634-641.

Taylor, M. A. 1993. Stomach Stones for Feeding or Buoyancy - the Occurrence and Function of Gastroliths in Marine Tetrapods. Philosophical Transactions of the Royal Society of London Series B-Biological Sciences 341(1296):163-175.

Thulborn, R. A. 1972. The post-cranial skeleton of the Triassic Ornithischian dinosaur *Fabrosaurus australis*. Palaeontology 15:29-60.

Upchurch, P. 1995. The Evolutionary History of Sauropod Dinosaurs. Philosophical Transactions of the Royal Society of London Series B-Biological Sciences 349(1330):365-390.

Upchurch, P. 1998. The phylogenetic relationships of sauropod dinosaurs. Zoological Journal of the Linnean Society 124:41-103.

Upchurch, P., P. M. Barrett, and P. Dodson. 2004. Sauropoda. Pp. 259-322. *In* D. B. Weishampel, P. Dodson, and H. Osmólska, eds. The Dinosauria. University of California Press, Berkeley, CA.

Upchurch, P., P. M. Barrett, and P. M. Galton. 2005. The phylogenetic relationships of basal sauropodomorphs: implications for the origin of sauropods. Journal of Vertebrate Paleontology 25:126A.

Upchurch, P., P. M. Barrett, and P. M. Galton. 2007. The phylogenetic relationships of basal sauropodomorphs: implications for the origin of sauropods. Special Papers in Palaeontology 77.

Wedel, M. J. 2003a. The evolution of vertebral pneumaticity in sauropod dinosaurs. Journal of Vertebrate Paleontology 23(2):344-357.

Wedel, M. J. 2003b. Vertebral pneumaticity, air sacs, and the physiology of sauropod dinosaurs. Paleobiology 29(2):243-255.

Wedel, M. J. 2006. Pneumaticity, neck length, and body size in sauropods. Journal of Vertebrate Paleontology 26:137A.

Weishampel, D. B., and R. E. Chapman, eds. 1990. Morphometric Study of *Plateosaurus* from Trossingen (Baden-Württemberg, Federal Republic of Germany). Cambridge University Press., Cambridge.

Welles, S. P. 1984. *Dilophosaurus wetherilli* (Dinosauria, Theropoda) Osteology and Comparisons. Palaeontographica.Abteilung A,; Paläozoologie, Stratigraphie 185:85-180.

Whittle, C. H., and L. Onorato. 2000. On the origins of gastroliths -determining the weathering environment of rounded and polished stones by scanning-electron-microscope examination. Pp. 69-73. *In* S. G. Lucas, and A. B. Heckert, eds. Dinosaurs of New Mexico, New Mexico Museum of Natural History and Science Bulletin No. 17. Albuquerque.

Wiley, E. O., D. Siegel-Causey, D. R. Brooks, and V. A. Funk. 1991. The Compleat Cladist, A Primer of Phylogenetic Procedures. Museum of Natural History The University of Kansas.

Wilhite, R. 1999. Ontogenetic variation in the appendicular skeleton of the genus *Camarasaurus*. Masters. Bringham Young University.

Wilson, J. A. 1999. A nomenclature for vertebral laminae in sauropods and other saurischian dinosaurs. Journal of Vertebrate Paleontology 19(4):639-654.

Wilson, J. A., and P. C. Sereno. 1998. Early evolution and higher-level phylogeny of sauropod dinosaurs. Journal of Vertebrate Paleontology 18(Supplement to 2):72.

Wings, O. 2005. Taphonomy, gastroliths, and the lithophagic behaviour of sauropodomorph dinosaurs. Journal of Vertebrate Paleontology 25(3):131A.

Witmer, L. M. 1997. The evolution of the antorbital cavity of archosaurs: A study in soft-tissue reconstruction in the fossil record with an analysis of the function of pneumaticity. Journal of Vertebrate Paleontology, Memoir 3 17:1-73.

Wu, X.-C., H. D. Sues, and Z.-M. Dong. 1997. *Sichuanosuchus Shuhanensis*, a new ?Early Cretaceaous Protosuchian (Archosauria: Crocodyliformes) from Sichuan (China), and the monophyly of Protosuchia. Journal of Vertebrate Paleontology 17(1):89-103.

Yates, A. 2002. A re-examination of the phylogenetic position of the unusual sauropodomorph, *Anchisaurus*. The Palaeontological Association Newsletter 50:55.

Yates, A. 2003a. A new species of the primitive dinosaur *Thecodontosaurus* (Saurischia: Sauropodomorpha) and its implications for the systematics of early dinosaurs. Journal of Systematic Palaeontology 1:1-42.

Yates, A. 2003b. The species taxonomy of the sauropodomorph dinosaurs from the Löwenstein Formation (Norian, Late Triassic) of Germany. Palaeontology 46(2):317-337.

Yates, A. 2004. *Anchisaurus polyzelus* (Hitchcock): the smallest known sauropod dinosaur and the evolution of gigantism amongst sauropodomorph dinosaurs. Postilla 230:1-58.

Yates, A. M. 2003c. A definite prosauropod dinosaur from the Lower Elliot Formation (Norian: Upper Triassic) of South Africa. Palaeontologia Africana 39:63-68.

Yates, A. M. 2005. The skull of the Triassic sauropodomorph, *Melanorosaurus readi*, from South Africa and the definition of Sauropoda. Journal of Vertebrate Paleontology 25:132A.

Yates, A. M. 2006. Solving a dinosaurian puzzle: the identity of *Aliwalia rex* Galton. Historical Geology:1-31.

Yates, A. M. 2007. The first complete skull of the Triassic dinosaur *Melanorosaurus* Haughton (Sauropodomorpha: Anchisauria). Special Papers in Palaeontology 77.

Yates, A. M., and J. W. Kitching. 2003. The earliest known sauropod dinosaur and the first steps towards sauropod locomotion. Proceedings of the Royal Society of London Series B-Biological Sciences 270(1525):1753-1758.

Yates, A. M., and C. C. Vasconcelos. 2005. Furcula-like clavicles in the prosauropod dinosaur *Massospondylus*. Journal of Vertebrate Paleontology 25(2):466-468.

Young, C. C. 1941. A complete osteology of *Lufengosaurus huenei* Young (gen. et sp. nov.) from Lufeng, Yunnan, China. Palaeontologia Sinica, Series C 7:1-53.

Young, C. C. 1947. On *Lufengosaurus magnus* Young (sp. nov.) and additional finds of *Lufengosaurus huenei* Young. Palaeontologia Sinica 12:1-53.

Young, C. C. 1951. The Lufeng Saurischian Fuana in China. Palaeontologia Sinica 134(13):1-96.

Zhang, Y. 1988. Sauropod Dinosaur (I) *Shunosaurus*. Sichuan Publishing House of Science and Technology, Chengdu, China.